Journal of Applied Mechanics

(Contributions of the ASME Applied Mechanics Division)

Reflection of Flexural Waves at the Edge of a Plate . . . . . *T. R. Kane* 213
Forced Motions of Elastic Rods . . . . . *G. Herrmann* 221
Creep Tests of Rotating Disks at Elevated Temperature and Comparison With Theory . . . . . *A. M. Wahl, G. O. Sankey, M. J. Manjoine, and E. Shoemaker* 225
Elasticity of Cubic Polycrystals . . . . . *A. V. Hershey* 236
Plasticity of Face-Centered Cubic Polycrystals . . . . . *A. V. Hershey* 241
Measurement of Mobility . . . . . *R. Plunkett* 250
Internal Damping of Machine Members . . . . . *A. W. Cochardt* 257
On Bending of a Flat Slab Supported by Square-Shaped Columns and Clamped . . . . . *S. Woinowsky-Krieger* 263
Impulsive Response of Beams in the Elastic and Plastic Regions . . . . . *W. T. Thomson* 271
Abstracts of Papers Presented at the Second U. S. National Congress of Applied Mechanics . . . 279

Design Data

A Simple Nomogram for the Ratios of Octahedral to Maximum Shearing Stresses and Its Physical Interpretation . . . . . *G. A. Zizicas* 291

Brief Notes

Impulsive Loading on an Elastic Half-Space . . . . . *J. H. Huth and J. D. Cole* 294
Influence of Primary Creep on Column Buckling . . . . . *F. K. G. Odqvist* 295
Bending of Plates Bounded by Conics and Clamped . . . . . *S. Woinowsky-Krieger* 296
On the Rate of Growth of Fatigue Cracks . . . . . *F. A. McClintock and F. J. Ryan* 296
Rounded Corner of a 90-Deg Elbow—Two-Dimensional Potential Flow . . . . *Robert Loury* 297
Discussion on previously published papers by *L. A. Pipes; H. D. Conway; Morris Morduchow; and J. L. Bogdanoff* 299
Book Reviews 305

SEPTEMBER, 1954

VOL. 21, NO. 3

Transactions of The American Society of Mechanical Engineers

Journal of Applied Mechanics

Papers Contributed to the Transactions by the ASME Applied Mechanics Division

[illegible] Committee on the Series [illegible]

E. H. Lee, Chairman

E. J. Hoer, Secretary

Jesse M. Lessells, Technical Editor

Published Quarterly by

The American Society of Mechanical Engineers

Publication Office, 20th and Northampton Streets, Easton, Pa.
Editorial Department at the Headquarters of the Society, 29 West Thirty-Ninth Street, New York 18, N. Y.

OFFICERS OF THE SOCIETY
[illegible], President

C. B. Davis, Secretary

[illegible] Treasurer, Assistant Secretary

[illegible]

[illegible], Vice-President

Stephen A. Kinnear, Editor
E. W. Cunningham, Mgr. Editor

Statement [illegible] made as responsible for statements or opinions advanced in papers or . . . printed in its publications (B13, Par. 4).

[illegible] by the American Society of Mechanical Engineers, Publication office at 20th and Northampton Streets, Easton, Pa. The editorial [illegible] York 18, N. Y. [illegible] Price [illegible] $4.00. Changes of address must be received at Society headquarters seven weeks before they are to be effective. Please send old label and new address. Allow one month for change of address. Subscriptions to the Journal of Applied Mechanics are included in the membership dues of the Applied Mechanics Division. Entered as second-class matter March 14, 1918, at the [illegible] Act of August 24, 1912. Acceptance for mailing at the special rate of postage provided for in paragraph (d-2) Section 34.40, P. L. & R. of 1948. Authorized March 14, 1918.

It is understood that the statements and opinions advanced in papers, discussions, and [illegible] are those of the individual contributors and not those of the Society. The Society shall not be responsible for statements or opinions advanced in papers or discussions at meetings of the Society or of its divisions or sections, or printed in its publications. Discussion is printed only if the paper is published in an ASME publication.

Released for general publication upon receipt of final manuscript and the author, and date of publication

Reflection of Flexural Waves at the Edge of a Plate[1]

By T. R. KANE,[2] PHILADELPHIA, PA.

The reflection of straight-crested flexural waves at the edge of a semi-infinite plate is studied in terms of a two-dimensional plate theory. It is found that, in general, a flexural wave propagated toward the edge at an arbitrary angle of incidence gives rise to three reflected waves: two flexural waves and a shear wave. A number of special cases, involving degenerate forms of these motions, are investigated in detail.

1 Introduction

IN this paper Mindlin's[3] equations of flexural motions of plates are used to study the reflection of a straight-crested wave at the edge of a semi-infinite plate. The equations accommodate three modes of motion: two types of flexural waves and a thickness-shear wave. It is found that, in general, all three of these motions are excited upon incidence of any one of them at a free edge. The shear motion, here encountered, is of particular interest; for this motion is absent in the classical theory of plates, whence the applicability of that theory is restricted to a range of frequencies considerably below that corresponding to the first mode of thickness-shear vibration. By the same token, the present theory does not include the higher modes of motion which are to be found in three-dimensional elasticity theory; thus the solution set forth in the paper may be expected to furnish an adequate description for frequencies which do not materially exceed that of the first thickness-shear mode.

The character of the reflected waves is affected by both the angle of incidence and the ratio of plate thickness to wave length of the incident wave. Appropriate values of these two parameters give rise to such special cases as waves whose amplitudes decrease exponentially with distance from the edge, vibrations, resonance, disappearance of some of the reflected waves, and, for grazing incidence, complete disappearance of the motion.

Following a résumé of the plate equations in Section 2, straight-crested waves are considered in Section 3. Incident and emergent waves are described in Section 4 and, in terms of these, a formal solution is reached in Section 5. In Sections 6 and 7 various cases of normal and oblique incidence are discussed in detail. Section 8 deals with grazing incidence.

[1] This investigation was supported by the Office of Naval Research under Contract Nonr-266(09) with Columbia University.

[2] Formerly, Research Associate in Civil Engineering, Columbia University; now Assistant Professor of Mechanical Engineering, University of Pennsylvania.

[3] "Influence of Rotatory Inertia and Shear on Flexural Motions of Isotropic, Elastic Plates," by R. D. Mindlin, JOURNAL OF APPLIED MECHANICS, Trans. ASME, vol. 73, 1951, pp. 31–38.

Contributed by the Applied Mechanics Division and presented at the Annual Meeting, New York, N. Y., November 29–December 4, 1953, of THE AMERICAN SOCIETY OF MECHANICAL ENGINEERS.

Discussion of this paper should be addressed to the Secretary, ASME, 29 West 39th Street, New York, N. Y., and will be accepted until October 11, 1954, for publication at a later date. Discussion received after the closing date will be returned.

NOTE: Statements and opinions advanced in papers are to be understood as individual expressions of their authors and not those of the Society. Manuscript received by ASME Applied Mechanics Division, March 23, 1953. Paper No. 53—A-42.

2 Plate Displacements, Equations of Motion and Stresses

For a plate of thickness h, oriented as in Fig. 1, plate displacements $\psi_x(x,y,t)$, $\psi_y(x,y,t)$, and $w(x,y,t)$ are given by[3]

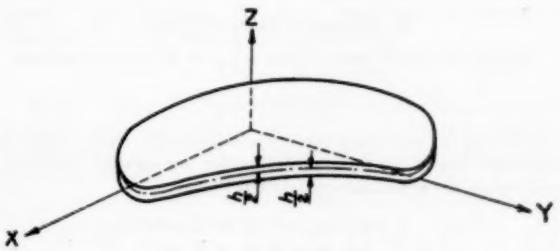

FIG. 1

$$\left.\begin{aligned}\psi_x &= \left[(\sigma_1 - 1)\frac{\partial w_1}{\partial x} + (\sigma_2 - 1)\frac{\partial w_2}{\partial x} + \frac{\partial H}{\partial y}\right]\exp(ipt)\\ \psi_y &= \left[(\sigma_1 - 1)\frac{\partial w_1}{\partial y} + (\sigma_2 - 1)\frac{\partial w_2}{\partial y} - \frac{\partial H}{\partial x}\right]\exp(ipt)\\ w &= (w_1 + w_2)\exp(ipt)\end{aligned}\right\} \quad \ldots [1]$$

The functions $w_1(x,y)$, $w_2(x,y)$, and $H(x,y)$ are governed, respectively, by equations of motion

$$\left.\begin{aligned}(\nabla^2 + \delta_1^2)w_1 &= 0\\ (\nabla^2 + \delta_2^2)w_2 &= 0\\ (\nabla^2 + \omega^2)H &= 0\end{aligned}\right\} \quad \ldots [2]$$

In the foregoing

$$(\sigma_1,\sigma_2) = (\delta_2^2, \delta_1^2)(R\delta_0^4 - S^{-1})^{-1} = (\delta_1^{-2},\delta_2^{-2})S\delta_0^4$$

$$2(\delta_1^2,\delta_2^2) = \delta_0^4[S + R \pm [(S-R)^2 + 4\delta_0^{-4}]^{1/2}] \quad \ldots [3]$$

$$(1-\nu)\omega^2 = 2(R\delta_0^4 - S^{-1}) \quad \ldots [4]$$

$$D\delta_0^4 = \rho p^2 h \quad \ldots [5]$$

$$\left.\begin{aligned}R &= \frac{h^2}{12}, \quad S = \frac{D}{\kappa^2\mu h}\\ D &= \frac{Eh^3}{12(1-\nu^2)}\end{aligned}\right\} \quad \ldots [6]$$

p is the circular frequency associated with the wave motion. E, ν, ρ are, respectively, Young's Modulus, Poisson's ratio, and the mass density of the plate material.

Plate bending moments M_x, M_y, shears Q_x, Q_y, and twisting moment M_{yx} are given by

$$\left.\begin{aligned} M_x &= D\left(\frac{\partial \psi_x}{\partial x} + \nu \frac{\partial \psi_y}{\partial y}\right) \\ M_y &= D\left(\frac{\partial \psi_y}{\partial y} + \nu \frac{\partial \psi_x}{\partial x}\right) \\ 2M_{yx} &= D(1-\nu)\left(\frac{\partial \psi_y}{\partial x} + \frac{\partial \psi_x}{\partial y}\right) \\ Q_x &= \kappa^2 \mu h \left(\psi_x + \frac{\partial w}{\partial x}\right) \\ Q_y &= \kappa^2 \mu h \left(\psi_y + \frac{\partial w}{\partial y}\right) \end{aligned}\right\} \quad \ldots\ldots [7]$$

μ is the modulus of rigidity of the plate material. The definition of κ^2 is given by Mindlin.[3]

3 Straight-Crested Waves

Taking any one of the functions w_1, w_2, or H to be of the form

$$A \exp(i\gamma x), \ \gamma > 0$$

and letting the remaining two vanish identically, we find that, in each case, two of the equations of motion are satisfied automatically while the remaining one requires that

$$\gamma^2 = \left\{\begin{array}{l} \delta_1^2; \ w_1 \neq 0, \ w_2 = H = 0 \\ \delta_2^2; \ w_2 \neq 0, \ w_1 = H = 0 \\ \omega^2; \ H \neq 0, \ w_1 = w_2 = 0 \end{array}\right\} \quad \ldots\ldots [8]$$

Letting

$$p^2 = (\gamma c)^2, \ c > 0$$

this leads to (see Equations [3], [4], [5]) three possible types of relationships between phase velocity c and wave number γ

$$\frac{c}{c_s} = \left\{\begin{array}{l} \dfrac{\kappa}{\gamma}\left[\dfrac{\Gamma - (\Gamma^2 - 4\gamma^4 RS)^{1/2}}{2R}\right]^{1/2}; \ w_1 \neq 0, \ w_2 = H = 0 \\ \dfrac{\kappa}{\gamma}\left[\dfrac{\Gamma + (\Gamma^2 - 4\gamma^4 RS)^{1/2}}{2R}\right]^{1/2}; \ w_2 \neq 0, \ w_1 = H = 0 \\ \dfrac{\kappa}{\gamma}\left[\dfrac{2 + \gamma^2(1-\nu)S}{2R}\right]^{1/2}; \ H \neq 0, \ w_1 = w_2 = 0 \end{array}\right\} \quad \ldots\ldots [9]$$

where

$$\Gamma = 1 + \gamma^2(R + S)$$

and c_s is the velocity of shear waves in an infinite medium. A plot of c/c_s versus $h\gamma$ (with $\nu = 1/4$) for each of these cases is shown in Fig. 2. It is seen that $c/c_s \to 0$ as $h\gamma \to 0$ for a w_1-wave, while $c/c_s \to \infty$ as $h\gamma \to 0$ for w_2 and H-waves. In the sequel we shall call w_1 a "slow" flexural wave, w_2 a "fast" flexural wave, and H a shear wave. (The fact that the preceding discussion involves waves propagated in the x-direction, does not result in any loss of generality.)

4 Incident and Emergent Waves

Referring the semi-infinite plate to axes x, y, z as shown in Fig. 3, we consider a slow flexural wave[4] propagated toward the edge of the plate

$$w_1 = A \exp(i\gamma\psi), \ w_2 = H = 0 \quad \ldots\ldots [10]$$

where

$$\psi = y \sin \alpha - x \cos \alpha$$

[4] The case of a fast incident wave is similar in nature and will not be discussed in the present paper.

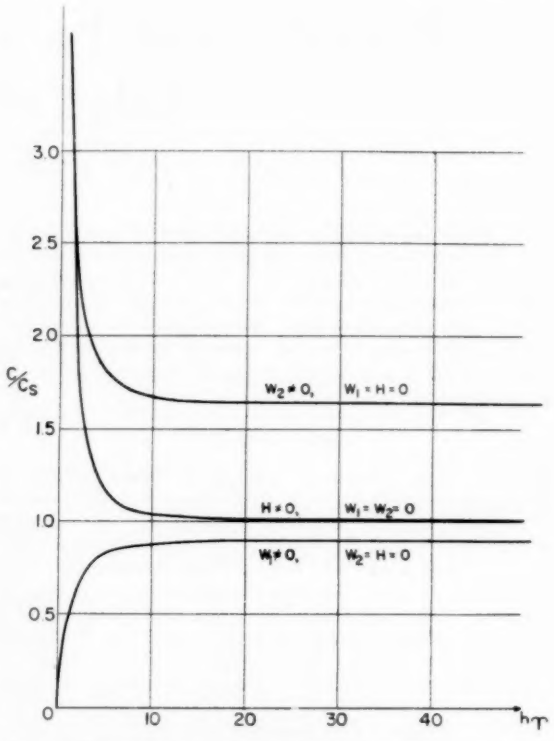

Fig. 2 Relationship Between Phase Velocity and Wave Number

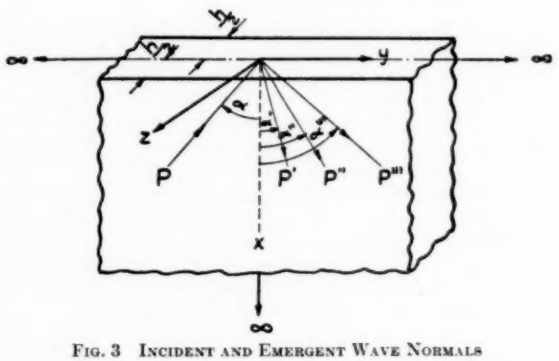

Fig. 3 Incident and Emergent Wave Normals

We postulate three emergent waves, propagated, respectively, toward P', P'', P''' as shown in Fig. 3. These are as follows:

(a) A slow flexural wave

$$w_1' = A' \exp(i\gamma'\psi'), \ w_2' = H' = 0 \quad \ldots\ldots [11]$$

(b) A fast flexural wave

$$w_2'' = A'' \exp(i\gamma''\psi''), \ w_1'' = H'' = 0 \quad \ldots\ldots [12]$$

(c) A shear wave

$$H''' = A''' \exp(i\gamma'''\psi'''), \ w_1''' = w_2''' = 0 \quad \ldots\ldots [13]$$

where

$$\psi^j = y \sin \alpha^j + x \cos \alpha^j, j = ', '', '''$$

and the α^j are the angles of emergence shown in Fig. 3.

In accordance with Equations [9], these waves are propagated with velocities c^j which depend on their respective wave numbers γ^j.

The displacements corresponding to these waves are obtained from Equations [1]. Denoting the incident wave by w, ψ_x, and ψ_y, and calling the displacement components of the emergent waves w^j, $\psi_x{}^j$, $\psi_y{}^j$ ($j = ', '', '''$), we observe that, since the equations of motion, Equations [2], are linear, the state of motion given by

$$\left.\begin{aligned} w^* &= w + \sum_j w^j \\ \psi_x{}^* &= \psi_x + \sum_j \psi_x{}^j \\ \psi_y{}^* &= \psi_y + \sum_j \psi_y{}^j \end{aligned}\right\} \quad \ldots\ldots\ldots\ldots [14]$$

is a possible state of motion for an infinite plate. For the semi-infinite plate under consideration, three boundary conditions must be satisfied on the edge $x = 0$.

5 Boundary Conditions

Plate stresses $M_x{}^*$, $M_y{}^*$, etc., corresponding to the motion defined by Equations [14], may be computed from Equations [7]. To obtain a traction-free edge, we must have, on $x = 0$

$$M_x{}^* = M_{yx}{}^* = Q_x{}^* = 0 \ldots\ldots\ldots\ldots [15]$$

In order that these equations be satisfied for all values of the time t and all values of the space variable y, it is necessary that the circular frequencies p and p^j associated with the various waves be identical, i.e.

$$\gamma c = \gamma^j c^j \ldots\ldots\ldots\ldots [16]$$

and that the angles α and α^j satisfy

$$\gamma \sin \alpha = \gamma^j \sin \alpha^j \ldots\ldots\ldots\ldots [17]$$

Now, the relation between c and γ is of the same form as that between c' and γ', both being slow flexural waves. Thus it follows from Equations [16] and [17] that the angle of emergence α' of the slow flexural wave is equal to the angle of incidence α of the incident wave, and that the wave numbers and phase velocities of these two waves are identical. Equations [16] and [17] show, furthermore, that the condition of vanishing traction at the edge of the plate, Equation [15], leads to a determination of the phase velocity, wave number, and angle of emergence of each of the postulated emergent waves when the angle of incidence and wave number (or phase velocity) of the incident wave are specified.

The Boundary Conditions [15] also impose restrictions on the amplitude ratios A^j/A. From Equations [10] to [13], [14], and [7] we get, upon substitution into Equations [15], a system of three nonhomogeneous linear algebraic equations governing these amplitude ratios

$$\sum_j \phi_n{}^j \frac{A^j}{A} = -\sqrt{2}\ \phi_n{}' \cos\left[(2n-1)\frac{\pi}{4}\right], j = ', '', '''; \quad n = 1, 2, 3 \ldots [18]$$

where

$$\left.\begin{aligned} \phi_1{}^j &= M^j \theta^j, j = ', '' \\ \phi_1{}''' &= (1-\nu)\gamma'''^2 \sin \alpha''' \cos \alpha''' \\ \phi_2{}^j &= M^j \sin 2\alpha^j, j = ', '' \\ \phi_2{}''' &= -\gamma'''^2 \cos 2\alpha''' \\ \phi_3{}^j &= S\delta_0{}^4 \gamma (\gamma^j)^{-1} \cos \alpha^j, j = \\ \phi_3{}''' &= \gamma\gamma''' \sin \alpha \end{aligned}\right\} \quad \ldots\ldots [19]$$

with

$$M^j = S\delta_0{}^4 - (\gamma^j)^2$$

$$\theta^j = \cos^2 \alpha^j + \nu \sin^2 \alpha^j$$

The analog, in the present theory, to F. Neumann's uniqueness theorem[5] guarantees that the foregoing constitutes the unique solution of the problem. We may say then that a slow incident flexural wave produces, in general, three reflected waves: a slow flexural, a fast flexural, and a shear wave.

6 Normal Incidence

We now proceed to study the character of the reflected waves in terms of the angle of incidence α and the wave number γ of the incident wave. We begin by examining the case of normal incidence, i.e., $\alpha = 0$.

The wave numbers γ'' and γ''' of the fast reflected wave and of the shear wave are given by (see Equations [8], [4], [5])

$$2(\gamma'')^2 = \delta_0{}^4[S + R - [(S-R)^2 + 4\delta_0{}^{-4}]^{1/2}] \ldots [20]$$

$$(\gamma''')^2 = 2(1-\nu)^{-1}(R\delta_0{}^4 - S^{-1}) \ldots\ldots [21]$$

Both γ'' and γ''' vanish when $RS\delta_0{}^4 = 1$, i.e., when $\gamma^2 RS = R + S$. For $\gamma^2 RS < R + S$, γ'' and γ''' are imaginary while for $\gamma^2 RS > R + S$, both are real. The physical significance of $\gamma^2 RS = 1$ will be discussed when the motion corresponding to that value of the wave number of the incident wave has been determined. We first consider

$$\gamma^2 RS < R + S$$

From Equation [17] we have, for $\alpha = 0$

$$\alpha^j = 0, j = ', '', '''$$

The amplitude ratios are found from Equations [18]

$$\left.\begin{aligned} \frac{A'}{A} &= \frac{a_1}{A} + \frac{ib_1}{A} \\ \frac{A''}{A} &= \frac{a_2}{A} + \frac{ib_2}{A} \\ \frac{A'''}{A} &= 0 \end{aligned}\right\} \quad \ldots\ldots\ldots\ldots [22]$$

where

$$\frac{a_1}{A} = \frac{(\bar\gamma'')^2(S\delta_0{}^4 + \bar\gamma''^2)^2 - \gamma^2(S\delta_0{}^4 - \gamma^2)^2}{(\bar\gamma'')^2(S\delta_0{}^4 + \bar\gamma''^2)^2 + \gamma^2(S\delta_0{}^4 - \gamma^2)^2}$$

$$\frac{b_1}{A} = -\frac{2\bar\gamma''\gamma(S\delta_0{}^4 + \bar\gamma''^2)(S\delta_0{}^4 - \gamma^2)}{(\bar\gamma'')^2(S\delta_0{}^4 + \bar\gamma''^2)^2 + \gamma^2(S\delta_0{}^4 - \gamma^2)^2}$$

$$\frac{a_2}{A} = -\frac{2\bar\gamma''^2(S\delta_0{}^4 + \bar\gamma''^2)(S\delta_0{}^4 - \gamma^2)}{(\bar\gamma'')^2(S\delta_0{}^4 + \bar\gamma''^2)^2 + \gamma^2(S\delta_0{}^4 - \gamma^2)^2}$$

$$\frac{b_2}{A} = \frac{2\bar\gamma''\gamma(S\delta_0{}^4 - \gamma^2)^2}{(\bar\gamma'')^2(S\delta_0{}^4 + \bar\gamma''^2)^2 + \gamma^2(S\delta_0{}^4 - \gamma^2)^2}$$

and $\bar\gamma'' = -i\gamma''$, so that $\bar\gamma''$ is real.

[5] "Theory of Elasticity," by A. E. H. Love, Cambridge University Press, London, England, fourth edition, 1927, p. 176.

The incident wave is given by (see Equations [1] and [10])

$$\left.\begin{aligned} w &= A\cos\gamma(x+ct)\\ \psi_x &= -AM'\gamma^{-1}\sin\gamma(x+ct)\\ \psi_y &= 0\end{aligned}\right\}\quad\ldots\ldots\ldots[23]$$

The slow reflected wave, Equations [11] becomes

$$\left.\begin{aligned} w' &= A\cos\gamma(x-ct+l_1)\\ \psi_x' &= -AM'\gamma^{-1}\sin\gamma(x-ct+l_1)\\ \psi_y' &= 0\end{aligned}\right\}\quad\ldots\ldots\ldots[24]$$

and the fast reflected wave, Equations [12] is given by

$$\left.\begin{aligned} w'' &= (a_2^2+b_2^2)^{1/2}\exp(-\tilde{\gamma}''x)\cos(\gamma ct-l_2)\\ \psi_x'' &= (\tilde{\gamma}'')^{-1}(S\delta_0^4-\tilde{\gamma}''^2)w''\\ \psi_y'' &= 0\end{aligned}\right\}\quad..[25]$$

In the foregoing

$$l_\kappa = \arctan(b_\kappa/a_\kappa),\ \kappa = 1, 2$$

We see that the slow reflected wave has the same amplitude, wave length, and velocity as the incident wave, but is out of phase with it. The fast reflected "wave" is, in fact, a *vibration*, the amplitude of which decreases exponentially as the distance from the edge of the plate increases. As $A''' = 0$ by Equations [22], no other waves are reflected.

Now consider

$$\gamma^2RS > R + S$$

Equations [22] are then replaced by

$$\frac{A'}{A} = \frac{\gamma''(S\delta_0^4-\gamma''^2)+\gamma(S\delta_0^4-\gamma^2)}{\gamma''(S\delta_0^4-\gamma''^2)-\gamma(S\delta_0^4-\gamma^2)}$$

$$\frac{A''}{A} = \frac{2(S\delta_0^4-\gamma^2)\gamma''}{\gamma(S\delta_0^4-\gamma^2)-\gamma''(S\delta_0^4-\gamma''^2)}$$

$$\frac{A'''}{A} = 0$$

The incident wave remains unchanged (Equations [23]); the slow reflected wave becomes

$$\left.\begin{aligned} w' &= A'\cos\gamma(x-ct)\\ \psi_x' &= -A'M'\gamma^{-1}\sin\gamma(x-ct)\\ \psi_y' &= 0\end{aligned}\right\}\quad\ldots\ldots\ldots[26]$$

the fast reflected wave is given by

$$\left.\begin{aligned} w'' &= A''\cos\gamma''(x-c''t)\\ \psi_x'' &= -A''M''(\gamma'')^{-1}\sin\gamma''(x-c''t)\\ \psi_y'' &= 0\end{aligned}\right\}\quad\ldots\ldots[27]$$

and the reflected shear wave again vanishes. (The amplitude ratios A'/A and A''/A for this case are plotted versus $h\gamma$ in Fig. 4.)

The incident wave is seen to give rise to two reflected flexural waves; we may examine the manner in which the energy per unit length of wave front, per cycle, of the incident wave is distributed to the two reflected waves. Using the expressions for energy given by Mindlin[3] we find

$$\frac{E'}{E} = \left(\frac{A'}{A}\right)^2$$

$$\frac{E''}{E} = \left(\frac{A''}{A}\right)^2\left(\frac{\gamma}{\gamma''}\right)\frac{\delta_0^4+M''^2}{\delta_0^4+M''^2}$$

Here E, E', and E'' are, respectively, the energy per cycle, per unit length of wave front of the incident wave, for the incident, slow reflected, and fast reflected waves. The ratios E'/E and E''/E are plotted versus $h\gamma$ in Fig. 5.

The motion corresponding to

$$\gamma^2RS = R + S$$

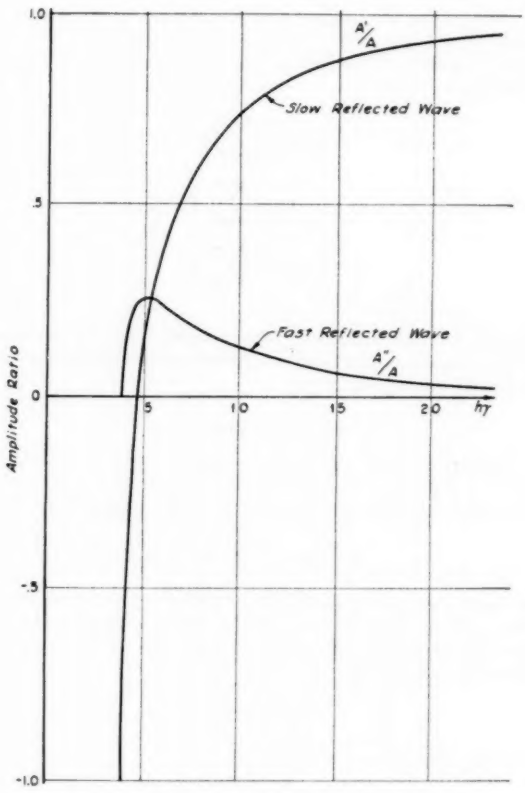

FIG. 4

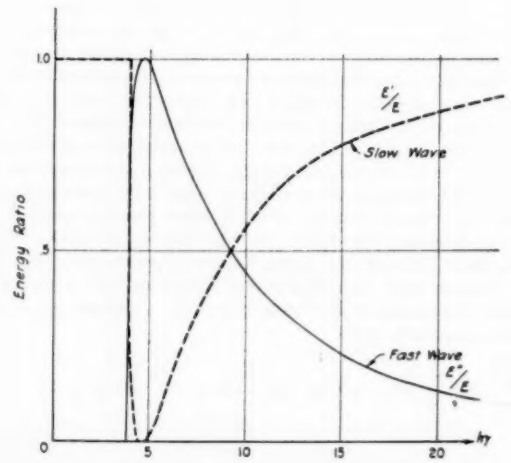

FIG. 5 ENERGY PARTITION—NORMAL INCIDENCE

may be found by proceeding to the limit, as $\gamma^2 RS \to R + S$, in either of the preceding cases. By either method it may be verified that an incident wave

$$\left.\begin{aligned} w &= A\cos\gamma(x+ct) \\ \psi_x &= A\left[\frac{R}{S(R+S)}\right]^{1/2}\sin\gamma(x+ct) \\ \psi_y &= 0 \end{aligned}\right\} \quad \ldots\ldots [28]$$

now gives rise to a slow reflected wave

$$\left.\begin{aligned} w' &= -A\cos\gamma(x-ct) \\ \psi_x' &= -A\left[\frac{R}{S(R+S)}\right]^{1/2}\sin\gamma(x-ct) \\ \psi_y' &= 0 \end{aligned}\right\} \quad \ldots\ldots [29]$$

and to a *thickness-shear vibration*

$$\left.\begin{aligned} w'' &= 0 \\ \psi_x'' &= 2A\left[\frac{S}{R(R+S)}\right]^{1/2}\sin\gamma ct \\ \psi_y'' &= 0 \end{aligned}\right\} \quad \ldots\ldots [30]$$

The circular frequency p for this vibration is (see Equations [3], [5], [6], [8], [9])

$$p = \kappa c_s \frac{\sqrt{12}}{h}$$

Now, the circular frequency $\bar{p}$, of the first antisymmetric mode of thickness-shear vibration of an infinite plate, according to the three-dimensional theory of elasticity, is $\bar{p} = \pi c_s/h$
Thus it seems appropriate to let $\kappa = \pi/\sqrt{12}$
so that the thickness-shear vibration in the present case will occur at the frequency predicted by exact theory for an infinite plate of the same thickness.

It is interesting to notice that the motion here being considered is one of the possible modes of motion of an infinite strip of thickness h and width b (according to Mindlin[6]) provided

$$b = \frac{hn\pi}{[3(R/S+1)]^{1/2}},\ n = 1,2,\ldots$$

Hence, for $\gamma^2 RS = R + S$, i.e., for $p = \bar{p}$, the semi-infinite plate may be regarded as consisting of an infinite number of independently vibrating strips, each with its infinite dimension parallel to the edge of the plate.

To conclude the discussion of normal incidence, we consider two limiting cases:

When the wave length of the incident wave is large in comparison with the thickness of the plate, we find, by proceeding to the limit in Equations [22] to [25], as $h\gamma \to 0$

$$w = A\cos\gamma(x+ct)\quad \psi_x = A\gamma\sin\gamma(x+ct)\quad \psi_y = 0$$

$$\begin{aligned} w' &= -A\sin\gamma(x-ct) \\ \psi_x' &= -A\gamma\cos\gamma(x-ct) \\ \psi_y' &= 0 \end{aligned}$$

$$\begin{aligned} w'' &= A(\cos\gamma ct + \sin\gamma ct)\exp(-\gamma x) \\ \psi_x'' &= -A\gamma(\cos\gamma ct + \sin\gamma ct)\exp(-\gamma x) \\ \psi_y'' &= 0 \end{aligned}$$

$$w''' = 0\quad \psi_x''' = 0\quad \psi_y''' = 0$$

These expressions show that the incident wave is reflected without change in amplitude or phase velocity, and that a vibration, confined primarily to a region near the edge of the plate, takes place. The classical theory of plates (whose range of applicability is restricted to the limiting case under consideration) predicts the same results.

For wave lengths which are very small in comparison with the plate thickness,[7] we let $h\gamma$ approach infinity in Equations [26], [27] with the result

$$\begin{aligned} w &= A\cos\gamma(x+ct),\ \psi_x = \psi_y = 0 \\ w' &= A\cos\gamma(x-ct),\ \psi_x' = \psi_y' = 0 \\ w'' &= \psi_x'' = \psi_y'' = 0 \\ w''' &= \psi_x''' = \psi_y''' = 0 \end{aligned}$$

The total motion is

$$w^* = 2A\cos\gamma x\cos\gamma ct$$

which is a standing wave.

7 Oblique Incidence

We have seen that fundamentally different states of motion obtain according as the circular frequency of the incident wave is less than, equal to, or greater than the circular frequency of thickness-shear vibration of an infinite plate. Hence, for $0 < \alpha < \pi/2$ we shall again examine separately the cases $p < \bar{p}$, $p > \bar{p}$, and $p = \bar{p}$

$p < \bar{p}$

As $p < \bar{p}$ is equivalent to $RS\delta_0^4 < 1$, we see from Equations [20] and [21] that γ'' and γ''' are imaginary.

Setting

$$\bar{\gamma}'' = -i\gamma'',\ \bar{\gamma}''' = -i\gamma'''$$

we get, from Equation [17]

$$\sin\alpha^j = -\frac{i\gamma}{\bar{\gamma}^j}\sin\alpha,\ j = '',\ '''$$

whence

$$\cos\alpha^j = \left[1 + \left(\frac{\gamma}{\bar{\gamma}^j}\right)^2\sin^2\alpha\right]^{1/2} = m^j,\ \text{say.}$$

(For all values of α and γ we have, as noted earlier, $\gamma' = \gamma$, $c' = c$, $\alpha' = \alpha$.) Substituting into the general expressions for the various reflected waves, Equations [11], [12], [13], we get from Equations [1]

$$\left.\begin{aligned} w' &= A'\exp[i\gamma(x\cos\alpha + \xi)] \\ \psi_x' &= w'M'\gamma^{-1}\cos\alpha \\ \psi_y' &= w'M'\gamma^{-1}i\sin\alpha \\ w'' &= A''\exp(i\gamma\xi - \bar{\gamma}''m''x) \\ \psi_x'' &= w''M''m'' \\ \psi_y'' &= -w''M''(\bar{\gamma}'')^{-1}\gamma\sin\alpha \\ w''' &= 0 \\ \psi_x''' &= A'''i\gamma\sin\alpha\exp(i\gamma\xi - \bar{\gamma}'''m'''x) \\ \psi_y''' &= A'''\bar{\gamma}'''m'''\exp(i\gamma\xi - \bar{\gamma}'''m'''x) \end{aligned}\right\} \quad \ldots [31]$$

where $\xi = y\sin\alpha - ct$.

These expressions are valid for all α with the possible exception of $\alpha = \pi/2$, i.e., "grazing" incidence. For that case, the solution of Equations [18] is

[6] "Thickness-Shear and Flexural Vibrations of Crystal Plates," by R. D. Mindlin, *Journal of Applied Physics*, vol. 22, 1951, pp. 316–323.

[7] The theory is not expected to be good for very short waves. This limiting case is included for the sake of completeness.

$$\frac{A'}{A} = -1,\ A'' = A''' = 0$$

and we get, in place of Equations [31]

$$w' = -w,\ \psi_x' = -\psi_x,\ \psi_y' = -\psi_y$$
$$w^j = \psi_x^j = \psi_y^j = 0,\ j = '', '''$$

so that the entire motion is then (see Equations [14])

$$w^* = \psi_x^* = \psi_y^* = 0 \qquad [32]$$

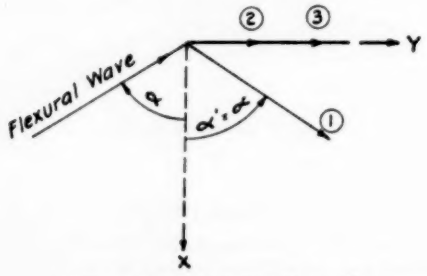

FIG. 6 OBLIQUE INCIDENCE, $p < \bar{p}$

This complete disappearance of the motion is analogous to the case of grazing incidence in the reflection of plane waves from the plane boundary of a semi-infinite solid. We shall return to this question later on.

The waves described by Equations [31] are as follows (Fig. 6):

① A slow flexural wave, reflected at an angle equal to the angle of incidence of the incident wave.

② A fast flexural wave of amplitude decreasing exponentially with departure from the edge, and propagated in a direction parallel to the edge.

③ A shear wave of exponentially decreasing amplitude, propagated along the edge.

Turning now to the case

$$p > \bar{p}$$

we note that, from Equations [20] and [21]

$$\gamma''/\gamma < 1,\ \gamma'''/\gamma < 1 \text{ and } \gamma''/\gamma < \gamma'''/\gamma \text{ for all } \gamma.$$

(Fig. 7 illustrates these facts for $\nu = 1/4$.)

Equation [17] permits us to construct a table which shows the relationship between α and α', α'', α''' in terms of trigonometric functions of these angles, Table 1.

With the help of Table 1 and Equations [10] to [13] we can now describe the motion associated with various angles of incidence.

For $0 \leq \sin\alpha < \gamma''/\gamma$, the reflected waves are as follows:

① A slow flexural wave.
② A fast flexural wave.
③ A shear wave.

These emerge at angles α', α'', α''' with

$$\alpha = \alpha' < \alpha''' < \alpha'' < \pi/2$$

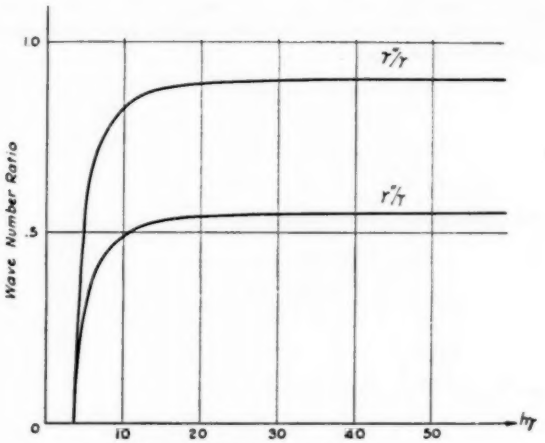

FIG. 7 WAVE NUMBER RATIOS

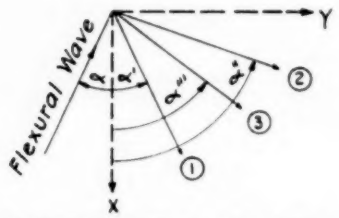

FIG. 8 OBLIQUE INCIDENCE. $p > \bar{p}$, $0 \leq \sin\alpha < \gamma''/\gamma$

as shown in Fig. 8. For instance, with $h\gamma = 5$, we have $\gamma''/\gamma = 0.302$, $\gamma'''/\gamma = 0.593$. Taking $\alpha = 15$ deg (so that $\sin\alpha < 0.302$) we get

$$\alpha' = 15 \text{ deg}$$

$$\alpha'' = \arcsin\frac{0.259}{0.302} = 59.1 \text{ deg}$$

$$\alpha''' = \arcsin\frac{0.259}{0.593} = 25.9 \text{ deg}$$

For $\sin\alpha = \gamma''/\gamma$, the amplitude ratios (see Equations [18]) are

$$\frac{A'}{A} = 1,\ \frac{A''}{A} = \frac{2(S\delta_0^4 - \gamma^2)}{\nu(S\delta_0^4 - \gamma''^2)}\left[\left(\frac{\gamma''}{\gamma}\right)^2(1-\nu) - 1\right],\ \frac{A'''}{A} = 0$$

Thus we have only two reflected waves, Fig. 9, as follows:

① A slow flexural wave whose angle of emergence is equal to the angle of incidence of the incident wave.

② A fast flexural wave propagated along the free edge.

With $h\gamma = 5$, as in the previous numerical example, the critical angle, α_c, for which the shear wave vanishes, is

$$\alpha_c = \arcsin(0.302) = 17.6 \text{ deg}$$

TABLE 1 RELATIONSHIP BETWEEN α, α', α'', and α'''

$\sin\alpha = 0$	$\sin\alpha' = 0$	$\sin\alpha'' = 0$	$\cos\alpha'' = 1$			
$0 < \sin\alpha < \gamma''/\gamma$	$0 < \sin\alpha' < \gamma''/\gamma$	$\sin\alpha < \sin\alpha'' < 1$	$0 < \cos\alpha'' < 1$	$\sin\alpha < \sin\alpha''' < \sin\alpha''$		$0 < \cos\alpha''' < 1$
$\sin\alpha = \gamma''/\gamma$	$\sin\alpha' = \gamma''/\gamma$	$\sin\alpha'' = 1$	$\cos\alpha'' = 0$	$\sin\alpha < \sin\alpha''' = \gamma''/\gamma''' < 1$		$0 < \cos\alpha''' < 1$
$\gamma''/\gamma < \sin\alpha < \gamma'''/\gamma$	$\gamma''/\gamma < \sin\alpha' < \gamma'''/\gamma$	$\sin\alpha'' > 1$	$\cos\alpha''$ imag.	$\sin\alpha < \sin\alpha''' < 1$		$0 < \cos\alpha''' < 1$
$\sin\alpha = \gamma'''/\gamma$	$\sin\alpha' = \gamma'''/\gamma$	$1 < \sin\alpha'' = \gamma'''/\gamma''$	$\cos\alpha''$ imag.	$\sin\alpha''' = 1$		$\cos\alpha''' = 0$
$\gamma'''/\gamma < \sin\alpha < 1$	$\gamma'''/\gamma < \sin\alpha' < 1$	$\sin\alpha'' > 1$	$\cos\alpha''$ imag.	$1 < \sin\alpha'''$		$\cos\alpha'''$ imag.
$\sin\alpha = 1$	$\sin\alpha' = 1$	$1 < \sin\alpha'' = \gamma/\gamma''$	$\cos\alpha''$ imag.	$1 < \sin\alpha''' = \gamma/\gamma'''$		$\cos\alpha'''$ imag.

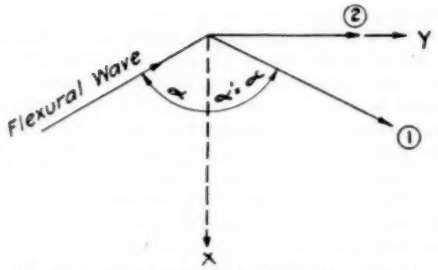

FIG. 9 OBLIQUE INCIDENCE, $p > \bar{p}$, $\sin \alpha = \gamma''/\gamma$

Letting α increase further, until $\gamma''/\gamma < \sin \alpha < \gamma'''/\gamma$, we find that the fast flexural wave (Equations [12]) changes in character since $\cos \alpha''$ is now imaginary. The shear wave reappears and we have, Fig. 10:

① A slow flexural wave.
② An exponentially decaying fast flexural wave, propagated parallel to the edge.
③ A shear wave emerging at an angle, α''', with $\alpha < \alpha''' < \pi/2$.

Another critical value of α is reached when $\sin \alpha = \gamma'''/\gamma$. We then find (Fig. 11):

① A slow flexural wave.
② An exponentially decaying fast flexural wave.
③ A shear wave.

Both ② and ③ are now propagated along the edge. With $h\gamma = 5$, the critical value for α is 36.4 deg.

Finally, for $\gamma'''/\gamma < \sin \alpha < 1$, the shear wave also acquires an exponentially decaying amplitude, giving us (Fig. 12):

① A slow flexural wave.
② An exponentially decaying fast flexural wave.
③ An exponentially decaying shear wave.

Grazing incidence, i.e., $\alpha = 90$ deg, leads to vanishing motion, as it did for $p < \bar{p}$.

To complete the discussion of oblique incidence, we consider the case

$$p = \bar{p}$$

As the circular frequency of the incident wave approaches the thickness-shear frequency, the amplitudes of the fast reflected wave and of the reflected shear wave become infinite. The resonance encountered here results from the fact that reflection at the edge of the plate is equivalent to "forcing" the plate at a frequency equal to a "natural" frequency. For it may easily be verified that the vibration

$$w = \psi_x = 0$$
$$\psi_y = B \exp(ipt)$$

is a motion which satisfies the equations of motion, Equations [2], and leaves the edge $x = 0$ free of traction.

8 GRAZING INCIDENCE

We have seen (Equation [32]) that the wave motion in a semi-infinite plate disappears as the angle of incidence approaches 90 deg. A similar situation obtains in the case of waves reflected from the plane boundary of a semi-infinite solid. By application of a suitable limiting process, wave motions for the latter case recently have been found by Goodier and Bishop.[8] A similar limiting process for the present case will now be considered.

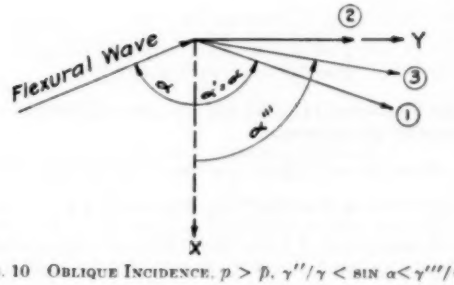

FIG. 10 OBLIQUE INCIDENCE, $p > \bar{p}$, $\gamma''/\gamma < \sin \alpha < \gamma'''/\gamma$

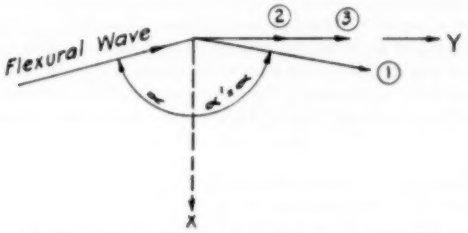

FIG. 11 OBLIQUE INCIDENCE, $p > \bar{p}$, $\sin \alpha = \gamma'''/\gamma$

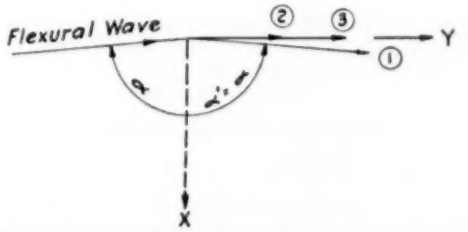

FIG. 12 OBLIQUE INCIDENCE, $p > \bar{p}$, $\gamma'''/\gamma < \sin \alpha < 1$

Letting

$$\epsilon = \pi/2 - \alpha$$

and neglecting higher powers of ϵ, we have, from Equations [17]

$$\sin \alpha^j = \frac{\gamma}{\gamma^j}\left(1 - \frac{\epsilon^2}{2}\right), \quad j = ', ''$$

Substituting into Equations [18], the amplitude ratios are found to be of the form

$$\frac{A'}{A} = -(1 + a'\epsilon), \quad \frac{A''}{A} = a''\epsilon, \quad \frac{A'''}{A} = a'''\epsilon \quad \ldots\ldots [33]$$

Expanding the exponentials which appear in the expressions for displacements, we get from Equations [10] to [13] and Equation [1]

$$\left.\begin{aligned} w &= A(1 - i\gamma\epsilon x)\exp(i\gamma\zeta) \\ w' &= A'(1 + i\gamma\epsilon x)\exp(i\gamma\zeta) \\ w'' &= A''\exp(i\gamma\zeta - xf'') \\ H''' &= A'''\exp(i\gamma y - xf''') \end{aligned}\right\} \quad \ldots\ldots [34]$$

[8] "A Note on Critical Reflections of Elastic Waves at Free Surfaces," by J. N. Goodier and R. E. D. Bishop, *Journal of Applied Physics*, vol. 23, 1952, pp. 124–126.

where

$$\zeta = y - ct$$
$$f^j = [\gamma^2 - (\gamma^j)^2]^{1/2},\ j = '',\ '''$$

From Equations [14], [33], and [34], the total motion is characterized by the expressions

$$w^* = A\epsilon[-a' - 2i\gamma x + a'' \exp(-f''x)] \exp(i\gamma\zeta) \quad [35]$$

$$H''' = A\epsilon a''' \exp(i\gamma y - xf''') \quad [36]$$

If we now permit A to become infinite as ϵ approaches zero, and let the approach to infinity be such that the product $A\epsilon$ remains finite, we see that the first term of Equation [35] represents an incident flexural wave while the second term corresponds to the P_y-wave found by Goodier and Bishop. The third term and Equation [36] indicate, respectively, a flexural and a shear wave, each propagated along the edge of the plate, and each having an exponentially increasing or decreasing amplitude, according as p is less than or greater than $\bar{p}$; for $p = \bar{p}$ we again have resonance.

The limiting solution obtained by Goodier and Bishop satisfies the three-dimensional equations of motion exactly. Similarly, the motion defined by Equations [35] and [36] constitutes an exact solution of the two-dimensional equations of motion. Hence these waves could be obtained directly, without a limiting process, but the connection between these waves and those arising from the general case of oblique incidence would then be less evident. Furthermore, these waves contain components whose amplitude increases, without limit, with increasing distance from the free edge; as omission of higher-order terms, in the expansion of the exponentials, requires that the product of the wave number and the distance from the free edge remain finite, it is seen that the limiting process leads to a description of the behavior of the waves, valid in the neighborhood of the free edge.

Acknowledgment

The author wishes to thank Prof. R. D. Mindlin of Columbia University both for suggesting this problem, and for his helpful advice in its solution.

Forced Motions of Elastic Rods[1]

By G. HERRMANN,[2] NEW YORK, N. Y.

In a recent paper by Mindlin and Herrmann, a one-dimensional theory of compressional waves in an elastic rod was described. This theory takes into account both radial inertia and radial shear stress and, accordingly, contains two dependent variables instead of the one axial displacement of classical rod theory. The solution of the equations for the case of forced motions thus involves complications not usually encountered. The difficulties may be surmounted in several ways, one of which is presented in this paper. The method described makes use of Lagrange's equation of motion and reduces the most general problem of forced motion to a free vibration problem and a quadrature.

Statement of Problem

An approximate, one-dimensional, theory of vibrations of rods,[3] in which the effect of radial inertia and radial shear deformation are taken into account, is contained in the equations of motion

$$\left.\begin{aligned} a^2\kappa^2\mu u'' - 8\kappa_1^2(\lambda+\mu)u - 4a\kappa_1^2\lambda w' + 4aR &= \rho a^2\ddot{u} \\ 2a\lambda u' + a^2(\lambda+2\mu)w'' + 2aZ &= \rho a^2\ddot{w} \end{aligned}\right\} \quad \ldots\ldots [1]$$

the stress-displacement relations

$$\left.\begin{aligned} 2P_r = 2P_\theta &= \kappa_1^2[2a(\lambda+\mu)u + a^2\lambda w'] \\ 2P_z &= 2a\lambda u + a^2(\lambda+2\mu)w' \\ 4Q &= \kappa^2 a^2\mu u' \end{aligned}\right\} \quad \ldots\ldots [2]$$

the following boundary conditions:

$$\left.\begin{aligned} &1\ \text{At each point along the length of the bar, one member of each of the products } \dot{u}R \text{ and } \dot{w}Z \text{ must be specified} \\ &2\ \text{At each end of the bar one member of each of the products } \dot{u}Q \text{ and } \dot{w}P_z \text{ must be specified} \end{aligned}\right\} \quad \ldots [3]$$

and the initial conditions:

The initial displacements and velocities must be specified.. [4]

In Equations and Conditions [1] to [4] the symbols have the following meanings:

λ, μ = Lamé's constants of elasticity
ρ = density
u, w = radial and axial displacements, respectively
a = radius of the rod
R, Z = radial and tangential components of traction, respectively, on cylindrical surface of rod
κ, κ_1 = correction factors
$\left.\begin{matrix} P_r, P_\theta \\ P_z, Q \end{matrix}\right\}$ = rod-stress components, defined previously[3]

Primes indicate differentiation with respect to z, the co-ordinate along the axis of the rod, and dots indicate differentiation with respect to time.

The object of this paper is to describe the development of a formal solution of the foregoing equations for a rod of finite length l, and any admissible combination of time-dependent boundary conditions and arbitrary initial conditions.

The solution will be developed by making use of Lagrange's equation of motion

$$\frac{d}{dt}\left(\frac{\partial T}{\partial \dot{q}_n}\right) - \frac{\partial T}{\partial q_n} + \frac{\partial V}{\partial q_n} = Q_n \quad \ldots\ldots [5]$$

where T is the kinetic energy of the mechanical system considered, V is the potential energy, q_n is the nth generalized co-ordinate, $\dot{q}_n$ the nth generalized velocity, and Q_n the nth generalized force. As a convenience in specifying the boundary conditions, the following notation will be employed

$B_1 = u$ or Q at $z = 0$
$B_2 = w$ or P_z at $z = 0$
$B_3 = u$ or Q at $z = l$
$B_4 = w$ or P_z at $z = l$

Accordingly, the Boundary Conditions [3] become

$$B_i = f_i(t), \qquad i = 1, 2, 3, 4 \quad \ldots\ldots [3a]$$

in which the four functions $f_i(t)$ are prescribed.

The Initial Conditions [4] are specified by the four arbitrary functions

$$\left.\begin{aligned} u(z, 0) &= u_0(z) \\ w(z, 0) &= w_0(z) \\ \dot{u}(z, 0) &= \dot{u}_0(z) \\ \dot{w}(z, 0) &= \dot{w}_0(z) \end{aligned}\right\} \quad \ldots\ldots [4a]$$

Kinetic Energy

The form of the kinetic energy of the rod may be obtained by performing the appropriate integrations in the expression of the kinetic energy in terms of the general three-dimensional displacements. Thus, in general, the kinetic energy is

$$T = \frac{\rho}{2}\int_V (\dot{u}_r^2 + \dot{u}_\theta^2 + \dot{u}_z^2)d\tau \quad \ldots\ldots [6]$$

where u_r, u_θ, u_z are the components of displacement in cylindrical co-ordinates and the integration is throughout the volume of the rod. With the assumed displacements of the one-dimensional theory,[3] which were

$$\left.\begin{aligned} u_r &= \frac{r}{a}u(z, t) \\ u_\theta &= 0 \\ u_z &= w(z, t) \end{aligned}\right\} \quad \ldots\ldots [7]$$

the kinetic energy of the rod becomes

$$T = \frac{\rho}{2}\int_0^{2\pi}\int_0^a\int_0^l \left(\frac{r^2}{a^2}\dot{u}^2 + \dot{w}^2\right) r\, dr\, d\theta\, dz \quad \ldots [8]$$

[1] This investigation was supported by the Office of Naval Research under Contract Nonr-266(09) with Columbia University.

[2] Assistant Professor of Civil Engineering, Columbia University.

[3] "A One-Dimensional Theory of Compressional Waves in an Elastic Rod," by R. D. Mindlin and G. Herrmann, Proceedings of the First U. S. National Congress of Applied Mechanics, Chicago, Ill., 1951.

Contributed by the Applied Mechanics Division and presented at the Annual Meeting, New York, N. Y., November 29–December 4, 1953, of The American Society of Mechanical Engineers. Discussion of this paper should be addressed to the Secretary, ASME, 29 West 39th Street, New York, N. Y., and will be accepted until October 11, 1954, for publication at a later date. Discussion received after the closing date will be returned.

Note: Statements and opinions advanced in papers are to be understood as individual expressions of their authors and not those of the Society. Manuscript received by ASME Applied Mechanics Division, January 30, 1953. Paper No. 53—A-59.

Performing the integrations with respect to θ and r, the volume integral in Equation [8] reduces to a simple integral, extended over the length l of the rod

$$T = \frac{\pi\rho a^2}{2}\int_0^l \left(\frac{\dot{u}^2}{2} + \dot{w}^2\right) dz \quad \ldots\ldots [9]$$

Potential Energy

The potential energy of the rod is obtained, similarly, by performing appropriate integrations in the general expression for the potential energy. The latter is

$$V = \int_V W d\tau \quad \ldots\ldots [10]$$

where the integration is over the volume of the rod and

$$W = \frac{1}{2}\left[\sigma_{rr}\frac{\partial u_r}{\partial r} + \ldots . \sigma_{\theta z}\left(\frac{1}{r}\frac{\partial u_z}{\partial \theta} + \frac{\partial u_\theta}{\partial z}\right) + \ldots .\right] \ldots . [11]$$

The Assumed Displacements [7] are now inserted into Equation [11] and the integrations are performed with respect to r and θ, thus obtaining an expression in terms of u, w, P_r, P_θ, P_z, and Q. Use of the stress-displacement Relations [2] reduces the result to

$$V = \pi\int_0^l \left[2(\lambda+\mu)u^2 + 2\lambda a u w' + \frac{a}{2}(\lambda+2\mu)w'^2 + \frac{\mu\kappa^2 a^2}{4}u'^2\right] dz \ldots\ldots [12]$$

For the sake of simplicity, the correction factor κ_1 has been set equal to unity.

Free Vibrations

As a preliminary to the study of forced vibrations, we shall be concerned with the problem of free vibrations, specified by the homogeneous differential equations of motion

$$\left.\begin{aligned} a^2\kappa^2\mu u'' - 8(\lambda+\mu)u - 4a\lambda w' &= \rho a^2 \ddot{u} \\ 2a\lambda u' + a^2(\lambda+2\mu)w'' &= \rho a^2 \ddot{w} \end{aligned}\right\} \ldots\ldots [13]$$

and homogeneous boundary conditions

$$B_i = 0, \qquad i = 1, 2, 3, 4 \ldots\ldots [14]$$

Considering solutions in the form

$$\left.\begin{aligned} u(z,t) &= U(z)\sin\omega t \\ w(z,t) &= W(z)\sin\omega t \end{aligned}\right\} \ldots\ldots [15]$$

we may show that the equations of motion, Equations [13], together with the Boundary Conditions [14], are satisfied for an infinite set of discrete frequencies ω_n, each of which corresponds to a mode shape given by functions $U_n(z)$ and $W_n(z)$, which are determined except for a multiplying factor, common to both functions.

The kinetic energy of the rod, vibrating in the nth principal mode, is, according to Equation [9]

$$T_n(t) = \frac{\omega_n^2\pi\rho a^2}{2}\int_0^l \left(\frac{1}{2}U_n^2 + W_n^2\right) dz \cos^2\omega_n t \ldots . [16]$$

and its maximum value is

$$T_{n\,max} = \frac{\omega_n^2\pi\rho a^2}{2}\int_0^l \left(\frac{1}{2}U_n^2 + W_n^2\right) dz \ldots\ldots [17]$$

Similarly, the maximum potential energy of the rod is, from Equation [12]

$$V_{n\,max} = \pi\int_0^l \left[2(\lambda+\mu)U_n^2 + 2\lambda a U_n W_n' + \frac{a^2}{2}(\lambda+2\mu)W_n'^2 + \frac{\mu\kappa^2 a^2}{4}U_n'^2\right] dz \ldots . [18]$$

Employing the principle of conservation of energy, we restate, for future reference, the well-known relationship

$$T_{n\,max} = V_{n\,max} \ldots\ldots [19]$$

Time-Dependent Boundary Displacements

Whenever a number m, of time-dependent displacements is specified at the ends of the rod, in a forced-vibration problem, it is convenient to solve m static problems in advance; each problem being governed by the equilibrium equations

$$\left.\begin{aligned} a^2\kappa^2\mu u'' - 8(\lambda+\mu)u - 4a\lambda w' &= 0 \\ 2a\lambda u' + a^2(\lambda+2\mu)w'' &= 0 \end{aligned}\right\} \ldots\ldots [20]$$

The boundary conditions for each static problem are obtained by setting one of the m end displacements equal to unity and letting the remaining three conditions be homogeneous. For example, if the boundary conditions of the forced-vibration problem are

$$\begin{aligned} u(0,t) &= f_1(t) \\ P_z(0,t) &= f_2(t) \\ Q(l,t) &= f_3(t) \\ w(l,t) &= f_4(t) \end{aligned}$$

then $m = 2$ and two static problems have to be solved; one with boundary conditions

$$\left.\begin{aligned} u(0,t) &= 1 \\ P_z(0,t) &= 0 \\ Q(l,t) &= 0 \\ w(l,t) &= 0 \end{aligned}\right\} \ldots\ldots [21]$$

and the other with boundary conditions

$$\left.\begin{aligned} u(0,t) &= 0 \\ P_z(0,t) &= 0 \\ Q(l,t) &= 0 \\ w(l,t) &= 1 \end{aligned}\right\} \ldots\ldots [22]$$

The m static solutions $u(z)$, $w(z)$, which are readily obtained, will be designated $g_{iu}(z)$, $g_{iw}(z)$, where i runs from 1 to m.

General Forced-Vibration Problem

The solution of the general forced-vibration problem, specified by Equations [1], [3a], and [4a], will be sought in the form

$$\left.\begin{aligned} u(z,t) &= \sum_{i=1}^{m} g_{iu}(z)f_i(t) + \sum_{n=1}^{\infty} U_n(z)q_n(t) \\ w(z,t) &= \sum_{i=1}^{m} g_{iw}(z)f_i(t) + \sum_{n=1}^{\infty} W_n(z)q_n(t) \end{aligned}\right\} \ldots\ldots [23]$$

All the functions in Equations [23] have been introduced in preceding sections and are assumed to have been determined, with the exception of $q_n(t)$, which will be found from Lagrange's Equation [5]. It should be noted that Equations [23] satisfy the Boundary Conditions [3a].

Inserting the Forms [23] into Expression [9] for the kinetic energy T, we obtain

$$T = \frac{\pi\rho a^2}{2}\int_0^l \left\{\frac{1}{2}\left[\sum_{i=1}^{m} g_{iu}\dot{f}_i + \sum_{n=1}^{\infty} U_n\dot{q}_n\right]^2 + \left[\sum_{i=1}^{m} g_{iw}\dot{f}_i + \sum_{n=1}^{\infty} W_n\dot{q}_n\right]^2\right\} dz \ldots\ldots [24]$$

Thus

$$\frac{\partial T}{\partial q_n} = 0 \quad \ldots\ldots [25]$$

and

$$\frac{d}{dt}\frac{\partial T}{\partial \dot{q}_n} = \frac{\pi\rho a^2}{2}\int_0^l \left[\sum_{i=1}^{m} g_{iu}U_n\ddot{f}_i + 2\sum_{i=1}^{m} g_{iw}W_n\ddot{f}_i\right] dz + T_{n\max}\frac{2}{\omega_n^2}\ddot{q}_n \quad \ldots\ldots [26]$$

where use has been made of Equation [17] and of

$$\int_0^l \left(\frac{1}{2}U_rU_s + W_rW_s\right) dz = 0, \quad \omega_r \neq \omega_s \quad \ldots\ldots [27]$$

The Relationship [27], which expresses the property of orthogonality of the principal modes of free vibration, can be obtained by substituting the assumed Displacements [7] and [15] into Clebsch's theorem[4] and performing the integrations with respect to r and θ. Alternatively, Relationship [27] may be obtained from Equations [13] and [14], using Rayleigh's method.[5]

Insertion of the Displacements [23] into the Expression [12] for the potential strain energy V yields

$$V = \pi\int_0^l \left\{2(\lambda+\mu)\left[\sum_{i=1}^{m} g_{iu}f_i + \sum_{n=1}^{\infty} U_nq_n\right]^2 + 2\lambda a\left[\sum_{i=1}^{m} g_{iu}f_i + \sum_{n=1}^{\infty} U_nq_n\right]\left[\sum_{i=1}^{m} g_{iw}'f_i + \sum_{n=1}^{\infty} W_n'q_n\right] + \frac{a^2}{2}(\lambda+2\mu)\left[\sum_{i=1}^{m} g_{iw}'f_i + \sum_{n=1}^{\infty} W_n'q_n\right]^2 + \frac{\mu\kappa^2a^2}{4}\left[\sum_{i=1}^{m} g_{iu}'f_i + \sum_{n=1}^{\infty} U_n'q_n\right]^2\right\} dz \quad \ldots\ldots [28]$$

Partial differentiation with respect to q_n results in

$$\frac{\partial V}{\partial q_n} = \pi\int_0^l \left\{4(\lambda+\mu)\sum_{i=1}^{m} g_{iu}f_iU_n + 2\lambda a\sum_{i=1}^{m}\left[g_{iu}f_iW_n' + g_{iw}f_iU_n\right] + a^2(\lambda+2\mu)\sum_{i=1}^{m} g_{iw}'f_iW_n' + \frac{\mu\kappa^2a^2}{2}\sum_{i=1}^{m} g_{iu}'f_iU_n'\right\} dz + 2V_{n\max}q_n \quad \ldots\ldots [29]$$

where use has been made of Equation [18] and of

$$\int_0^l \left[4(\lambda+\mu)U_rU_s + 2\lambda a(U_rW_s' + U_sW_r') + (\lambda+2\mu)a^2W_r'W_s' + \frac{\mu\kappa^2a^2}{2}U_r'U_s'\right] dz = 0, \ \omega_r \neq \omega_s \quad \ldots\ldots [30]$$

which states, in another way, the orthogonality property of the principal modes and can be transformed to the Relationship [27] by use of the equations of motion, Equations [13].

Referring to the integral in Equation [29], the primed terms may be integrated by parts. Then, noting that U_n, W_n satisfy Equations [13] and [14], while g_{iu}, g_{iw} satisfy Equations [20] and boundary conditions of the type exemplified by Equations [21], we arrive at

$$\int_0^l \left\{4(\lambda+\mu)g_{iu}U_n + 2\lambda a(g_{iu}W_n' + g_{iw}'U_n) + (\lambda+2\mu)a^2g_{iw}'W_n' + \frac{\mu\kappa^2a^2}{2}g_{iu}'U_n'\right\} dz = 0 \quad \ldots\ldots [31]$$

Thus, the integral in Equation [29] vanishes and we find, from Equations [29], [31], and [19]

$$\frac{\partial V}{\partial q_n} = 2q_nV_{n\max} = 2q_nT_{n\max} \quad \ldots\ldots [32]$$

The vanishing Integral [31] also can be used advantageously to simplify the integral in Equation [26]. Assuming, temporarily, the largest possible number of specified, time-dependent displacements at the ends of the rod ($m = 4$) we obtain, by partial integration

$$\int_0^l \left[\sum_{i=1}^{4} g_{iu}U_n + 2\sum_{i=1}^{4} g_{iw}W_n\right] dz = \frac{4}{\rho\omega_n^2a^2}\left[Q_n(0) + P_{sn}(0) - Q_n(l) - P_{sn}(l)\right] \quad \ldots\ldots [33]$$

where Q_n and P_{sn} are tractions produced by the displacements of U_n and W_n.

Entering this result into Equation [26], we obtain

$$\frac{d}{dt}\frac{\partial T}{\partial \dot{q}_n} = \frac{2\pi}{\omega_n^2}\left[\ddot{f}_1Q_n(0) + \ddot{f}_2P_{sn}(0) - \ddot{f}_3Q_n(l) - \ddot{f}_4P_{sn}(l)\right] + T_{n\max}\frac{2}{\omega_n^2}\ddot{q}_n \quad \ldots\ldots [34]$$

The generalized force Q_n in Equation [5], defined as the coefficient of the increment δq_n of the generalized co-ordinate q_n, in the expression for the work δW_n, done by the applied physical forces in the displacement produced by δq_n, has to be determined on the basis of this definition. We note, at this point, that not only the q_n but also the m-functions f_i have to be regarded as generalized co-ordinates. Consequently, Q_n will not be affected by the presence or absence of any of the functions f_i.

An increment δq_n produces, according to Equations [23], the infinitesimal displacements

$$\left.\begin{aligned}\delta u &= U_n\delta q_n\\ \delta w &= W_n\delta q_n\end{aligned}\right\} \quad \ldots\ldots [35]$$

The work δW, done by the applied forces on the surfaces of the rod, has been derived in another paper[3] and is

$$\delta W = 2\pi a\int_0^l (R\delta u + Z\delta w)dz + 2\pi\left[Q(l)\delta u(l) + P_s(l)\delta w(l) - Q(0)\delta u(0) - P_s(0)\delta w(0)\right] \quad \ldots\ldots [36]$$

Considering the largest possible number of specified, time-dependent forces, inserting Equations [35] in the foregoing expression and factoring δq_n, we obtain the generalized force $Q_n(t)$

$$Q_n(t) = 2\pi a\int_0^l [RU_n + ZW_n]dz + 2\pi\left[Q(l)U_n(l) + P_s(l)W_n(l) - Q(0)U_n(0) - P_s(0)W_n(0)\right] \quad \ldots [37]$$

Comparing this with Equation [36], Q_n is seen to be the work done by the applied surface tractions in the displacements of the nth principal mode.

[4] "Theory of Elasticity," by A. E. H. Love, Cambridge University Press, London, England, fourth edition, 1927, p. 180.

[5] "Theory of Sound," by Lord Rayleigh, Dover Publications, New York, N. Y., second edition, vol. 1, 1945, p. 262.

In computing

$$\frac{d}{dt}\frac{\partial T}{\partial \dot{q}_n}$$

of Equation [34], we have assumed, as an extreme case, four time-dependent displacements specified at the ends of the rod ($m = 4$). The generalized force Q_n, Equation [37], on the other hand, was derived under the presupposition of four time-dependent tractions acting at the ends of the rod ($m = 0$). Now, whatever the value of m, the total number of the terms in the bracket of Equation [34] and in the bracket of Equation [37] will always be four. In view of this, it is convenient to define four quantities H_i, $i = 1, 2, 3, 4$, as follows

$$\left.\begin{aligned}
-H_1 &= \frac{2\pi}{\omega_n^2} f_1 Q_n(0) \quad \text{or } 2\pi U_n(0)Q(0), \text{ according as}\\
B_1 &= u \qquad\qquad \text{or } Q\\
-H_2 &= \frac{2\pi}{\omega_n^2} f_2 P_{zn}(0) \text{ or } 2\pi W_n(0)P_z(0), \text{ according as}\\
B_2 &= w \qquad\qquad \text{or } P_z\\
H_3 &= \frac{2\pi}{\omega_n^2} f_3 Q_n(l) \quad \text{or } 2\pi U_n(l)Q(l), \text{ according as}\\
B_3 &= u \qquad\qquad \text{or } Q\\
H_4 &= \frac{2\pi}{\omega_n^2} f_4 P_{zn}(l) \quad \text{or } 2\pi W_n(l)P_z(l), \text{ according as}\\
B_4 &= w \qquad\qquad \text{or } P_z
\end{aligned}\right\} \quad [38]$$

Also we define the quantity

$$Q_n^* = \frac{\omega_n^2}{2T_{n\max}}\left[2\pi a\int_0^l (RU_n + ZW_n)dz + \sum_{i=1}^{4} H_i\right] \quad [39]$$

Then Lagrange's Equation [5] becomes

$$\ddot{q}_n + \omega_n^2 q_n = Q_n^* \quad [40]$$

The general integral of this ordinary differential equation is

$$q_n(t) = A_n \cos\omega_n t + B_n \sin\omega_n t + \frac{1}{\omega_n}\int_0^t Q_n^*(\tau)\sin\omega_n(t-\tau)d\tau \quad [41]$$

It remains to determine the constants of integration A_n and B_n, employing the Initial Conditions [4a]. At $t = 0$ we have

$$\left.\begin{aligned}
u(z,0) &= \sum_{i=1}^{m} g_{iu}(z)f_i(0) + \sum_{n=1}^{\infty} A_n U_n\\
w(z,0) &= \sum_{i=1}^{m} g_{iw}(z)f_i(0) + \sum_{n=1}^{\infty} A_n W_n\\
\dot{u}(z,0) &= \sum_{i=1}^{m} g_{iu}(z)\dot{f}_i(0) + \sum_{n=1}^{\infty} B_n U_n\omega_n\\
\dot{w}(z,0) &= \sum_{i=1}^{m} g_{iw}(z)\dot{f}_i(0) + \sum_{n=1}^{\infty} B_n W_n\omega_n
\end{aligned}\right\} \quad [42]$$

In view of the orthogonality Relationship [27] we multiply the first of Equations [42] by $U_n/2$, the second by W_n, add the two and integrate both sides over the length of the bar.

Solving for A_n we obtain

$$A_n = \frac{\displaystyle\int_0^l \left\{\frac{1}{2}\left[u_0 - \sum_{i=1}^{m} g_{iu}(z)f_i(0)\right]U_n + \left[w_0 - \sum_{i=1}^{m} g_{iw}(z)f_i(0)\right]W_n\right\}dz}{\displaystyle\int_0^l \left(\frac{1}{2}U_n^2 + W_n^2\right)dz} \quad [43a]$$

B_n is obtained from the third and fourth of Equation [42] in an analogous manner

$$B_n = \frac{\displaystyle\int_0^l \left\{\frac{1}{2}\left[\dot{u}_0 - \sum_{i=1}^{m} g_{iu}(z)\dot{f}_i(0)\right]U_n + \left[\dot{w}_0 - \sum_{i=1}^{m} g_{iw}(z)\dot{f}_i(0)\right]W_n\right\}dz}{\omega_n\displaystyle\int_0^l \left(\frac{1}{2}U_n^2 + W_n^2\right)dz} \quad [43b]$$

This completes the formal solution of the problem.

Acknowledgment

The author wishes to express his gratitude to Prof. R. D. Mindlin of Columbia University for help and advice in the preparation of this paper.

Creep Tests of Rotating Disks at Elevated Temperature and Comparison With Theory

By A. M. WAHL,[1] G. O. SANKEY,[2] M. J. MANJOINE,[3] AND E. SHOEMAKER,[4] EAST PITTSBURGH, PA.

A theoretical and experimental program involving methods of calculating creep in rotating disks at elevated temperatures is described. This program consisted primarily of the following: (*a*) Obtaining forged disks from the same ingot of 12 per cent chrome steel, all disks being forged and heat-treated in the same manner; (*b*) making spin tests at 1000 F on three of these disks for periods up to about 1000 hr; ( ) making long-time tension-creep tests at 1000 F on many specimens cut out circumferentially from several of the other disks at stresses approximating those of the spin tests; (*d*) investigating theoretical methods of calculation of creep deformation in such disks; and (e) comparison of spin-test results with those calculated theoretically using average tension-creep data. It was found that available methods of calculating rotating disks based on the Mises criterion gave creep deformations too low compared to the test values, i.e., on the unsafe side for design. Considerably better agreement between test and theoretical results is obtained if the latter is based on the maximum-shear theory. Some discussion is given of the reasons for the better agreement obtained using the latter theory; these are believed to be related in part to the anisotropy of the forged material tested. Further tests on other materials are necessary before general conclusions can be drawn; however, in the absence of test data it is suggested that a conservative course in design for such disks is to apply the maximum-shear theory.

1 Introduction

In the design of gas turbines and jet engines, the problem of long-time creep deformations and stresses in the turbine disks operating at high temperature is an important one. For this reason, several years ago the authors' company instituted a theoretical and experimental program at its Research Laboratories with two primary objectives: (*a*) Checking experimentally on presently used methods of calculating creep deformations and stresses in rotating disks operating for long periods at elevated temperature; and (*b*) developing better and more accurate methods of calculation for design use. To this end a precision testing machine was developed at the Research Laboratories of the company for spinning disks at high speeds and temperatures while maintaining close control of these variables; this machine has been reported on previously (1).[5] Tests of a more immediately practical nature are carried out on jet-engine disks and blade fastenings at the Aviation Gas Turbine Division using a machine described some time ago (2), while the tests at the Research Laboratories are carried out from a more fundamental viewpoint.

Although a great many theoretical investigations of rotating disks have been reported in the technical literature, most of these consider only elastic deformations and stresses, or the problem of plastic flow when the disk is brought up to speed; only a very few deal with the theoretical calculation of creep and stress in rotating disks operating for long periods at elevated temperature. In so far as the authors are aware, no investigations have so far been reported wherein an accurate comparison has been made between the long-time creep deformations observed in spin tests of disks at high temperature and those calculated theoretically on the basis of long-time tension-creep test data as is done in this paper.

Because of the complicated nature of the creep problem when temperatures vary radially in the disk, it was decided to simplify the problem by carrying out the first phase of the investigation using constant-thickness disks of 12 in. OD subjected to constant temperature.

Some preliminary spin tests were made some years ago on disks forged from a commonly used gas-turbine material (19-9-DL). Long-time tension-creep tests also were obtained from specimens cut out from these 19-9-DL disks, but these latter showed wide scatter in the creep rates at the same stress even though the specimens were cut out from the same disk. However, using available methods of calculating creep deformations employing the Mises criterion (distortion-energy theory), calculated creep deformations, using average tensile-creep data, of the order of half the spin-test results were obtained. At that time this discrepancy was attributed to the variability of the material.

On account of this wide variability in the tension-creep results obtained on the 19-9-DL disk material in the preliminary phase of the investigation, it was then decided to make further tests on a 12 per cent chrome steel which was expected to be more uniform and stable. Briefly the procedure was to forge several disks from a single ingot, the disks to be heat-treated to as uniform properties as possible. Several of these machined disks were spun at 1000 F for periods up to about 950 hr; several more were cut up for long-time tension-creep tests.

In spite of precautions to obtain uniform material it was found that this 12 per cent chrome steel also showed considerable scatter in creep-test results although not as much as that found for the 19-9-DL. Therefore it was necessary to make a great many creep tests in order to obtain average values of statistical significance. This matter is discussed further in Section 3. Comparison is then made between test and theoretical values of strains as measured by spin tests on the 12 per cent chrome steel disks at various radii and at various times. This also will be discussed further in Section 4.

The results of these comparisons appear to indicate that, using average values of tensile-creep data as a basis, these data being obtained from specimens cut in a tangential direction, the

[1] Advisory Engineer, Westinghouse Research Laboratories. Fellow ASME.

[2] Westinghouse Research Laboratories. Assoc. Mem. ASME.

[3] Research Engineer, Westinghouse Research Laboratories. Mem. ASME.

[4] Westinghouse Research Laboratories.

Contributed by the Applied Mechanics Division and presented at the Annual Meeting, New York, N. Y., November 29–December 4, 1953, of The American Society of Mechanical Engineers.

Discussion of this paper should be addressed to the Secretary, ASME, 29 West 39th Street, New York, N. Y., and will be accepted until October 11, 1954, for publication at a later date. Discussion received after the closing date will be returned.

Note: Statements and opinions advanced in papers are to be understood as individual expressions of their authors and not those of the Society. Manuscript received by ASME Applied Mechanics Division, June 25, 1953. Paper No. 53—A-61.

[5] Numbers in parentheses refer to the Bibliography at the end of the paper.

theoretical creep deformations in the disks calculated using the Mises criterion are too low compared with the results of long-time spin tests at 1000 F. By using the maximum-shear theory, however, instead of the Mises criterion (as discussed in the following), closer agreement between average test and theoretical values of creep deformations in the disks was obtained for the disks tested. This result obtained on the 12 per cent chrome steel is now seen to be at least roughly consistent with the results obtained previously on the 19-9-DL material.

It can be stated further that the maximum-shear theory in this case leads to somewhat simpler expressions and is also on the safe side for design since it yields higher creep deformations than if the Mises criterion is used. Some reasons why the maximum-shear theory gives better results in this case are discussed in Section 4; these are believed to be connected in part with the anisotropy of the forged material tested.

Further studies of methods of taking into account this anisotropy are now in progress and will be reported on later.

2 Theoretical Considerations

Assumptions. In making an analysis of creep deformations for the long-time spin tests reported here (see Section 3) the following assumptions will be made:

1 Elastic deformations, being relatively small for the disks tested, may be neglected in comparison with deformations due to creep.

2 Stresses at any radius r of the disk remain constant in time; i.e., a steady-steady condition of stress is reached. (This neglects the transient condition during the first few hours of operation; the justification for this is discussed more fully later.)

3 A biaxial state of stress exists with tangential stress σ_t and radial stress σ_r, Fig. 1, the axial stress σ_z being zero.

4 A power function relation of the form $\dot{\epsilon} = k\sigma^n f(t)$ exists between strain rate $\dot{\epsilon}$, stress σ, and time t in simple tension, where $f(t)$ = function of time; k and n are constants. (Use of a power function is believed justified since the tangential stress does not change too much along a radius of the disk.)

5 For a biaxial state of stress (σ_t, σ_r) the tangential, radial, and axial strain rates $\dot{\epsilon}_t$, $\dot{\epsilon}_r$, $\dot{\epsilon}_z$ may be expressed in the following form, similar to equations based on the so-called rules of stationary plastic flow (3)

$$\left.\begin{aligned}\dot{\epsilon}_t &= ks^n f(t)\left[\frac{\sigma_t - \frac{1}{2}\sigma_r}{s}\right]\\ \dot{\epsilon}_r &= ks^n f(t)\left[\frac{\sigma_r - \frac{1}{2}\sigma_t}{s}\right]\\ \dot{\epsilon}_z &= ks^n f(t)\left[\frac{-(\sigma_r + \sigma_t)}{2s}\right]\end{aligned}\right\} \quad \ldots\ldots\ldots\ldots [1]$$

The stress s in Equations [1] refers to an "equivalent" stress (also called "effective" stress) which depends on the strength criterion employed. Thus, for example, if we have only a simple tension stress σ_t acting, $s = \sigma_t$ and $\dot{\epsilon}_t = k\sigma_t^n f(t)$; on the other hand, if a tension stress σ_r acts alone ($\sigma_t = 0$), $s = \sigma_r$ and $\dot{\epsilon}_t = -{}^1/_2 k\sigma_r^n f(t)$ as would be expected from the constant-volume relation.

In this paper the stress s in Equations [1] will be based on either the Mises criterion (as is frequently done at present) or on the maximum-shear theory. Note that these equations assume isotropy of the material.

Analysis Using Mises Criterion. Assuming that the stress s in Equations [1] is based on the Mises criterion (also known as distortion-energy or octahedral-stress theory) we obtain for a biaxial state of stress

$$s = [\sigma_t^2 - \sigma_r\sigma_t + \sigma_r^2]^{1/2} \ldots\ldots\ldots\ldots [2]$$

Using this in Equations [1], and taking $\dot{w} = dw/dt$ as the radial deformation rate we obtain

$$\left.\begin{aligned}\dot{w}/r = \dot{\epsilon}_t &= k[\sigma_t^2 - \sigma_r\sigma_t + \sigma_r^2]^{(n-1)/2}\left[\sigma_t - \frac{1}{2}\sigma_r\right]f(t)\\ d\dot{w}/dr = \dot{\epsilon}_r &= k[\sigma_t^2 - \sigma_r\sigma_t + \sigma_r^2]^{(n-1)/2}\left[\sigma_r - \frac{1}{2}\sigma_t\right]f(t)\\ \dot{\epsilon}_z &= -(\dot{\epsilon}_t + \dot{\epsilon}_r)\end{aligned}\right\} \quad \ldots\ldots [3]$$

These equations are essentially the same as those proposed by Soderberg (4) except that strain rates are used instead of strains. Equations [3] also reduce to those proposed by Odquist (5) if $f(t)$ is taken as unity. In addition, the Mises criterion has been utilized by Bailey (6) in calculating rotating disks under creep; however, Bailey's equations assume that the creep rate does not vary with time and are more complicated than Equations [3] since they involve an additional constant which must be determined experimentally using creep tests under biaxial stress systems. However, by a suitable choice of this constant it is possible to express Bailey's equations in the form of Equations [3], taking $f(t) = 1$. In view of the lack of experimental data for determining the additional constant in Bailey's equation, the simpler Equations [3] are used here.

Equations [3], taking $f(t) = 1$ and basing s on the Mises criterion, also have been used for rotating disks under creep conditions by Popov (7) and by Millenson and Manson (8).

In determining the stress distribution in a rotating disk of constant thickness the following equation based on the equilibrium

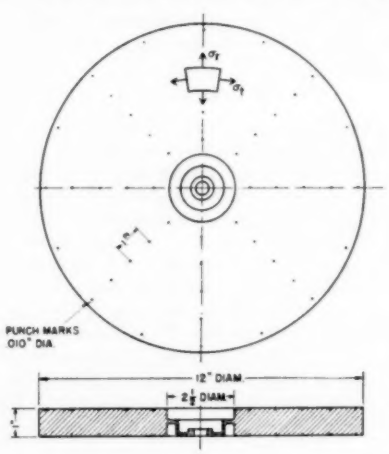

Fig. 1 Disk of Uniform Thickness With Hole

condition of an element, Fig. 1, subjected to radial and tangential stresses, σ_r and σ_t, is used

$$\frac{d}{dr}(r\sigma_r) - \sigma_t + \frac{\gamma}{g}\omega^2 r^2 = 0 \ldots\ldots\ldots\ldots [4]$$

In this, γ = weight of material, lb per cu in., g = gravitational acceleration in/sec^2, ω = angular velocity, radians per sec.

The first two of Equations [3] and Equation [4] suffice to determine the three unknowns σ_t, σ_r, and $\dot{w}$. In determining the dis-

tributions of σ_t and σ_r as a function of r, the authors have used the successive-approximation method suggested by Bailey (6), which was found to converge very rapidly. (See Appendix for details and example calculation.) With the stresses known, the tangential, radial, and axial strain rates $\dot{\epsilon}_t$, $\dot{\epsilon}_r$, and $\dot{\epsilon}_z$ may be found from Equations [3]. If the strain rates are known at various times the strains can be obtained by simple integration.

The distribution of σ_t and σ_r along a radius obtained in this manner based on the Mises criterion for a 12-in-diam disk with a $2^1/_2$-in. bore and operating at 15,000 rpm (γ = 0.283 lb per cu in.) is shown in Fig. 2 for various values of n.

The distribution of radial, tangential, and axial strains ϵ_r, ϵ_t, and ϵ_z as a function of radius for n = 6 to 9 is indicated in Fig. 3. These strains are plotted in terms of ratios ϵ_t/ϵ_{ti}, ϵ_r/ϵ_{ti}, ϵ_z/ϵ_{ti} where ϵ_{ti} = maximum tangential strain at r_i. The curves for n = 6, 8, and 9 were found to nearly coincide so that average curves only are given.

Analysis Using Maximum-Shear Theory. A similar analysis may be carried out employing the maximum-shear theory instead of the Mises criterion. This means that in Equations [1] the equivalent or effective stress s is based on the maximum-shear theory; since in the case of the rotating disk considered $\sigma_t > \sigma_r > 0$, the minimum principal stress is zero and hence s may be taken as σ_t in Equations [1]. Thus we obtain

$$\left.\begin{aligned} \dot{w}/r = \dot{\epsilon}_t &= k\sigma_t^n \left(1 - \frac{\sigma_r}{2\sigma_t}\right) f(t) \\ d\dot{w}/dr = \dot{\epsilon}_r &= k\sigma_t^n \left(\frac{\sigma_r}{\sigma_t} - \frac{1}{2}\right) f(t) \\ \dot{\epsilon}_z &= -(\dot{\epsilon}_t + \dot{\epsilon}_r) \end{aligned}\right\} \quad \ldots\ldots\ldots [5]$$

Similar equations based on maximum-shear theory for creep also have been proposed by Coffin, Shepler, and Cherniak (9) who have applied the results to tubes under internal pressure.

By utilizing Equation [4] and the first two of Equations [5], stress and strain distribution as a function of disk radius may be obtained on the basis of the maximum-shear theory. (See Appendix for details.) The results of these calculations for various n-values are shown in Figs. 3 and 4. The strain-distribution curves when plotted in terms of ratios ϵ_t/ϵ_{ti}, and so on, were found practically to coincide with the values obtained using the Mises criterion for n = 6 to 9, Fig. 3.

In general, higher strains and strain rates will be obtained using the maximum-shear theory as compared with the Mises criterion, since the equivalent stress s in Equations [1] is higher if the maximum-shear theory is used.

Transient Condition at Start. When the disk is first brought up to speed at 1000 F, the stress distribution will approximate the

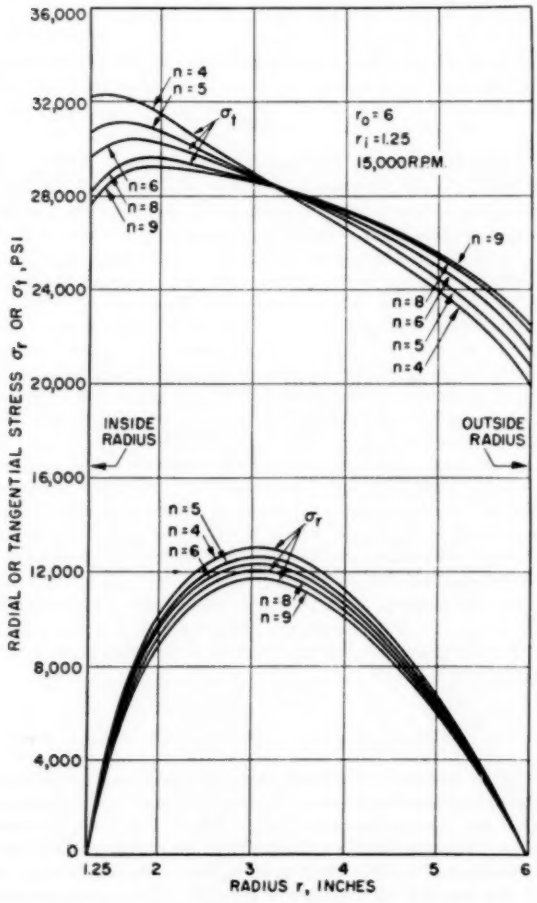

FIG. 2 STRESS DISTRIBUTION ALONG RADIUS OF ROTATING DISK FOR VARIOUS VALUES OF n
(Mises criterion assumed.)

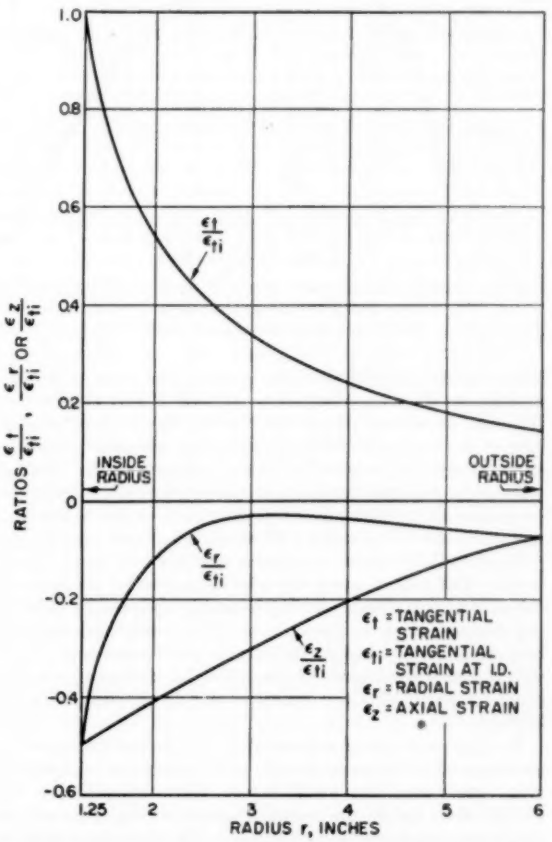

FIG. 3 THEORETICAL STRAIN DISTRIBUTIONS IN ROTATING DISK
(Curves apply for n = 6 to 9 and for either Mises or maximum-shear criteria.)

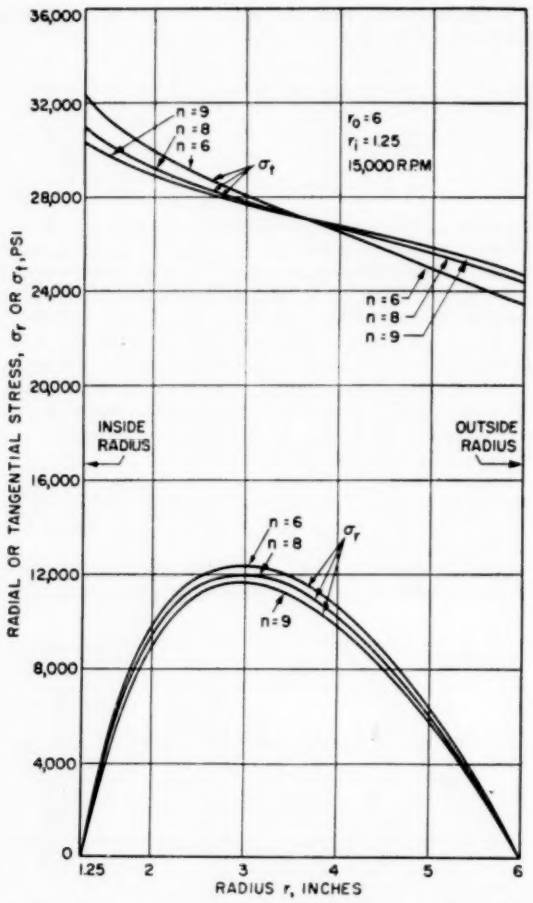

FIG. 4 STRESS DISTRIBUTION ALONG RADIUS OF ROTATING DISK FOR VARIOUS VALUES OF n
(Maximum-shear theory assumed.)

elastic stress distribution except near the bore where a stress roughly equal to the yield stress at 1000 F may be expected. However, because of this rather high tangential stress near the bore at the start, rapid creep at this point will occur; this bore stress relaxes rapidly toward the steady-state condition. A rough estimate of the time necessary to reach practically steady-state conditions at 15,000 rpm was made (for $n = 5$) by assuming successive small increments of tangential stress linearly distributed radially while maintaining constant average tangential stress. The time necessary to allow relaxation of the stress by this amount was then computed, assuming a power-function relation between stress and creep rate. The results indicated that relaxation to practically steady-state conditions would occur within a very short time (of the order of a few hours). This is small compared with test operation during times up to nearly 1000 hr.

For higher values of n (around 6 to 8 as was found for the stresses used in the present tests) even more rapid relaxation to steady-state conditions would occur. Hence it is believed that for the disks tested, the transient condition may be neglected and steady-state conditions assumed. This conclusion also was reached by Bailey (6). It is possible, however, that there are cases, particularly where operating stresses are very low, for which the transient condition would have to be considered for accurate results.

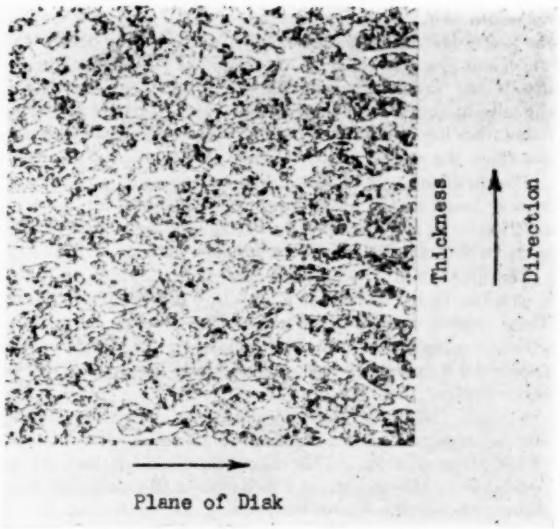

FIG. 5 PHOTOMICROGRAPH OF DISK 13 AT RIM; ×100

3 TESTS

Disk Material. (*a*) *Selection and Preparation.* To select an alloy for the disk forgings, several alloys for steam and gas-turbine service were forged. Specimens selected from the rim and center of these disks were tested in creep. As a result of these tests Allegheny 418 was selected from a uniformity standpoint. Thirteen forgings were ordered with the co-operation of the Allegheny Ludlum Corporation. The following conditions and procedure were carried out: (*a*) All thirteen billets were taken from one ingot. (*b*) Billets from the ingot were forged the same amount to approximate disk size and marked 1 through 13 starting at the bottom of the ingot. (*c*) All forgings were heat-treated together as follows: (1) 1650 F for 3 hr, air-cooled; (2) 1150 F for 12 hr, furnace-cooled. The forgings were then machined to approximately final disk size and examined for cracks or flaws. For the latter, ultrasonic, zyglo, and x-ray methods were employed. Finally, a hardness survey across four diameters (two on each face) was made on each disk. The average hardness of individual disks was about the same, varying from 210 to 218 DPH with a standard deviation of 3.

(*b*) *Composition.* This Allegheny 418 material is a 12 per cent Cr, 3 per cent W stainless steel (designated 12 per cent chrome steel throughout this paper). Analysis of the ingot in per cent is as follows:

C	Mn	Si	W	Cr	Ni	S	P
0.11	0.37	0.48	2.91	12.55	0.39	0.017	0.017

(*c*) *Microstructure.* Photomicrographs were made of parts of the disks which were cut up for creep specimens both before and after test. A portion of the rim of disk 13, Fig. 5, shows a two-phase structure which is typical of all of the disk specimens tested in tensile creep. The bright second phase, delta iron, strings out in the direction of the plane of the disk. The average amount of hot-cold work is very small in these disks since the diameter of the disk is about the same as that of the original ingot. These stringers are formed because of the free ferrite, delta iron, present.

The stringers become longer, finer, and more broken up as the center of the disk is approached. Only a slight difference in orientation of the stringers was noted in the thickness direction.

(*d*) *Anisotropy.* As a result of these stringers in the plane of the disk a pronounced anisotropy of the specimens from the disks was observed. In the tensile-creep tests the original circular cross section of the specimens deformed into an ellipse with the minor diameter corresponding to the thickness or axial direction, and the major diameter, to the radial direction in the disk. For the tangential specimens, the ratio of the strain in the axial direction to that in the radial direction varied from 1.3 to 2.7 with an average of around 2.0 for the disks tested. We can conclude that the material has a lower creep strength in the thickness direction. The consequences of this anisotropy will be discussed in Section 4.

(*e*) *Metallurgical Stability.* The creep specimens were checked for metallurgical stability by hardness measurements and photomicrographs of the stressed and unstressed portions of the specimens. Diamond-pyramid hardness measurements were made on all specimens before and after test on a portion of the specimen not subjected to stress. No significant change in hardness was found. A comparison of the photomicrographs taken before and after tests on creep specimens selected at random led to the following observations: (*a*) No change in the microstructure of the unstressed part due to exposure at 1000 F, and (*b*) slight breaking up of the second (bright) phase of the stressed part of the specimen. It also was noted that the stressed part etched slightly darker than the unstressed. These observations were made on specimens tested well beyond the 900-hr limit represented by the spin tests.

Long-Time Spin Tests of Disks at 1000 F. The spin tests were carried out in a high-speed high-temperature testing machine (1) shown in Fig. 6. The disk specimen is mounted with the rotational axis vertical on a flexible shaft and driven by a 3-phase induction motor.

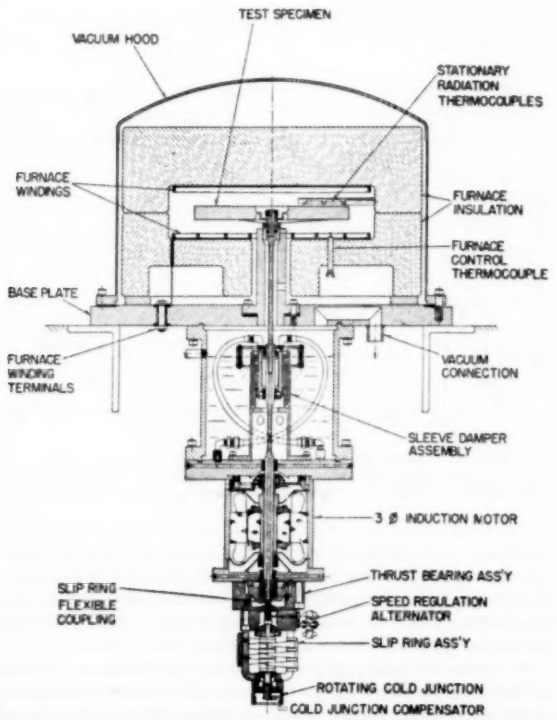

FIG. 6 CROSS SECTION OF HIGH-SPEED DISK TESTER

In the design of the machine primary emphasis was placed on accurate measurement and control of the test parameters of speed (stress) and temperature, and the determination of creep strains. Speed regulation is achieved by automatic means using 60-cycles-per-sec (cps) line supply as a reference. Periodic checks of machine frequency using a precision Frahm meter showed maximum short-time errors of less than 0.3 per cent and the average error for a run was estimated to be less than 0.01 per cent. Calibrated thermocouple wire was spot-welded to the disk at various radii with the leads being brought out to a precision potentiometer in parallel with an electronic recorder through slip rings. Calibration of the thermocouple circuits indicated the disk temperature was measured within 5 deg F. The specimen was heated by means of a winding supported in close proximity to the disk faces. By test, with thermocouples located at inner, outer, and intermediate radii, and throughout the disk thickness, this heater gave uniformity of specimen temperature within 5 deg F.

Strains in the disk were measured by punch marks placed 1 in. apart across four equally spaced diameters on each face of the specimens, Fig. 1. Punch-mark spacings were measured before and after each test by means of a traveling microscope. Specimen ID and OD were measured with micrometer calipers along with disk thickness and profile. The accuracy of these strain measurements was within 5 per cent.

Three disks (1, 2, and 12) were selected for plastic-flow and creep tests. The plastic-flow test consisted of bringing disks 1 and 2 to temperature (1000 F) and speed (15,000 rpm, average stress 27,200 psi) for several seconds. When cool, the permanent expansion in each disk was measured and was found to be about 0.002 in. on the OD, an amount very small in comparison with the creep values obtained later. A creep test of 180 hr was carried out subsequently on each disk. Disk 2 was then run for an additional 271 hr at slightly reduced speeds such that the initial peripheral speed was maintained approximately constant considering the expansion of the OD. The initial test on disk 12 was for $6^1/_2$ hr. It was then run out to 206 hr at a constant speed of 15,000 rpm. Thereafter the spin speed was reduced slightly to maintain constant peripheral speed and the specimen run on out until a total of 957 hr was reached. The test results showing OD and ID expansion versus time for each disk are plotted in Figs. 7 and 8, respectively, with a scatter band shaded between points. Radial, tangential, and axial-strain values along the disk radius for each disk after 180 hr are shown in Fig. 9. Here again test points are plotted and scatter bands shown. It can be seen from the data plotted that the summation of the three strains at any radius leads to a nearly zero value which is in agreement with the usual assumption made in creep problems of a constant-volume relation.

Tensile-Creep Tests of Specimens From Disks at 1000 F. To obtain tensile-creep data at various stresses, four disks (Nos. 5, 9, 10, and 13) were cut into blanks as indicated in Fig. 10. Most of the specimens were cut in the tangential direction since the major stress is tangential. The specimens were machined from these blanks, marked with the number of the blank, and prefixed with the number of the disk forging. The gage length was 3 in. and the diameter 0.505 in.

The tests were performed in conventional lever-arm and spring-loaded creep machines (10) at a constant load and a temperature of 1000 F $\pm$ 2 deg F.

Tensile-Creep-Test Results. The results of the tensile-creep tests are summarized in Table 1. The stress given is the nominal stress based on the original area. Since this material is characterized by a long first stage of creep, that is, the creep rate diminishes with time during most of the creep test, the strain and creep rates are given at 180, 300, 600, and 900 hr. To indicate the duration of the test the final strain and creep rates also are tabulated. At the higher stresses all three stages of creep were ob-

TABLE 1 CREEP DATA OF SPECIMENS FROM DISKS

Spec. no.	Stress,[a] psi	180 hr		300 hr		600 hr		900 hr		Final			Remarks
		ϵ[b]	$\dot{\epsilon}$[c]	ϵ	$\dot{\epsilon}$	ϵ	$\dot{\epsilon}$	ϵ	$\dot{\epsilon}$	ϵ	$\dot{\epsilon}$	t	
5-5	25000	1.27	3.72	1.67	3.06	2.46	2.38	3.10	2.12	5.10	0.127	3570	d
-8	25000	1.39	3.43	1.78	3.20	2.65	2.51	3.17	0.63	6.0	0.128	8075	d
-11	25000	0.97	2.42	1.24	2.42	1.93	2.22	2.60	2.17	7.45	0.74	7500	d
-18	25000	1.00	1.98	1.16	1.80					1.10	1.98	258	d
-9	25000	1.05	2.16							1.05	2.16	180	d
Average	25000	1.14	2.74	1.46	2.62	2.35	2.37	2.96	1.64				
9-3	25000	0.70	1.71	0.90	1.60	1.33	1.33	1.68	0.96	2.82	0.09	4850	d
-5	25000	1.11	3.6	1.52	3.24	2.23	1.93	2.72	1.5	4.5	0.106	6050	d
-7	25000	0.89	2.13	1.11	1.73	1.55	1.29	1.87	0.84	2.55	0.88	1665	d
Average	25000	0.90	2.45	1.18	2.19	1.70	1.52	2.09	1.10				
13-2	25000	0.80	1.9	1.02	1.84	1.50	1.42	1.88	1.04	2.70	0.525	2020	d
-4	25000	1.02	2.0	1.25	1.92	1.83	1.91	2.39	1.48	3.51	0.39	2520	d
-6	25000	0.88	2.46	1.11	1.59	1.42	0.97	1.70	0.97	2.40	0.27	2000	d,e
-9	25000	1.32	3.60	1.71	3.22	2.67	3.22	3.5	2.59	5.83	1.25	2000	d
-11	25000	1.54	3.22	1.81	2.33	2.50	2.30	3.10	1.72	7.55	0.065	30400	d,e
-16	25000	1.05	2.97	1.40	2.91	2.23	2.62	2.92	1.81	4.16	0.89	2000	d
-17	25000	1.37	3.94	1.78	2.47	2.35	1.73	2.80	1.59	4.03	0.30	2110	d,e
-19	25000	1.20	3.54	1.63	3.46	2.62[f]	3.24			2.30	3.24	500	d
-21	25000	1.58	5.13	2.16	4.84	3.60	4.78	4.73	2.66	6.10	2.14	1510	d
-22	25000	1.45	4.83	2.01	4.55	3.33	3.75	4.25	2.69	6.11	1.27	1700	d
Average	25000	1.22	3.36	1.59	2.91	2.40	2.59	3.03	1.84				
Average	25000	1.09	2.85	1.41	2.57	2.15	2.16	2.69	1.53				Disks 5, 9 & 13
5-4	29000	3.33	11.5	4.7	11.5					6.0	11.5	412	g
-9	29000	2.54	10.5	3.16[f]	9.7					3.1	9.7	240	d
-14	29000	2.31	9.4	4.02	8.6	6.23	8.6			6.3	8.6	608	g
-17	29000	4.46	13.8							4.7	13.8	194	g
Average	29000	3.28	11.3	3.96	9.9								
9-8	29000	2.33	6.8	3.22	6.0	4.6	4.4	6.02[f]	3.9	8.3	3.9	880	d
9-14	29000	3.05	10.7	4.26	9.2					5.4	9.2	428	d
Average	29000	2.69	8.75	3.74	7.6								
13-15	29000	3.05	10.6	4.2	10.6					4.75	10.6	350	g
-12	29000	2.4	9.3	3.4[f]	9.0					2.75	9.3	225	d, h
-13	29000	2.72	9.7	3.5[f]	6.5					3.29	6.5	260	d, h
Average	29000	2.72	9.9	3.70	8.7								
Average	29000	2.90	10.0	3.80	8.7								Disks 5, 9 & 13
5-1	30000	4.3	17.0	6.4[f]	17.0					6.0	17.0	275	g
-13	30000	4.42	18.3	6.62[f]	18.3					6.1	18.3	274	g
-16	30000	5.8	25.3	8.8[f]						5.9	25.3	180	g
-21	30000	4.38	13.9							4.42	13.9	186	d
-22	30000	7.4[f]	36.0							6.9	36.0	162	g
Average	30000	5.26	22.1										
10-14	30000	4.9[f]	21.8							3.4	2.18	122	g
-19	30000	4.51	15.0	6.5	13.0					[i]			
-20	30000	6.18	28.2							7.28	25.8	260	g
-22	30000	3.5	14.8							4.95	14.8	280	g
Average	30000	4.77	20.0										

[a] Stress based on original area.
[b] Plastic strain in per cent.
[c] Creep rate in 10^{-3} in/in/hr.
[d] Test stopped.
[e] Poor temperature control.
[f] Estimated.
[g] Transition point.
[h] Intermittent loading—same loading and heating cycle as used in spin tests 1 and 2 (first 180 hr).
[i] Test disturbed.

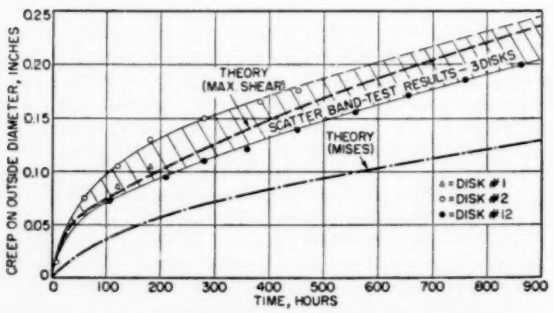

FIG. 7 CREEP ON OUTSIDE DIAMETER OF ROTATING DISK
(Theoretical results based on average tensile-creep data. Temp = 1000 F; initial speed = 15,000 rpm; constant peripheral speed maintained approximately.)

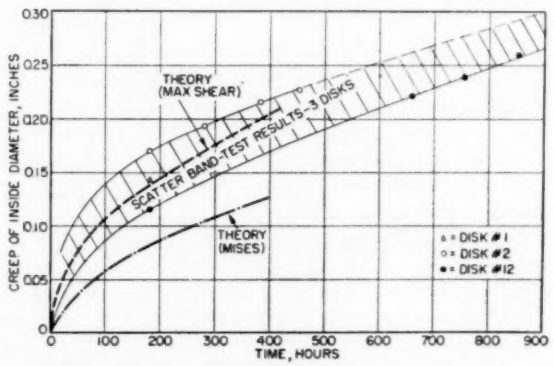

FIG. 8 CREEP ON INSIDE DIAMETER OF ROTATING DISK
(Theoretical results based on average tensile-creep data. Temp = 1000 F; initial speed = 15,000 rpm; constant peripheral speed maintained approximately.)

served; for these tests the strain and time at the transition point and the minimum creep rate are given. The greatest number of tests were made at 25,000 psi. The creep curves for this stress are shown in Fig. 11 where the logs of the plastic strains are plotted as a function of the log of time.

The curves in the upper half of Fig. 11 are for specimens from disks 5 and 9 and those in the lower half are from disk 13. These curves are practically straight lines after about 180 hr, which indicates that the creep rate diminishes with time. The creep curves for the other stresses are similar and are, therefore, not plotted here. However, as the stress is increased the time to the transition point from second to third stage of creep decreases. As the transition point is approached, the creep rate and creep strain increase at the portions of the specimen where local necking starts. The true stress, therefore, increases more than that calculated from an assumption of uniform plastic flow.

To utilize the tension-creep data in the theoretical calculations of creep deformations in the spin tests the average properties of disks 5, 9, and 13 were taken as being representative of all the disk forgings. Most of the creep tests were made on specimens

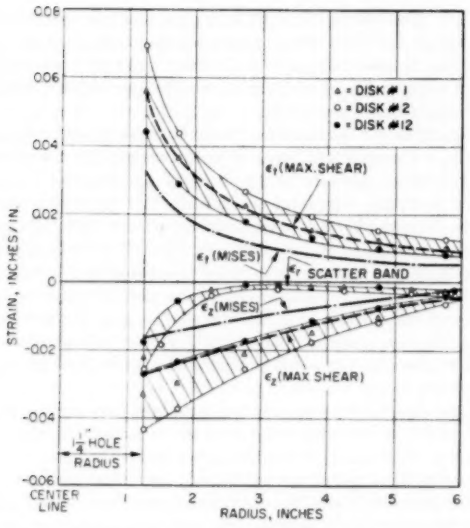

FIG. 9 RADIAL, TANGENTIAL, AND AXIAL CREEP STRAINS VERSUS DISK RADIUS AT 180 HR

(Cross-hatched regions represent scatter bands of test results.)

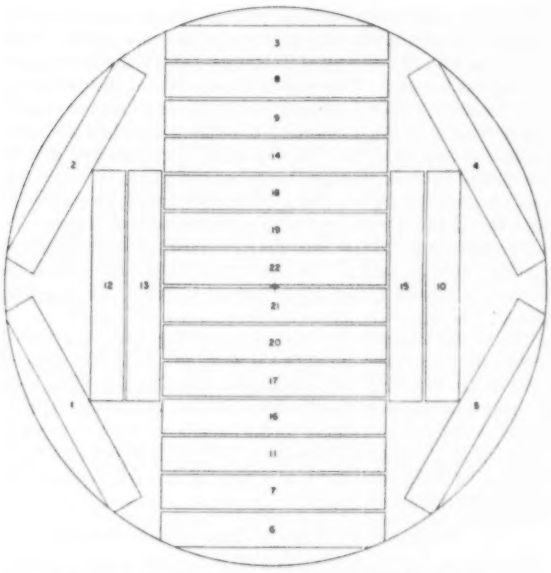

FIG. 10 PLAN OF CUTTING SPECIMENS FROM DISK

(Disk, 12 1/8 in. diam × 1 1/8 in. thick. All blanks, 3/4 in. × 3/4 in. × 5 in.)

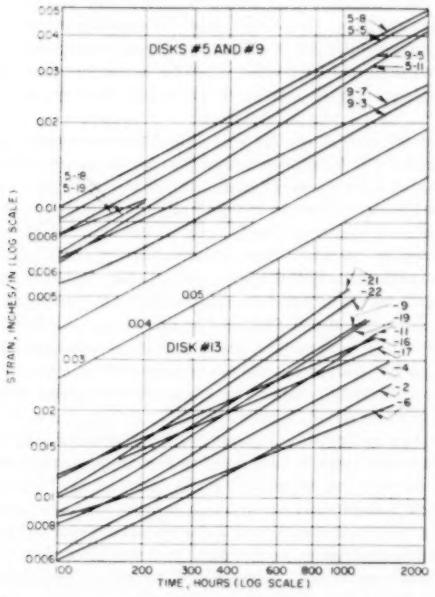

FIG. 11 CREEP CURVES AT 25,000 PSI AND 1000 F

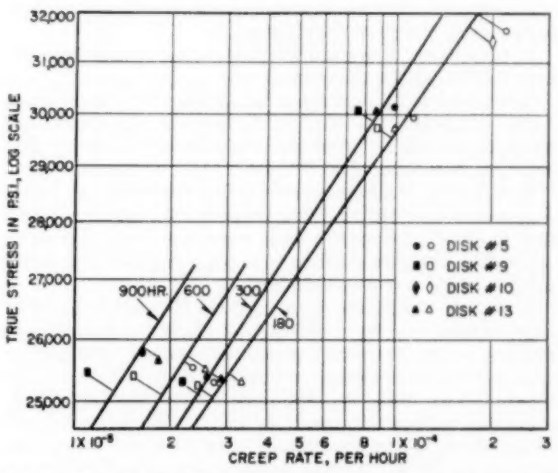

FIG. 12 TRUE STRESS VERSUS CREEP RATE FOR TENSILE SPECIMENS CUT FROM VARIOUS DISKS AT 1000 F

(Open points, 180 and 600 hr; solid points, 300 and 900 hr.)

from these disks and the majority of tests were made at two nominal stress levels (25,000 and 29,000 psi).

The data from tests made at other stress levels are not included in the table except those at 30,000 psi. The true stress at 180, 300, 600, and 900 hr is given as a function of creep rate in Fig. 12 for those stress levels where sufficient tests were made to obtain a representative average. Each point on this figure represents the average of several specimens cut from a given disk. The straight lines shown for 180 and 300 hr represent average values for 3 disks between 25,000 and 29,000 psi nominal stress levels. This amounts to assuming a power-function relation between these stress levels. The lines for 600 and 900 hr are drawn approximately parallel to the curve for 300 hr but are not extrapolated to high stress levels (around 29,000 psi) since no tests were available at such values of true stress beyond about 300 hr, and it was felt that such extrapolation may be somewhat uncertain. Data from this figure are used in the theoretical calculations (Section 4).

Discussion of Results. As mentioned previously, this alloy was selected because it was hoped that the properties would be uniform for various positions in the disk. Disk No. 13 was selected for a study of the creep properties at a nominal stress of 25,000 psi and 1000 F because it showed the greatest variation in the hard-

ness survey and hence it might be expected to show a greater variation in creep properties than would the other disks. From the ten tests for No. 13 disk at 25,000 psi, Fig. 11, the wide spread of creep can be noted. The ratio of the strains from the weakest to the strongest specimen is about 2.5 to 1. This variation in properties is related to the amount of hot-cold work which occurred during the forging of the disk. It should be mentioned that no correlation between average hardness and creep strength was found among the various disks. The variations in properties of disks Nos. 5 and 9 were less but so were the number of tests.

Two tests at 29,000 psi with the same intermittent loading and heating cycle as used in the spin tests 1 and 2 indicated no anomalous change in the creep rate when compared to a continuous loading.

The straight lines in the log-log plot of Fig. 12, as mentioned previously, are drawn through the average of the disk tests at nominal stresses of 25,000 and 29,000 psi. The data from tests at other stresses lower than 29,000 psi were consistent with these curves if recognition is given to the relative strength of the particular disk. The data at stresses higher than 29,000 psi are influenced by the initiation of local necking and are therefore not used in the analysis.

4 Discussion of Test and Theoretical Results

General. In evaluating the two methods of theoretical calculation (based on the Mises and maximum-shear criteria as discussed in Section 2) it was felt that the following comparisons between test and theoretical results would be of interest:

1 Comparison of test and theoretical strain distributions along radius of disk at a given time (180 hr).

2 Comparison of test and theoretical expansions of both OD and ID of the disk as a function of time.

Comparison of Theoretical and Test Strain Distributions Along Radius at 180 Hr. To calculate the theoretical distributions of strains in the disk at 180 hr the average tension-creep-test data were used as follows:

From Table 1 the average strain at the end of 180 hr at a mean true stress $\bar{\sigma}$ of 25,150 psi during the period (25,000 start, 25,300 end) was 0.0109 in/in; at a mean stress $\bar{\sigma}$ of 29,450, the strain was 0.029. Using these values an average n equal to 6.2 during the first 180-hr period was obtained.

To find the strains, the stress σ_{ti} at the ID was first found by interpolation from Fig. 2 (Mises) and Fig. 4 (maximum shear) taking $n = 6.2$. However, because of the expansion of the disk after 180 hr, these stresses are increased slightly since r_o and r_i become larger while the disk cross section becomes slightly trapezoidal because ϵ_z is greater at the ID. These factors cause an increase in average tangential stress σ_{ti} of about $3^1/_2$ per cent at the end of 180 hr. To take this effect into account the stresses σ_{ti} previously found for the two criteria were increased by half this percentage to obtain average values during the 180-hr period. These values were then used in the power-function relation between strain and stress taking $n = 6.2$ and using the data of Table 1 to find the theoretical strain ϵ_{ti} at the ID at the end of the 180-hr period. Knowing ϵ_{ti}, the values of ϵ_t, ϵ_r, ϵ_z at various radii r may be found using Fig. 3. The theoretical values of tangential and axial strains thus found are shown in Fig. 9 by the dashed curves (maximum shear) and by the dot-dash curves (Mises criterion).

For comparison, the tangential, radial, and axial strains obtained experimentally along a radius at 180 hr are indicated by the points of Fig. 9 for three different disks, the scatter band of these results being shown by the shaded areas.

In general, it may be seen that the theoretical strains calculated in this manner by using the maximum-shear theory agree better with average test results than those obtained using the Mises criterion. The average axial strain is appreciably larger than that obtained on the basis of the maximum-shear theory; this is no doubt due to anisotropy of the material and corresponds to the greater contraction in the thickness direction observed in the tensile-creep tests (section 3).

Comparison of Test and Theoretical Expansions of the Disk OD and ID as Functions of Time. The theoretical expansion of the OD and ID of the disk at 180 hr may be obtained using the tangential strains calculated previously. To obtain the disk expansion beyond 180 hr, tangential strain rates at both OD and ID were first calculated at 180, 300, 600, and 900 hr taking into account the slight increase in average tangential stress due to increases in r_o and r_i and distortion of the disk cross section; the results are then integrated numerically to give the increase in tangential strain at the OD and ID of the disk after 180 hr. These values are then added to the strains determined previously for 180 hr.

To get the strain rates at various times, the log-log plot of strain rate $\dot{\epsilon}$ versus true stress $\bar{\sigma}$ based on average tension-creep data, Fig. 12, is used. From this figure, values of $n = 7.8$ at 180 hr and $n = 7.2$ at 300 hr were obtained; using Figs. 2 and 4, stress values corresponding to these n-values could be found. At 600 and 900 hr to obtain stresses, the value of n was taken as 7.2. These stresses were then corrected slightly as before, for the expansion of the disk diameter and the distortion of the cross section; in this way tangential strain rates $\dot{\epsilon}_{to}$ at $t = 180$, 300, 600, and 900 hr could be found for the OD. By integration the strains and diametral expansion at the OD may be found. The results are shown in Fig. 7 by the dashed curve (maximum shear) and by the dot-dash curve (Mises) which represent diametral expansion at the OD versus time. For comparison, the scatter band of the spin-test results (three disks) is indicated by the shaded area.

The strain rates at the ID were calculated in a similar manner at 180 and at 300 hr and by integration the tangential strain and expansion of the ID could be found up to about 400 hr. The results are shown by the theoretical curves in Fig. 8 for the Mises and maximum-shear criteria; again the scatter of the experimental results on three disks is indicated by the shaded area. In this case the theoretical curves are not extended beyond about 400 hr since no creep-test data were available at true stresses near the σ_{ti} values (around 30,000 psi) for times beyond about 300 hr.

Again it may be seen that use of the Mises criterion gives too low values of diametral creep deformations when compared with average test results while the agreement obtained using the maximum-shear theory is much better.

Discussion of Results. A possible explanation for these results lies in the following: As indicated in Section 3, owing to anisotropy, a lower creep strength for this material may be expected in the axial (thickness) direction as compared with the tangential. Thus the average creep strength for specimens cut out from all directions including the axial would be lower than that obtained from creep tests made on tangential specimens only as is done here. If this lower value of average creep strength were then used in the theoretical calculations, better agreement between test results and those calculated using the Mises criterion (which is based on an isotropic material) would be expected. Since the equivalent stress based on maximum shear in this case is higher than that based on the Mises criterion, use of the former apparently tends to compensate in some degree at least for using too high values of average creep strength in the theoretical calculations, all directions in the disk being considered.

Another qualitative way of looking at this is as follows: Use of the maximum-shear theory gives greater weight to the effects of tangential stresses (i.e., the maximum stresses in the disk) and less weight to the effects of radial stresses (compare Equations

[3] and [5]). Since these maximum stresses also act in the direction of the tangential specimens used for evaluating creep strength, for a material with this type of anisotropy it seems reasonable that these tangential stresses should be given greater weight as is the case where the maximum-shear theory is used.

A more satisfactory way of evaluating the test results would be to apply available theoretical methods which take into account effects of anisotropy. Studies of such methods, which also require the obtaining of additional creep-test data, are now in progress and will be reported on later.

5 Conclusions

Based on the results of spin tests on disks of 12 per cent chrome steel at 1000 F the following conclusions appear justified:

1 If long-time creep tests are made on tension specimens cut out tangentially from disks forged in the usual manner, and if the average results of these creep tests are used to calculate creep strains and strain rates in rotating disks at 1000 F using the Mises criterion (which assumes an isotropic material) the theoretically calculated creep deformations may be too low.

2 One reason for the lack of agreement between test results and theoretical values obtained here using the Mises criterion is believed to lie in the anisotropy of the material used; however, anisotropy is probably characteristic of material as used in forged turbine disks.

3 For the material tested and the stresses used, closer agreement is obtained between the average results of the spin tests at 1000 F and the creep deformations calculated theoretically by applying the maximum-shear theory.

4 Distributions of stress using the maximum-shear and Mises criteria do not differ greatly, Figs. 2 and 4. However, because of the high value of n in the stress-creep rate relation (around 6 to 8 for the stresses used) small differences in stress can mean large differences in creep rates.

5 At much lower stresses than those used in this investigation where the exponent n may be less, the difference between the theoretical creep distortions obtained using the Mises and maximum-shear criteria may be expected to be less. Hence, if spin tests are made at lower stresses than those used in this investigation, agreement between the theoretical results obtained using the Mises criterion and the test results may be better than that obtained here.

6 If tensile-creep tests had been made on specimens cut from the various disks in all directions (including the axial) and if the average of these tests were used as a basis, better agreement between the results of spin tests and those based on the Mises criterion would be expected.

7 One possible reason for the better results obtained by using the maximum-shear theory is that the latter gives greater weight to the effects of tangential stress which acts in the direction of the tangential specimens used for evaluating creep strength.

8 Further tests on other high-temperature materials will be necessary before general conclusions can be drawn. However, in the absence of such data it is suggested that a conservative course in design is to apply the maximum-shear theory since this will give larger creep deformations (i.e., values on the safe side), as compared with those obtained using the Mises criterion.

Acknowledgment

This program was initiated by Mr. R. E. Peterson to whom the authors are indebted for valuable advice and guidance during the course of the work. Acknowledgment also should be made as follows: to Dr. J. A. Hutcheson, Vice-President, and Mr. R. P. Kroon of the A.G.T. Division of the Westinghouse Electric Corporation, for their support of and interest in this project; to various members of the Mechanics Department of the Research Laboratories, particularly Messrs. P. G. McVetty, A. C. Hagg, and E. A. Davis for assistance and advice from time to time during the course of the investigation.

Bibliography

1 "A High-Speed High-Temperature Precision Testing Machine for Gas Turbine Disk Research," by A. C. Hagg, B. Cametti, and G. O. Sankey, Proceedings of the Society for Experimental Stress Analysis, vol. 8, 1951, pp. 17–28.

2 "Hot-Spin Tests of Bladed Jet-Engine Rotors," by H. B. Saldin and P. G. DeHuff, Jr., Trans. ASME, vol. 71, 1949, pp. 605–612.

3 "Theory of Flow and Fracture of Solids," by A. Nadai, McGraw-Hill Book Company, Inc., New York, N. Y., 1950, p. 236.

4 "Interpretation of Creep Tests for Machine Design," by C. R. Soderberg, Trans. ASME, vol. 58, 1936, p. 734.

5 "Theory of Creep Under the Action of Combined Stresses With Application to High Temperature Machinery," by F. K. G. Odquist, Proceedings of the Royal Swedish Institution for Engineering Research, No. 141, 1936; see also Proceedings of the Fourth International Congress for Applied Mechanics, 1934.

6 "The Utilization of Creep Test Data in Engineering Design," by R. W. Bailey, The Institution of Mechanical Engineers, London, England, vol. 131, November, 1935, p. 260.

7 "Stresses in Turbine Disks," by E. P. Popov, *Journal of The Franklin Institute*, vol. 243, 1947, p. 365.

8 "Determination of Stresses in Gas Turbine Disks Subjected to Plastic Flow and Creep," by M. B. Millenson and S. S. Manson, NACA Report No. 906, 1948.

9 "Primary Creep in Design of Internal Pressure Vessels," by L. F. Coffin, Jr., P. R. Shepler, and G. S. Cherniak, Journal of Applied Mechanics, Trans. ASME, vol. 71, 1949, p. 229.

10 "New Machines for Creep and Creep Rupture Tests," by M. J. Manjoine, Trans. ASME, vol. 67, 1945, p. 111.

Appendix

Calculation of Stress and Strain Distributions in Rotating Disk Using Mises Criterion[8]

We assume a constant-thickness disk of outside radius r_o and inside radius r_i and that the Mises criterion governs. Taking $x = \sigma_r/\sigma_i$, the plastic rates, Equations [3], can be written as follows

$$\left.\begin{aligned} \dot{\epsilon}_i &= \dot{w}/r = k\sigma_i^n[f(t)][1 - x + x^2]^{(n-1)/2}\left(1 - \frac{x}{2}\right) \\ \dot{\epsilon}_r &= d\dot{w}/dr = k\sigma_i^n[f(t)][1 - x + x^2]^{(n-1)/2}\left(x - \frac{1}{2}\right) \\ \dot{\epsilon}_a &= -(\dot{\epsilon}_i + \dot{\epsilon}_r) \end{aligned}\right\} \quad \ldots\ldots [6]$$

Dividing the second of these equations by the first, we have

$$\frac{d\dot{w}}{\dot{w}}\frac{r}{dr} = \frac{2x - 1}{2 - x} = \phi(r) \quad \ldots\ldots [7]$$

Integrating between r_i and r

$$\dot{w} = \dot{w}_i \exp\left[\int_{r_i}^{r} \frac{\phi(r)}{r}\, dr\right] \quad \ldots\ldots [8]$$

where $\dot{w}_i$ = radial deformation rate at the ID.

Dividing Equation [8] by r and using the first of Equations [6]

$$\dot{w}/r = \dot{\epsilon}_i = \frac{\dot{w}_i}{r} \exp\left[\int_{r_i}^{r} \frac{\phi(r)}{r}\, dr\right]$$

$$= k\sigma_i^n\,[1 - x + x^2]^{(n-1)/2}\left(1 - \frac{x}{2}\right) f(t)$$

Solving for σ_i

[8] This follows a similar method to that suggested by Bailey (6).

$$\sigma_i = \left[\frac{\dot{w}_i}{k[f(t)]}\right]^{1/n} \psi(r) \quad \ldots\ldots\ldots\ldots [9]$$

where

$$\psi(r) = \left[\frac{\exp\left[\int_{r_i}^{r} \frac{\phi(r)}{r}\,dr\right]}{r(1-x+x^2)^{(n-1)/2}\left(1-\frac{x}{2}\right)}\right]^{1/n} \quad \ldots\ldots [10]$$

Integrating the equilibrium Equation [4] between the limits r_i and r_o we obtain (since no radial stress acts at the OD or ID)

$$r\sigma_r\Big]_{r_i}^{r_o} = \int_{r_i}^{r_o} \sigma_t\,dr - \frac{\gamma\omega^2}{3g}(r_o^3 - r_i^3) = 0$$

Substituting the value of σ_i given by Equation [9] in this, we can solve for

$$\left[\frac{\dot{w}_i}{k[f(t)]}\right]^{1/n}$$

which then can be used in Equation [9] to give the following equation

$$\sigma_i = \left[\frac{(r_o - r_i)\sigma_{t\,\text{avg}}}{\int_{r_i}^{r_o} \psi(r)dr}\right]\psi(r) \quad \ldots\ldots\ldots\ldots [11]$$

In this $\sigma_{t\,\text{avg}}$ = average tangential stress over the cross section

$$\sigma_{t\,\text{avg}} = \frac{\gamma\omega^2}{3g}\left(\frac{r_o^3 - r_i^3}{r_o - r_i}\right) \quad \ldots\ldots\ldots\ldots [12]$$

Integrating Equation [4] from r_i to r we obtain

$$\sigma_r = \frac{1}{r}\int_{r_i}^{r} \sigma_t\,dr - \frac{\gamma\omega^2}{3gr}(r^3 - r_i^3) \quad \ldots\ldots \ldots [13]$$

To find a first approximation for x, i.e. $(x)_1$ for use in Equations [7], [10], and [11] we assume $\sigma_t = \sigma_{t\,\text{avg}}$ in Equation [13] and integrate. This gives a first approximation for σ_r, i.e. $(\sigma_r)_1$. Then

$$(x)_1 = \frac{(\sigma_r)_1}{\sigma_{t\,\text{avg}}} = 1 - \frac{r_i}{r} - \left(\frac{r^3 - r_i^3}{r_o^3 - r_i^3}\right)\left(\frac{r_o - r_i}{r}\right) \ldots [14]$$

Using this value of $(x)_1$ for x in Equation [7] we can determine $\phi(r)$ as a function of r; from this by numerical integration we find

$$\exp\left[\int_{r_i}^{r} \frac{\phi(r)}{r}\,dr\right]$$

Using this in Equation [10] together with $(x)_1$ for x, the first approximation for $\psi(r)$ is found. Using this in Equation [11] the first approximation for σ_t, i.e. $(\sigma_t)_1$ is obtained. Using $(\sigma_t)_1$ for σ_t in Equation [13] the second approximation for σ_r, i.e. $(\sigma_r)_2$ is found by numerical integration and from this the second approximation of x, i.e. $(x)_2$ is found. The whole process is then repeated using $(x)_2$ instead of $(x)_1$ to find a second approximation of σ_t, i.e. $(\sigma_t)_2$. In general, it is found that the process converges very rapidly and it is seldom necessary to obtain more than two approximations for σ_t.

An example calculation for $(\sigma_t)_1$ and $(\sigma_r)_2$ for the disk tested, using $n = 6$ is shown in Table 2 where the steps in calculation are indicated.

A check was also made using increments Δr equal to half those in Table 2. This showed no appreciable difference in final results.

To calculate strain-rate distributions, values of σ_t and x as obtained by this method for various r-values (Table 2) may be used in Equations [6]. Since the stress is taken constant in time at any radius r (steady-state condition), Equations [6] may be integrated, giving the following strains

$$\left.\begin{aligned}
\epsilon_t &= k\sigma_t^n(1-x+x^2)^{(n-1)/2}\left(1-\frac{x}{2}\right)\int_0^t f(t)dt \\
\epsilon_r &= k\sigma_t^n(1-x+x^2)^{(n-1)/2}\left(x-\frac{1}{2}\right)\int_0^t f(t)dt \\
\epsilon_z &= -(\epsilon_t + \epsilon_r)
\end{aligned}\right\} \quad [14a]$$

If we take σ_{ti} and ϵ_{ti} to be the stress and plastic strain at the ID of the disk at time t, then

$$\epsilon_{ti} = k\sigma_{ti}^n \int_0^t f(t)dt$$

and we can write for the strains at any radius r and time t

$$\left.\begin{aligned}
\epsilon_t &= \epsilon_{ti}(\sigma_t/\sigma_{ti})^n(1-x+x^2)^{(n-1)/2}\left(1-\frac{x}{2}\right) \\
\epsilon_r &= \epsilon_{ti}(\sigma_t/\sigma_{ti})^n(1-x+x^2)^{(n-1)/2}\left(x-\frac{1}{2}\right) \\
\epsilon_z &= -(\epsilon_t + \epsilon_r)
\end{aligned}\right\} \quad \ldots [15]$$

TABLE 2 ROTATING DISK[a] WITH HOLE

Example calculation of first approximation for σ_t, i.e. $(\sigma_t)_1$ for $n = 6$. (Mises criterion)

(1) r	(2) $(x)_1$	(3) $\phi(r)$	(4) $\frac{\phi(r)}{r}$	(5) $\int_{r_i}^{r}\frac{\phi(r)}{r}dr$	(6) $\exp\left[\int_{r_i}^{r}\frac{\phi(r)}{r}dr\right]$	(7) $\psi(r)$	(8) $\int_{r_i}^{r}\psi(r)dr$	(9) $(\sigma_t)_1$	(10) $\frac{1}{r}\int_{r_i}^{r}(\sigma_t)_1 dr$	(11) $\frac{\gamma\omega^2}{3g}\left(\frac{r^3-r_i^3}{r}\right)$	(12) $(\sigma_r)_2$	(13) $(x)_2 = \frac{(\sigma_r)_2}{(\sigma_t)_1}$
1.25	0	−0.500	−0.400	0	1.000	0.963	0	29800	0	0	0	0
1.5	0.146	−0.382	−0.254	−0.083	0.920	0.987	0.243	30600	5020	570	4450	0.145
2.0	0.308	−0.227	−0.114	−0.171	0.843	0.984	0.736	30500	11400	1830	9570	0.314
2.5	0.378	−0.150	−0.060	−0.213	0.808	0.960	1.22	29800	15100	3310	11790	0.395
3.0	0.398	−0.139	−0.0434	−0.238	0.788	0.930	1.69	28800	17500	5040	12460	0.432
3.5	0.383	−0.144	−0.0411	−0.259	0.772	0.900	2.15	27900	19000	7050	11970	0.429
4.0	0.344	−0.188	−0.0471	−0.231	0.755	0.868	2.59	26900	20150	9350	10750	0.399
4.5	0.283	−0.253	−0.0562	−0.306	0.736	0.833	3.02	25800	20800	11950	8850	0.343
5.0	0.204	−0.330	−0.0660	−0.337	0.715	0.795	3.42	24600	21200	14850	6350	0.258
5.5	0.106	−0.418	−0.0760	−0.372	0.690	0.745	3.80	23100	21400	18000	3400	0.147
6.0	0	−0.500	−0.0833	−0.414	0.662	0.692	4.16	21450	21500	21500	0	0

[a] Methods of calculating values for each column are indicated as follows:
Data: N = 15,000 rpm, γ = 0.283 lb per cu in., r_o = 6 in., r_i = 1.25 in., $\gamma\omega^2/g$ = 1810, $\sigma_{t\,\text{avg}}$ = 27 150 psi
Col. (2) $(x)_1$ calculated from Equation [14].
Col. (3) $\phi(r)$ calculated from Equation [7] using $x = (x)_1$.
Col. (5) Integration may be carried out numerically.
Col. (6) Obtained from Col. 5 using tables of functions of e^{-x}.
Col. (7) Calculated from Equation [10] using Col. 6 and first approx. $(x)_1$ given by Col. 2, taking $n = 6$.
Col. (8) Values obtained by numerical integration from Col. 7.
Col. (9) Calculated by using Col. 7 in Equation [11].
Col. (10) Calculated using Col. 8 since σ_t = 31,000 $\psi(r)$ (see Equation [11]).
Col. (12) Equals Col. (10) minus Col. (11) (see Equation [13]).
Col. (13) Equals Col. (12) divided by Col. (9).

A similar method can be used for disks of variable thickness (Reference 6).

Calculation of Stress and Strain Distributions in Rotating Disk Using Maximum-Shear Theory

In this case we proceed in the same way as was done for the Mises criterion, except that we start with Equations [5] using $x = \sigma_r/\sigma_t$. The term $\phi(r)$ is again given by Equation [7] while $\psi(r)$ becomes

$$\psi(r) = \left[\frac{\exp \int_{r_i}^{r} \frac{\phi(r)dr}{r}}{r(1 - x/2)}\right]^{1/n} \quad \ldots\ldots\ldots\ldots [16]$$

The procedure for determining stress distribution as a function of r is the same as that given in the first section of the Appendix, except that Equation [16] instead of Equation [10] is used for the term $\psi(r)$; the numerical procedure illustrated in Table 2 also may be used in this case except that column 7 is based on Equation [16] rather than on Equation [10].

With the stress distribution thus found the strain distributions are obtained in the same way as was done in the previous example starting with Equations [5]. This yields the following equations

$$\left.\begin{aligned} \epsilon_t &= \epsilon_{ti}\left(\frac{\sigma_t}{\sigma_{ti}}\right)^n\left(1 - \frac{x}{2}\right) \\ \epsilon_r &= \epsilon_{ti}\left(\frac{\sigma_t}{\sigma_{ti}}\right)^n\left(x - \frac{1}{2}\right) \\ \epsilon_z &= -(\epsilon_t + \epsilon_r) \end{aligned}\right\} \quad \ldots\ldots\ldots\ldots [17]$$

The Elasticity of an Isotropic Aggregate of Anisotropic Cubic Crystals

By A. V. HERSHEY,[1] DAHLGREN, VA.

The elasticity of a polycrystalline aggregate is expressed in terms of the elasticity of the individual grains. The stress within each grain is estimated with the aid of an analysis of the stress distribution around a spherical cavity in an isotropic medium. The strain within each grain is expressed in terms of the average stress in the polycrystal as a whole by pseudoelastic constants which are related to the actual elastic constants. The calculated elasticities for physical tests and for x-ray diffraction measurements in polycrystals are given for a few cubic metals.

Introduction

THE elasticity of a polycrystalline aggregate can be calculated from the elasticity of the monocrystalline grains. Such calculations have been published previously on the basis of various assumptions. Thus Voigt (1)[2] calculated the average stress on the assumption that the local strain is everywhere uniform, while Reuss (2) calculated the average strain on the assumption that the local stress is everywhere uniform. Laurent and Eudier (4) calculated the average stress on the assumption that the principal axes of stress and strain are uniform. Huber and Schmid (5) found the average values of the elastic moduli over all orientations of a free single crystal. Bruggeman (6) introduced boundary conditions at the grain boundaries, but assumed that the grains are lamellar with various distributions of orientation. The present paper is an analysis of the stress distribution in a polycrystalline cubic metal with isometric and randomly oriented crystalline grains.

Comparisons (7 to 9) between the experimental data and the calculated averages show that the data agree more closely with Bruggeman's theory than with the other previous theories. The present theory gives values of the elastic moduli which agree with Bruggeman's values to within a fraction of a per cent, but are derived from simpler formulas.

The crystal grains of a polycrystalline aggregate are irregular polyhedra which vary in size and orientation from grain to grain. The environment of each grain contains many other grains, which must remain in contact over their intergranular boundaries as they deform. The interactions between adjacent grains create local deformations in each grain. The local strain is derived from the local displacement by a differential operation which is linear in the limiting case of elastic deformations and the local stress at equilibrium is a solution of a linear differential equation. If all of the grains with the same orientations were superimposed and their strain patterns were added together, the composite strain would still be obtained from the composite displacement by the same differential operation as the local strain, and the composite stress would still be a solution of the same differential equation as the local stress. The average strain pattern in the neighborhood of a grain is therefore the same as the strain pattern for a prototype grain immersed in a continuous medium with average properties which vary gradually from those of the crystal lattice at the center of the grain to those of the polycrystalline aggregate at a great distance from the grain. If the actual grains have a completely random distribution of properties, the prototype grain is essentially spherical and the polycrystalline aggregate is isotropic.

It is assumed that the average elastic moduli of the polycrystal are the same for a divergent average strain as they are for a homogeneous average strain. The diffuse boundary of the prototype grain then can be replaced by a sharp boundary. The elasticity of a spherical boundary and the elasticity of a single crystal are used in finding the elasticity of the prototype grain.

Elasticity of a Spherical Boundary in an Isotropic Medium

The displacement $\Delta \boldsymbol{r}$ of a point in the medium at equilibrium is a solution of the three-dimensional equation (10)

$$(\lambda + \mu)\nabla\nabla\cdot\Delta\boldsymbol{r} + \mu\nabla\cdot\nabla\Delta\boldsymbol{r} = 0 \quad \ldots\ldots\ldots [1]$$

in which λ, μ are elastic constants. The stress tensor is given by the expression (10)

$$\lambda\nabla\cdot\Delta\boldsymbol{r}\boldsymbol{I} + \mu(\nabla\Delta\boldsymbol{r} + \nabla'\Delta\boldsymbol{r}) \quad \ldots\ldots\ldots\ldots [2]$$

in which $\boldsymbol{I}$ is the identity tensor and $\nabla'\Delta\boldsymbol{r}$ is the transposed form of $\nabla\Delta\boldsymbol{r}$. Let r, θ, φ be spherical polar co-ordinates and let $\boldsymbol{e}_1$, $\boldsymbol{e}_2$, $\boldsymbol{e}_3$, be vectors of unit length in the directions of increasing r, θ, φ. In the special case of a spherical boundary of radius a whose interior is subject to a uniaxial strain along the polar axis, the displacement $\Delta \boldsymbol{r}$ per unit strain is given by the equation

$$\Delta\boldsymbol{r} = -\frac{3}{2}\frac{(\lambda+\mu)}{(3\lambda+8\mu)}\left(\frac{a^3}{r^2} - \frac{a^4}{r^4}\right)a\boldsymbol{e}_1 + \left[\frac{5}{2}\frac{(3\lambda+5\mu)}{(3\lambda+8\mu)}\frac{a^2}{r^2} - \frac{9}{2}\frac{(\lambda+\mu)}{(3\lambda+8\mu)}\frac{a^4}{r^4}\right]a\cos^2\theta\,\boldsymbol{e}_1 - \left[\frac{5\mu}{(3\lambda+8\mu)}\frac{a^2}{r^2} + 3\frac{(\lambda+\mu)}{(3\lambda+8\mu)}\frac{a^4}{r^4}\right]a\sin\theta\cos\theta\,\boldsymbol{e}_2 \quad [3]$$

The components of stress σ_{11}, σ_{22}, σ_{33}, σ_{12}, when referred to the unit vectors $\boldsymbol{e}_1$, $\boldsymbol{e}_2$, $\boldsymbol{e}_3$, are given by the equations

$$\frac{1}{2\mu}\sigma_{11} = \frac{1}{2}\frac{(11\lambda+6\mu)}{(3\lambda+8\mu)}\frac{a^3}{r^3} - 6\frac{(\lambda+\mu)}{(3\lambda+8\mu)}\frac{a^5}{r^5} - \left[\frac{5}{2}\frac{(9\lambda+10\mu)}{(3\lambda+8\mu)}\frac{a^3}{r^3} - 18\frac{(\lambda+\mu)}{(3\lambda+8\mu)}\frac{a^5}{r^5}\right]\cos^2\theta \quad [4]$$

$$\frac{1}{2\mu}\sigma_{22} = \frac{1}{2}\frac{(2\lambda+7\mu)}{(3\lambda+8\mu)}\frac{a^3}{r^3} + \frac{9}{2}\frac{(\lambda+\mu)}{(3\lambda+8\mu)}\frac{a^5}{r^5} + \left[\frac{5}{2}\frac{\mu}{(3\lambda+8\mu)}\frac{a^3}{r^3} - \frac{21}{2}\frac{(\lambda+\mu)}{(3\lambda+8\mu)}\frac{a^5}{r^5}\right]\cos^2\theta \quad [5]$$

$$\frac{1}{2\mu}\sigma_{33} = \frac{1}{2}\frac{(2\lambda-3\mu)}{(3\lambda+8\mu)}\frac{a^3}{r^3} + \frac{3}{2}\frac{(\lambda+\mu)}{(3\lambda+8\mu)}\frac{a^5}{r^5}$$

[1] U. S. Naval Proving Ground.

[2] Numbers in parentheses refer to the Bibliography at the end of the paper.

Contributed by the Applied Mechanics Division and presented at the Annual Meeting, New York, N. Y., November 29–December 4, 1953, of The American Society of Mechanical Engineers.

Discussion of this paper should be addressed to the Secretary, ASME, 29 West 39th Street, New York, N. Y., and will be accepted until October 11, 1954, for publication at a later date. Discussion received after the closing date will be returned.

Note: Statements and opinions advanced in this paper are to be understood as individual expressions of the author and not those of the Society or of the Navy Department. Manuscript received by ASME Applied Mechanics Division, January 13, 1953. Paper No. 53—A-62.

$$+\left[\frac{15}{2}\frac{\mu}{(3\lambda+8\mu)}\frac{a^3}{r^3}-\frac{15}{2}\frac{(\lambda+\mu)}{(3\lambda+8\mu)}\frac{a^5}{r^5}\right]\cos^2\theta \quad [6]$$

$$\frac{1}{2\mu}\sigma_{12}=-\left[\frac{5}{2}\frac{(3\lambda+2\mu)}{(3\lambda+8\mu)}\frac{a^3}{r^3}-12\frac{(\lambda+\mu)}{(3\lambda+8\mu)}\frac{a^5}{r^5}\right]\sin\theta\cos\theta \quad [7]$$

At the boundary $r = a$ the equations are reduced to

$$\frac{1}{2\mu}\sigma_{11}=-\frac{1}{2}\frac{(\lambda+6\mu)}{(3\lambda+8\mu)}-\frac{1}{2}\frac{(9\lambda+14\mu)}{(3\lambda+8\mu)}\cos^2\theta \quad (r=a) \quad [8]$$

$$\frac{1}{2\mu}\sigma_{12}=+\frac{1}{2}\frac{(9\lambda+14\mu)}{(3\lambda+8\mu)}\sin\theta\cos\theta \quad (r=a) \quad [9]$$

The force on the interior of the boundary is equivalent to a uniform pressure which is equal to

$$\frac{(\lambda+6\mu)}{(3\lambda+8\mu)}\mu \quad [10]$$

in combination with a uniaxial compression stress along the polar axis which is equal to

$$\frac{(9\lambda+14\mu)}{(3\lambda+8\mu)}\mu \quad [11]$$

Combinations of similar solutions with the polar axes in different directions give any combination of uniform strains in the interior of the boundary.

Elastic Constants of a Single Crystal

Let the stress and strain be referred to a set of orthogonal axes with Cartesian co-ordinates x, y, z. The components of the three-dimensional strain tensor are given by the matrix

$$\begin{Vmatrix} e_{11} & e_{12} & e_{13} \\ e_{21} & e_{22} & e_{23} \\ e_{31} & e_{32} & e_{33} \end{Vmatrix}$$

and the components of the three-dimensional stress tensor are given by the matrix

$$\begin{Vmatrix} \sigma_{11} & \sigma_{12} & \sigma_{13} \\ \sigma_{21} & \sigma_{22} & \sigma_{23} \\ \sigma_{31} & \sigma_{32} & \sigma_{33} \end{Vmatrix}$$

Since these three-dimensional tensors are symmetric, it is convenient to represent them by six-dimensional vectors (11). Let the engineering components of strain be the covariant components

$$(e_{11}, e_{22}, e_{33}, 2e_{23}, 2e_{31}, 2e_{12})$$

of a six-dimensional strain vector Π, and let the conventional components of stress be the contravariant components

$$(\sigma_{11}, \sigma_{22}, \sigma_{33}, \sigma_{23}, \sigma_{31}, \sigma_{12})$$

of a six-dimensional stress vector Σ. The matrix of elastic constants is then symmetric, as required by the first law of thermodynamics. The conventional elastic constants c_{11}, c_{12}, c_{44} of a cubic lattice are elements of the contravariant matrix of a six-dimensional tensor $\boldsymbol{C}_i$ and the conventional elastic constants s_{11}, s_{12}, s_{44} are elements of the covariant matrix of the six-dimensional tensor $\boldsymbol{C}_i^{-1}$ when the matrices are referred to crystallographic axes. The matrix of elastic constants is illustrated by Table 1. The stress-strain relationship for the crystal is given by the equation

$$\Sigma = \boldsymbol{C}_i \cdot \Pi \quad [12]$$

TABLE 1 CONTRAVARIANT ELASTIC CONSTANTS OF A CUBIC LATTICE

$\boldsymbol{C}_i$

	e_{11}	e_{22}	e_{33}	$2e_{23}$	$2e_{31}$	$2e_{12}$
σ_{11}	c_{11}	c_{12}	c_{13}	0	0	0
σ_{22}	c_{12}	c_{11}	c_{12}	0	0	0
σ_{33}	c_{13}	c_{13}	c_{11}	0	0	0
σ_{23}	0	0	0	c_{44}	0	0
σ_{31}	0	0	0	0	c_{44}	0
σ_{12}	0	0	0	0	0	c_{44}

If Π or Σ represent the strain or stress when referred to fixed axes, then there is a six-dimensional rotation tensor $\boldsymbol{H}$ such that $\boldsymbol{H}\cdot\Pi$ or $\boldsymbol{H}\cdot\Sigma$ gives the components of strain or stress when referred to rotated axes. For example, the contravariant components of the tensor $\boldsymbol{H}$ for a rotation through the angle χ about the z-axis are given by Table 2. The rotation tensor $\boldsymbol{H}$ for three successive rotations through the Eulerian angles χ, θ, φ, about the stationary z, y, z-axes is the product $\boldsymbol{H}_\chi\cdot\boldsymbol{H}_\theta\cdot\boldsymbol{H}_\varphi$ of three tensors, with one tensor for each rotation. The tensor $\boldsymbol{H}$ is orthogonal.

TABLE 2 CONTRAVARIANT COMPONENTS OF THE ROTATION TENSOR $\boldsymbol{H}$ FOR ROTATION THROUGH χ ABOUT z AXIS

$\boldsymbol{H}_\chi$

	σ_{11}	σ_{22}	σ_{33}	$2\sigma_{23}$	$2\sigma_{31}$	$2\sigma_{12}$
σ_{11}	$\cos^2\chi$	$\sin^2\chi$	0	0	0	$+\frac{1}{2}\sin 2\chi$
σ_{22}	$\sin^2\chi$	$\cos^2\chi$	0	0	0	$-\frac{1}{2}\sin 2\chi$
σ_{33}	0	0	1	0	0	0
σ_{23}	0	0	0	$\frac{1}{2}\cos\chi$	$-\frac{1}{2}\sin\chi$	0
σ_{31}	0	0	0	$+\frac{1}{2}\sin\chi$	$\frac{1}{2}\cos\chi$	0
σ_{12}	$-\frac{1}{2}\sin 2\chi$	$+\frac{1}{2}\sin 2\chi$	0	0	0	$\frac{1}{2}\cos 2\chi$

TABLE 3 COMPARISON BETWEEN CONTRAVARIANT COMPONENTS OF VARIOUS TENSORS OF SAME CLASS

Tensor	Components		
$\boldsymbol{C}_i$	e_{11}	e_{12}	e_{44}
$\boldsymbol{C}$	$\lambda+2\mu$	λ	μ
$\boldsymbol{C}_o$	$-10\frac{(\lambda+2\mu)}{(3\lambda+8\mu)}\mu$	$-\frac{(\lambda+6\mu)}{(3\lambda+8\mu)}\mu$	$-\frac{1}{2}\frac{(9\lambda+14\mu)}{(3\lambda+8\mu)}\mu$
$\boldsymbol{J}_1$	j_1	0	0
$\bar{\boldsymbol{J}}_1$	$\frac{1}{3}j_1$	$\frac{1}{3}j_1$	$\frac{1}{3}j_1$
$\boldsymbol{J}_2, \bar{\boldsymbol{J}}_2$	j_2	j_2	0
$\boldsymbol{J}_3, \bar{\boldsymbol{J}}_3$	j_3	0	$\frac{1}{3}j_3$
$\boldsymbol{C}_i^{-1}$	s_{11}	s_{12}	$\frac{1}{4}s_{44}$
$\boldsymbol{C}_i^{-1}\cdot\boldsymbol{J}$	ξ_{11}	ξ_{12}	$\frac{1}{4}\xi_{44}$

Elastic Moduli of a Polycrystalline Medium

The elasticity of an isotropic medium may be represented by a six-dimensional tensor $\boldsymbol{C}$, and the elasticity of a spherical boundary in the medium may be represented by a six-dimensional tensor $\boldsymbol{C}_o$. The tensors $\boldsymbol{C}$, $\boldsymbol{C}_o$, $\boldsymbol{C}_i$ all belong to the same class of symmetry in so far as the same components in each tensor are equal to each other or are equal to zero. The sum, product, or reciprocals of any tensors in this class are also tensors in the same class. The components of the tensors are compared in Table 3.

If Π is the six-dimensional vector strain at a distance from the grain boundary, then the six-dimensional stress Σ at a distance is given by the product $\boldsymbol{C}\cdot\Pi$. If Π_i is the six-dimensional vector strain in the interior of the grain, then that part of the strain which contributes to the distortion of the boundary is $\Pi_i - \Pi$. The six-dimensional stress Σ_i on the interior of the boundary is given by the equation

$$\Sigma_i = \Sigma + \boldsymbol{C}_o\cdot(\Pi_i - \Pi) \quad [13]$$

The stress Σ_i in the interior is also given by the equation

$$\Sigma_i = \boldsymbol{C}_i\Pi_i \quad [14]$$

Elimination of Π and Π_i from Equations [13] and [14], and definition of a new tensor $\boldsymbol{J}$ by the equation

$$\boldsymbol{J} \equiv (\boldsymbol{I} - \boldsymbol{C}_o\cdot\boldsymbol{C}_i^{-1})^{-1}\cdot(\boldsymbol{I} - \boldsymbol{C}_o\cdot\boldsymbol{C}^{-1}) \quad [15]$$

in which $\boldsymbol{I}$ is the six-dimensional identity tensor, leads to the equation

$$\Sigma_i = \boldsymbol{J}\cdot\Sigma \quad [16]$$

The tensor $\boldsymbol{J}$ can be expressed as the sum of three tensors $\boldsymbol{J}_1$, $\boldsymbol{J}_2$, $\boldsymbol{J}_3$ whose components are given in Table 3 when the matrices of the tensors are referred to crystallographic axes. The average $\bar{\boldsymbol{J}}$ of the tensor $\boldsymbol{J}$ is given by the equation

$$\bar{\boldsymbol{J}} = \frac{1}{8\pi^2}\int\int\int \boldsymbol{H}^{-1}\cdot\boldsymbol{J}\cdot\boldsymbol{H}\sin\theta\, d\varphi\, d\theta\, d\chi \quad [17]$$

The components of the averages $\bar{\boldsymbol{J}}_1$, $\bar{\boldsymbol{J}}_2$, $\bar{\boldsymbol{J}}_3$ of the tensors $\boldsymbol{J}_1$, $\boldsymbol{J}_2$, $\boldsymbol{J}_3$ are given in Table 3. The average internal stress is equal to the external stress if $\bar{\boldsymbol{J}}$ is equal to $\boldsymbol{I}$, or if the quantities j_1, j_2, j_3 satisfy the equations

$$j_1 + 3j_2 + j_3 = 1 \quad [18]$$

$$-2j_2 + j_3 = 1 \quad [19]$$

The first of these equations leads to the equation

$$3\lambda + 2\mu = c_{11} + 2c_{12} = 3\kappa \quad [20]$$

which may be used to simplify the evaluation of $\boldsymbol{J}$. The quantities j_1, j_2, j_3 are then expressed by the equations

$$j_1 + j_2 + j_3 = \frac{1}{3}\,\frac{[(9\lambda + 14\mu)\mu + 2(9\lambda + 19\mu)(c_{11} - c_{12})]}{[(9\lambda + 14\mu)\mu + (3\lambda + 8\mu)(c_{11} - c_{12})]} \quad [21]$$

$$j_2 = \frac{1}{3}\,\frac{[(9\lambda + 14\mu)\mu - \tfrac{1}{2}(9\lambda + 14\mu)(c_{11} - c_{12})]}{[(9\lambda + 14\mu)\mu + (3\lambda + 8\mu)(c_{11} - c_{12})]} \quad [22]$$

$$j_3 = \frac{15(\lambda + 2\mu)c_{44}}{(9\lambda + 14\mu)\mu + 2(3\lambda + 8\mu)c_{44}} \quad [23]$$

Elimination of λ from Equations [19], [20], [22], [23] leads to the quartic equation

$$\begin{aligned}&64\mu^4 + 16(4c_{11} + 5c_{12})\mu^3\\ &+ [3(c_{11} + 2c_{12})(5c_{11} + 4c_{12}) - 8(7c_{11} - 4c_{12})c_{44}]\mu^2\\ &- (29c_{11} - 20c_{12})(c_{11} + 2c_{12})c_{44}\mu\\ &- 3(c_{11} + 2c_{12})^2(c_{11} - c_{12})c_{44} = 0\end{aligned} \quad [24]$$

Application of the rule of Descartes shows that this equation has only one positive real root as long as c_{11} is greater than c_{12}. Negative real roots would be physically unstable.

The tensor of elasticity of the polycrystal is given by the equation

$$\boldsymbol{C}^{-1} = \frac{1}{8\pi^2}\int\int\int \boldsymbol{H}^{-1}\cdot\boldsymbol{C}_i^{-1}\cdot\boldsymbol{J}\cdot\boldsymbol{H}\sin\theta\, d\varphi\, d\theta\, d\chi \quad [25]$$

Pseudoelastic constants ξ_{11}, ξ_{12}, ξ_{44} are defined by the equations

$$\xi_{11} = s_{11} - 2j_2(s_{11} - s_{12}) \quad [26]$$

$$\xi_{12} = s_{12} + j_2(s_{11} - s_{12}) \quad [27]$$

$$\xi_{44} = j_3 s_{44} \quad [28]$$

and are the covariant components of the tensor $\boldsymbol{C}_i^{-1}\cdot\boldsymbol{J}$. The Young's modulus of the polycrystal is given by the equation

$$E = \frac{5}{3\xi_{11} + 2\xi_{12} + \xi_{44}} \quad [29]$$

and the shear modulus is given by the equation

$$\mu = \frac{5}{4(\xi_{11} - \xi_{12}) + 3\xi_{44}} \quad [30]$$

These are just the equations of Reuss (2) when $\boldsymbol{J} \equiv \boldsymbol{I}$.

Elastic Moduli From Direct Measurements

It is not easy to obtain data (12) on truly isotropic specimens of polycrystalline metals. The grains in specimens which are prepared by casting or by electrolysis have preferred orientations (13). The specimens can be recrystallized by heating after cold work, but the preferred orientations tend to persist. Diffusion of the orientations during recrystallization is increased by alloying elements which give solution-hardening effects. Nearly random orientations are produced in steel by the polymorphic transformation from austenite to ferrite.

A necessary although not sufficient indication of the isotropy of a specimen is provided by the accuracy with which a set of three or more independent elastic moduli satisfies the relationships for isotropic media. Direct measurements of the bulk modulus would not be influenced by the presence of preferred orientations, and measurements of the Young's modulus and the shear modulus should be consistent with the bulk modulus.

The published data have been determined by both static measurements of stress-strain relations and dynamic measurements of vibration frequencies. Vibrations and supersonic pulses have been adiabatic in free bars, but flexural vibrations have been isothermal in bars which were so heavily weighted that the vibrations could be counted by eye. The adiabatic data can be reduced to isothermal values with the aid of the second law of thermodynamics (1). The adiabatic compressibility differs from the isothermal compressibility by the amount $-(\alpha^2 VT)/C_p$ in which α is the cubical coefficient of thermal expansion, V is the molal volume, T is the absolute temperature, and C_p is the molal heat capacity at constant pressure. The differences between the adiabatic and isothermal values of c_{11}, c_{12}, κ are equal, while the differences for c_{44}, μ are zero. The most nearly consistent values of the shear modulus μ and the bulk modulus κ, which have been calculated from the elastic data (27 to 41) for single crystals, are compared with the most nearly consistent measurements (14 to 26) on polycrystalline aggregates in Fig. 1. Solid symbols designate the values for the polycrystal where $\boldsymbol{J} \neq \boldsymbol{I}$, and hollow symbols designate the values for crystals without constraint, for which $\boldsymbol{J} \equiv \boldsymbol{I}$. The possible range of μ from $\frac{1}{3}(c_{11} - c_{12})$ to c_{44} is indicated by arrows. The unit of stress is 10^{12} (dyne)/(cm)^2.

Elastic Moduli From X-Ray Diffraction

The x-ray diffraction camera selects a set of coplanar atomic planes in the polycrystalline aggregate and determines the average change in the interplanar spacing which is produced by an external stress. Let the normals of the diffracting planes be oriented at the polar angles α, β with respect to the crystallographic axes, and let the normals be oriented at the polar angles θ, φ with respect to fixed axes. The crystallographic axes are brought into a position for diffraction if they are rotated successively through the angles $-\beta$, $-\alpha$, χ, θ, φ about the fixed z, y, z, y, z-axes. The rotation tensor $\boldsymbol{H}$ for these rotations is given by the equation

$$\boldsymbol{H} = \boldsymbol{H}_{-\beta}\cdot\boldsymbol{H}_{-\alpha}\cdot\boldsymbol{H}_{\chi}\cdot\boldsymbol{H}_{\theta}\cdot\boldsymbol{H}_{\varphi} \quad [31]$$

The average internal strain $\bar{\Pi}_i$ of the diffracting grains, when referred to crystallographic axes, is given by the equation

$$\bar{\Pi}_i = \frac{1}{2\pi}\int_0^{2\pi} \boldsymbol{C}_i^{-1}\cdot\boldsymbol{J}\cdot\boldsymbol{H}\cdot\Sigma\, d\chi \quad [32]$$

The x-ray diffraction measurements give that component of the average internal strain $\boldsymbol{H}_{\alpha}\cdot\boldsymbol{H}_{\beta}\cdot\bar{\Pi}_i$ which is in the polar axis.

If the penetration of the x rays into the specimen is deep, the measured strain $\bar{\epsilon}$ for unit uniaxial stress in the z-axis is given by the equation

$$\begin{aligned}\bar{\epsilon} &= \xi_{12} + (\xi_{11} - \xi_{12})\cos^2\theta\\ &\quad + (\xi_{11} - \xi_{12} - \tfrac{1}{2}\xi_{44})\Gamma(1 - 3\cos^2\theta)\end{aligned} \quad [33]$$

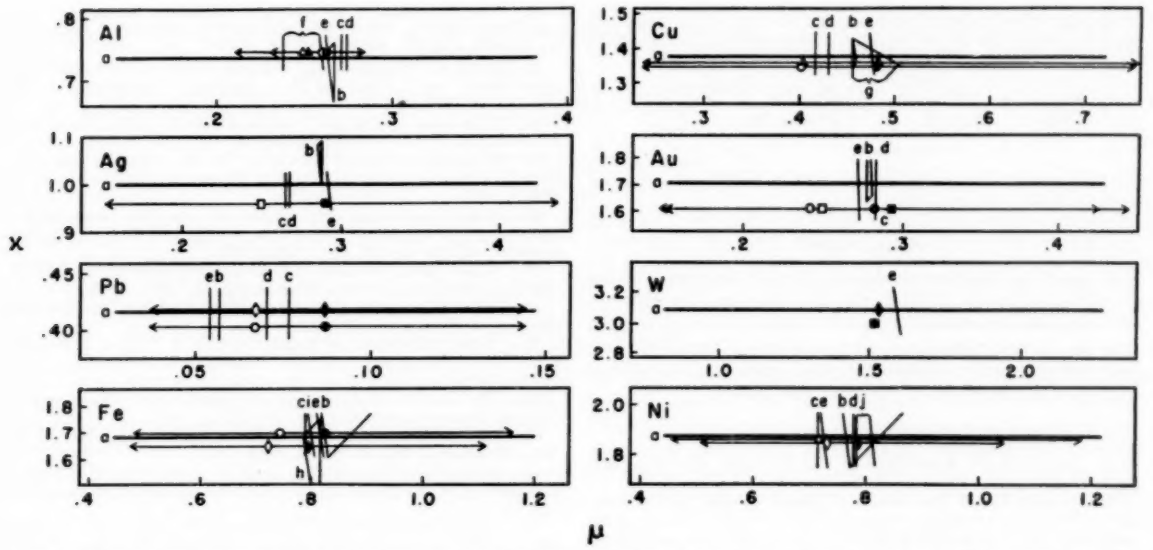

FIG. 1 COMPARISON BETWEEN EXPERIMENTAL AND THEORETICAL VALUES OF ISOTHERMAL ELASTIC MODULI FOR POLYCRYSTALLINE AGGREGATES

(Experimental curves based on measurements of polycrystals by: *a*, Bridgman (15, 16); *b*, Grüneisen (17); *c*, Koch and Dannecker (18); *d*, Kikuta (19); *e*, Köster (20); *f*, Moore (21); *g*, Schneider and Burton (22); *h*, Lyse and Godfrey (23); *i*, Abram (24) or Cleaves and Hiegel (25); *j*, Mudge and Luff (26). Theoretical values based on measurements of single crystals by: ○—● [Al] Goens (28); [Cu, Au, Pb] Goens and Weerts (29); [Fe] Goens and Schmid (30); □—■ [Ag, Au] Röhl (31); [W] Wright (32); ◇—◆ [Pb] Swift and Tyndall (33); [W] Bridgman (34); [Fe] Kimura (35); [Ni] Honda and Shirakawa (36, 37); △—▲ [Al, Cu] Lazarus (38); [Ni] Bozorth, Mason, McSkimin, and Walker (39–41). The arrows indicate the range of μ from $\frac{1}{2}[c_{11} - c_{12}]$ to c_{44}.)

in which Γ is given by the equation

$$\Gamma = (\sin^2\alpha\cos^2\alpha + \sin^4\alpha\sin^2\beta\cos^2\beta) \ldots\ldots [34]$$

These are just the equations of Möller and Martin (46) when $\boldsymbol{J} \equiv \boldsymbol{I}$.

In most of the experimental work[3] the x rays have not penetrated appreciably beyond the surface layer of grains. The boundary stress at the free surface of the specimen is zero. The strain at the free surface may be estimated if the tensor $\boldsymbol{J}$ is replaced by the tensor $\boldsymbol{H}\cdot\boldsymbol{\mathfrak{I}}\cdot\boldsymbol{H}^{-1}\cdot\boldsymbol{J}$, in which the tensor $\boldsymbol{\mathfrak{I}}$ differs from the tensor $\boldsymbol{I}$ by having those three diagonal elements missing which would preserve a boundary stress. The effect of the boundary surface is illustrated in Fig. 2 by a comparison between curve (*a*), which illustrates the limiting case of deep penetration, curve (*b*) which illustrates the limiting case of superficial penetration, and curve (*c*) which illustrates the case of crystals without constraint. These curves should straddle the experimental data. Included in the figure are some measured values of $\bar{\epsilon}$. Early measurements (42 to 45) of strain by x rays tended to show that the measured elasticity is isotropic, but recent measurements (46 to 51) show definite evidence of anisotropy.

Smith and Wood (47 to 50) have published x-ray measurements of the elastic constants of diffracting planes in copper and iron. The incident x-ray beam was perpendicular to the axis of stress. The diffracted x-ray beam was coplanar with the axis of stress and the normal of the surface of the specimen. The theoretical values of $\bar{\epsilon}$ which would be observed in the interior of a polycrystal, or in crystals without constraint, are compared in Table 4 with the experimental values.

Kemmnitz (51) has published x-ray measurements with cobalt $K\alpha_1$ and chromium $K\alpha_1$ radiation in iron. Average values were given for the difference between the displacements of the two

[3] For example, the grains in a metal with No. 7 ASTM grain size are approximately 0.04 mm diam, while the mean penetration of Co $K\alpha$-radiation in iron is 0.02 mm.

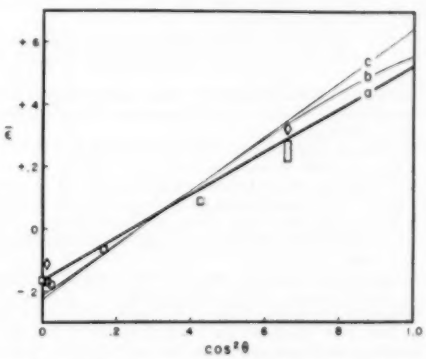

FIG. 2 COMPARISON BETWEEN EXPERIMENTAL AND THEORETICAL VALUES OF LATTICE STRAIN PER UNIT STRESS FOR 103 PLANES IN IRON OR STEEL

(Measurements by □ Möller, Barbers, and Strunk (46); ◇ Bennett and Vacher (45); ○ Smith and Wood (48 to 50). Curves for *a*, deep penetration of x rays; *b*, superficial penetration of x rays; *c*, free crystals.)

diffracted rays which make maximum and minimum angles with the axis of stress. This method is equivalent to a direct comparison between the slopes of lines which connect $\bar{\epsilon}$ with $\cos^2\theta$. X-ray stresses have been computed, from the reported data, on the assumption that the crystal lattice is isotropic. The theoretical values for these stresses, which would be observed in the interior

TABLE 4 COMPARISON BETWEEN X-RAY MEASUREMENTS OF ELASTIC CONSTANTS, REPORTED BY SMITH AND WOOD, AND THEORETICAL ELASTIC CONSTANTS CALCULATED FROM DATA FOR SINGLE CRYSTALS

Diffracting planes	$\cos^2\theta$	$\bar{\epsilon}$ Polycrystal	$\bar{\epsilon}$ Observed	$\bar{\epsilon}$ Free crystal
103 in Fe	0.026	—0.145	—0.183 ± 0.007	—0.203
004 in Cu	0.021	—0.342	—0.447	—0.578
331 in Cu	0.046	—0.181	—0.175	—0.182

TABLE 5 COMPARISON BETWEEN X-RAY STRESSES, CALCULATED BY KEMMNITZ ON THE ASSUMPTION THAT CRYSTAL LATTICE IS ISOTROPIC, AND THEORETICAL VALUES FOR THESE STRESSES, BASED ON ACTUAL ELASTICITY OF CRYSTAL LATTICE

Diffracting planes	X-ray stress per unit external stress		
	Polycrystal	Observed	Free crystal
103	1.13	1.29 ± 0.10	1.41
112	0.94	0.86 ± 0.12	0.96

of a polycrystal, and in crystals without constraint, are compared in Table 5 with the experimental values.

Conclusion

Although the experimental data confirm the magnitude of the elasticity which is predicted by the theoretical analysis, they are not comprehensive enough to provide a quantitative check of the analysis. A determination of all twenty-one of the elastic constants of each polycrystalline specimen would make possible a correction for the effects of preferred orientation.

BIBLIOGRAPHY

1 "Lehrbuch der Kristallphysik," by W. Voigt, Teubner, Leipsig, Germany, 1928. Cf. reference 3.

2 "Calculation of Flow Limits of Mixed Crystals on the Basis of the Plasticity of Single Crystals," by A. Reuss, *Zeitschrift für angewandte Mathematik und Mechanik*, vol. 9, 1929, p. 49. Cf. ref. 3.

3 "The Elastic Behavior of a Crystalline Aggregate," by R. Hill, Proceedings of the Physical Society, series A, vol. 65, 1952, p. 349.

4 "Crystalline Interactions and the Brittleness of Metals," by P. Laurent and M. Eudier, *Revue de Metallurgie*, vol. 47, 1950, p. 582.

5 "Determination of the Elastic Properties of Quasi-Isotropic Polycrystals by Averaging," by A. Huber and E. Schmid, *Helvetica Physica Acta*, vol. 7, 1934, p. 620.

6 "Elastizitätskonstanten von Kristallaggregaten," by D. A. G. Bruggeman, Utrecht Dissertation (J. B. Wolters, Groningen-den Haag, 1930). Cf. reference 31.

7 "On the Calculation of Physical Constants of Quasi-Isotropic Polycrystals," by W. Boas and E. Schmid, *Helvetica Physica Acta*, vol. 7, 1934, p. 628.

8 "Calculation of the Elastic Moduli for the Various Textures of the Regular Metals," by D. A. G. Bruggeman, *Zeitschrift für Physik*, vol. 92, 1934, p. 561.

9 "The Elastic Behavior of Polycrystalline Iron," by H. Möller, *Archiv für das Eisenhüttenwesen*, vol. 13, 1939, p. 59.

10 "A Treatise on the Mathematical Theory of Elasticity," by A. E. H. Love, Cambridge University Press, England, 1927.

11 "A Review of the Definitions of Finite Strain," by A. V. Hershey, First National Congress of Applied Mechanics, Chicago, Ill., June 12, 1951.

12 "Anisotropy in Metals," by W. Boas and J. K. Mackenzie, *Progress in Metal Physics*, vol. 2, 1950, p. 90.

13 "Structure of Metals," by C. S. Barrett, McGraw-Hill Book Company, Inc., New York, N. Y., 1943, chapters 19 and 20.

14 "Mechanical Properties of Metals and Alloys," by J. L. Everhart, W. E. Lindlief, J. Kanegis, P. G. Weissler, and F. Siegel, U. S. National Bureau of Standards, Washington, D. C. Circular C447, 1943.

15 "Compressibilities and Electrical Resistance Under Pressure, With Special Reference to Intermetallic Compounds," by P. W. Bridgman, Proceedings of the American Academy of Arts and Sciences, vol. 70, 1935, p. 285.

16 "Recent Work in the Field of High Pressures," by P. W. Bridgman, *Reviews of Modern Physics*, vol. 18, 1946, p. 1.

17 "The Elastic Constants of Metals at Small Deformations. I, Modulus of Elasticity Measured Dynamically and Statically," by E. Grüneisen, *Annalen der Physik*, vol. 22, 1907, p. 801: II, "Modulus of Rigidity Ratio of Transverse Contraction to Longitudinal Dilatation and Cubic Compressibility," by E. Grüneisen, *Annalen der Physik*, vol. 25, 1908, p. 825.

18 "The Elasticity of a Few Metals and Alloys Up to Temperatures Which Are Near Their Melting Points," by K. R. Koch and C. Dannecker, *Annalen der Physik*, vol. 47, 1915, p. 197.

19 "The Change of Rigidity and Logarithmic Decrement in Different Metals and Alloys at High Temperatures," by T. Kikuta, Scientific Reports, Tohoku Imperial University, vol. 10, 1921, p. 139.

20 "The Dependence of the Modulus of Elasticity of Pure Metals on Temperature," by W. Köster, *Zeitschrift für Metallkunde*, vol. 39, 1948, p. 1.

21 "Some Fatigue Tests on Non-Ferrous Metals," by R. R. Moore, Proceedings, ASTM, vol. 25, (2), 1925, p. 66.

22 "Determination of the Elastic Constants of Solids by Ultrasonic Methods," by W. C. Schneider and C. J. Burton, *Journal of Applied Physics*, vol. 20, 1949, p. 48.

23 "Shearing Properties and Poisson's Ratio of Structural and Alloy Steels," by I. Lyse and H. J. Godfrey, Proceedings, ASTM, vol. 33, (2), 1933, p. 274.

24 "The Value of Young's Modulus for Steel," by H. H. Abram, *Journal of the Iron and Steel Institute*, vol. 129, 1934, p. 325.

25 "Properties of High Purity Iron," by H. E. Cleaves and J. M. Hiegel, *Journal of Research*, National Bureau of Standards, vol. 28, 1942, p. 643.

26 "Some Mechanical Properties of Nickel, Manganese-Nickel, and Copper-Nickel Alloys," by W. A. Mudge and L. W. Luff, Proceedings, ASTM, vol. 28, (2), 1928, p. 278.

27 "The Elastic Constants of Anisotropic Materials," by R. F. S. Hearmon, *Reviews of Modern Physics*, vol. 18, 1946, p. 409.

28 "Elastic Constants of Aluminum Single Crystals," by E. Goens, *Annalen der Physik*, vol. 17, 1933, p. 233.

29 "Elastic Constants of Single Crystals of Copper, Gold, and Lead," by E. Goens and J. Weerts, *Physikalische Zeitschrift*, vol. 37, 1936, p. 321.

30 "On the Elastic Anisotropy of Iron," by E. Goens and E. Schmid, *Naturwissenschaften*, vol. 19, 1931, p. 520.

31 "Elastic Properties of Gold-Silver Single Crystals," by H. Röhl, *Annalen der Physik*, vol. 16, 1933, p. 887.

32 "Elasticity of Pintsch Crystals of Tungsten," by S. J. Wright, Proceedings of the Royal Society, London, England, series A, vol. 126, 1930, p. 613.

33 "Elasticity and Creep of Lead Single Crystals," by I. H. Swift and E. P. T. Tyndall, *Physical Review*, vol. 61, 1942, p. 359.

34 "Some Properties of Single Metal Crystals," by P. W. Bridgman, Proceedings of the National Academy of Sciences, 1924, p. 411.

35 "Elastic Moduli of Ferromagnetic Materials," by R. Kimura, Proceedings of the Physico-Mathematical Society of Japan, vol. 21, 1939, p. 686.

36 "Young's Modulus of Elasticity of Single Crystals of Nickel and Cobalt," by K. Honda and Y. Shirakawa, Scientific Reports, Research Institute, Tohoku University, Japan, vol. 1, 1949, p. 9.

37 "Elastic Constants of Nickel Crystals," by M. Yamamoto, *Physical Review*, vol. 77, 1950, p. 566.

38 "The Variation of the Adiabatic Elastic Constants of Potassium Chloride, Sodium Chloride, Copper-Zinc, Copper, and Aluminum With Pressure to 10,000 Bars," by D. Lazarus, *Physical Review*, vol. 76, 1949, p. 545.

39 "Elastic Constants and Internal Loss of Single Nickel Crystals," by R. M. Bozorth, W. P. Mason, H. J. McSkimin, and J. G. Walker, *Physical Review*, vol. 75, 1949, p. 1954.

40 "Frequency Dependence of Elastic Constants and Losses in Nickel," by R. M. Bozorth, W. P. Mason, and H. J. McSkimin, *Bell System Technical Journal*, vol. 30, 1951, p. 970.

41 "The Elastic Constants of Nickel," by J. R. Neighbours, F. W. Bratten, and C. S. Smith, *Journal of Applied Physics*, 1952, p. 389.

42 "Mechanical and X-Ray Measurements of the Torsion Modulus of Iron," by R. Glocker and O. Schaaber, *Ergebnisse der Technischer Röntgenkunde*, vol. 6, 1938, p. 34.

43 "X-Ray Stress Measurements on the Beginning of the Flow Process in Carbon Steels," by R. Glocker and H. Hasenmaier, *Zeitschrift Vereines deutscher Ingenieure*, vol. 84, 1940, p. 825.

44 "The Measurement of Stress by X-Rays," by D. E. Thomas, *Journal of Scientific Instruments*, vol. 18, 1941, p. 135.

45 "Calibration of X-Ray Measurement of Strain," by J. A. Bennett and H. C. Vacher, *Journal of Research*, National Bureau of Standards, vol. 40, 1948, p. 285.

46 "Elastic Anisotropy and X-Ray Stress Measurement," by H. Möller and G. Martin, Düsseldorf, Germany, *Mitteilungen aus dem Kaiser-Wilhelm-Institut für Eisenforschung*, vol. 21, 1939, p. 261.

47 "X-Ray Structure and Elastic Strains in Copper," by S. L. Smith and W. A. Wood, Proceedings of the Royal Society, London, England, series A, vol. 176, 1940, p. 398.

48 "A Stress-Strain Curve for the Atomic Lattice of Iron," by S. L. Smith and W. A. Wood, Proceedings of the Royal Society, London, England, series A, vol. 178, 1941, p. 93.

49 "A Stress-Strain Curve for the Atomic Lattice of Mild Steel and the Physical Significance of the Yield Point of a Metal," by S. L. Smith and W. A. Wood, Proceedings of the Royal Society, London, England, series A, vol. 179, 1942, p. 450.

50 "A Stress-Strain Curve for the Atomic Lattice of Mild Steel in Compression," by S. L. Smith and W. A. Wood, Proceedings of the Royal Society, London, England, series A, vol. 181, 1942, p. 72.

51 "The Use of X-Ray Back-Reflection Technique for the Determination of Deformation and Stress," by G. Kemmnitz, *Zeitschrift für Metallkunde*, vol. 39, 1948, p. 254.

The Plasticity of an Isotropic Aggregate of Anisotropic Face-Centered Cubic Crystals

By A. V. HERSHEY,[1] DAHLGREN, VA.

The plasticity of a polycrystalline aggregate is expressed in terms of the plasticity of the individual grains. It is assumed that the local deviation of stress from the average stress is proportional to the local deviation of strain from the average strain, and it is assumed that plastic flow begins when there is an average of three active slip systems per grain. The plastic states of a grain are mapped as a function of the orientation of the crystallographic axes. A coexistence of different states of strain with different rotations of the axes at the same state of stress can be correlated with the occurrence of deformation bands. A range of orientations is illustrated in which the axes tend to congregate quickly and then move more slowly toward a stable end orientation. The residual strain which would be observed by x-ray diffraction after the release of stress is calculated for three sets of diffracting planes. The applications of the theory have so far been limited to face-centered cubic polycrystals with intrinsic elastic isotropy.

Introduction

THE possible slip planes and slip directions in face-centered cubic single crystals have been identified by Taylor, Elam, and Farren (1 to 4).[2] Slip in the crystals was confined to the primary slip system which had the largest resolved shear stress, until a secondary slip system was brought into an orientation where both slip systems had the same resolved shear stress. The slip then continued in both slip systems if the metal was pure. The critical slip stress in aluminum has been determined by a number of investigators (5 to 15). The critical slip stress is usually independent (5 to 10) of orientation of the crystallographic axes in a range of orientations.

A few theories of plasticity for polycrystalline aggregates have been published on the basis of information about the slip in single crystals. Thus Sachs (16) has calculated the average stress on the assumption that the local stress in each grain is the same as that stress which would be required to initiate slip in a free single crystal. Batdorf and Budiansky (19) have calculated the average strain on the assumption that the local stress is uniform in free crystals with work hardening. Calnan and Clews (20) have calculated the average stress on the assumption that the local stress is the same as that stress which would cause slip in four or more slip systems but only one or two of the slip systems were assumed to be active. Boas and Schmid (21) have calculated stable orientations in deformation textures on the assumption that there are three active slip systems per grain. Those slip systems were assumed to be active which would have the greatest resolved shear stress in a free crystal. The rotation of the crystallographic axes during slip in each slip system was assumed to be the same as the rotation which would occur in a single crystal.

Taylor (6, 7) has emphasized that an aggregate of free crystals would not fit together after plastic deformation and has therefore assumed that the local strain is everywhere uniform. There must then be five active slip systems in grains of random orientation. Taylor has calculated the average plastic work for uniaxial strain on the assumption that the five active slip systems in each grain are those for which the plastic work is the least. More than one set of slip systems were possible for many of the orientations of a single grain. Bishop and Hill (24) have extended the calculations to a series of biaxial strains. Slibar and Vitovec (22) have assumed that the constraint which is imposed on each grain by adjacent grains is a probability function of the number of independent sets of five slip systems. If five independent shear stresses were equal to the critical slip stress, then all of the components of stress would be determined except for an isotropic component. The boundary stress between grains with different orientations would not be in equilibrium. That the strain is not uniform within grains or from grain to grain, even though there is intergranular continuity, has been shown experimentally by Aston (25), Boas and Hargreaves (26 to 28) with strain and hardness surveys in large-grained specimens of aluminum. In no case were more than three active slip planes reported.

At equilibrium, the divergence of the stress is zero throughout the medium. Integration of the divergence of stress throughout any volume can be converted by Gauss's theorem into an integration over the surface which encloses the volume.

The transformation which expresses the differential change in displacement for any differential change in location is the gradient of the displacement. The curl of the transformation is therefore zero throughout a continuous medium. Integration of the curl of the transformation throughout any volume can be converted by Gauss's theorem into an integration over the surface which encloses the volume.

Let the polycrystal be partitioned, by surfaces of integration, into cells within which the stress and strain are constant. The cells coincide with the grains in an approximate analysis, while the cells would be subdivided indefinitely in an accurate analysis. In a number N of cells there are $6N$ components of stress, there are $6N$ components of strain, and there are $3N$ components of rotation. The surface integrals which express the equilibrium are vectors with three components each. There are therefore $3N$ equations of equilibrium among the $6N$ components of stress. The surface integrals which express the continuity are tensors with nine components each, but only six of the components are linearly independent. There are therefore $6N$ equations of continuity among the $9N$ components of strain and rotation. In an elastic medium there are $6N$ stress-strain relations and the $15N$ components of stress, strain, and rotation are fully determined by a total of $15N$ equations. If $3N$ independent shear stresses were equal to a con-

[1] U. S. Naval Proving Ground.

[2] Numbers in parentheses refer to the Bibliography at the end of the paper.

Contributed by the Applied Mechanics Division and presented at the Annual Meeting, New York, N. Y., November 29–December 4, 1953, of The American Society of Mechanical Engineers.

Discussion of this paper should be addressed to the Secretary, ASME, 29 West 39th Street, New York, N. Y., and will be accepted until October 11, 1954, for publication at a later date. Discussion received after the closing date will be returned.

Note: Statements and opinions advanced in this paper are to be understood as individual expressions of the author and not those of the Society or of the Navy Department. Manuscript received by the ASME Applied Mechanics Division, January 13, 1953. Paper No. 53—A-63.

stant critical slip stress, the $6N$ components of stress would be fully determined by $6N$ equations and the stress would be independent of strain. It is therefore assumed in the present paper that plastic flow begins when there is an average of three active slip systems per cell.

If slip occurs in a solitary cell, a stress is transferred elastically to the surrounding cells. The transferred stress varies with direction and decreases rapidly with distance. The average of the transferred stress is zero.

The environments of all cells with the same orientations have a local stress pattern which differs from the average stress in the polycrystal as a whole. The active slip systems in the environments have a distribution of multiplicity which varies with the deviation of the local stress pattern from the average stress, and have a distribution of orientation which is symmetric with respect to the principal axes in the local stress pattern. An increment of stress in the polycrystal may be represented by the sum of three increments.

In the first increment, the polycrystal is loaded elastically, and the resolved shear stresses in the active slip systems are increased. In the second increment, each cell slips individually by the amount which would remove the initial increment in its own active shear stresses, but a residual increment is thus restored to the active shear stresses of the other cells. The local variation of stress is increased. In the third increment, the slip in the cells is so readjusted as to eliminate the residual increment in the active shear stresses. The local variation of stress is reduced by a major amount which is proportional to the local variation of stress and by a minor amount which is distorted by the distribution of the active slip systems. Plastic flow begins when the net increment in the variation of local stress is zero.

It is assumed in the present paper that the third increment of stress is a linear combination of the first and second increments of stress. An accurate assessment of the error which is introduced by this assumption would require the solution of an elaborate integral equation with the aid of an electronic digital calculator. A first-order approximation of the solution, which has been computed for the case of a nearly uniform uniaxial stress, has indicated that the average error is probably not more than a few per cent.

The environments of all cells with the same orientations contain adjacent cells with nearly the same orientations but contain distant cells with random orientations. It is therefore assumed that the partitioned polycrystal may be represented adequately by prototype grains with sharp boundaries in continuous media.

The gradient of the displacement is the sum of a strain tensor with the matrix

$$\begin{Vmatrix} e_{11} & e_{12} & e_{31} \\ e_{12} & e_{22} & e_{23} \\ e_{31} & e_{23} & e_{33} \end{Vmatrix}$$

and a rotation tensor with the matrix

$$\begin{Vmatrix} 0 & +\theta_{12} - \theta_{31} \\ -\theta_{12} & 0 & +\theta_{23} \\ +\theta_{31} - \theta_{23} & 0 \end{Vmatrix}$$

in the limiting case of small deformations. A representation of stress and strain by six-dimensional vectors has been presented in a previous paper (29). The conventional components of the three-dimensional strain tensor are replaced by the covariant components

$$(e_{11}, e_{22}, e_{33}, 2e_{23}, 2e_{31}, 2e_{12})$$

of a six-dimensional strain vector, and the three components of rotation are replaced by the covariant components

$$(0, 0, 0, 2\theta_{23}, 2\theta_{31}, 2\theta_{12})$$

of a six-dimensional rotation vector. The conventional components of the three-dimensional stress tensor with the matrix

$$\begin{Vmatrix} \sigma_{11} & \sigma_{12} & \sigma_{31} \\ \sigma_{12} & \sigma_{22} & \sigma_{23} \\ \sigma_{31} & \sigma_{23} & \sigma_{33} \end{Vmatrix}$$

are replaced by the contravariant components

$$(\sigma_{11}, \sigma_{22}, \sigma_{33}, \sigma_{23}, \sigma_{31}, \sigma_{12})$$

of a six-dimensional stress vector. The elasticity of an isotropic medium, the elasticity of a spherical boundary in the medium, and the elasticity of an anisotropic crystal may be represented by six-dimensional tensors $\boldsymbol{C}$, $\boldsymbol{C}_0$, $\boldsymbol{C}_i$.

The components of vectors and tensors may be referred to fixed Cartesian x, y, z-axes, or may be referred to crystallographic axes which are rotated in succession through Eulerian angles χ, θ, φ with respect to the fixed x, y, z-axes. There is a six-dimensional rotation tensor $\boldsymbol{H}$ which expresses the components of any six-dimensonal vector with respect to rotated axes in terms of the components with respect to fixed axes.

The present analysis is limited to systems at zero pressure.

Plasticity of a Polycrystalline Medium

Arbitrary Variation of Stress. During an elastic increment of stress, the six-dimensional stress vector $\boldsymbol{\Sigma}_i$ and the six-dimensional strain vector $\boldsymbol{\Pi}_i$ for the interior of a spherical boundary are related to the six-dimensional stress vector $\boldsymbol{\Sigma}$ and the six-dimensional strain vector $\boldsymbol{\Pi}$ for an external isotropic medium by the equation

$$d\boldsymbol{\Sigma}_i = d\boldsymbol{\Sigma} + \boldsymbol{C}_0 \cdot (d\boldsymbol{\Pi}_i - d\boldsymbol{\Pi}) \quad [1]$$

During slip in a crystal grain within the boundary, the six-dimensional stress $\boldsymbol{\Sigma}_i$ for the interior is related to the six-dimensional plastic strain $\boldsymbol{\Pi}_s$ in the interior by the equation

$$d\boldsymbol{\Sigma}_i = \boldsymbol{C}_i \cdot (d\boldsymbol{\Pi}_i - d\boldsymbol{\Pi}_s) \quad [2]$$

Elimination of $d\boldsymbol{\Pi}_i$ from Equations [1] and [2], representation of the identity tensor by $\boldsymbol{I}$, definition of a new tensor $\boldsymbol{J}$ by the equation

$$\boldsymbol{J} \equiv (\boldsymbol{I} - \boldsymbol{C}_0 \cdot \boldsymbol{C}_i^{-1})^{-1} \cdot (\boldsymbol{I} - \boldsymbol{C}_0 \cdot \boldsymbol{C}^{-1}) \quad [3]$$

and definition of a new tensor $\boldsymbol{K}$ by the equation

$$\boldsymbol{K} \equiv (\boldsymbol{I} - \boldsymbol{C}_0 \cdot \boldsymbol{C}_i^{-1})^{-1} \cdot \boldsymbol{C}_0 \quad [4]$$

lead to the equation

$$d\boldsymbol{\Sigma}_i = \boldsymbol{J} \cdot d\boldsymbol{\Sigma} + \boldsymbol{K} \cdot d\boldsymbol{\Pi}_s \quad [5]$$

The tensors $\boldsymbol{J}$ and $\boldsymbol{K}$ are in the same class of symmetry with the tensor $\boldsymbol{C}_i$ for an elastic anisotropic crystal and each may be expressed as the sum of three tensors $\boldsymbol{J}_1$, $\boldsymbol{J}_2$, $\boldsymbol{J}_3$, or $\boldsymbol{K}_1$, $\boldsymbol{K}_2$, $\boldsymbol{K}_3$. The components of the tensors are compared with the conventional elastic constants of a cubic crystal in Table 1. The components j_1, j_2, j_3, and k_1, k_2, k_3 satisfy the identity

$$\frac{j_1}{j_2} = \frac{k_1}{k_2} \quad [6]$$

The slip in a crystal is confined to a limited number of directions in a limited number of planes. The plastic strain $\boldsymbol{\Pi}_s$ is given in terms of the strain $\boldsymbol{\Pi}_m$ per unit slip strain and the slip strain s_m in the mth slip system by the equation

$$d\boldsymbol{\Pi}_s = \boldsymbol{\Pi}_m ds_m \quad [7]$$

TABLE 1. COMPARISON BETWEEN CONTRAVARIANT COMPONENTS OF VARIOUS TENSORS OF THE SAME CLASS

Tensor	Components		
$\boldsymbol{C}_i$	c_{11}	c_{12}	c_{44}
$\boldsymbol{J}_1$	j_1	0	0
$\boldsymbol{J}_2$	j_2	j_2	0
$\boldsymbol{J}_3$	j_3	0	$\frac{1}{2}\, j_3$
$\boldsymbol{K}_1$	k_1	0	0
$\boldsymbol{K}_2$	k_2	k_2	0
$\boldsymbol{K}_3$	k_3	0	$\frac{1}{2}\, k_3$

in which the repetition of the dummy index m signifies summation in accordance with the summation convention. The plastic work which would occur during unit slip strain in the mth slip system is $\boldsymbol{\Pi}_m \cdot \boldsymbol{\Sigma}_i$, which is therefore just the resolved shear stress. The slip strains in a crystal with constant slip stress are solutions of the system of equations

$$\boldsymbol{\Pi}_k \cdot d\boldsymbol{\Sigma}_i = 0 \qquad [8]$$

Let a new tensor $\boldsymbol{X}$ be defined by the equation

$$\boldsymbol{X} \equiv \gamma^{mk} \boldsymbol{K} \cdot \boldsymbol{\Pi}_m \boldsymbol{\Pi}_k \qquad [9]$$

in which m, k are summation indexes and γ^{mk} is the mkth element of the inverse of that matrix[3] whose kmth element γ_{km} is equal to $\boldsymbol{\Pi}_k \cdot \boldsymbol{K} \cdot \boldsymbol{\Pi}_m$. The increment of internal stress is then given by the equation

$$d\boldsymbol{\Sigma}_i = (\boldsymbol{I} - \boldsymbol{X}) \cdot \boldsymbol{J} \cdot d\boldsymbol{\Sigma} \qquad [10]$$

During slip in the external medium adjacent to the boundary, an increment of stress is transferred to the interior of the boundary. Let the increment of transferred stress be represented by the expression

$$\alpha \boldsymbol{J} \cdot d\boldsymbol{\Sigma} - \beta \boldsymbol{K} \cdot d\boldsymbol{\Pi}_s \qquad [11]$$

in which α, β are uniform scalars, and β is equal to unity when there is an average of three active slip systems per grain.

During slip in the polycrystal as a whole, the average of the internal stress $\boldsymbol{\Sigma}_i$ is equal to the external stress $\boldsymbol{\Sigma}$ if the increment of internal stress is given by the equation

$$d\boldsymbol{\Sigma}_i = (\boldsymbol{I} - \boldsymbol{X}) \cdot \boldsymbol{J} \cdot (\boldsymbol{I} - \overline{\boldsymbol{X}})^{-1} \cdot d\boldsymbol{\Sigma} \qquad [12]$$

The average $\overline{\boldsymbol{X}}$ of the tensor $\boldsymbol{X}$ is defined by the equation

$$\overline{\boldsymbol{X}} = \frac{1}{8\pi^2} \int\int\int \boldsymbol{H}^{-1} \cdot \boldsymbol{X} \cdot \boldsymbol{J} \cdot \boldsymbol{H} \sin\theta \, d\varphi \, d\theta \, d\chi \qquad [13]$$

in which the components of $\boldsymbol{X}$, $\boldsymbol{J}$ are referred to crystallographic axes. The increment of plastic strain is given by the equation

$$\boldsymbol{K} \cdot d\boldsymbol{\Pi}_s = -\frac{1}{(1-\beta)} \boldsymbol{X} \cdot \boldsymbol{J} \cdot (\boldsymbol{I} - \overline{\boldsymbol{X}})^{-1} \cdot d\boldsymbol{\Sigma} \qquad [14]$$

and becomes infinite as β approaches unity.

The internal stress $\boldsymbol{\Sigma}_i$ in a crystal with unit slip stress satisfies the equations

$$\boldsymbol{\Pi}_k \cdot \boldsymbol{\Sigma}_i = \pm 1 \qquad [15]$$

The plastic strain contributes, to the internal stress, a total stress which is a linear function of $\boldsymbol{K} \cdot \boldsymbol{\Pi}_m$.

If no slip has occurred in any slip system except the active slip systems, then Equations [15] lead to the equation

$$\boldsymbol{\Sigma}_i = \boldsymbol{\Sigma}_a + (\boldsymbol{I} - \boldsymbol{X}) \cdot \boldsymbol{J} \cdot \hat{\boldsymbol{J}} (\boldsymbol{I} - \overline{\boldsymbol{X}})^{-1} \cdot d\boldsymbol{\Sigma} \qquad [16]$$

in which $\boldsymbol{\Sigma}_a$ is defined by the equation

$$\boldsymbol{\Sigma}_a \equiv \gamma^{mk} \boldsymbol{K} \cdot \boldsymbol{\Pi}_m \boldsymbol{\Pi}_k \cdot \boldsymbol{\Sigma}_i = \boldsymbol{X} \cdot \boldsymbol{\Sigma}_i \qquad [17]$$

[3] The quantities γ_{km} and γ^{mk} are two-index scalar invariants.

and is a constant as long as the active slip systems remain constant.

If slip in any slip system has been discontinued, then $\boldsymbol{\Sigma}_a$ is replaced by a constant of integration in a finite interval which begins and ends with a change in the active slip systems.

The same slip systems are active in a range of orientation of the crystallographic axes. A slip system is active on one side and is inactive on the other side of each boundary of the range of orientation.

Proportional Variation of Stress. If the polycrystal is initially free of internal stress and the external stress $\boldsymbol{\Sigma}$ is proportional to a constant stress $\boldsymbol{\Sigma}_o$, then the condition for plastic flow is a unique function of the stress.

If the average number of active slip systems is nearly zero, slip is limited to slip systems with a maximum resolved shear stress. The largest difference between the principal components of $\boldsymbol{\Sigma}$ is given by the expression

$$\frac{2\sqrt{3}}{\sqrt{j_3^2 + 2(j_1 + j_3)^2}} \qquad [18]$$

and the limiting stress satisfies a Tresca (30) yield condition. The plastic strain is a pure shear.

If the average number of active slip systems could approach five, the ranges of orientation with five active slip systems would grow into large zones, and the ranges of orientation with four or less active slip systems would shrink into thin boundary regions. Wherever there are four active slip systems, the internal stresses $\boldsymbol{\Sigma}_i$ and $\boldsymbol{\Sigma}_a$ are linear combinations of two limiting stresses $\boldsymbol{\Sigma}_a'$ and $\boldsymbol{\Sigma}_a''$, which initiate slip in a fifth slip system, and the symmetric tensor $(\boldsymbol{I} - \boldsymbol{X}) \cdot \boldsymbol{J}$ is equivalent to the dyad

$$\frac{(\boldsymbol{\Sigma}_a' - \boldsymbol{\Sigma}_a'')(\boldsymbol{\Sigma}_a' - \boldsymbol{\Sigma}_a'')}{(\boldsymbol{\Sigma}_a' - \boldsymbol{\Sigma}_a'') \cdot (\boldsymbol{\Sigma}_a' - \boldsymbol{\Sigma}_a'')} \qquad [19]$$

Slipping in four active slip systems continues indefinitely if $\boldsymbol{\Sigma}$ satisfies the equation

$$(\boldsymbol{I} - \boldsymbol{X}) \cdot \boldsymbol{J} \cdot (\boldsymbol{I} - \overline{\boldsymbol{X}})^{-1} \cdot d\boldsymbol{\Sigma} = 0 \qquad [20]$$

The tensor $\boldsymbol{X}$ is equal to the tensor $\boldsymbol{I}$ everywhere except in the thin boundary regions where this equation is satisfied. The plastic strain $\boldsymbol{\Pi}_s$ is therefore the same for nearly all orientations and is collinear with $(\boldsymbol{I} - \overline{\boldsymbol{X}})^{-1} \cdot d\boldsymbol{\Sigma}$. The internal stress is equal to a constant stress $\boldsymbol{\Sigma}_a'$ or $\boldsymbol{\Sigma}_a''$ on either side of the boundary region. If the stress $\boldsymbol{\Sigma}_o$ were varied, the boundary would be shifted. The internal stress would be changed by $\boldsymbol{\Sigma}_a' - \boldsymbol{\Sigma}_a''$, in the range of variation of the boundary, and the external stress would be changed by an average of $\boldsymbol{\Sigma}_a' - \boldsymbol{\Sigma}_a''$, which is orthogonal to the plastic strain. The plastic strain is therefore the gradient of a von Mises (32) plastic potential. In the case of tension the average stress satisfies the equation

$$\boldsymbol{\Sigma} \cdot \boldsymbol{\Sigma} = 6.27 \text{ (tension)} \qquad [21]$$

and in the case of shear the average stress satisfies the equation

$$\boldsymbol{\Sigma} \cdot \boldsymbol{\Sigma} = 5.48 \text{ (shear)} \qquad [22]$$

The same results have been obtained by Bishop and Hill (23, 24).

Plastic States of a Face-Centered Cubic Crystal

Slip in a face-centered cubic crystal is limited to the 110 axes in the 111 planes. There are three 110 axes in each of four 111 planes. There are therefore twelve different slip systems in a face-centered cubic crystal. Expressions for the strain $\boldsymbol{\Pi}_m$ per unit slip strain and the rotation Θ_m per unit slip strain are given in Table 2.

If slip in a crystal with unit slip stress is limited to the $1\bar{1}0$ axis

TABLE 2 SLIP SYSTEMS IN FACE-CENTERED CUBIC CRYSTAL

System			$\sqrt{6}\,\Pi_m$						$\sqrt{6}\,\Theta_m$		
Code	Plane	Axis	σ_{11}	σ_{22}	σ_{33}	$2\sigma_{23}$	$2\sigma_{31}$	$2\sigma_{12}$	$2\theta_{23}$	$2\theta_{31}$	$2\theta_{12}$
A	111	$1\bar{1}0$	+1	−1	0	−1	+1	0	+1	+1	−2
B	111	$01\bar{1}$	0	+1	−1	0	−1	+1	−2	+1	+1
C	111	$\bar{1}01$	−1	0	+1	+1	0	−1	+1	−2	+1
D	$\bar{1}11$	$\bar{1}\bar{1}0$	+1	−1	0	−1	−1	0	+1	−1	+2
E	$\bar{1}11$	$01\bar{1}$	0	+1	−1	0	+1	−1	−2	−1	−1
F	$\bar{1}11$	101	−1	0	+1	+1	0	+1	+1	+2	−1
G	$1\bar{1}1$	110	+1	−1	0	+1	+1	0	−1	+1	+2
H	$1\bar{1}1$	$0\bar{1}\bar{1}$	0	+1	−1	0	−1	−1	+2	+1	−1
I	$1\bar{1}1$	$\bar{1}01$	−1	0	+1	−1	0	+1	−1	−2	−1
J	$\bar{1}\bar{1}1$	$\bar{1}10$	+1	−1	0	+1	−1	0	−1	−1	−2
K	$\bar{1}\bar{1}1$	$0\bar{1}\bar{1}$	0	+1	−1	0	+1	+1	+2	−1	+1
L	$\bar{1}\bar{1}1$	101	−1	0	+1	−1	0	−1	−1	+2	+1

in the 111 plane, then the components of stress have the following properties

$$\sigma_{11} - \sigma_{22} - \sigma_{23} + \sigma_{31} = \sqrt{6} \quad [23]$$

$$-\sqrt{6} < \sigma_{23} < 0 \quad [24]$$

$$0 < \sigma_{31} < +\sqrt{6} \quad [25]$$

$$0 < \sigma_{11} - \sigma_{22} < +\sqrt{6} \quad [26]$$

$$-\sqrt{6} + \sigma_{31} < \sigma_{22} - \sigma_{33} + \sigma_{12} < +\sqrt{6} - \sigma_{31} \quad [27]$$

$$-\sqrt{6} + \sigma_{31} < \sigma_{22} - \sigma_{33} - \sigma_{12} < +\sqrt{6} - \sigma_{31} \quad [28]$$

$$-\sqrt{6} - \sigma_{23} < \sigma_{33} - \sigma_{11} + \sigma_{12} < +\sqrt{6} + \sigma_{23} \quad [29]$$

$$-\sqrt{6} - \sigma_{23} < \sigma_{33} - \sigma_{11} - \sigma_{12} < +\sqrt{6} + \sigma_{23} \quad [30]$$

$$(\sigma_{22} - \sigma_{33}) + (\sigma_{33} - \sigma_{11}) \equiv -(\sigma_{11} - \sigma_{22}) \quad [31]$$

The possible ranges of stress may be investigated with the aid of a series of diagrams. Fig. 1 is a representative plot of σ_{23} versus σ_{31}, while Fig. 2 is a plot of σ_{12} versus $\sigma_{22} - \sigma_{33}$ superimposed on a plot of σ_{12} versus $\sigma_{33} - \sigma_{11}$. Any points in either figure which can represent the stress must fall within the dot-dash boundaries. For any point in Fig. 1, the points in Fig. 2 must also fall within the heavy boundaries. The points for multiple slip are located at the boundaries in the figures. The range of points for each level of multiplicity is bounded by points for a higher level of multiplicity.

The sum of the shear stresses on the three axes in any 111 plane is zero, and a linear combination of the shear stresses on the four axes in any 100 plane is zero. The twelve shear stresses are thus connected by seven independent linear equations and only five of the shear stresses are independent at one time.

The slip stress in any one slip system may be positive or negative. If the sum of any two shear stresses is equal to the slip stress, both shear stresses have the same sign as the slip stress. If the sum of any two shear stresses is equal to twice the slip stress, both shear stresses are equal to the slip stress. Not more than two shear stresses can be equal to the slip stress on any one 111 plane. If the shear stresses are equal to the slip stress on any three axes in one 100 plane, the shear stress on the fourth axis is also equal to the slip stress. Not more than eight shear stresses can be equal to the slip stress at any one time. These limitations greatly simplify the discovery of those sets of stresses which have six or eight shear stresses equal to the slip stress. The sets of stresses with lower levels of multiplicity can be found by matching pairs of sets to find the shear stresses which are common to both.

The plastic states which include slip on the $1\bar{1}0$ axis in the 111 plane have been located graphically and have been checked analytically. Only twenty three of these plastic states need to be analyzed in detail. The other states may be derived by cyclical permutations or reflections of the crystallographic axes. A representative set of states is given in Table 3. Letters without parentheses designate fundamental slip systems, whose shear stresses are linearly independent, while letters within parentheses designate incidental slip systems, whose shear stresses happen also to be equal to the slip stress.

If the analysis were repeated for each of the twelve slip systems there would be many duplications. For many of the states of

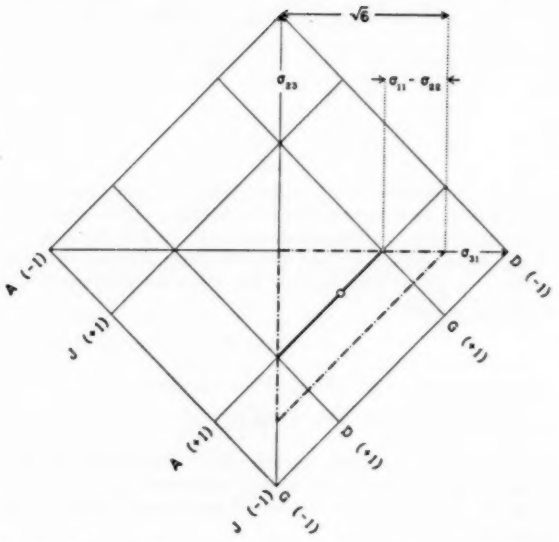

FIG. 1 POSSIBLE RANGE OF STRESS FOR SLIP ALONG THE $1\bar{1}0$ AXIS IN THE 111 PLANE

(○, Plot of σ_{23} versus σ_{31}. Fine lines mark maximum range without slip in each of slip systems A. . .J, [±1] is the slip stress. Dot-dash line marks maximum range for slip in slip system A without slip in any other slip system.)

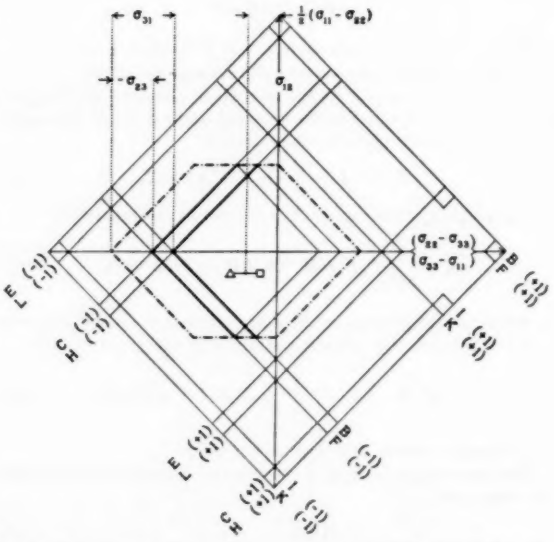

FIG. 2 POSSIBLE RANGE OF STRESS FOR SLIP ALONG THE $1\bar{1}0$ AXIS IN THE 111 PLANE

(Δ, Plot of σ_{12} versus $\sigma_{22} - \sigma_{33}$; □, plot of σ_{12} versus $\sigma_{33} - \sigma_{11}$. Fine lines mark maximum range for slip in each of slip systems B. . .L, [±1] is slip stress. Heavy lines mark limiting stress for double slip. Dot-dash line marks maximum range for slip in slip system A without slip in any other slip system.)

TABLE 3 REPRESENTATIVE PLASTIC STATES FOR FACE-CENTERED CUBIC CRYSTAL

A	AB	ABE	ABEF	ABEFG(I)
	AE	ABF	ABEG	ABEFJ(L)
	AG	ABG	ABEJ	AB(D)EG(H)J(K)
	AJ	AEG	ABGH	ACDFG(I)(J)(L)
		ADG(J)	AEGK	ACEFG(I)(K)(L)
		AFG(I)	AEFG(I)	
			ACFG(I)(L)	

TABLE 4 NUMBER OF PLASTIC STATES FOR FACE-CENTERED CUBIC CRYSTAL

Systems		States	
Fundamental	Incidental	Stress	Strain
1	0	12	12
2	0	66	66
3	0	120	120
3	1	15	60
4	0	72	72
4	1	24	96
4	2	12	144
5	1	16	72
5	3	12	312
Total		349	954

stress there is a multiplicity of states of strain. The numbers of independent states of stress and strain are listed in Table 4. The 28 states of stress with slip in five fundamental slip systems have been analyzed by Bishop and Hill (24), while the 384 states of strain with slip in five fundamental slip systems have been analyzed by Kochendörfer (33).

Plasticity of an Aggregate of Isotropic Crystals

Distribution of Plastic States. The general theory has so far been applied only to the special cases of tension and shear in an intrinsically isotropic polycrystal. The tensors $\boldsymbol{J}$ and $-\boldsymbol{K}$ can then be simplified to unity, and the tensor $(\boldsymbol{I} - \bar{\boldsymbol{A}})^{-1}$ can be replaced by a scalar $1 + \alpha$. The external stress $\boldsymbol{\Sigma}$ is proportional to the constant stress $\boldsymbol{\Sigma}_o$. The factor of proportionality is given in terms of a scalar ω by the equation

$$\boldsymbol{\Sigma} = \boldsymbol{\Sigma}_o \int \frac{d\omega}{1 + \alpha} \quad \ldots\ldots [32]$$

The internal stress is given in terms of ω by the equation

$$\frac{1}{\omega}(\boldsymbol{\Sigma}_i - \boldsymbol{\Sigma}_a) = (\boldsymbol{I} - \boldsymbol{X}) \cdot \boldsymbol{\Sigma}_o \quad \ldots\ldots [33]$$

The internal stress $\boldsymbol{\Sigma}_i$ is thus a linear function of ω in a finite interval. The same slip systems are active in a range of orientation which is bounded by the Eulerian angles where the shear stress is unity in an inactive slip system. The value of $1/\omega$ at each boundary of the range of orientation is a linear function of the components of $\boldsymbol{\Sigma}_o$ and is therefore also a linear harmonic function of the Eulerian angles χ, θ, φ. Each boundary is therefore located at the Eulerian angles where some function $Q(\chi, \theta, \varphi)$ is zero. The functions $Q(\chi, \theta, \varphi)$ happen to be linear harmonic functions of 2φ or 2θ, and the Eulerian angles at the boundary are related by an equation of the form

$$Q(\chi,\theta,\varphi) = Q_0(\chi,\theta) + Q_1(\chi,\theta) \sin 2\varphi + Q_2(\chi,\theta) \cos 2\varphi = 0 \quad \ldots\ldots [34]$$

or by an analogous equation in 2θ. The values of φ or θ at the boundary are given by the expression

$$-\frac{1}{2}\left(\sin^{-1}\frac{Q_0}{\sqrt{Q_1^2 + Q_2^2}} + \tan^{-1}\frac{Q_2}{Q_1}\right) \quad \ldots\ldots [35]$$

and it is thus possible to map out the range of orientations with the aid of a straightforward algorithm.

A total of forty-five boundaries must be analyzed in detail, while other boundaries may be derived by cyclical permutations and reflections of the crystallographic axes. The analysis is complicated by the fact that a few of the states with a high level of multiplicity actually may be unstable with respect to other states with a lower level of multiplicity. One or more shear stresses, which are equal to the slip stress in the unstable states, are reduced below the slip stress by slip in the stable states. The instability occurs only in a limited range of orientation of the crystallographic axes.

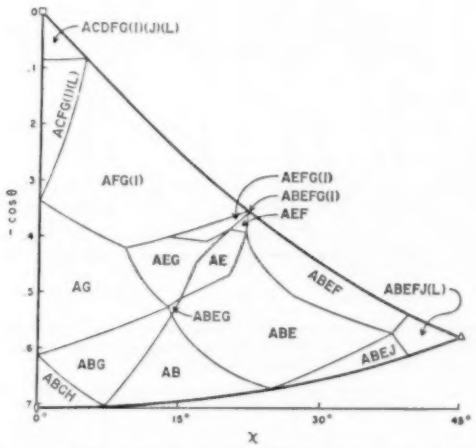

FIG. 3 MAP OF PLASTIC STATES FOR PLASTIC FLOW IN TENSION WITH EXTENSION IN z-AXIS

(□, ◇, △ are orientations of crystallographic axes when axis of tension coincides with 100, 101, 111 axes. Heavy line marks range of orientations in which slip system A is first system to slip.)

The plastic states are mapped as a function of orientation in Fig. 3 for plastic flow in tension. The plastic states AEF and AEFG(I) are unstable for large values of θ. The map of plastic states as a function of orientation is three-dimensional in the case of shear. The map has an axis of symmetry, and only half of the map need therefore be analyzed in detail. Sections through the map are illustrated in Figs. 4 to 6. The plastic states ABL, ACGH(L), and ABDF(K) are unstable for extreme values of φ.

The boundaries in the maps for a real polycrystal would be blurred by local variations in the environments of the grains.

In the plastic states A, AB, there is only one slip plane, while the plastic states with five active slip systems have three or four slip planes. The theory is thus in agreement with experimental determinations of the number of slip planes, in so far as there is only one slip plane for a finite range of orientations. An absence of slip bands at the free surface of a polycrystal may not be a reliable indication of the absence of slip in the interior of the polycrystal.

Other evidence of possible limitations on the formation of slip bands has been reported in the literature. The distribution of the orientations of slip bands on the surface of polycrystalline aluminum has been determined by Hedgepeth, Batdorf, and Sanders (34 to 36). The maximum angle between slip bands and the cross section of a tensile specimen was observed to be only 58 deg, whereas the maximum angle for a grain with a 111 axis in the axis of tension would be 70.53 deg. The spacing between slip bands on single crystals of aluminum have been studied by Honeycombe (45) and by Chen and Mathewson (45). The slip bands became clustered when the 111 axis or the 100 axis of the crystal was near the tension axis. The effect of surface condition has been studied by Brown and Honeycombe (50). The spacing between slip bands was wide where the surface was polished

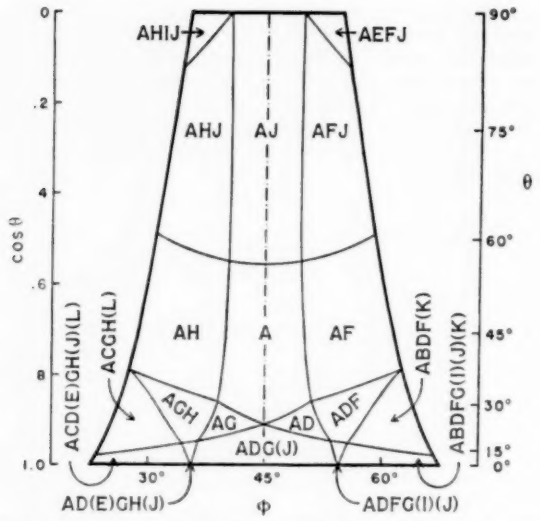

FIG. 4 SECTION AT $\chi = -45$ DEG THROUGH MAP OF PLASTIC STATES FOR PLASTIC FLOW IN SHEAR WITH EXTENSION IN x-AXIS AND CONTRACTION IN y-AXIS

(Dot-dash line marks an axis of symmetry. Heavy line marks range of orientations in which slip system A is first system to slip.)

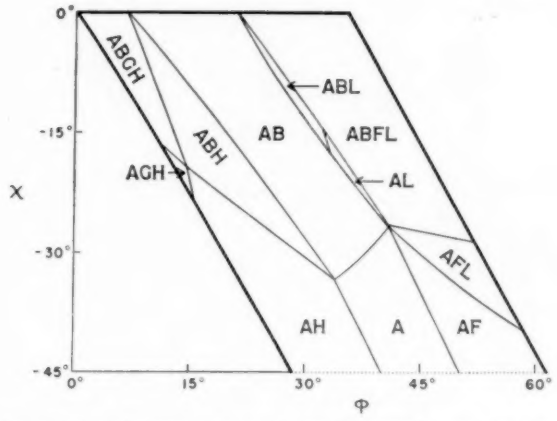

FIG. 5 HALF SECTION AT $\theta = 45$ DEG THROUGH MAP OF PLASTIC STATES FOR PLASTIC FLOW IN SHEAR

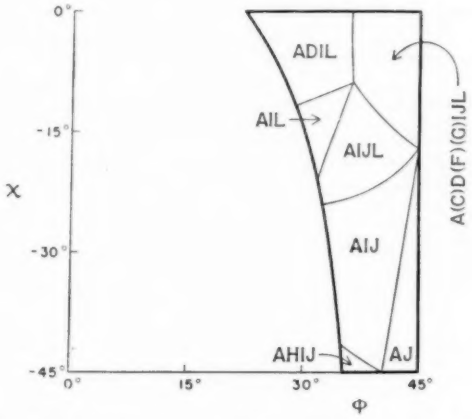

FIG. 6 HALF SECTION AT $\theta = 90$ DEG THROUGH MAP OF PLASTIC STATES FOR PLASTIC FLOW IN SHEAR

mechanically and was narrow where the surface was polished electrolytically. Hardening of an aluminum crystal without the formation of slip bands has been reported by Heidenreich, Roros, and Shockley (51, 52), and elementary slip lines between the visible slip bands have been detected by Kuhlmann-Wilsdorf, van der Merwe, and Wilsdorf (53) in electron micrographs.

Stress for Plastic Flow. The theoretical stress for plastic flow has been calculated for the case of tension, where the average stress satisfies the equation

$$\Sigma\cdot\Sigma = 5.34 \text{ (tension)} \quad [36]$$

and for the case of shear, where the average stress satisfies the equation

$$\Sigma\cdot\Sigma = 4.99 \text{ (shear)} \quad [37]$$

The plastic work $\Sigma\cdot\Pi$ and the average of $|s_m|$ for the same strain are not equal as a result of local distortion of the grains near the grain boundaries.

Values[4] of the plastic work are given by the following:

Strain	$\Sigma\cdot\Pi$	$\overline{\lvert s_m \rvert}$
Elongation	2.83	2.59
Shear	2.74	2.61

for an elongation equal to unity and for a shear equal to $\sqrt{3}$.

Experimental comparisons between the stresses for plastic flow in single crystals and in polycrystals of the same metal have been made by Elam (5, 7) and by Karnop and Sachs (10). Representative values of the uniaxial stress in the polycrystal per unit slip stress in the single crystals have been calculated on the assumption that the work hardening can be expressed as a function of the amount of plastic work. The experimental values are larger than the theoretical value. This discrepancy may be the result of differences in the distribution of imperfections in the crystals.

Other examples of possible effects of structure have been reported in the literature. The elastic limit of aluminum has been measured by Sugihara (54) and the hardness of copper has been measured by Angus and Summers (55). Both the elastic limit and the hardness increased linearly with increase in the reciprocal of the grain size. Different stress-strain curves for cast or recrystallized single crystals of aluminum have been reported by Dehlinger and Gisen (56, 57). Slip on slip bands in single crystals is so heterogeneous that the crystals may become divided into deformation bands which have been studied by Barrett and Levenson (37). Primary slip, primary cross slip, secondary slip, and secondary cross slip may all be stimulated in different parts of the same crystal, as several investigators (41 to 45) have observed in alpha-brass and aluminum. The critical slip stress may vary (10 to 15) with the orientation of the crystallographic axes in a range of orientation. The slip stress is a maximum when the 111 axis or the 100 axis is in the axis of tension. Slip in especially thin crystals of aluminum has been studied by Wu and Smoluchowski (58). The critical slip stress was proportional to the path of slip through the crystals. Slip in slip bands is blocked by kink bands which have been studied in aluminum by Collins and Mathewson (40) and by numerous other investigators (43 to 49). Slip in slip bands is blocked by grain boundaries to an extent which has been illustrated by Lacombe and Beaujard (59).

Representative values of the stresses for plastic flow in poly-

[4] Bishop and Hill's values are 3.06 for elongation and 2.86 for shear.

crystals have been selected from the literature (60 to 64). The triaxial stresses after equal amounts of plastic work have been reduced proportionately by such an amount as to reduce the uniaxial stress to the theoretical value for a unit slip stress. The plotted values of the principal stresses σ_1, σ_2, σ_3 in a three-dimensional diagram are projected on an octahedral plane in Fig. 7. The Tresca (30) yield condition is represented in such a figure by a hexagon, and the von Mises (31) yield condition is represented by a circle. That the experimental data deviate by a perceptible amount from a circle was observed by Lode (60).

The scalar invariants in the three-dimensional stress tensor have been used by Drucker (65) in a function of the sixth degree to correlate the stress-strain curves. The experimental relationship between increments of the principal strains and the principal stresses has been integrated by Taylor (66) to obtain a von Mises plastic potential. A power law has been used by Bailey (67) to express the relationship between increments of the principal strains and the principal stresses. An exponent of four in the power law has been found by Davis (62) to be in good agreement with the experimental data. The power law is collinear with the gradient of a von Mises plastic potential of the form

$$|\sigma_2 - \sigma_3|^n + |\sigma_3 - \sigma_1|^n + |\sigma_1 - \sigma_2|^n \ldots\ldots\ldots [38]$$

in which the exponent $n = 5$. This plastic potential correlates the Tresca yield condition, for which $n = \infty$, with the von Mises yield condition, for which $n = 2$. The present theory is consistent with $n = 6$ and is supported by the experimental data in Fig. 7.

Growth of Preferred Orientations. If the co-ordinates of orientation χ, $\cos\theta$, φ of a large number of grains in an isotropic polycrystal were plotted in a three-dimensional Cartesian diagram, the density of points in the diagram would be initially uniform. Each point would be displaced by a vector with components $\Delta\chi$, $\Delta\cos\theta$, $\Delta\varphi$ during an increment of strain. In the limiting case of a small strain, the components are given by the equations

$$\Delta\chi = -(\theta_{23}\cos\chi - \theta_{31}\sin\chi)\cot\theta - \theta_{12} \ldots\ldots [39]$$

$$\Delta\cos\theta = +(\theta_{23}\sin\chi + \theta_{31}\cos\chi)\sin\theta \ldots\ldots [40]$$

$$\Delta\varphi = +(\theta_{23}\cos\chi - \theta_{31}\sin\chi)\csc\theta \ldots\ldots [41]$$

The density of points is changed within each zone of the map of plastic states by an amount which is proportional to the divergence of the displacement of the points. The density may change instantaneously by severalfold along a boundary between zones where the displacement is discontinuous. The change of density at the boundary is in a band which grows in width as the strain increases.

The displacement for a 10 per cent elongation in tension is plotted in Fig. 8. In the orientations where there are incidental slip systems, two or more states occur with divergent directions of rotation. The multiplicity occurs in about the same range of orientation as Barrett and Levenson (37) have observed deformation bands in polycrystalline aluminum.

The theory leads to a stable orientation during compression when the axis of compression is in a 110 axis and leads to a stable orientation at

$$\chi = 0°,\ \theta = 45°,\ \varphi = 27.37°$$

during shear with extension in the x-axis and contraction in the y-axis. The orientations congregate quickly in a band which contains the stable orientation, and then the orientations move more slowly along the band as the strain increases. Stereographic projections of the approximate location of the bands are illustrated in Fig. 9. Analogous bands have been found experimentally by Barrett and Levenson (37 to 39) in the case of compression and by

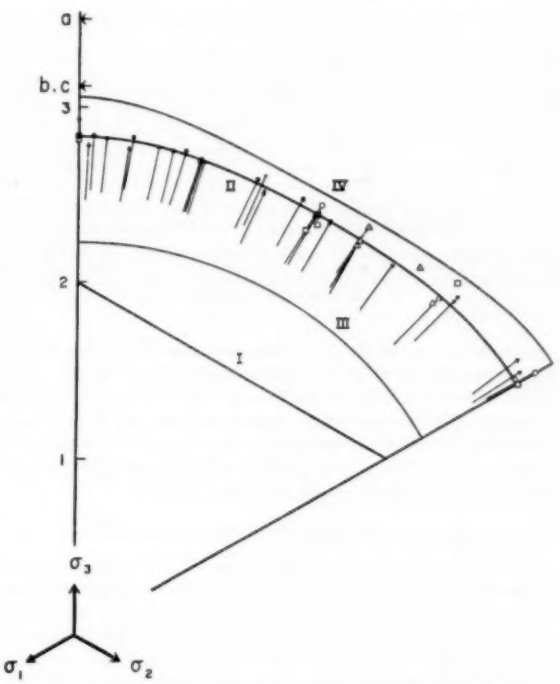

FIG. 7 COMPARISON OF STRESSES FOR PLASTIC FLOW

(Projection on octahedral plane of three-dimensional Cartesian plot of principal stresses σ_1, σ_2, σ_3. Curve I, plastic potential for initiation of slip [Tresca (30), $n = \infty$]; Curve II, plastic potential for plastic flow [$n = 6$]; Curve III, plastic potential for free crystals [von Mises (31), Sachs (16), $n = 2$]; Curve IV, plastic potential for five active slip systems [Bishop and Hill (24)]. Experimental stress in a polycrystal for unit slip stress in a single crystal of same metal [Al] from measurements by: *a*, Elam (5, 7); *b*, Karnop and Sachs (10). Theoretical stress from calculations by: *c*, Taylor (7). Experimental triaxial stresses for same uniaxial stress from measurements by: Δ[Cu], ○[Ni], Lode (60); ▲[Cu], ■[Al], Taylor and Quinney (61); ▼[Cu], Davis (62); □[24S-T Al], Osgood (63), Marin and Kotalik (64). Tails attached to symbols represent increments of plastic strain.)

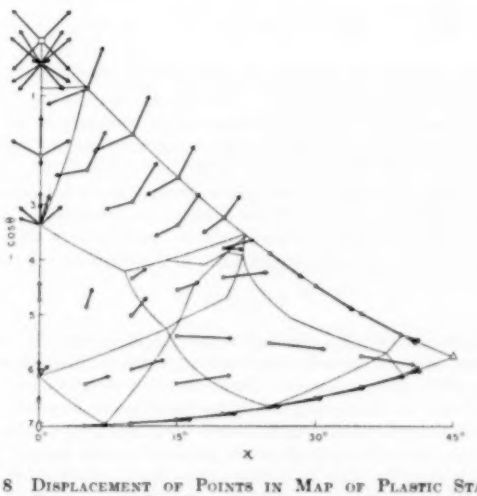

FIG. 8 DISPLACEMENT OF POINTS IN MAP OF PLASTIC STATES DURING A 10 PER CENT ELONGATION IN TENSION

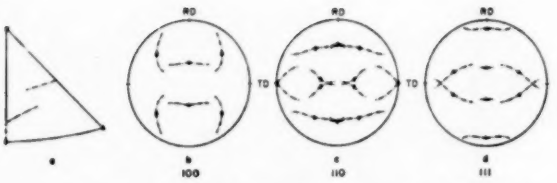

FIG. 9 CENTER LINES OF BANDS IN WHICH ORIENTATIONS OF CRYSTALLOGRAPHIC AXES TEND TO CONGREGATE

(Stereographic projections of: a, axis of compression; b, c, d, the 100, 110, 111 axes in shear; ■, ◆, ▲, theoretically stable orientations. Axes of shear in rolled metals are oriented by RD, the rolling direction and by TD, the transverse direction.)

von Göler and Sachs (68, 69) in the case of shear. Consistent data also have been obtained by other investigators (70 to 72). The bands of preferred orientation during shear are rotated through an angle of 17.63 deg or less during torsion, and they have a somewhat symmetric distribution with respect to the plane of shear. The preferred orientation has been measured experimentally by Backofen (73) in the case of torsion.

RESIDUAL STRESSES BY X-RAY DIFFRACTION

The release of external stress is known (74) to leave a residual internal stress which varies with the orientation of the crystallographic axes. The presence of the residual stress is revealed by x-ray diffraction measurements of the strain between selected lattice planes. The average residual stress has been calculated from the stress difference $\Sigma_i - \Sigma$ for all orientations in which the 100, 110, 111 axes are perpendicular to the axis of tension. The residual strain $\bar{\epsilon}$, which would be determined by x rays in a polycrystal with intrinsic elastic isotropy and unit slip stress, is tabulated in Table 5.

TABLE 5 COMPARISON BETWEEN X-RAY MEASUREMENTS OF RESIDUAL STRAINS REPORTED BY GREENOUGH AND THEORETICAL RESIDUAL STRAINS FOR AN INTRINSICALLY ISOTROPIC POLYCRYSTAL WITH UNIT SLIP STRESS

Diffracting planes	$(10^6) \times$ (measured strains) Al	Cu	Ni	$\frac{\bar{\epsilon}}{(\sigma_{11} - \sigma_{12})}$	Strain axis
400	+8	+6		+0.509	100
511	+7				
311	+8	+4	−1		
422	+5	+2			
222	−3	−1	−11	−0.480	111
331	0	−1	−3		
330				−0.124	110
420	+5		+3		
400	+8	+6		+0.509	100

The residual strains in a few metals after tension have been measured by Greenough (75). The normals of all of the diffracting planes happened to be located on the boundary of the unit triangle in the map of plastic states, and the data are therefore arranged in Table 5 in serial order for a circuit around the boundary. The theoretical and experimental values show the same trend of variation. If the theory were corrected for anisotropy, the theoretical values would be corrected in the right direction to make them proportional to the experimental values.

CONCLUSION

Although there is a qualitative agreement between the experimental data and the theoretical analysis, a quantitative comparison cannot be made because of differences in the materials which are involved. An interesting test of the theory would be provided by the discovery of abrupt variations in the intensity of a diffraction pattern where discontinuities are predicted by the theory. Such details may, however, be scattered and lost by the local fluctuations in the environment of the grains.

ACKNOWLEDGMENT

The author is indebted to Miss T. E. Haislip, Mrs. V. L. Nichols, and Mr. J. M. Foster who performed the bulk of the computations for this paper. The work is part of a research program for the Bureau of Ordnance, U. S. Navy Department.

BIBLIOGRAPHY

1 "Distortion of an Aluminum Crystal During a Tensile Test," by G. I. Taylor and C. F. Elam, Proceedings of the Royal Society, London, England, series A, vol. 102, 1923, p. 643.

2 "The Plastic Extension and Fracture of Aluminum Crystals," by G. I. Taylor and C. F. Elam, Proceedings of the Royal Society, London, England, series A, vol. 108, 1925, p. 28.

3 "The Distortion of Crystals of Aluminum Under Compression," by G. I. Taylor and W. S. Farren, Proceedings of the Royal Society, series A, vol. 111, 1926, p. 529; G. I. Taylor, Proceedings of the Royal Society, London, England, series A, vol. 116, 1927, p. 16.

4 "Tensile Tests of Large Gold, Silver, and Copper Crystals," by C. F. Elam, Proceedings of the Royal Society, London, England, series A, vol. 112, 1926, p. 289.

5 "Experiments on the Distortion of Single Crystal Test Pieces of Aluminum," by H. C. H. Carpenter and C. F. Elam, Proceedings of the Royal Society, London, England, series A, vol. 107, 1925, p. 171.

6 "Analysis of Plastic Strain in a Cubic Crystal" by G. I. Taylor, Stephen Timoshenko 60th Anniversary Volume, The Macmillan Company, New York, N. Y., 1938, p. 218.

7 "Plastic Strain in Metals," by G. I. Taylor, *Journal of the Institute of Metals*, vol. 62, 1938, p. 307. Cf. reference 18.

8 "On the Temperature Dependence of Crystal Plasticity," by W. Boas and E. Schmid, *Zeitschrift für Physik*, vol. 71, 1931, p. 703.

9 "A Study of the Plastic Behavior of High Purity Aluminum Single Crystals at Various Temperatures," by F. D. Rosi and C. H. Mathewson, *Journal of Metals*, vol. 188, 1950, p. 1159.

10 "The Behavior of Aluminum Crystals in the Tension Test," by R. Karnop and G. Sachs, *Zeitschrift für Physik*, vol. 41, 1927, p. 116.

11 "Influence of Temperature on Elastic Limit of Single Crystals of Aluminum, Silver, and Zinc," by R. F. Miller and W. E. Milligan, Trans. AIME, vol. 124, 1937, p. 229.

12 "Mechanical Recovery of Aluminum Single Crystals," by G. Masing and J. Raffelsieper, *Zeitschrift für Metallkunde*, vol. 41, 1950, p. 65.

13 "Recent Results on the Hardening of Crystals by Plastic Deformation," by F. Röhm and A. Kochendörfer, *Zeitschrift für Metallkunde*, vol. 41, 1950, p. 265; cf. discussion by W. T. Read, "A Symposium on the Plastic Deformation of Crystalline Solids," Carnegie Institute of Technology and Office of Naval Research, May, 1950, p. 111.

14 "On the Form of the Strain-Hardening Curve of Super Pure Aluminum Crystals and the Formation of Deformation Bands," by K. Lücke and H. Lange, *Zeitschrift für Metallkunde*, vol. 43, 1952, p. 55.

15 "Contribution to the Study of the Form of the Tension Curves of Metals and to Its Physical Interpretation," by C. Crussard and B. Jaoul, *Revue de Metallurgie*, vol. 47, 1950, p. 589.

16 "On the Derivation of a Condition for Flow," by G. Sachs, *Zeitschrift, VDI*, vol. 72, 1928, p. 734. Cf. references 17 and 18.

17 "Effect of Orientation on Stresses in Single Crystals, and of Random Orientation on Strength of Polycrystalline Aggregates," by H. L. Cox and D. G. Sopwith, Proceedings of the Physical Society, London, England, vol. 49, 1937, p. 134.

18 "Influence of Grain Boundaries on the Plastic Properties of Metals," by F. R. N. Nabarro, Some Recent Developments in Rheology, United Trade Press, Ltd., London, England, 1950, p. 38.

19 "A Mathematical Theory of Plasticity Based on the Concept of Slip," by S. B. Batdorf and B. Budiansky, NACA Technical Note No. 1871, April, 1949.

20 "Deformation Textures in Face-Centered Cubic Metals," by E. A. Calnan and C. J. B. Clews, *Philosophical Magazine*, vol. 41, 1950, p. 1085.

21 "The Interpretation of Deformation Textures of Metals," by W. Boas and E. Schmid, *Zeitschrift für Technische Physik*, vol. 12, 1931, p. 71.

22 "On the Effective Range of Stress Hardening," by A. Slibar and F. Vitovec, *Schweizer Archiv für angewandte Wissenschaft und Technik*, vol. 16, 1950, p. 80.

23 "A Theory of the Plastic Distortion of a Polycrystalline Aggregate Under Combined Stresses," by J. F. W. Bishop and R. Hill, *Philosophical Magazine*, vol. 42, 1951, p. 414.

24 "A Theoretical Derivation of the Plastic Properties of a

Polycrystalline Face-Centered Metal," by J. F. W. Bishop and R. Hill, *Philosophical Magazine*, vol. 42, 1951, p. 1298.

25 "The Tensile Deformation of Large Aluminum Crystals at Crystal Boundaries," by R. L. Aston, Proceedings of the Cambridge Philosophical Society, Cambridge, England, vol. 23, 1926, p. 549.

26 "On the Inhomogeneity of Plastic Deformation in the Crystals of an Aggregate," by W. Boas and M. E. Hargreaves, Proceedings of the Royal Society, London, England, series A, vol. 193, 1948, p. 89.

27 "Inhomogeneity of Plastic Deformation in Metals," by W. Boas, *Helvetica Physica Acta*, vol. 23, 1950, p. 159.

28 "The Interaction Between Crystals of an Aggregate During Plastic Deformation," by W. Boas, Proceedings of the 7th International Congress of Applied Mechanics, vol. 1, 1948, p. 356.

29 "The Elasticity of an Isotropic Aggregate of Anisotropic Cubic Crystals," by A. V. Hershey, published in this issue, pp. 236–240.

30 "Memoir on the Flow of Solid Bodies Under Strong Pressure," by H. Tresca, C. R. Academy of Science, Paris, France, vol. 59, 1864, p. 754.

31 "Mechanics of Solid Bodies in the Plastic Deformable State," by R. von Mises, Nachrichten von der Gesellschaft der Wissenschaften zu Göttingen, Mathematisch-Physikalische Klasse, 1913, p. 582.

32 "Mechanics of the Plastic Deformation of Crystals," by R. von Mises, *Zeitschrift für angewandte Mathematik und Mechanik*, vol. 8, 1928, p. 161.

33 "Plastische Eigenschaften von Kristallen und Metallischen Werkstoffen," by A. Kochendörfer, Julius Springer, Berlin, Germany; Edwards Bros., Inc., Ann Arbor, Mich., 1941, p. 284.

34 "A Study of Slip Formation in Polycrystalline Aluminum," by A. E. Johnson, Jr., and S. B. Batdorf, NACA Technical Note 2576, December, 1951.

35 "On the Angular Distribution of Slip Lines in Polycrystalline Aluminum Alloy," by J. M. Hedgepeth, S. B. Batdorf and J. L. Sanders, Jr., NACA Technical Note 2577, December, 1951.

36 "Theoretical Distribution of Slip Angles in an Aggregate of Face-Centered Cubic Crystals," by J. M. Hedgepeth, NACA Technical Note 2777, August, 1952.

37 "The Structure of Aluminum After Compression," by C. S. Barrett and L. H. Levenson, Trans. AIME, vol. 137, 1940, p. 112.

38 "Recrystallization Texture of Aluminum After Compression," by C. S. Barrett, Trans. AIME, vol. 137, 1940, p. 128.

39 "Structure of Metals," by C. S. Barrett, McGraw-Hill Book Company, Inc., New York, N. Y., 1943, p. 386.

40 "Plastic Deformation and Recrystallization of Aluminum Single Crystals," by J. A. Collins and C. H. Mathewson, Trans. AIME, vol. 137, 1940, p. 150.

41 "The Active Slip Systems in the Simple Axial Extension of Single Crystalline Alpha Brass," by R. Maddin, C. H. Mathewson, and W. R. Hibbard, *Journal of Metals*, vol. 1, 1949, p. 527.

42 "Particular Aspects of Slipping Produced by Alternating Stress in Annealed Aluminum Crystals," by P. H. Laurent, *Revue de Metallurgie*, vol. 48, 1951, p. 441.

43 "Slip and Polygonization in Aluminum," by R. W. Cahn, *Journal of the Institute of Metals*, vol. 79, 1951, p. 129.

44 "Inhomogeneities in the Plastic Deformation of Metal Crystals," by R. W. K. Honeycombe, *Journal of the Institute of Metals*, vol. 80, 1951, p. 45.

45 "Structural Studies of Plastic Deformation in Aluminum Single Crystals," by N. K. Chen and C. H. Mathewson, *Journal of Metals*, vol. 3, 1951, p. 653; cf. discussion by E. A. Calnan, H. Wilsdorf, D. Kuhlmann-Wilsdorf, and R. R. Hasiguti, *Journal of Metals*, vol. 4, 1952, p. 526.

46 "The Mechanical Behavior of Single Crystals of Certain Face-Centered Cubic Metals," by E. N. da C. Andrade and C. Henderson, Philosophical Transactions of the Royal Society, series A, vol. 244, 1951, p. 177.

47 "X-Ray Asterisms From Deformed Crystals," by P. Gay and R. W. K. Honeycombe, Proceedings of the Physical Society, series A, vol. 64, 1951, p. 844.

48 "A Study of Cold-Worked Aluminum by an X-Ray Micro-Beam Technique," by P. B. Hirsch and J. N. Kellar, *Acta Crystallographica*, vol. 5, 1952, p. 162; P. B. Hirsch, *Acta Crystallographica*, vol. 5, 1952, pp. 168 and 172.

49 "Extent of Strain of Primary Glide Planes in Extended Single Crystalline Alpha Brass," by R. Middin, *Journal of Metals*, vol. 4, 1952, p. 270.

50 "Microslip in Metal Crystals," by A. F. Brown and R. W. K. Honeycombe, *Philosophical Magazine*, vol. 42, 1951, p. 1146.

51 "Study of Slip in Aluminum Crystals by Electron Microscope and Electron Diffraction Methods," by R. D. Heidenreich and W. Shockley, Report on a Conference on Strength of Solids, The Physical Society, London, England, 1948, p. 57.

52 "Solid State Physics in Electronics and in Metallurgy," by W. Shockley, *Journal of Metals*, vol. 4, 1952, p. 829.

53 "Elementary Structure and Slip Band Formation in Aluminum," by D. Kuhlmann-Wilsdorf, J. H. van der Merwe, and H. Wilsdorf, *Philosophical Magazine*, vol. 43, 1952, p. 632.

54 "Elastic Limit of an Aluminum Rod and the Size of the Crystal Grains," by M. Sugihara, Memoirs of the College of Science, Kyoto Imperial University, vol. A20, 1937, p. 173.

55 "The Effect of Grain Size Upon Hardness and Annealing Temperature," by H. T. Angus and P. F. Summers, *Journal of the Institute of Metals*, vol. 33, 1925, p. 115.

56 "Plasticity and Mosaic Structure in Cast and in Recrystallized Metals," by U. Dehlinger and F. Gisen, *Physikalische Zeitschrift*, vol. 35, 1934, p. 862.

57 "Differing Behavior of Cast and Recrystallized Single Crystals of Aluminum of Various Degrees of Purity," by F. Gisen, *Zeitschrift für Metallkunde*, vol. 27, 1935, p. 256.

58 "A New Criterion for the Occurrence of Slip in Thin Single Crystals," by T. L. Wu and R. Smoluchowski, *Physical Review*, vol. 78, 1950, p. 468.

59 "The Application of Etch Figures on Pure Aluminum to the Study of Some Micrographic Problems," by P. Lacombe and L. Beaujard, *Journal of the Institute of Metals*, vol. 74, 1947, p. 1.

60 "The Influence of the Middle Principal Stress on the Flow of Metals," by W. Lode, *Forschungsarbeiten, VDI*, vol. 303, 1928, p. 1.

61 "The Plastic Distortion of Metals," by G. I. Taylor and H. Quinney, Philosophical Transactions of the Royal Society, London, England, vol. 230, 1931, p. 323.

62 "Increase of Stress With Permanent Strain and Stress-Strain Relations in the Plastic State for Copper Under Combined Stresses," by E. A. Davis, JOURNAL OF APPLIED MECHANICS, Trans. ASME, vol. 65, 1943, p. A-187.

63 "Combined Stress Tests on 24S-T Aluminum Alloy Tubes," by W. R. Osgood, JOURNAL OF APPLIED MECHANICS, Trans. ASME, vol. 69, 1947, p. A-147.

64 "Plastic Biaxial Stress-Strain Relations for Alcoa 24S-T Subjected to Variable Stress Ratios," by J. Marin and B. J. Kotalik, JOURNAL OF APPLIED MECHANICS, Trans. ASME, vol. 72, 1950, p. 372.

65 "Relation of Experiments to Mathematical Theories of Plasticity," by D. C. Drucker, Trans. ASME, vol. 71, 1949, pp. 349–357.

66 "A Connection Between the Criterion of Yield and the Strain Ratio Relationship in Plastic Solids," by G. I. Taylor, Proceedings of the Royal Society, London, England, series A, vol. 191, 1947, p. 441.

67 "The Utilization of Creep Test Data in Engineering Design," by R. W. Bailey, Proceedings of The Institution of Mechanical Engineers, London, England, vol. 131, 1935, p. 131.

68 "Rolling and Recrystallization Texture of Regular Face-Centered Metals," by F. von Göler and G. Sachs, *Zeitschrift für Physik*, vol. 41, 1927, p. 873.

69 "Rolling and Recrystallization Texture of Regular Face-Centered Metals," by F. von Göler and G. Sachs, *Zeitschrift für Physik*, vol. 56, 1929, p. 477.

70 "Structure of Copper After Rolling," by C. S. Barrett and F. W. Steadman, Trans. AIME, vol. 147, 1942, p. 57.

71 "Texture of Rolled Alpha Brass," by W. Iweronowa and G. Schdanow, Tech. Phys. USSR, vol. 1, 1934, p. 64.

72 "Rolling Textures in Face-Centered Cubic Metals," by H. Hu, P. R. Sperry, and P. A. Beck, *Journal of Metals*, vol. 4, 1952, p. 76.

73 "Torsion Texture of Copper," by W. A. Backofen, *Journal of Metals*, vol. 188, 1950, p. 1454.

74 "Internal Strains in Cold-Wrought Metals and Some Troubles Caused Thereby," by E. Heyn, *Journal of the Institute of Metals*, vol. 12, 1914, p. 3.

75 "Residual Lattice Strains in Plastically Deformed Polycrystalline Metal Aggregates," by G. B. Greenough, Proceedings of the Royal Society, London, England, series A, vol. 197, 1949, p. 556.

Experimental Measurement of Mechanical Impedance or Mobility

By R. PLUNKETT,[1] SCHENECTADY, N. Y.

A device for the experimental measurement of mechanical impedance as a function of frequency is described. The measured values for two systems are shown. It is also shown that the performance of a modified system may be predicted in some respects. These measurements show that this function is extremely complex and that the systems are very limber at audio frequencies.

Nomenclature

The following nomenclature is used in the paper:

E = Young's modulus

g = acceleration of gravity, 386 in/sec^2

$j = \sqrt{-1}$

m = mass

$Z = \dfrac{v}{F}$ = mobility

ω = frequency, radians per sec

Introduction

The concept of mechanical mobility or its inverse, impedance, has been used for some years in the calculation of the response of vibratory systems (1, 2, 3, 4, 6).[2] The computation quickly becomes difficult as the complexity increases. The same computational methods may be used in discussing the effects of changes and combinations of complex systems if the mobility is experimentally measured. A start in this direction was made by Muster (6), who found very peculiar effects in the transmissibility of vibration isolation mounts at audio frequencies. However, Muster measured transmissibility, which is not mobility directly, although closely related to it.

The Impedance Head

The principles of this measurement are relatively simple. Apply a sinusoidal vibratory force of known frequency to a point in a structure, measure the resulting velocity and its phase with the force, and plot the ratio of velocity to force as a function of frequency. Some preliminary tests indicated considerable practical difficulties. The first was to get a satisfactory force gage, one which would have satisfactory sensitivity without being so flexible it would be hard to drive. The measurement of velocity was not so difficult; almost any commercial self-generating vibration pickup with a suitable frequency range would do.

It was first thought that the application of sufficient force would be difficult, but it was soon found that very little force was required; i.e., the mobility of most mechanical systems is relatively high.

A barium-titanate ceramic transducer was designed as a force gage and proved very satisfactory, being very stiff (E = 15,000,000 psi) and having relatively large sensitivity in compression (approximately 0.1 volt per lb for a 2-in-square piece $^3/_8$ in. thick). The first measurements were taken with this force gage driven by an electromagnetic vibration motor; the velocity was measured with a vibration pickup mounted as close to the force gage as possible. These measurements on a relatively massive foundation indicated that the pickup could not be located as much as 2 in. away from the force gage at 1000 cps without serious error in the measured values.

In addition, it was found that the vibration pickup must be fastened down securely to follow vibrations of this frequency. Hand pressure was not satisfactory above about 200 cycles per sec (cps), and a magnetic stand was not satisfactory above 1000 cps even when the surface was prepared carefully. A relatively large acceleration (1 g or 386 in/sec^2) at 1000 cps represents only a small displacement (10 microin.); this is comparable to surface roughness, which means that both the pickup and force gage must be pressed firmly against the surface to eliminate relative movement. All of these considerations led to the development of a device which could be attached securely by means of a stud, and screwed down firmly against a shoulder with a large pressure.

An accelerometer is basically simpler than a velocity pickup and has a higher top-frequency limit. While it is possible to build an integrating circuit to convert acceleration readings to velocity, it is not worthwhile for an impedance head which works on single frequency signals. Thus, it was decided to measure the acceleration for a unit force (1 lb) and plot this as a function of frequency on the proper graph paper, Fig. 1, from which the velocity per unit force (mobility) would be read directly.

The preliminary tests indicated the necessary range of frequency and mobility to be covered. For the time being, it was decided to work in the frequency range from 10 cps to 3000 cps with the possibility of going to 10,000 cps in the future. Since all the measured mobilities, so far, have fallen in the range from 0.001 to 10 in/sec per lb and forces from 0.1 to 10 lb have proved adequate for driving, acceleration measurements from 0.001 g to 10 g cover most of the range, Fig. 1. Using a force of 10 lb drops the lower limit by a factor of 10, and a force of 0.1 lb raises the upper limit by a factor of 10 in terms of a unit force (dashed lines 0.0001 and 100 g). A further physical limit of 1 microin. and 0.01 in. seemed reasonable, which would be expanded by a factor of 10 at each end by changing the driving force (dash-dot lines). Thus, the shaded portion gives the useful range of measurements.

This can be done with a sensitivity of 0.5 volt/g for the accelerometer, since 1 millivolt is a comparatively easy measurement in this frequency range. Likewise, a sensitivity of 0.03 volt/lb is adequate for the force gage.

A cross section of the complete unit is shown in Fig. 2. All of the major components have a circular cross section. The bottom ④ is drilled and tapped for a $^1/_4$-28 stud and is screwed down

---

[1] Engineer, General Engineering Laboratory, General Electric Company. Assoc. Mem. ASME.

[2] Numbers in parentheses refer to the Bibliography at the end of the paper.

Contributed by the Applied Mechanics Division and presented at the Annual Meeting, New York, N. Y., November 29–December 4, 1953, of The American Society of Mechanical Engineers.

Discussion of this paper should be addressed to the Secretary, ASME, 29 West 39th Street, New York, N. Y., and will be accepted until October 11, 1954, for publication at a later date. Discussion received after the closing date will be returned.

Note: Statements and opinions advanced in papers are to be understood as individual expressions of their authors and not those of the Society. Manuscript received by ASME Applied Mechanics Division, February 7, 1953. Paper No. 53—A-45.

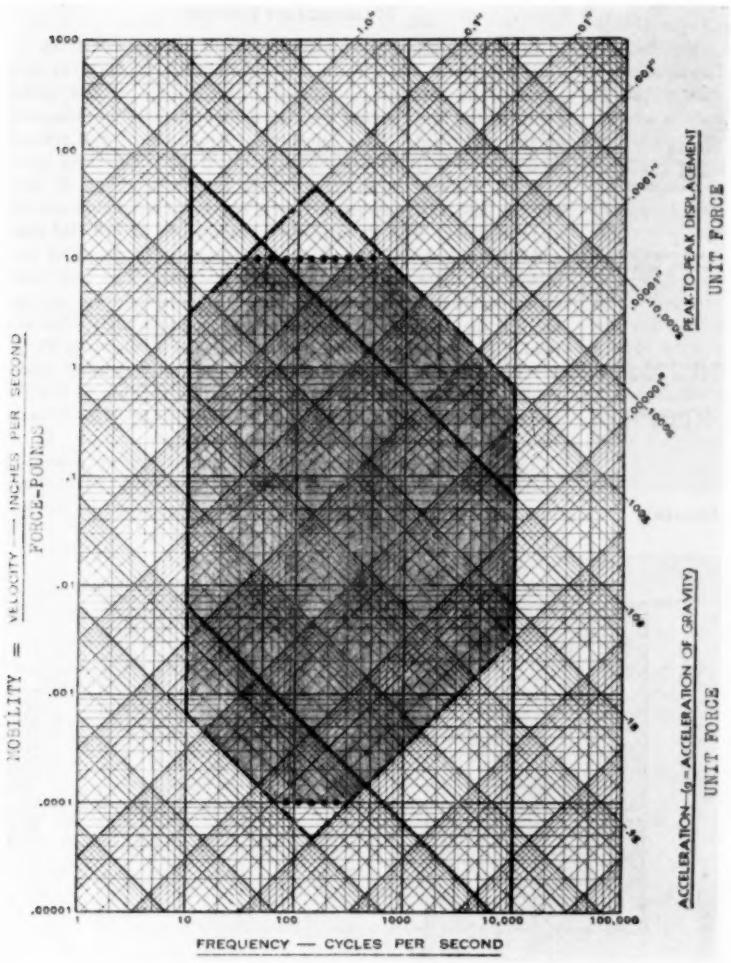

FIG. 1 USEFUL RANGE OF MECHANICAL IMPEDANCE HEAD

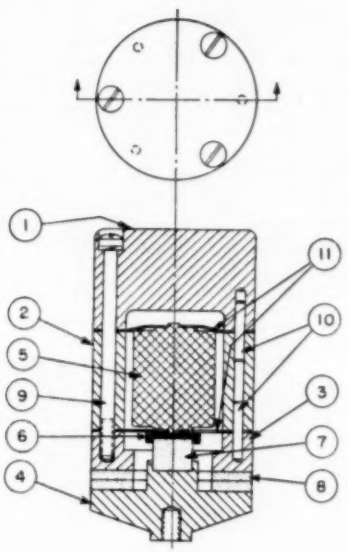

FIG. 2 CROSS SECTION OF MECHANICAL IMPEDANCE HEAD

tightly to shoulder on the point to be measured. A cylindrical barium-titanate element ⑦ is glued to the middle of the base piece and a mass of approximately 0.3 lb is mounted on the top for a seismic weight ⑤ forming an accelerometer. The weight is positioned by two diaphragms which are pretensioned to allow mounting in any direction and to permit acceleration exceeding 10 g; this requires a preload exceeding 3 lb for this mass. The natural frequency of this system is about 5500 cps, giving a useful range of 3500 cps. This can be increased to 10,000 cps by decreasing the mass to 0.03 lb; this reduces the sensitivity from 0.5 volt/g to 0.05 volt/g which is satisfactory at the higher frequencies, Fig. 1.

An annular disk of barium titanate ⑧ is glued to the base, surrounding the accelerometer; this has a sensitivity of 0.03 volt/lb. The hollow body ③ is mounted above the force gage and is closed with a cap ① to furnish a place to apply the force from a vibration motor. All portions of the body subjected to bending are made relatively thick to raise the resonant frequencies above 10,000 cps. Suitable leads are brought out from the two sides of both sensitive elements to connectors in the body of the gage. The sensitive elements have the electrical characteristics of capacitances. The force gage has a capacitance of 9000 mmfd and the accelerometer 300 mmfd. This means that the lower cutoff frequency is 1 cps when used with a cathode follower with an input impedance of 1000 megohms. There is no measurable cross-talk between the gages when used with these circuits and suitable shielded leads.

Since the parts of the gage below the force-sensing element, the base and accelerometer mass, appear as part of the measured system, these were kept as light as possible. Their combined weight is about 0.5 lb; even so it will be shown that this is enough to affect the fine detail of the measurements at the higher frequencies. We have been using a Model SD, MB vibration motor suitably modified to make a boot-strap driver, Fig. 3; i.e., a driver which reacts against its own mass only. We have yet to find a system that this does not have sufficient force to drive. The field, which is fairly massive, is supported on an inflated inner tube for vibration isolation. Even this is not satisfactory at higher frequencies when the tripod legs are mounted directly on the driven piece, and more elaborate measures must be taken to keep the leg force below 1 per cent of the armature force. The device is essentially driving against the mass of the field in this application since the field is floating on the very limber inner tube which acts as a soft spring.

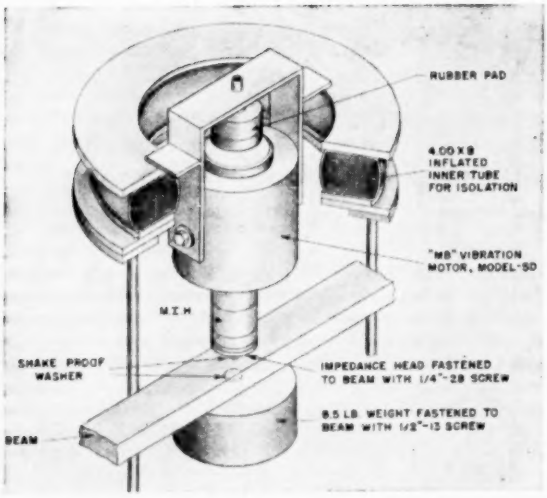
RUBBER PAD
4.00 X 8 INFLATED INNER TUBE FOR ISOLATION
"MB" VIBRATION MOTOR, MODEL-50
M I H
SHAKE PROOF WASHER
IMPEDANCE HEAD FASTENED TO BEAM WITH 1/4"-28 SCREW
8.5 LB. WEIGHT FASTENED TO BEAM WITH 1/2"-13 SCREW
BEAM

FIG. 3 VIBRATION MOTOR DRIVE SHOWING ISOLATION

MEASUREMENT RESULTS

As an illustration, the measured mobility of a steel bar 48 in. long, 2 in. wide, and 1 in. thick is shown in Fig. 4. The bar was mounted on soft sponge rubber approximately at the nodal points of the first free-free resonance, and the mobility measured at the mid point. The calculated frequencies of the normal modes up to 1210 cps are shown in Fig. 5 (7). The three symmetrical free-free beam modes were calculated to be 91 cps, 492 cps, and 1210 cps, respectively, Fig. 5; these should appear as resonances. The three modes calculated at 57 cps, 358 cps, and 1000 cps should appear as antiresonances or points of low mobility; these separate the previous three. The two antisymmetrical resonances at 251 and 812 cps should not appear at all if the driving and support systems are absolutely symmetrical. The actual measured frequencies were as shown in Table 1. These are in good enough agreement for the rather crude setup. The resonance at 18 cps is that of the beam as a rigid body on the sponge-rubber supports, and the one at 33.5 cps is that of rocking motion on the same supports.

The maxima and minima of the mobility curve coincided exactly with a phase angle of 90 deg between force and acceleration, as estimated from a cathode-ray picture with the ac-

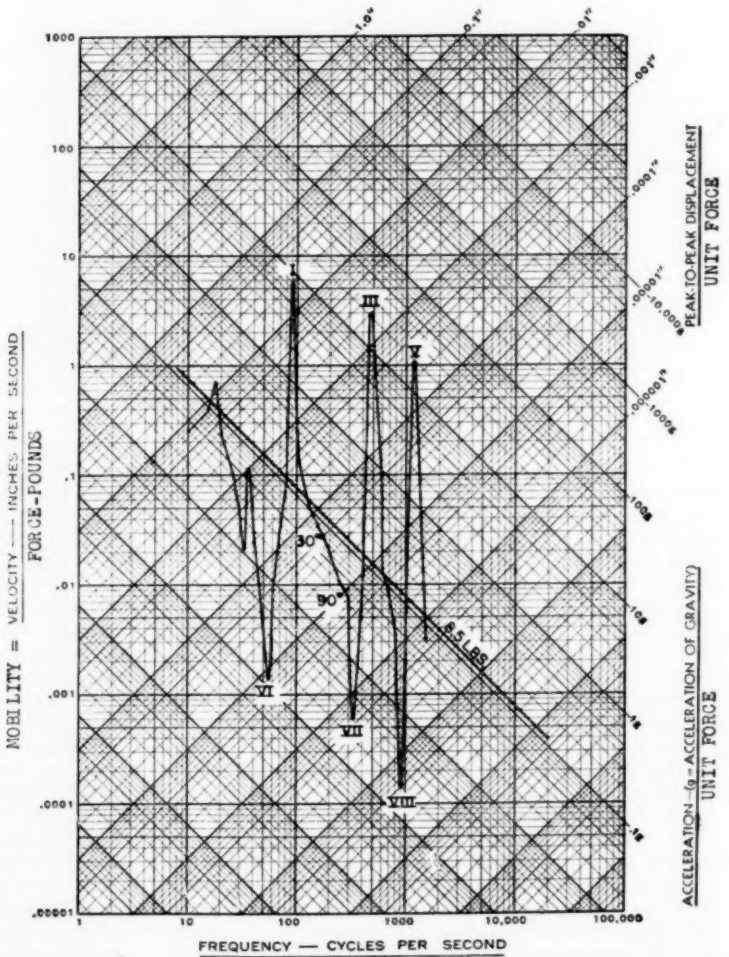

FIG. 4 MOBILITY OF CENTER OF 48-IN. × 2-IN. × 1-IN. FREE-FREE STEEL BAR

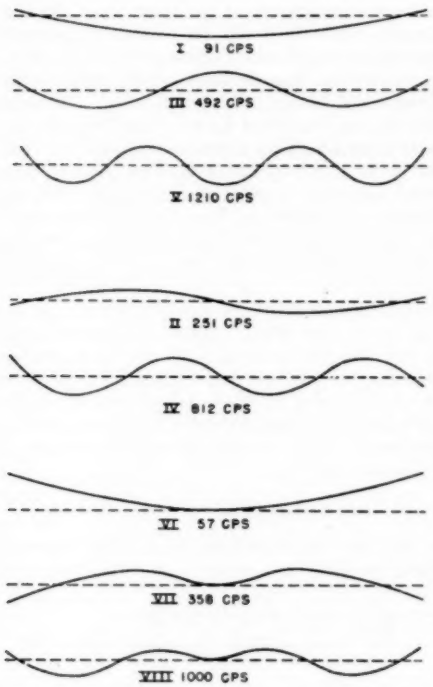

FIG. 5 RESONANCES AND ANTIRESONANCES OF BAR

celeration voltage horizontal and the force voltage vertical. Consideration of a polar plot of mobility (8) indicates that the phase angle between force and acceleration must vary from greater than 90 deg through 90 deg to less than 90 deg as the frequency is increased through a resonance point. It must vary from less than 90 deg through 90 deg to greater than 90 deg as the frequency is increased through an antiresonance point. Thus, the system is spring-controlled if the mobility increases with frequency and mass-controlled if it decreases with frequency; at resonance, where the system is damping-controlled, the slope is approximately zero. In general, the phase angle was almost 180 deg, as estimated from the oscilloscope, for increasing mobility, 90 deg as noted before at the maxima and minima, and almost 0 deg for decreasing mobility, except for the regions indicated. These regions were associated with subsidiary pseudoresonances, such as those corresponding to antisymmetrical free-free beam modes.

The effective spring compliances (reciprocal spring constants) in inches per pound and reciprocal damping in inches per second

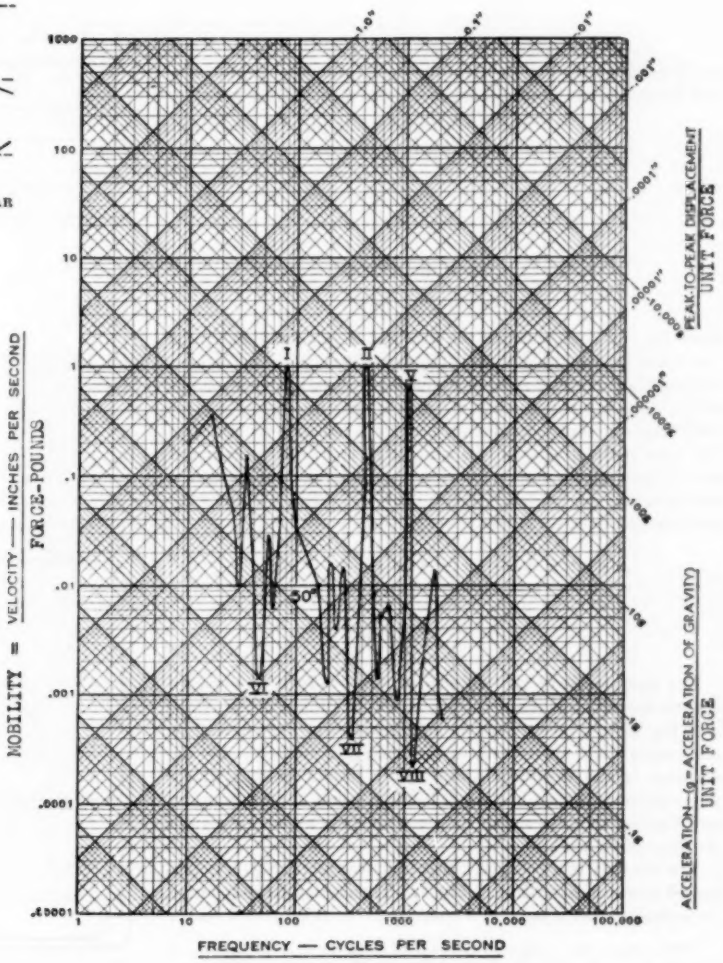

FIG. 6 MOBILITY OF BAR WITH 8.5-LB WEIGHT

TABLE 1 MEASURED FREQUENCIES

	Calculated frequencies, cps	Measured frequencies, cps
Free-free symmetrical beam resonances	91	91
	492	475
	1210	1160
Antiresonances	57	55
	358	320
	1000	900
Unsymmetrical beam resonances	251	?
	812	?

per pound can be read directly from Fig. 4.[3] A force of 1 lb causes an acceleration of 1 g on a mass which weighs 1 lb. Thus the effective mass in weight units is the reciprocal of the acceleration mobility in g's. The effective mass of the bar varies as the distance between nodes; this distance varies roughly as the inverse square root of the frequency. Thus, the general trend of the mobility diagram should follow a straight line on this log-log chart, at an angle halfway between lines of constant velocity and constant acceleration, or $-22^1/_2$ deg, which it appears to do.

A weight of 8.5 lb was fastened securely to the bottom of the bar and the mobilities remeasured, Fig. 6. The mobility of a mass (2) is

$$Z_m = \frac{-j}{\omega m} \quad [1]$$

and is given by the line at 0.118 g (= 1/8.5) in Fig. 4. The mass and bar constitute a parallel system, the new mobility is given by

$$\frac{1}{Z} = \frac{1}{Z_m} + \frac{1}{Z_B} \quad [2]$$

where

$$Z_m = \frac{-j}{\omega m} = \text{mobility of mass}$$

$$Z_B = ja + b = \text{mobility of bar}$$

$$Z = \text{mobility of system}$$

Since the real component of the mobility is very small except at the peaks (phase angle almost 0 deg or 180 deg), it can be seen that resonance should occur at frequencies where the bar-mobility line crosses the mass-mobility line with positive slope (spring-controlled or positive imaginary part). Resonance occurs when the total mobility has a zero imaginary part; for example, a simple mass-spring system is resonant when the mobility of the spring equals the mobility of the mass (2). Table 2 gives the predicted and measured values of the new resonances.

TABLE 2 VALUES OF NEW RESONANCES

Predicted	Measured
80	80
405	410
1010	1030

The frequencies of the mobility minima should be increased slightly by the same reasoning but should be practically the same as in Fig. 6, since the phase-angle shift is so rapid. The subsidiary resonances and antiresonances are changed markedly by the addition of the weight; this probably results from relatively minor changes in the direction of loading, points of beam support, and the fact that the weight was not precisely at the location of the impedance head.

The mobility of a point on a cast-iron base plate, Fig. 7, weighing 60 lb was measured next, Fig. 8. The casting was supported on sponge-rubber blocks on a concrete floor which rested on the ground. The extreme complexity of the response of the base is immediately apparent. It would be possible to estimate the first natural frequency and make a guess at the height of the first peak from the physical characteristics and dimensions of the system. The rest would be impossible to calculate. The same trend of $-22^1/_2$ deg may be noted up to about 700 cps, then the trend seems to be up along a line of constant compliance. This is probably due to the local response of the base plate at these frequencies, which seems to be relatively independent of lateral dimension. Preliminary calculations show that this effect should occur at about 1000 cps for a $^1/_2$-in-round steel surface bearing on steel; the details of this calculation have not been worked out fully.

The 8.5-lb weight was next screwed down to the casting and the mobility again measured, Fig. 9. Again the measured resonances agree with the intersections with the mass-mobility line. The interesting thing here is that the general level of the mobility curve is decreased at those frequencies where the mass mobility is less than the general trend of the casting mobility (above 700 cps) and the trend toward the constant-compliance line is delayed to about 2000 cps.

Conclusions

1 A device has been constructed for the practical measurement of mechanical mobility.

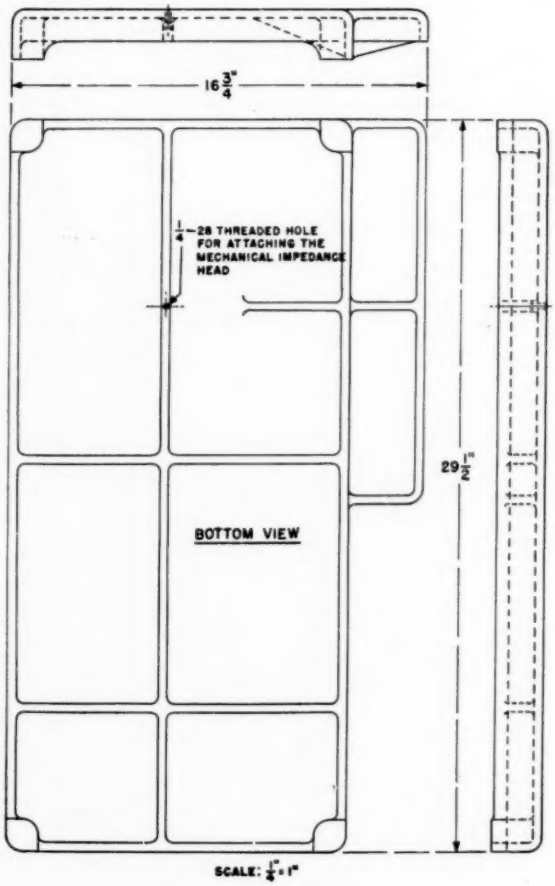

Fig. 7 Motor Base Plate

[3] This chart was originally devised in 1942, for the calibration of pickups by R. W. Samsel, General Electric Company. It shows displacement in peak to peak; thus, all compliance values are multiplied by 2.

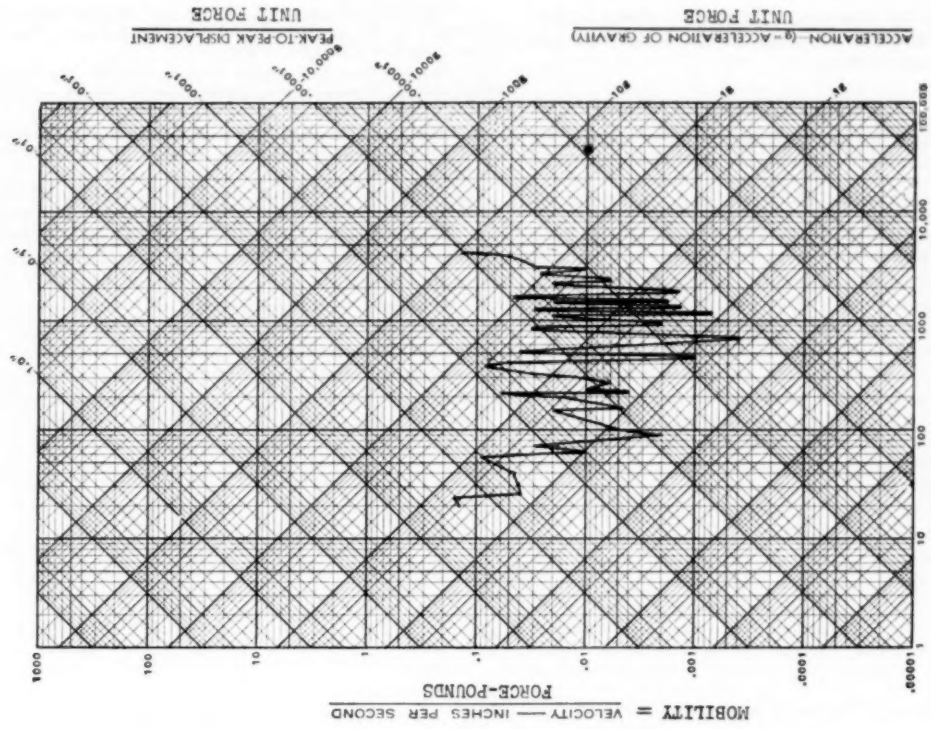

FIG. 9 MOBILITY OF BASE PLATE WITH 8.5-LB WEIGHT

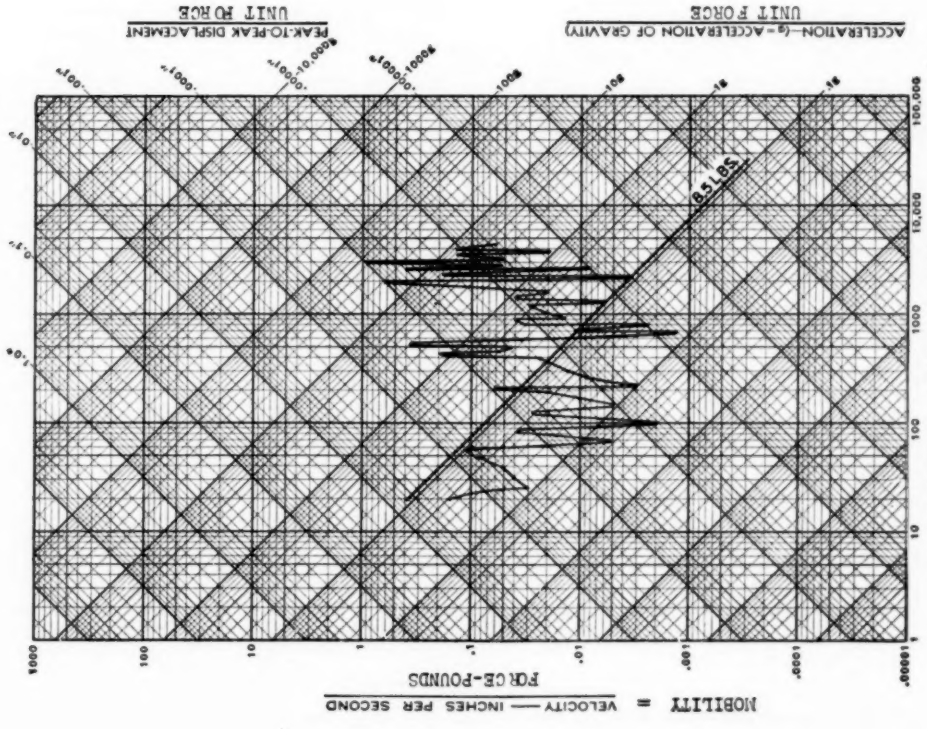

FIG. 8 MOBILITY OF BASE PLATE

2 The experimental measurement of mobility gives a method for predicting the vibration characteristics of complex structures when changes are made in them.

BIBLIOGRAPHY

1 "Mathematical Methods in Engineering," by Th. von Kármán and M. A. Biot, McGraw-Hill Book Company, Inc., New York, N. Y., 1940, 373 ff.

2 "Elements of Mechanical Vibrations," by C. R. Freberg and E. N. Kemler, John Wiley & Sons, Inc., New York, N. Y., 1943.

3 "Vibration and Sound," by F. A. Firestone, Edwards Bros., Inc., Ann Arbor, Mich., 1939.

4 "On the Application of the Impedance Method to Continuous Systems," by P. F. Chenea, JOURNAL OF APPLIED MECHANICS, Trans. ASME, vol. 75, 1953, p. 233.

5 "Wave Effects in Isolation Mounts," by M. Harrison, A. O. Sykes, and M. Martin, *Journal of the Acoustical Society*, vol. 24, 1952, p. 62.

6 "Resilient Mountings," Annual Report No. 2, Contract N7-onr-32904, Mechanical Engineering Department, Illinois Institute of Technology, 1950.

7 "Mechanical Vibrations," by J. P. DenHartog, McGraw-Hill Book Company, Inc., New York, N. Y., third edition, 1947, p. 459.

8 "Electric Circuits," by E. E. Staff, M.I.T., John Wiley & Sons Inc., New York, N. Y., 1943, chapter 9.

A Method for Determining the Internal Damping of Machine Members

By A. W. COCHARDT,[1] EAST PITTSBURGH, PA.

A method is described by which the internal damping of a machine member can be evaluated in a simple way. It is shown that the results of a conventional damping test on a simple shaped specimen of the chosen material can be combined with a newly introduced quantity, the stress-distribution function, to yield the internal damping of a particular member. The suggested method eliminates the necessity for testing expensive specimens as was often the practice.

Nomenclature

The following nomenclature is used in the paper:

r = distance from center line
y = distance from I_{min}-axis of blade 5600
z = distance from bottom end of blade 5600
R = radius of cross section
L = length of circular bar
l = length of blade 5600
V = volume
A = area
τ = shear stress
τ_m = maximum shear stress
σ = normal stress
σ_m = maximum normal stress
σ_z = maximum normal stress of any given cross section
E = Young's modulus
U = strain energy
$\bar{U}$ = total strain energy
ΔU = energy absorbed per cycle per unit volume
$\overline{\Delta U}$ = total energy absorbed per cycle

Introduction

Structural failures in service generally are caused by dynamic forces that are excited in a member at or near resonance. These failures can be prevented if the excited forces are kept low; and this can often be attained by selecting members with sufficiently large internal damping. A high damping means that the excited vibrational energy is absorbed in the material before the vibration can be built up.

Internal damping is therefore an important property of machine members. Despite its significance, very little is known about its evaluation. In general, the internal damping of a complicated member may be determined in two ways: The particular member may be used as a specimen and tested under conditions analogous to the operating conditions. Yet this is costly, and often even impossible, to carry out. Or the damping may be measured in a conventional way on a simple-shaped specimen, and the results of this test may then be used to derive the internal damping of the complicated member. The latter procedure, undoubtedly, is superior to the first, if the data of the conventional test can be interpreted in a simple manner. But no simple method was hitherto available, probably because damping is a somewhat obscure property. It was therefore often general practice to test complicated and expensive specimens. That this is not necessary, is shown by the present paper.

B. J. Lazan (1)[2] has recently presented a treatment of this problem, but his analysis which disregards the low-stress damping is applicable only for specific cases. The method proposed here, on the other hand, can be used for all machine members and all materials. It is based on two quantities, the stress-distribution function and the energy-absorption function. The stress-distribution function depends only upon the shape of a member and not upon the material, contrary to the energy-absorption function which depends only upon the material and not upon the shape of the member. Once these two quantities are known, the problem is virtually solved.

Explanation of Term "Stress-Distribution Function"

The fraction of the total volume of a member in which the stress lies between σ and $\sigma + d\sigma$ may be written as

$$\frac{dV}{V} = f\left(\frac{\sigma}{\sigma_m}\right)\frac{d\sigma}{\sigma_m} \quad [1]$$

In this expression $f(\sigma/\sigma_m)$ is a dimensionless function of the ratio σ/σ_m which is called stress-distribution function.

Consider, for example, a torsion bar with circular cross section that has been twisted by a certain amount. On the assumption that every cross section of the bar remains plane and perpendicular to the axis after torsion, it is clear that the stress does not vary in the axial direction. But in a given cross section the stress increases linearly with the distance from the center; consequently, the curves of constant stress are circles with a radius r

$$r = \frac{\tau}{\tau_m} R \quad [2]$$

and the volume $V(\tau)$ of the torsion bar subjected to a stress lower than τ is

$$V(\tau) = \frac{\tau^3}{\tau_m^3} V \quad [3]$$

When Equation [3] is differentiated with respect to τ, the stress-distribution function is found to be

$$f\left(\frac{\tau}{\tau_m}\right) = 2\frac{\tau}{\tau_m}$$

or

$$f\left(\frac{\sigma}{\sigma_m}\right) = 2\frac{\sigma}{\sigma_m} \quad [4]$$

---

[1] Research Engineer, Metallurgy Department, Westinghouse Research Laboratories.

Contributed by the Applied Mechanics Division and presented at the Annual Meeting, New York, N. Y., November 29–December 4, 1953, of The American Society of Mechanical Engineers.

Discussion of this paper should be addressed to the Secretary, ASME, 29 West 39th Street, New York, N. Y., and will be accepted until October 11, 1954, for publication at a later date. Discussion received after the closing date will be returned.

Note: Statements and opinions advanced in papers are to be understood as individual expressions of their authors and not those of the Society. Manuscript received by ASME Applied Mechanics Division, February 17, 1953. Paper No. 53—A-44.

[2] Numbers in parentheses refer to the Bibliography at the end of the paper.

if τ is replaced by one of the principal stresses σ. This expression has a real physical meaning. It says that only a relatively small part of the bar is subjected to small stresses. To be exact, only 1 per cent of the bar is operated between 0 and $^1/_{10}$ of the maximum stress

$$\frac{V}{\tau_m}\int_0^{0.1\tau_m} f\left(\frac{\tau}{\tau_m}\right) d\tau = 1 \text{ per cent } V$$

Table 1 shows stress-distribution functions for some common types of stress systems; tension-compression, torsion, and bending. The function for direct stress is 1 because the stress is uniform throughout the member in this particular case. It is interesting to note that the function for the cantilever beam, which was calculated analytically (2), decreases considerably with increasing stress ratio, σ/σ_m. This means that a large part of the beam is subjected to only a fraction of the maximum stress, contrary to a torsion bar. A simple calculation shows that the stress lies between 90 and 100 per cent of the maximum value for only 0.5 per cent of the volume of the beam. This is illustrated in Fig. 1 where the two parts of the cross-sectional areas are drawn (shaded area) for which the stress lies between zero and one tenth of the maximum stress and between nine tenths and the maximum stress. The large difference in size between these two areas is apparent, and from this the real meaning of the term stress-distribution function is understood.

TABLE 1 STRESS-DISTRIBUTION FUNCTIONS FOR SOME COMMON STRESS SYSTEMS

Direct stress	Cantilever beam	Simply supported beam	Simple torsion
1	$-\ln\frac{\sigma}{\sigma_m}$	$0.5 \sin \pi\frac{\sigma}{\sigma_m} - 0.7 \ln\frac{\sigma}{\sigma_m}$	$2\frac{\tau}{\tau_m}$

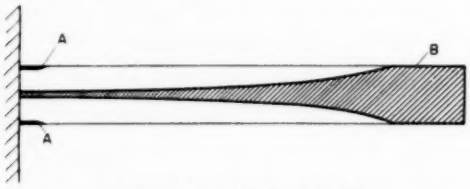

A = Stress between 90 and 100 per cent of maximum.
B = Stress between 0 and 10 per cent of maximum.

FIG. 1 A HIGH AND A LOW-STRESS INTERVAL IN A CANTILEVER BEAM

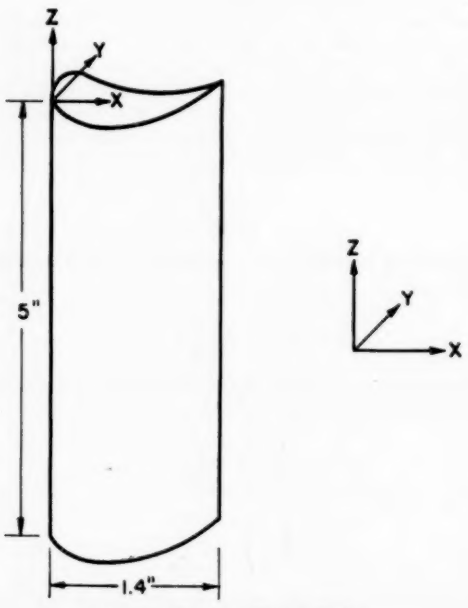

FIG. 2 TURBINE BLADE 5600

A machine member generally is subjected to a more complicated stress system, and a simple derivation of the stress-distribution function $f(\sigma/\sigma_m)$ may not exist. But it can be assumed that an approximate graphical solution can be found even in the most complicated cases. In order to demonstrate the procedure for a more complicated case, the stress-distribution function of a typical turbine blade in bending will now be calculated. The blade is shown in Fig. 2 and its cross section in Fig. 3. According to Rosard[1] the blade is subjected, to first approximation, to only one normal stress. This stress acts in the z-direction, Fig. 2, and varies in this direction as shown in Fig. 4. The negative values of σ_z/σ_m are due to the force of the shroud on the blade. In a given cross section, Fig. 3, the stress increases linearly with the distance from the I_{min}-axis, that is, linearly with y and does not vary in the x-direction. On the basis of Figs. 2 and 3 the stress is known at any point of the blade. The calculation of the stress-distribution function, which is carried out in the Appendix, leads to the following function

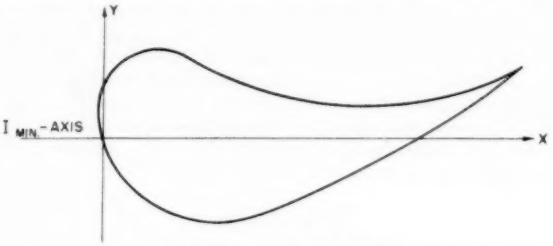

FIG. 3 SECTION OF BLADE 5600

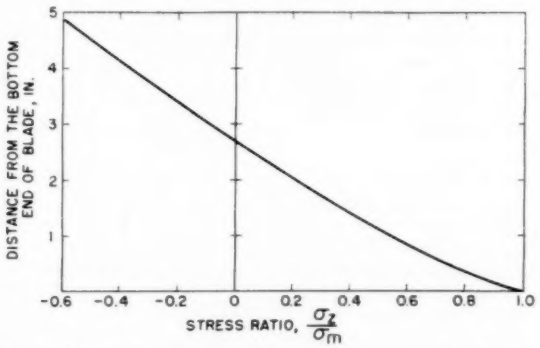

FIG. 4 STRESS DISTRIBUTION ALONG Z-DIRECTION OF TURBINE BLADE 5600 ACCORDING TO ROSARD

$$f\left(\frac{\sigma}{\sigma_m}\right) = 7.0063\,(0.0009)^{\sigma/\sigma_m} - 0.0063 \quad \ldots\ldots [5]$$

This expression is plotted in Fig. 5 and it is noted that, similar to a cantilever beam, a large part of the blade is at low stress even if the maximum stress is high. Equation [5] will be used after the second quantity used for evaluating the internal damping has been explained.

[1] Steam Division, Westinghouse South Philadelphia Works.

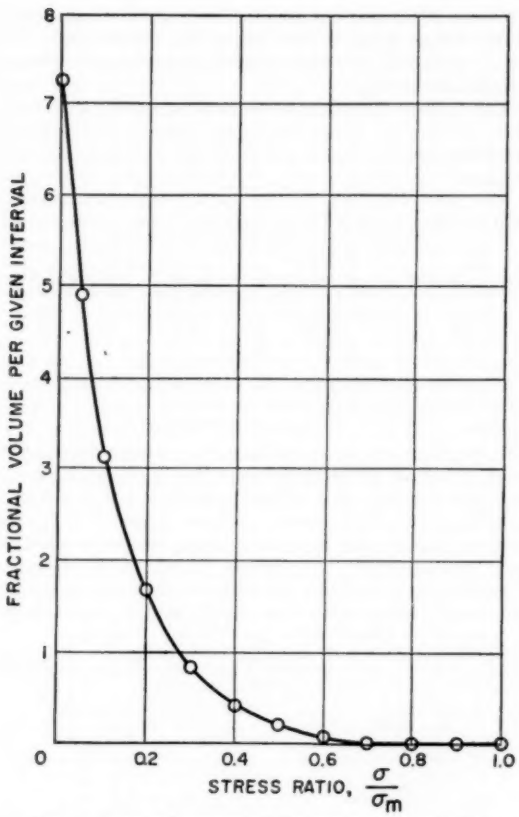

FIG. 5 STRESS-DISTRIBUTION FUNCTION OF BLADE 5600

EXPLANATION OF TERM "ENERGY-ABSORPTION FUNCTION"

The energy-absorption function is the energy loss per unit volume during a complete cycle of vibration if the stress is uniform throughout the material. This function, so defined, is determined only by the material and not by the shape of the member, contrary to the stress-distribution function. It will be denoted hereafter by ΔU. The magnitude of ΔU varies considerably for different materials. It may be so large in some cases that it by far outweighs other contributions to the total damping, such as slippage, joint, and aerodynamic effects; on the other hand, the energy absorption in the material may be, and often is, so small that it can be disregarded compared to those other contributions.

ΔU may depend upon temperature and stress history. It may further depend upon frequency although no influence of frequency has been found in a number of alloys (2, 3). But its dependence upon stress is the most important in practice. ΔU will thus be regarded hereafter as a function of stress only, and will be written $\Delta U(\sigma)$.

In general, there seems to be no simple relation between $\Delta U(\sigma)$ and σ throughout the entire range of stress, although the observed data frequently could be expressed by a simple function within a certain range. For example, at large stress $\Delta U(\sigma)$ was found (1, 4) to increase, due to plastic flow, in proportion to a power of the stress for a number of materials. But at low stresses such a simple relationship generally does not exist; this is understandable in view of the different origins of $\Delta U(\sigma)$ at low stress. At low stresses, the energy absorption may be caused by the thermoelastic effect (5, 6), the interstitial diffusion of atoms (7), or the magnetomechanical hysteresis (8). These contributions to the energy absorption superimpose with the contribution due to plastic flow, and explain why the resultant curve at low stress often has an odd shape.

For most alloys $\Delta U(\sigma)$ cannot be predicted from physical considerations. It must be determined experimentally and this can be done in a direct or indirect way. A direct measurement of $\Delta U(\sigma)$ is feasible if the stress is uniform throughout the specimen during the vibration. This condition is fulfilled, for example, for a specimen tested in Lazan's ingenious direct-loading machine (9) or approximately fulfilled in a hollow torsion specimen with a wall thickness small compared to its diameter. In these cases the damping test gives $\Delta U(\sigma)$ directly.

The other method, and the more efficient one, involves determination of $\Delta U(\sigma)$ by an indirect measurement. The damping test is performed using a conventional specimen, for example, a solid torsion bar. Such a specimen can be machined easily, but is not subjected to a uniform stress. Accordingly, the damping measurement does not give $\Delta U(\sigma)$ but the energy absorbed in the entire specimen which will be designated by $\overline{\Delta U}(\sigma_m)$ since it depends upon the maximum stress. The relation between $\Delta U(\sigma)$ and $\overline{\Delta U}(\sigma_m)$ is as follows

$$\overline{\Delta U}(\sigma_m) = \int \Delta U(\sigma) dV = V \int_0^{\sigma_m} \Delta U(\sigma) f\left(\frac{\sigma}{\sigma_m}\right) d\frac{\sigma}{\sigma_m} \quad \ldots [6]$$

For a torsion specimen a simple expression for $\Delta U(\sigma)$ is found. Equation [4] is substituted into Equation [6], and Equation [6] is differentiated with respect to σ_m. The energy-absorption function is then found as

$$\Delta U(\sigma_m) = \frac{1}{V}\left[\overline{\Delta U}(\sigma_m) + \frac{1}{2}\sigma_m \frac{d\,\overline{\Delta U}}{d\,\sigma_m}(\sigma_m)\right] \ldots [7]$$

In accordance with the prior notation, $\Delta U(\sigma_m)$ can be written

$$\Delta U(\sigma_m) = \Delta U(\sigma) \ldots [8]$$

For a torsion specimen $\Delta U(\sigma)$ is therefore easily obtained performing just a simple torsion test and applying Equation [7].

In order to demonstrate the procedure, the energy-absorption function of the standard turbine-blade material, a 12 per cent chrome steel, was determined using the Föppl-Pertz machine (10). The curve is shown in Fig. 6 where the shear stress has been replaced by the normal stress, making use of the Mises criterion (11). It can be seen that at large stress the measured curve (dotted line) can be fitted smoothly by Lazan's Equation [1]

$$\Delta U(\sigma) = J\sigma^n \ldots [9]$$

where the value of the constant J is 2×10^{-31} psi^{-4} and where $n = 5$. But at lower stresses, Lazan's equation does not quite hold. The measured values are somewhat larger; this was explained in terms of magnetomechanical hysteresis (2).

This example illustrates the appearance of a ΔU-curve. Moreover, it shows one of the differences between the present method and the one proposed by Lazan (1). His procedure does not consider the exact shape of the ΔU-curve at low stress which seems to be, at first sight, a reasonable approximation since the two curves in Fig. 6 differ only by a slight amount. However, the calculation to be carried out shows that serious errors result if the true low-stress damping is disregarded.

INTERNAL DAMPING OF A MEMBER

The internal damping may be expressed in several ways. Some

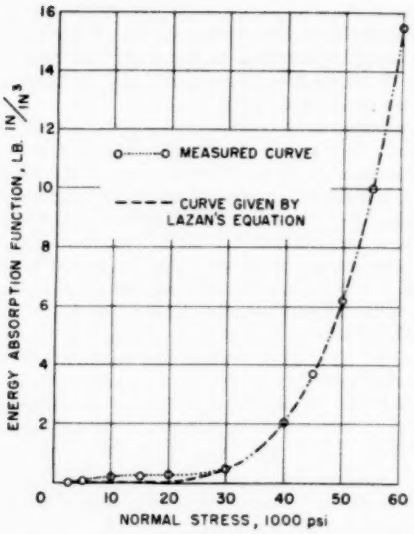

FIG. 6 ENERGY-ABSORPTION FUNCTION ΔU OF BLADE 5600

of its most common definitions are as follows: logarithmic decrement, relative energy loss per cycle, internal friction, half-width at maximum amplitude, stress-amplification factor at resonance, and the ratio between velocity-damping coefficient and critical velocity-damping coefficient. It can be shown that the confusingly large number of definitions can be reduced to just two quantities, stress-distribution function and energy-absorption function. The stress-amplification factor at resonance A_r, for example, is

$$A_r = 2\pi \frac{\bar{U}}{\overline{\Delta U}} = \frac{\pi}{E} \frac{\int_0^{\sigma_m} \sigma^2 f\left(\frac{\sigma}{\sigma_m}\right) d\sigma}{\int_0^{\sigma_m} \Delta U(\sigma) f\left(\frac{\sigma}{\sigma_m}\right) d\sigma} \quad \ldots [10]$$

A_r is a function of only $\Delta U(\sigma)$ and $f(\sigma/\sigma_m)$ at a given maximum stress. This clearly shows the significance of these two quantities. The integration in Equation [10] generally can be carried out easily using graphical methods. In other words, the internal damping of a member is essentially known if the stress-distribution function and the energy-absorption function have been evaluated.

Functions $f(\sigma/\sigma_m)$ and $\Delta U(\sigma)$ have been determined in the foregoing for a typical turbine blade. Using Equations [5] and [10] and Fig. 6, it is not difficult to find the total energy absorption $\overline{\Delta U}(\sigma_m)$, the total strain energy at the amplitude of vibration $\bar{U}(\sigma_m)$, and the stress-amplification factor A_r of the blade at resonance. The values of $\overline{\Delta U}$, $\bar{U}$, and A_r obtained in this manner for various values of the maximum stress, using the actual ΔU-curve (dotted curve in Fig. 6) are seen in Table 2. The change

TABLE 2 ACTUAL VALUES OF $\overline{\Delta U}$, $\bar{U}$, AND A_r AS A FUNCTION OF MAXIMUM STRESS FOR BLADE 5600

σ_m, maximum normal stress, psi	$\overline{\Delta U}$, total energy absorbed per cycle, lb-in.	$\bar{U}$, total strain energy, lb-in.	A_r, stress-amplification factor at resonance
40000	0.17	2.2	81
50000	0.22	3.5	99
60000	0.35	5.1	91

of the stress-amplification factor with stress requires particular mention. It is noted that A_r increases in the range between 40,000 and 50,000 psi; but from then on it decreases up to 60,000 psi, the fatigue strength of the 12 per cent chrome steel.[4] This peculiar variation of A_r with stress can be explained on the basis of magnetostriction (2).

Table 3 shows the results of the same calculation if $\Delta U(\sigma)$ is taken as given by Lazan's equation (dashed curve in Fig. 6). The difference between these values and those in Table 2 is readily apparent.

TABLE 3 VALUES OF $\overline{\Delta U}$, $\bar{U}$, AND A_r CALCULATED FOR VARIOUS STRESSES USING LAZAN'S EQUATION

σ_m, maximum normal stress, psi	$\overline{\Delta U}$, total energy absorbed per cycle, lb-in.	$\bar{U}$, total strain energy, lb-in.	A_r, stress-amplification factor at resonance
40000	0.015	2.2	920
50000	0.038	3.5	578
60000	0.120	5.1	267

There are, of course, cases where the low-stress damping is not important. This is exemplified by torsional vibration of a shaft consisting of 12 per cent chrome steel. Using Equations [4] and [10], the Mises criterion, and Fig. 6, the stress-amplification factor A_r of a shaft vibrating in torsion was calculated for various maximum stresses. It is evident from Table 4 that it does not make much difference whether the true values of $\Delta U(\sigma)$ are used, or Lazan's equation, if the maximum torsion stress is 35,000 psi. Needless to say, the low-stress damping would be even less important for the torsion vibration of materials that exhibit less damping at low stress than the 12 per cent chrome steel.

TABLE 4 COMPARISON OF ACTUAL STRESS-AMPLIFICATION FACTORS WITH THOSE CALCULATED USING LAZAN'S EQUATION FOR A TORSION BAR

Maximum torsion stress, τ, psi	A_r, stress-amplification factor at resonance	
	Lazan's values	Actual values
23000	143	123
29000	73	71
35000	43	42

The two examples have shown that the present method has one further advantage. It quickly answers the practically important question whether, in a particular case, the low or high-stress damping is more effective. This is readily recognized from the shape of the two basic functions $f(\sigma/\sigma_m)$ and $\Delta U(\sigma)$. The low-stress damping is more effective if the stress-distribution function decreases more rapidly with stress than the energy-absorption function increases. This condition generally is fulfilled for machine members, that vibrate in bending similarly to supported or clamped beams, such as turbine and compressor blades. In these cases almost the entire internal damping occurs in fibers which are at low stress; in other words, the damping of these members is essentially caused by the thermoelastic, magnetomechanical, or the Zener effect. This should be mentioned especially, because there seems to be the belief that the low-stress damping is of no practical importance.[5]

On the other hand, the high-stress damping is more effective if the energy-absorption function increases more rapidly than the stress-distribution function decreases, or if both functions increase with stress. This condition is fulfilled, as was shown, for a torsion vibration. But these considerations apply to the steady-state vibration only. When the transient state of vibration is considered, as is frequently done (12), the low-stress damping may prove to be more important, even in this case.

SUMMARY

A method is outlined by which damping properties of machine

[4] At 10^8 cycles and room temperature according to P. R. Toolin, Westinghouse Research Laboratories.

[5] See, for example, reference (4).

members may be determined in a simple way using the two quantities: stress-distribution function and energy-absorption function. The first quantity depends only upon the shape of the member and not upon the material, while the second quantity is dependent only upon the material and not upon the shape of the member.

The stress-distribution function can be determined analytically in simple cases or graphically for the more complicated parts. The energy-absorption function may be evaluated by testing a simple shaped specimen in a conventional way. For all practical purposes the problem can be considered solved once the two functions are known.

The method is illustrated using practical examples. As a by-product, it is found that the low-stress damping is sometimes more effective than the damping at higher stresses, and it is pointed out that the conclusions of some workers in this field are misleading since they disregard the low-stress damping.

Acknowledgment

The author wishes to express his great appreciation to Dr. C. Zener, Associate Director of the Westinghouse Research Laboratories, for his helpful criticism and suggestions.

BIBLIOGRAPHY

1 "Effect of Damping Constants and Stress Distribution on the Resonance Response of Members," by B. J. Lazan, JOURNAL OF APPLIED MECHANICS, Trans. ASME, vol. 75, 1953, pp. 201–209.

2 "The Origin of Damping in High-Strength Ferromagnetic Alloys," by A. W. Cochardt, JOURNAL OF APPLIED MECHANICS, Trans. ASME, vol. 75, 1953, pp. 196–200.

3 "Damping, Fatigue, and Dynamic Stress-Strain Properties of Mild Steel," by B. J. Lazan and T. Wu, Proceedings of the American Society for Testing Materials, vol. 51, 1951, p. 649.

4 "Internal Friction in Engineering Materials," by J. M. Robertson and A. J. Yorgiadis, JOURNAL OF APPLIED MECHANICS, Trans. ASME, vol. 68, 1946, pp. A-173–A-182.

5 "Internal Friction in Solids," by C. Zener, *Physical Review*, vol. 52, 1937, p. 230.

6 "Über die innere Reibung fester Körper," by K. Bennewitz and H. Rötger, *Physikalische Zeitschrift*, vol. 39, 1938, p. 835.

7 "Interstitial Atomic Diffusion Coefficients," by C. Wert and C. Zener, *Physical Review*, vol. 76, 1949, p. 1169.

8 "Einige magneto-elastische Torsionsversuche," by R. Becker and M. Kornetzki, *Zeitschrift für Physik*, vol. 88, 1934, p. 634.

9 "Some Mechanical Properties of Plastics and Metals Under Sustained Vibrations," by B. J. Lazan, Trans. ASME, vol. 65, 1943, pp. 87–104.

10 "Föppl-Pertz Damping Machine," *Metals and Alloys*, New Products Section, February, 1931, p. 28.

11 "Theory of Flow and Fracture of Solids," by A. Nadai, McGraw-Hill Book Company, Inc., New York, N. Y., 1950, p. 210.

12 "Turbine-Blade Vibration Due to Partial Admission," by R. P. Kroon, JOURNAL OF APPLIED MECHANICS, Trans. ASME, vol. 62, 1940, pp. A-161–A-165.

Appendix

In calculating the stress-distribution function of turbine blade 5600, a graphical method will be used: The blade is thought to be cut into 20 slices, each 0.25 in. thick, and the problem is approximated by assuming the stress σ_z to be constant and equal to the average value of σ_z in each slice. This then leads to a stress distribution along the z-direction as illustrated in Fig. 7, if only the absolute value of the stress is considered. The constant value of the ratio σ_z/σ_m in each slice will be denoted by λ_n where the index n refers to the number of the slice. Using this approximation, the stress-distribution function of each of the 20 slices is easily derived in the following way: The quantity

$$\frac{\Delta A}{\Delta \sigma}\frac{\sigma}{A} = g\left(\frac{\sigma}{\sigma_z}\right) \quad \ldots\ldots\ldots\ldots\ldots\ldots\ldots\ldots [11]$$

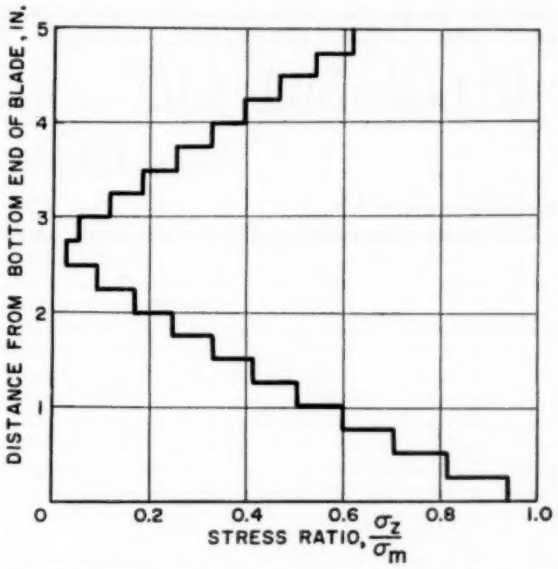

FIG. 7 APPROXIMATED STRESS DISTRIBUTION ALONG Z-DIRECTION

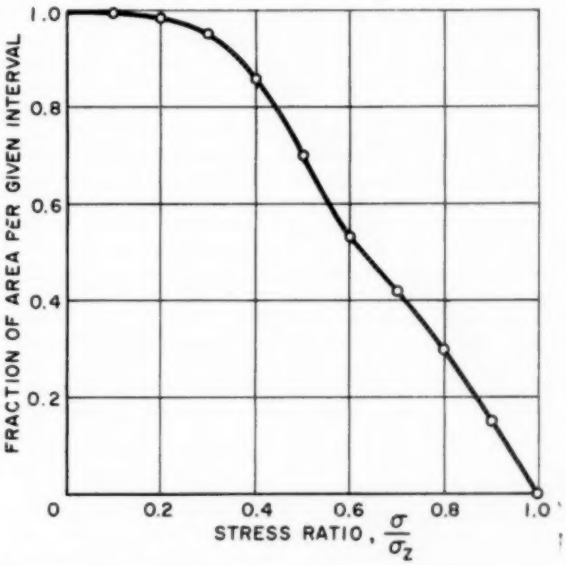

FIG. 8 STRESS-DISTRIBUTION FUNCTION OF CROSS-SECTIONAL AREA OF BLADE 5600

is determined for the cross section of the blade by measuring in Fig. 3 the fraction of the cross-sectional area for which the stress lies within a unit interval of stress. Taking $\Delta\sigma$ equal to $(1/20)\,\sigma_z$, the curve seen in Fig. 8 was obtained and, using the methods of least squares, this curve could be fitted smoothly by the analytic expression

$$g\left(\frac{\sigma}{\sigma_z}\right) = 1 - 9\left(\frac{\sigma}{\sigma_z}\right)^4 + 13\left(\frac{\sigma}{\sigma_z}\right)^5 - 5\left(\frac{\sigma}{\sigma_z}\right)^6 \quad \ldots [12]$$

This expression multiplied by $\Delta z/l = 1/20$ represents the stress-

distribution function of each of the 20 slices which may be written as

$$\varphi_n\left(\frac{\sigma}{\sigma_m}\right) = \frac{1}{20}\left[\frac{1}{\lambda_n} - \frac{9}{\lambda_n^5}\left(\frac{\sigma}{\sigma_m}\right)^4 + \frac{13}{\lambda_n^6}\left(\frac{\sigma}{\sigma_m}\right)^5 - \frac{5}{\lambda_n^7}\left(\frac{\sigma}{\sigma_m}\right)^6\right] \quad [13]$$

if σ_n is substituted by $\lambda_n\sigma_m$.

The total stress-distribution function of the blade is the sum of these 20 stress-distribution functions and thus becomes

$$f(\sigma/\sigma_m) = (1/20) \sum_n \varphi_n(\sigma/\sigma_m);\ n = 1, 2 \ldots 20 \quad [14]$$

Taking the 20 values of λ_n from Fig. 7, the stress-distribution function for the blade was computed for 12 different values of σ/σ_m. The result is seen graphically in Fig. 5. This curve can be fitted again by an analytic function, and the stress-distribution function of the blade can so finally be expressed as in Equation [5].

On Bending of a Flat Slab Supported by Square-Shaped Columns and Clamped

By S. WOINOWSKY-KRIEGER,[1] QUEBEC CITY, CANADA

A solution is given in this paper for the problem of bending of an infinite flat slab loaded uniformly and rigidly clamped in square-shaped columns arranged to form the square panels of the slab. The complex variable method in connection with conformal mapping is used for this aim. Although not perfectly rigorous, the solution obtained is sufficiently accurate for practical purposes and, besides, it can be improved at will. Stress diagrams traced in a particular case of column dimensions do not wholly confirm the stress distribution, generally accepted in design of flat slabs.

Statement of Problem

LET us consider an infinite elastic plate of constant thickness supported by rows of equidistant columns and submitted to a uniform load, Fig. 1. The column capitals, if any, have a square cross section as well as the columns themselves if they

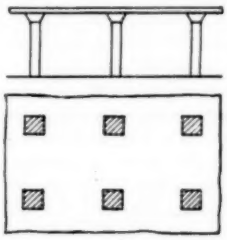

Fig. 1 Section of a Flat Slab in Ground Plan and Elevation

carry no capitals. The stress distribution throughout such an infinite plate is practically the same as that throughout a "flat slab" or "mushroom slab" of the usual type, provided that extreme panels and extreme columns of the slab are excluded from consideration and that the number of the columns in a row is not too small (say, three at least).

Flat slabs of reinforced concrete are used extensively in civil engineering, and their correct design is of a primary practical interest. Stress distribution in such a slab, on the other hand, is a stimulating object for mathematical investigation owing to the high-degree symmetry imposed by the geometrical conditions of the problem.

These latter suggest the use of double Fourier series in representing the deflection of the plate (1),[2] but the solution in simple series (2), although less elegant, is more convenient for numerical computation of stresses. A connection of the stress distribution in a flat slab with the double periodic properties of the elliptical functions first was established by A. Nadai (3) in the particular case of concentrated column reactions.

References (1) and (2) both assume these reactions as uniformly distributed over the area of the square-shaped capitals, the load being distributed uniformly over the plate. This assumption greatly simplifies the encountered problem; it disregards, however, the actual conditions of the deformation of the slab around the column. In fact, the capital of the column is extremely rigid in comparison with the plate, and the assumption of a built-in edge along the boundary of the capital responds better to the real conditions of the deformation of the slab than any other supposition.

If the capitals are circular, the slab in the vicinity of the column can be considered as a cantilever circular plate clamped along the edge of the capital. Turneaure and Maurer, American engineers, first succeeded in estimating the radius of such a fictitious plate with a fairly good approximation. A solution credited to F. Tölke (4) based on a similar idea is exact enough to meet all practical demands; unfortunately, the results of Tölke are not applicable to a slab on square capitals, which is the conventional type of the flat slab.

The method of finite differences used by many authors in handling the stress distribution in flat slabs (5, 6, 7) is, in principle, applicable to any given boundary conditions. However, it becomes less appropriate if a considerable stress concentration must be expected, as it is near the corners of a square capital rigidly connected with the slab.

The method used in this paper originally was developed by Muschelišvili (8) to handle the two-dimensional and the torsion problems in elasticity (9). It has been altered and applied to the theory of bending of anisotropic plates by S. G. Lechnickiĭ (10) and recently used by several authors (11, 12) in treating some problems of stress concentration around variously shaped holes in plates subjected to tension or bending.

Some Results of the Complex Variable Theory

Let us consider a plate which carries no surface load and is submitted merely to shearing forces and couples applied along its edge. The deflection w of the plate then obeys the bipotential equation $\Delta\Delta w = 0$ and is, therefore, expressible (13) in the form

$$w(x, y) = R[\bar{z}\Phi(z) + \mathbf{X}(z)] \quad \ldots\ldots\ldots\ldots [1]$$

where $\Phi(z)$ and $\mathbf{X}(z)$ are some analytical functions of the complex variable $z = x + iy$. The bending moments M_x, M_y, the twisting moment M_{xy}, and the shearing forces Q_x, Q_y are obtainable from Equation [1] by usual differentiation with respect to x and y (14). Three complex combinations of the foregoing quantities are expressible by the formulas

$$\left.\begin{aligned} M_x + M_y &= -2D(1+\nu)[\Phi'(z) + \overline{\Phi'(z)}] \\ M_y - M_x - 2iM_{xy} &= 2D(1-\nu)[\bar{z}\Phi''(z) + \Psi'(z)] \\ Q_x - iQ_y &= -4D\Phi''(z) \end{aligned}\right\} \ldots [2]$$

[1] Professor of Structural Engineering, Laval University.

[2] Numbers in parentheses refer to the Bibliography at the end of the paper.

Contributed by the Applied Mechanics Division and presented at the Annual Meeting, New York, N. Y., November 29–December 4, 1953, of The American Society of Mechanical Engineers.

Discussion of this paper should be addressed to the Secretary, ASME, 29 West 39th Street, New York, N. Y., and will be accepted until October 11, 1954, for publication at a later date. Discussion received after the closing date will be returned.

Note: Statements and opinions advanced in papers are to be understood as individual expressions of their authors and not those of the Society. Manuscript received by ASME Applied Mechanics Division, February 21, 1953. Paper No 53—A-60.

in which D is the flexural rigidity of the plate, ν the Poisson's ratio, and, finally

$$\Psi(z) = \frac{d\mathbf{X}(z)}{dz} \quad \ldots\ldots [3]$$

Suppose now the plate forms an infinite region around a hole, the origin of co-ordinates $x = 0$, $y = 0$ being inside the hole, Fig. 2. The plate may be submitted to a system of bending couples and shearing forces acting along the edge C of the hole and to another similar system acting at infinity. With regard to the problem under consideration, we assume the resulting moment vector of each previous system of loading to be zero. Under this restriction the functions contained in Equation [1] are of the form

$$\left.\begin{aligned} \Phi(z) &= \frac{P_0 z}{8\pi D} \log z + \Phi^*(z) \\ \mathbf{X}(z) &= A \log z + \mathbf{X}^*(z) \end{aligned}\right\} \quad \ldots\ldots [4]$$

where P_0, positive in the direction of positive deflections w, is the resultant of the shearing forces applied to the edge C, while $\Phi^*(z)$ and $\mathbf{X}^*(z)$ are functions, single valued and continuous throughout the region outside C.

Now, let s denote the arc of C and n the exterior normal to C, Fig. 2. Furthermore, let w and $\partial w/\partial n$, or $\partial w/\partial s$ and $\partial w/\partial n$

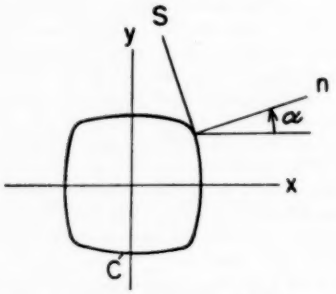

FIG. 2 INTERIOR BOUNDARY C OF SLAB

(which is the same but for a constant), be some given functions on C. One boundary condition on C then can be written as

$$\Phi(z) + z\overline{\Phi'(z)} + \overline{\Psi(z)} = e^{i\alpha}\left(\frac{\partial w}{\partial n} + i\frac{\partial w}{\partial s}\right) \quad \ldots\ldots [5]$$

in which α is the angle between x-axis and n, and the second boundary condition is a conjugate of Equation [5].

Next, let us map the given infinite region of the plate into the region $|\zeta| < 1$ interior to the unit circle γ by means of the transformation

$$z = \omega(\zeta) \quad \ldots\ldots [6]$$

in which $\zeta = \rho e^{i\theta}$. The curve C then is mapped on the unit circle γ and the rectangular co-ordinates x, y are replaced by curvilinear co-ordinates ρ = constant, θ = constant, Fig. 3. Writing for brevity

$$\left.\begin{aligned} \Phi(z) &= \Phi[\omega(\zeta)] = \varphi(\zeta) \\ \mathbf{X}(z) &= \mathbf{X}[\omega(\zeta)] = \chi(\zeta) \\ \Psi(z) &= \Psi[\omega(\zeta)] = \psi(\zeta) \end{aligned}\right\} \quad \ldots\ldots [7]$$

and, furthermore, introducing the notation

$$\mu(\zeta) = \frac{\varphi'(\zeta)}{\omega'(\zeta)} \quad \ldots\ldots [8]$$

the following system of equations can be established between the bending moments, the twisting moment, and the shearing forces which, this time, refer to an element of the plate bound by two curves ρ = const and two curves θ = const

$$\left.\begin{aligned} M_\theta + M_\rho &= -2D(1+\nu)[\mu(\zeta) + \overline{\mu(\zeta)}] \\ M_\theta - M_\rho - 2iM_{\rho\theta} &= \frac{2D(1-\nu)\zeta^2}{\rho^2\omega'(\zeta)}[\mu'(\zeta)\overline{\omega(\zeta)} + \psi'(\zeta)] \\ Q_\rho - iQ_\theta &= -\frac{4D\zeta}{\rho|\omega'(\zeta)|}\mu'(\zeta) \end{aligned}\right\} \quad \ldots [9]$$

In order to simplify the boundary conditions let us put

$$\zeta = e^{i\theta} = \sigma, \quad \bar{\zeta} = e^{-i\theta} = \frac{1}{\sigma} \quad \ldots\ldots [10]$$

for a point on the unit circle γ. Then Equation [5] allows a transformation into the form

$$\varphi(\sigma) + \frac{\omega(\sigma)}{\omega'(\sigma)}\overline{\varphi'(\sigma)} + \overline{\psi(\sigma)} = f_1 + if_2 \quad \ldots\ldots [11]$$

in which the function

$$f_1 + if_2 = \frac{\partial w}{\partial x} + i\frac{\partial w}{\partial y} = e^{i\alpha}\left(\frac{\partial w}{\partial n} + i\frac{\partial w}{\partial s}\right) \quad \ldots\ldots [12]$$

must be expressed through the variable σ.

Next, let us submit a plate without a hole to some bending couples and shearing forces at infinity and, possibly, to a load P_0 concentrated at $x = 0$, $y = 0$. Let the corresponding stress distribution throughout the plate be defined by some functions $\varphi_0(\zeta)$, $\psi_0(\zeta)$ referred to the curvilinear co-ordinates. Introducing once more the interior edge C let be $w = 0$, $\partial w/\partial\rho = 0$ on the unit circle γ which is the image of C. The resultant of shearing forces at C then is equal to $-P_0$ and the resultant of bending couples may be zero according to supposition.

The final stress distribution throughout the infinite plate outside C then will be governed by some functions

$$\left.\begin{aligned} \varphi(\zeta) &= \varphi_0(\zeta) + \varphi_c(\zeta) \\ \psi(\zeta) &= \psi_0(\zeta) + \psi_c(\zeta) \end{aligned}\right\} \quad \ldots\ldots [13]$$

where $\varphi_c(\zeta)$, $\psi_c(\zeta)$ are two compensating functions chosen in a manner as to satisfy the just mentioned edge conditions by the combined functions, Equations [13]. Substituting these functions in Equation [11] and making $\partial w/\partial n = \partial w/\partial s = 0$ on γ we arrive at the boundary condition

$$\varphi_c(\sigma) + \frac{\omega(\sigma)}{\overline{\omega'(\sigma)}}\overline{\varphi_c'(\sigma)} + \overline{\psi_c(\sigma)} = f_1^0 + if_2^0 \quad \ldots\ldots [14]$$

in which, this time

$$f_1^0 + if_2^0 = -\left[\varphi_0(\sigma) + \frac{\omega(\sigma)}{\omega'(\sigma)}\overline{\varphi_0'(\sigma)} + \overline{\psi_0(\sigma)}\right] \quad \ldots [15]$$

is expressed in terms of both given functions $\varphi_0(\zeta)$ and $\psi_0(\zeta)$. As for the second boundary condition, it is, once again, a conjugate of Equation [14].

Taking both unknown functions in form of expansions[3]

[3] It can be shown that the initial term either in the first of both expansions or in the second one can be nullified without any loss of generality.

$$\left.\begin{aligned}\varphi_e(\zeta) &= \alpha_0 + \alpha_1\zeta + \alpha_2\zeta^2 + \alpha_3\zeta^3 + \dots \\ \psi_e(\zeta) &= \beta_1\zeta + \beta_2\zeta^2 + \beta_3\zeta^3 + \dots\end{aligned}\right\} \dots\dots [16]$$

observing that $\zeta = \sigma$ on γ, and finally using Equation [14] and its conjugate, the values α and β could have been determined by equating to zero the coefficients of successive powers of σ. The determination of the functions $\varphi_e(\zeta)$ and $\psi_e(\zeta)$ is, however, much simplified by application of Harnack's theorem.[4] Hence multiplying both sides of Equation [14] by $d\sigma/2\pi i(\sigma - \zeta)$, in which ζ denotes a point inside γ, and integrating the result along γ one obtains the first of the following boundary conditions

$$\varphi_e(\zeta) + \frac{1}{2\pi i}\int_\gamma \frac{\omega(\sigma)}{\overline{\omega'(\sigma)}}\,\overline{\varphi_e'(\sigma)}\,\frac{d\sigma}{\sigma - \zeta} = \frac{1}{2\pi i}\int_\gamma (f_1^0 + if_2^0)\frac{d\sigma}{\sigma - \zeta} \dots\dots [17]$$

$$\psi_e(\zeta) + \frac{1}{2\pi i}\int_\gamma \frac{\overline{\omega(\sigma)}}{\omega'(\sigma)}\,\varphi_e'(\sigma)\,\frac{d\sigma}{\sigma - \zeta} = \frac{1}{2\pi i}\int_\gamma (f_1^0 - if_2^0)\frac{d\sigma}{\sigma - \zeta} \dots\dots [18]$$

while the second one is derived from a conjugate of Equation [14] by a similar procedure. If $w_0(x, y)$ is a biharmonic function, defined as such by $\varphi_0(\zeta)$ and $\psi_0(\zeta)$, the expressions $f_1^0 \pm if_2^0$ are given by Equation [15]. In the event of a surface load the function $w_0(x, y)$ is no longer biharmonic and the expression, Equation [12], then must be taken for substitution.

The exact mapping of the infinite region with a square hole into the interior of the unit circle should be performed by means of the Schwarz-Christoffel transformation taken for instance in the form

$$\omega(\zeta) = R\int_1^{1/\zeta}\left[\left(1 - \frac{e^{\frac{\pi i}{4}}}{t}\right)\left(1 - \frac{e^{\frac{3\pi i}{4}}}{t}\right)\left(1 - \frac{e^{\frac{5\pi i}{4}}}{t}\right)\left(1 - \frac{e^{\frac{7\pi i}{4}}}{t}\right)\right]^{\frac{1}{2}} dt \dots\dots [19]$$

where R is a constant. As $|t| \geq 1$, the integrand can be expanded near the infinity and the integration gives

$$\omega(\zeta) = R\left(\frac{1}{\zeta} - \frac{1}{6}\zeta^3 + \frac{1}{56}\zeta^7 - \frac{1}{176}\zeta^{11} + \dots\right) \dots [20]$$

The initial terms of this expansion rather than the exact transformation will be used in further consideration, a procedure usually followed in solving problems of stress concentration around a polygonal hole (12).

Construction of Solution

Returning to the basic problem, let us consider an annular region of the flat slab bounded by the contour line C of the capital and the straight lines $x = \pm a/2$, $y = \pm a/2$, Fig. 3. By means of the previous transformation this region is mapped into a region contained between the unit circle γ and some closed curve inside this circle. In order to simplify the solution the expansion Equation [20] may be restricted to

$$z = \omega(\zeta) = R\left(\frac{1}{\zeta} - \frac{1}{6}\zeta^3\right) \dots\dots [21]$$

[4] See, for instance, reference (9), p. 160.

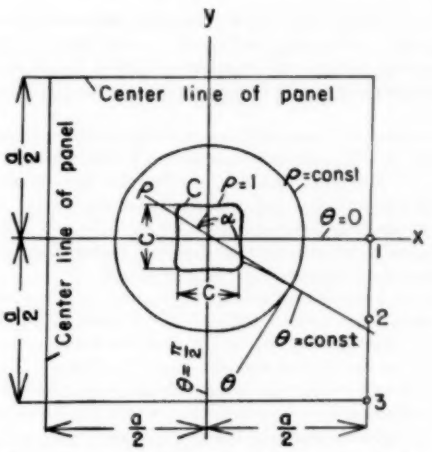

Fig. 3 Panel of Slab With Rectangular and Curvilinear Co-Ordinates

Since $\zeta = \rho e^{i\theta}$ this transformation leads to the relations

$$\left.\begin{aligned}x &= R\left(\frac{\cos\theta}{\rho} - \frac{\rho^3\cos 3\theta}{6}\right) \\ y &= -R\left(\frac{\sin\theta}{\rho} + \frac{\rho^3\sin 3\theta}{6}\right)\end{aligned}\right\} \dots\dots [22]$$

Putting in particular $\rho = 1$ one finds that the image of the unit circle has the shape shown in Figs. 3 and 4, and this shape will replace the square contour of the capital in all following considerations.

Letting q be the intensity of the uniformly distributed load we find that the deflection w of the annular region of the plate must satisfy the following:

(a) The differential equation $\Delta\Delta w = q/D$.

(b) The conditions of symmetry with respect to the axes $x = 0$, $y = 0$, and $x \pm y = 0$.

(c) The conditions $w = 0$, $\partial w/\partial n = 0$ on C, i.e., $w = 0$, $\partial w/\partial\rho$ on γ.

(d) The conditions of symmetry $\partial w/\partial x = 0$, $Q_x = 0$ on $x = a/2$, which, by condition (b), also secure the symmetry on $x = -a/2$ and $y = \pm a/2$.

Making a temporary use of polar co-ordinates $r = (x^2 + y^2)^{1/2}$, $\phi = \arctan(y/x)$ the conditions (a) and (b) are satisfied by taking $w(r, \phi)$ in the form

$$w = w_q + w_p + \sum_{n=1}^{5} A_n w_n \dots\dots [23]$$

in which

$$w_q = w_{0q} + w_{cq} \text{ with } w_{0q} = \frac{qr^4}{64D} \dots\dots [24]$$

$$w_p = w_{0p} + w_{cp} \text{ with } w_{0p} = \frac{qa^2r^2}{8\pi D}\log\frac{R}{r} \dots\dots [25]$$

$$\left.\begin{aligned}&w_n = w_{0n} + w_{cn}\ (n = 1, 2, 3, 4, 5) \text{ with} \\ &w_{01} = qR^2r^2,\ w_{02} = qr^4\cos 4\phi,\ w_{03} = \frac{qr^6}{R^2}\cos 4\phi \\ &w_{04} = \frac{qr^8}{R^4}\cos 8\phi,\ w_{05} = \frac{qr^{10}}{R^6}\cos 8\phi\end{aligned}\right\} \dots [26]$$

where, furthermore, w_{eq}, w_{ep}, w_{en} are some biharmonic functions, and A_n some coefficients. All functions contained in Equation [23] may hold throughout the infinite region of the plate outside C; they hold accordingly throughout the interior of γ after transformation.

The function w_{0q}, especially, is a particular solution of the equation $\Delta\Delta w = q/D$ and the corresponding uniform load is qa^2 for one panel of the slab. Similarly, the function w_{0p} represents the action of a load $P_0 = -qa^2$ concentrated at the origin. The resultant of shearing forces produced by $w_{0q} + w_{0p}$ on C is therefore in equilibrium with the load distributed over the annular region inside the square $x = \pm a/2$, $y = \pm a/2$.

As for the seven compensating functions w_{eq}, w_{ep}, w_{en} they must be chosen in a manner as to fulfill the conditions (c) by each of the combined functions w_q, w_p, w_n, a problem easily solvable by means of the method of complex variable. Finally the conditions (d) may be satisfied by making $\partial w/\partial x = 0$ at the points 1, 2, 3, and by making $Q_x = 0$ at the points 1 and 3, Fig. 3, which can be done by a suitable choice of the five[5] parameters A_n, still available.

Determination of Set of Functions w_n

Every given function w_{0p}, w_{0n} being expressed by two harmonic functions $\Phi_0(z)$, $\mathbf{X}_0(z)$, the associated function $\Psi_0(z)$ is readily obtained from Equation [3] and the functions $\varphi_0(\zeta)$, $\chi_0(\zeta)$ then are found by means of Equations [7] and [21]. Next, the coefficients α of the power series for $\varphi_e(\zeta)$ can be determined from the boundary condition, Equation [17], and the function $\psi_e(\zeta)$ then is found from the boundary condition, Equation [18], by integration. The relation

$$\chi_e'(\zeta) = \omega'(\zeta)\psi_e(\zeta) = -R\left(\frac{1}{\zeta^2} + \frac{\zeta^2}{2}\right)\psi_e(\zeta) \quad [27]$$

which follows from Equations [3], [7], and [21] defines the last yet unknown function $\chi_e(\zeta)$ and the final expression now is given by

$$w_n(\zeta) = R[\overline{\omega(\zeta)}\varphi_n(\zeta) + \chi_n(\zeta)] \quad [28]$$

where $\varphi_n = \varphi_{0n}(\zeta) + \varphi_{en}(\zeta)$ and $\chi_n(\zeta) = \chi_{0n}(\zeta) + \chi_{en}(\zeta)$.

A slightly different procedure needed to find the nonbiharmonic function w_q is exhibited in the Appendix.

The seven functions w_q, w_p, w_n constituting the final solution are assembled later, together with the associated functions $\varphi_{0n}(\zeta)$, $\chi_{0n}(\zeta)$, $\varphi_n(\zeta)$, and $\chi_n(\zeta)$. It is easy to verify that all partial solutions fulfill the boundary conditions $w_n = 0$, $\partial w_n/\partial\rho = 0$ on $\rho = 1$. The data concerning stress distribution and readily obtainable from Equations [9] may be restricted here to formulas for the bending moments M_ρ and $M_\theta = \nu M_\rho$ acting along the edge C of the capital.

Function w_q

$$w_{0q} = \frac{qR^4}{64D}\left(\frac{1}{\rho^2} + \frac{\rho^6}{36} - \frac{\rho^2}{3}\cos 4\theta\right)^2 \quad [29]$$

$$\left.\begin{aligned}\varphi_{eq} &= \frac{qR^3}{3456D}(73\zeta^3 - 6\zeta^7)\\ \chi_{eq} &= \frac{qR^4}{27648D}(2116\log\zeta - 296\zeta^4 + 24\zeta^8 - 383)\end{aligned}\right\} \quad [30]$$

$$w_q = \frac{qR^4}{82944D}[1296\rho^{-4} - 1149 + 144\rho^4 - 292\rho^8 + \rho^{12} + 6348\log\rho - (864 - 1752\rho^2 + 888\rho^4 + 24\rho^8 - 24\rho^{10})\cos 4\theta + (72\rho^4 - 144\rho^6 + 72\rho^8)\cos 8\theta] \quad [31]$$

$$M_\rho = -\frac{qR^2}{36}\frac{22 - 11\cos 4\theta + \cos 8\theta}{5 + 4\cos 4\theta} \quad [32]$$

Function w_p

$$\varphi_{0p} = -\frac{qa^2}{8\pi D}\, z\log\frac{z}{R},\quad \chi_{0p} = 0 \quad [33]$$

$$\left.\begin{aligned}\varphi_p &= -\frac{qa^2R}{288\pi D}\left[6\zeta^3 + \left(6\zeta^3 - \frac{36}{\zeta}\right)\log\zeta\right]\\ \chi_p &= -\frac{qa^2R^2}{288\pi D}(1 - 6\zeta^4 + 43\log\zeta)\end{aligned}\right\} \quad [34]$$

$$w_p = -\frac{qa^2R^2}{288\pi D}[1 - \rho^6 + 6(\rho^2 - \rho^4)\cos 4\theta - (36\rho^{-2} - 43 + \rho^6 - 12\rho^2\cos 4\theta)\log\rho] \quad [35]$$

$$M_\rho = \frac{qa^2}{3\pi}\frac{4 - \cos 4\theta}{5 + 4\cos 4\theta} \quad [36]$$

Function w_1

$$\varphi_{01} = \frac{qR^2}{D}\, z,\quad \chi_{01} = 0 \quad [37]$$

$$\left.\begin{aligned}\varphi_1 &= \frac{qR^3}{D}\left(\frac{1}{\zeta} + \frac{1}{6}\zeta^3\right)\\ \chi_1 &= \frac{qR^4}{36D}(78\log\zeta - 35)\end{aligned}\right\} \quad [38]$$

$$w_1 = \frac{qR^4}{36D}(36\rho^{-2} - 35 - \rho^6 + 78\log\rho) \quad [39]$$

$$M_\rho = -\frac{12qR^2}{5 + 4\cos 4\theta} \quad [40]$$

Function w_2

$$\varphi_{02} = 0,\quad \chi_{02} = \frac{qz^4}{D} \quad [41]$$

$$\left.\begin{aligned}\varphi_2 &= -\frac{4qR^3}{D}\,\zeta^3\\ \chi_2 &= \frac{qR^4}{3D}(3\zeta^{-4} - 2 + 9\zeta^4 - 12\log\zeta)\end{aligned}\right\} \quad [42]$$

$$w_2 = \frac{qR^4}{3D}[2(\rho^6 - 1) - 12\log\rho + 3(\rho^{-4} - 4\rho^2 + 3\rho^4)\cos 4\theta] \quad [43]$$

$$M_\rho = -96qR^2\frac{1 + 2\cos 4\theta}{5 + 4\cos 4\theta} \quad [44]$$

Function w_3

$$\varphi_{03} = \frac{qz^5}{DR^2},\quad \chi_{03} = 0 \quad [45]$$

[5] By results of Tölke's solution (4) the suppression of the condition $Q_x = 0$ at the point 2 is justified by the choice $P_0 = -qa^2$.

$$\left.\begin{aligned}\varphi_3 &= \frac{qR^3}{18D}\left(18\zeta^{-5} - 15\zeta^{-1} - 100\zeta^3 + 15\zeta^7\right)\\ \chi_3 &= \frac{qR^4}{72D}\left(328\zeta^4 - 48\zeta^3 - \frac{20}{3} - 520\log\zeta\right)\end{aligned}\right\} \quad \ldots\ldots [46]$$

$$w_3 = \frac{qR^4}{72D}\Big[-60\rho^{-2} - \frac{20}{3} + \frac{200}{3}\rho^6 - 520\log\rho + (72\rho^{-6} - 390\rho^2 + 328\rho^4 - 10\rho^{10})\cos 4\theta - (12\rho^{-2} - 60\rho^6 + 48\rho^8)\cos 8\theta\Big] \quad \ldots\ldots [47]$$

$$M_\rho = -\frac{40qR^2}{3}\,\frac{9 + 22\cos 4\theta - 4\cos 8\theta}{5 + 4\cos 4\theta} \quad \ldots\ldots [48]$$

Function w_4

$$\varphi_{04} = 0 \quad \chi_{04} = \frac{qz^5}{DR^4} \quad \ldots\ldots [49]$$

$$\left.\begin{aligned}\varphi_4 &= \frac{qR^3}{3D}(28\zeta^3 - 24\zeta^7)\\ \chi_4 &= \frac{qR^4}{3D}\left(3\zeta^{-3} - 4\zeta^{-4} + \frac{14}{3} - 28\zeta^4 + 21\zeta^8 + 28\log\zeta\right)\end{aligned}\right\} \quad \ldots\ldots [50]$$

$$w_4 = \frac{qR^4}{3D}\Big[\frac{14}{3}(1 - \rho^6) + 28\log\rho - (4\rho^{-4} - 28\rho^2 + 28\rho^4 - 4\rho^{10})\cos 4\theta + (3\rho^{-8} - 24\rho^6 + 21\rho^8)\cos 8\theta\Big] \quad \ldots\ldots [51]$$

$$M_\rho = 224\,qR^2\,\frac{1 - 4\cos 8\theta}{5 + 4\cos 4\theta} \quad \ldots\ldots [52]$$

Function w_5

$$\varphi_{05} = \frac{qz^9}{DR^8}, \quad \chi_{05} = 0 \quad \ldots\ldots [53]$$

$$\left.\begin{aligned}\varphi_5 &= \frac{qR^3}{6D}(6\zeta^{-9} - 9\zeta^{-3} + 6\zeta^{-1} + 79\zeta^3 - 66\zeta^7 + 9\zeta^{11})\\ \chi_5 &= \frac{qR^4}{12D}\left(\frac{43}{3} - 160\zeta^4 + 120\zeta^8 - 16\zeta^{12} + 182\log\zeta\right)\end{aligned}\right\} \quad \ldots [54]$$

$$w_5 = \frac{qR^4}{288D}\,[288\rho^{-2} + 344 - 632\rho^6 + 4368\log\rho - (432\rho^{-6} - 3744\rho^2 + 3840\rho^4 - 528\rho^{10})\cos 4\theta + (288\rho^{-10} + 72\rho^{-2} - 3168\rho^8 + 2880\rho^8 - 72\rho^{14})\cos 8\theta - (48\rho^{-6} - 432\rho^{10} + 384\rho^{12})\cos 12\theta] \quad \ldots\ldots [55]$$

$$M_\rho = 4qR^2\,\frac{75 + 32\cos 4\theta - 296\cos 8\theta + 48\cos 12\theta}{5 + 4\cos 4\theta} \quad \ldots\ldots [56]$$

In all previous expressions for φ_{0n} and χ_{0n} one has to put

$$z = R\left(\frac{1}{\zeta} - \frac{1}{6}\zeta^3\right)$$

Final Solution for $c/a = 0.2$

Let us establish the numerical solution of the problem in the particular case of $c/a = 0.2$, Fig. 3. By equating the area of the column section as given by Equation [22], that is the value

$$A = 4\int_{\theta=0}^{\pi/4}(x\,dy - y\,dx) = \frac{11}{12}\pi R^2 \quad \ldots\ldots [57]$$

to the area $A = c^2$ of a square, one obtains $R/c = 0.589277$ and, furthermore, $R/a = 0.11786$. Now the position of the points 1, 2, 3 is given by $x_1 = x_2 = x_3 = 0.5a = 4.2425R$, $y_1 = 0$, $y_2 = -2.12125R$, $y_3 = -4.2425R$ or, in curvilinear co-ordinates, Equation [22], by

$$\left.\begin{aligned}\rho_1 &= 0.234522, \quad \theta_1 = 0\\ \rho_2 &= 0.210845, \quad \theta_2 = 0.147483\pi\\ \rho_3 &= 0.1666937, \quad \theta_3 = 0.25\pi\end{aligned}\right\} \quad \ldots\ldots [58]$$

The angle α between the x-axis in the direction of the increasing ρ, Fig. 3, at point 2 is given by

$$\sin\alpha = \frac{2\sin\theta_2 - \rho_2^4\sin 3\theta_2}{4 + 4\rho_2^4\cos 4\theta_2 + \rho_2^8} = 0.446082 \quad \ldots\ldots [59]$$

and $\cos\alpha = -0.894992$. The conditions of symmetry at $x = a/2$ now can be written as

$$\left.\begin{aligned}&\frac{\partial w}{\partial\rho} = 0, \quad Q_\rho = 0 \text{ at point 1}\\ &\frac{\partial w}{\partial\rho}\cos\alpha - \frac{1}{\rho}\frac{\partial w}{\partial\theta}\sin\alpha = 0 \text{ at point 2}\\ &\frac{\partial w}{\partial\rho} = 0, \quad Q_\rho = 0 \text{ at point 3}\end{aligned}\right\} \quad \ldots\ldots [60]$$

where $w(\rho, \theta)$ must be taken in the form of Equation [23] while the shearing forces Q_ρ are defined by the third of Equations [9]. After having performed all necessary computations the five previous conditions yield the system of Equations [61] for the parameters A_n.

$$\left.\begin{aligned}&145.814A_1 + 5657.000A_2 + 153645A_3 + 3720094A_4 + 84462200A_5 = 764.082\\ &0.364335A_1 - 4.37201A_2 + 199664A_3 + 10.07785A_4 + 237141000A_5 = 19.00080\\ &363.440A_1 + 3463.77A_2 + 23229.3A_3 - 19325970A_4 - 517228000A_5 = 1951.999\\ &418.792A_1 - 31056.06A_2 - 1678100A_3 + 80545380A_4 + 3624302000A_5 = 2328.533\\ &0.0658462A_1 - 0.790155A_2 + 551837A_3 + 1.849386A_4 - 2574310000A_5 = 35.0010\end{aligned}\right\} \quad \ldots\ldots [61]$$

The solutions of this system

$$\left.\begin{aligned}A_1 &= 5.4179324\\ A_2 &= -0.00662653\\ A_3 &= 0.00008059416\\ A_4 &= -0.00000030850\\ A_5 &= 0.000000003820\end{aligned}\right\} \quad \ldots\ldots [62]$$

being finally introduced in Equation [23] make the solution of the problem complete and the stress distribution throughout the panel of the slab is now easily obtainable.

Bending Moments for $c/a = 0.2$

Table 1 contains the values of the bending moments in various points of the slab together with the corresponding values obtained by the usual theory,[6] distributing the column reaction uniformly

[6] See references (1, 2).

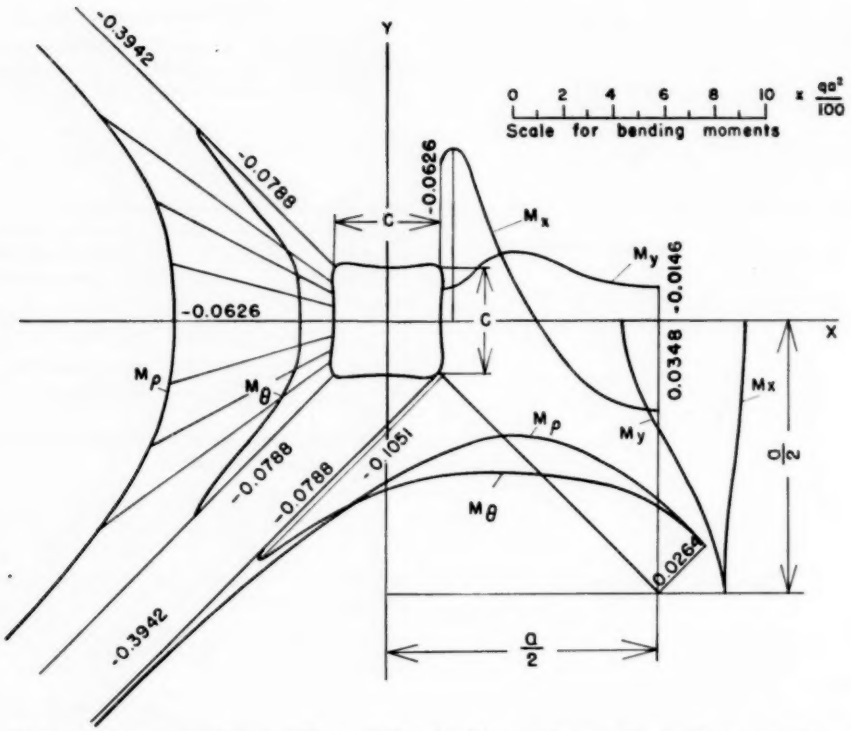

FIG. 4 DISTRIBUTION OF BENDING MOMENTS M_x, M_y, M_ρ, AND M_θ FOR A UNIFORM LOAD, $c = 0.2a$, AND $\nu = 0.2$

(Reactive moments M_ρ and $M_\theta = 0.2\,M_\rho$ acting along edge $\rho = 1$ of column are plotted in radial direction not coincident with normal to edge.)

TABLE 1 NUMERICAL FACTORS k FOR BENDING MOMENTS $M = kqa^2$ OF SLAB $c/a = 0.2$

Position in Fig. 4	Moment	Present theory	Usual theory
$x = \frac{a}{2}, y = \frac{a}{2}$	M_x	$0.0220(1 + \nu)$	$0.0268(1 + \nu)$
	M_y	$0.0220(1 + \nu)$	$0.0268(1 + \nu)$
$x = \frac{a}{2}, y = 0$	M_x	$0.0393 - 0.0225\nu$	$0.0544 - 0.0287\nu$
	M_y	$-0.0225 + 0.0393\nu$	$-0.0287 + 0.0544\nu$
$x \sim \frac{c}{2}, y \sim \frac{c}{2}$	M_ρ	-0.3942	$-0.0319 - 0.0807\nu$
	M_θ	-0.3942ν	$-0.0807 - 0.0319\nu$
$x \sim \frac{c}{2}, y = 0$	M_x	-0.0626	$-0.0622 - 0.0927\nu$
	M_y	-0.0626ν	$-0.0927 - 0.0622\nu$

over the area of the square capital. A diagram of bending moments computed for $\nu = 0.2$, which is a good average value of Poisson's ratio for the reinforced concrete, is given in Fig. 4.

The following conclusion can be made from consideration of Table 1 and of the moment distribution shown in Fig. 4.

1 All positive moments and the negative moments in the central part of the panel are considerably reduced by the restraining effect of the columns.

2 Contrary to the usual assumption the distribution of the negative moments M_y along $y = 0$ (respectively of M_x along $x = 0$) is nearly uniform between the columns, a fact making allowable a more economic design of the slab.

3 According to the usual theory the moments M_θ at the support are larger than the corresponding radial moments M_ρ and both vary but little along the edge of the capital. By the theory here established the moments $M_\theta = \nu M_\rho$ become secondary as compared with the moments M_ρ, which are moderately large near the middle of the side of the square support and increase progressively toward its corners.

By keeping still more terms in the expansion Equation [20] one obtains a series of shapes approaching rapidly the exact square. The fact that the radius of curvature at $\theta = 45$ deg then is steadily decreasing justifies the assumption that the theoretical stress concentration at the corners of the capital will increase infinitely at the same time.[7] The actual stress concentration is bounded of course by the elastic limit of the material of the plate. Its plastic deformation may produce somewhat the same effect on the stress distribution as a slight rounding off of the square shape of the support, assumed in this paper.

EXTENSION OF SOLUTION ON FURTHER CASES

The accuracy of the solution might be improved not only by use of a more exact mapping function as noted previously but also by satisfying the symmetry conditions on more points along the center lines of the panels and by increasing the number of the functions $A_n w_n$ accordingly. The practical value of this more elaborate procedure is, however, questionable since the anisotropy of the reinforced slab and the effect of shear deformation (15) in the vicinity of the columns are likely to cause greater errors than the mathematical shortcomings of the first approximation, used in this paper.

More important appears the extension of the solution on flat slabs with rectangular panels and especially on the load distribution shown in Fig. 5 and giving, in combination with the uniform load, maximum bending moments at the center of the panel.

[7] One is led to the same conclusion by considering the results obtained for stress distribution near a square hole in a plate subjected to tension, see reference (12) pp. 68–72.

Both cases can be handled by a suitable change of the symmetry properties of the fundamental expression Equation [23] with re-

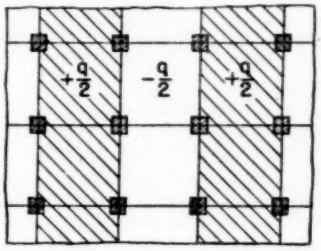

FIG. 5 ALTERNATING LOAD DISTRIBUTION OVER SLAB

spect to the axes x and y. In the instance of rectangular columns the Mapping Function [19] must be altered accordingly, together with the symmetry in the form of solution.

CONCLUSION

The application of complex variable theory leads to a solution sufficiently accurate for the purpose of the design of the slab and appearing in a closed form, convenient for the numerical computation of the stresses. The bending moments throughout the panels of the slab prove to be smaller than those obtained by the usual theory. As for the moments at the support, a considerable stress concentration, although of a localized character, must be taken into account at the corners of the supporting capitals. The foregoing method appears also applicable to flat slabs with rectangular panels or rectangular-shaped columns, as well as in the event of an alternating distribution of the load. All results previously obtained hold as well for a "reversed flat slab," i.e., for a mat foundation carrying a system of equidistant columns in rigid connection with the slab, provided the soil-pressure is distributed uniformly.

Appendix

DETERMINATION OF FUNCTION w_q

Assuming $w_{0q} = q(x^2 + y^2)^2/64D$, the problem is to find a biharmonic function w_{cq} such as to make both $w_q = w_{0q} + w_{cq}$ and $\partial w_q/\partial\rho$ zero on γ, i.e., for $\rho = 1$. Observing that

$$\frac{\partial w_{0q}}{\partial x} = \frac{q(x^2 + y^2)}{16D}\,x, \quad \frac{\partial w_{0q}}{\partial y} = \frac{q(x^2 + y^2)}{16D}\,y \qquad [63]$$

and using consecutively Equations [12], [22], and [10], one obtains on γ

$$f_1 + if_2 = \frac{q(x^2 + y^2)}{16D}\,z = \frac{qR^3}{1152D}\left(\frac{12}{\sigma^5} - \frac{76}{\sigma} + \frac{73}{3}\,\sigma^3 - 2\sigma^7\right) \qquad [64]$$

and furthermore, by integration

$$\frac{1}{2\pi i}\int_\gamma (f_1 + if_2)\,\frac{d\sigma}{\sigma - \zeta} = \frac{qR^3}{1152D}\left(\frac{73}{3}\,\zeta^3 - 2\zeta^7\right) \qquad [65]$$

for the right side of Equation [17]. On the left side of the same equation one has

$$\frac{\omega(\sigma)}{\omega'(\sigma)} = \frac{\sigma}{6} - \frac{13\sigma}{6(2\sigma^4 + 1)} \qquad [66]$$

since $\omega(\zeta) = \zeta^{-1} - \zeta^3/6$. Next, using the expansion $\varphi_{cq}(\zeta) = \alpha_0 + \alpha_1\zeta + \alpha_2\zeta^2 + \ldots$ for substitution in Equation [17] one arrives at

$$\frac{1}{2\pi i}\int_\gamma \left[\frac{\sigma}{6} - \frac{13\sigma}{6(2\sigma^4 + 1)}\right]\left(\bar\alpha_1 + \frac{2\bar\alpha_2}{\sigma} + \frac{3\bar\alpha_3}{\sigma^2} + \ldots\right)\frac{d\sigma}{\sigma - \zeta} = \frac{\bar\alpha_1}{6}\,\zeta + \frac{\bar\alpha_2}{3} \qquad [67]$$

This result is obtained most simply by use of the following formula, concerning the integrals of Cauchy's type;[8] let

$$F(\zeta) = a_0 + a_1\zeta + a_2\zeta^2 + \ldots \qquad [68]$$

be a function holomorphic inside γ and continuous up to γ. Then

$$\frac{1}{2\pi i}\int_\gamma \frac{\sigma^k\overline{F(\sigma)}}{\sigma - \zeta}\,d\sigma = \bar a_0\zeta^k + \bar a_1\zeta^{k-1} + \ldots + \bar a_k \qquad [69]$$

for every ζ inside γ and $k = 0, 1, 2, \ldots$

Equation [17] now yields zero values for all coefficients α, except for α_2 and α_7 and the result then is

$$\varphi_{cq} = \frac{qR^3}{3456D}\,(73\zeta^3 - 6\zeta^7) \qquad [70]$$

In similar manner we obtain

$$f_1 - if_2 = -\frac{qR^3}{1152D}\left(\frac{2}{\sigma^7} - \frac{73}{3\sigma^3} + 76\sigma - 12\sigma^5\right) \qquad [71]$$

which leads to the expression

$$\frac{1}{2\pi i}\int_\gamma (f_1 - if_2)\,\frac{d\sigma}{\sigma - \zeta} = -\frac{qR^3}{1152D}\,(76\zeta - 12\zeta^5) \qquad [72]$$

on the right side of Equation [18], while the integrand on the left side is given by

$$\frac{\overline{\omega(\sigma)}}{\omega'(\sigma)} = \frac{1}{6\sigma} - \frac{13\sigma^3}{6(2 + \sigma^4)} \qquad [73]$$

and

$$\varphi_{0q}'(\sigma) = \frac{qR^3}{1152D}\,(73\sigma^2 - 14\sigma^6) \qquad [74]$$

Now the second term in Equation [18]

$$\frac{qR^3}{6912D}\,\frac{1}{2\pi i}\int_\gamma \left(\frac{1}{\sigma} - \frac{13\sigma^3}{2 + \sigma^4}\right)\frac{73\sigma^2 - 14\sigma^6}{\sigma - \zeta}\,d\sigma = \frac{qR^3}{6912D}\left(73\zeta^3 - \frac{977\zeta^5 - 168\zeta^9}{2 + \zeta^4}\right) \qquad [75]$$

can be obtained by means of the theory of residues and the result

$$\psi_{cq} = -\frac{qR^3}{6912D}\,\frac{1058\zeta - 592\zeta^5 + 96\zeta^9}{2 + \zeta^4} \qquad [76]$$

then is readily established. Next, taking into account Equation [27] we have by integration

$$\chi_{cq} = \frac{qR^4}{27648D}\,(2116\log\zeta - 296\zeta^4 + 24\zeta^8) + c_0 \qquad [77]$$

in which c_0 is a constant. The function w_{0q}, but for this constant, now is defined by the fundamental relation, Equation [28], while the constant c_0 is obtainable from the condition $w_{0q} + w_{cq} = 0$ on γ. The final result then is that given by Equation [31].

Lastly, let us determine the bending moments which correspond

[8] See reference (8) p. 275.

to the nonbiharmonic part w_{0q} of the solution. According to Equation [24]

$$M_\theta + M_\rho = -(1+\nu)D\Delta w_{0q} = -\frac{q(x^2+y^2)}{4} \quad \ldots [78]$$

and in order to express this sum of moments in terms of ρ,θ we have only to use Equation [22]. As for the difference $M_\theta - M_\rho$ it can be obtained most simply by means of the relation

$$M_\theta - M_\rho - 2iM_{\rho\theta} = (M_y - M_x - 2iM_{xy})e^{2i\alpha} \quad \ldots [79]$$

which results from purely geometrical considerations.[9] The bending moments M_x, M_y, M_{xy} herein contained are readily found from the expression $w_{0q} = qr^4/64D$ by usual differentiation[10] followed by transformation, while the factor $e^{2i\alpha}$ is given by the formula

$$e^{2i\alpha} = \frac{\omega'(\zeta)}{\omega'(\zeta)}\, e^{2i\theta} \quad \ldots [80]$$

As for the moments due to the part w_{cq} of the deflection they are given by Equations [9] in which the Functions [70] and [77] must be substituted.

BIBLIOGRAPHY

1 "Die Lösung des Pilzdeckenproblems durch Fouriersche Reihen," by V. Lewe, *Bauingenieur*, vol. 1, 1920, p. 631.

2 "Beitrag zur Theorie der Pilzdecken," by S. Woinowsky-Krieger, *Zeitschrift für angewandte Mathematik und Mechanik*, vol. 14, 1934, p. 13.

3 "Über die Biegung durchlaufender Platten und der rechteckigen Platte mit freien Rändern," by A. Nadai, *Zeitschrift für angewandte Mathematik und Mechanik*, vol. 2, 1922, p. 1.

4 "Über Spannungszustände in dünnen Rechteckplatten," by F. Tölke, *Ingenieur-Archiv*, vol. 5, 1934, p. 187.

5 "Moments and Stresses in Slabs," by H. M. Westergaard and W. A. Slater, Proceedings of the American Concrete Institute, vol. 17, 1921.

6 "Bestemmelse af Spændinger i Plader," by N. J. Nielsen, Copenhagen, Denmark, first edition, 1920, p. 171.

7 "Die Theorie elastischer Gewebe und ihre Anwendung auf die Berechnung biegsamer Platten," by H. Marcus, Julius Springer, Berlin, Germany, first edition, 1924.

8 "Nekotorye Osnovnye Zadaci Matematičeskoj Teorii Uprugosti" ("Some Fundamental Problems in Mathematical Elasticity"), by N. I. Muscheliśvili, Moscow-Leningrad, USSR, third edition, 1949.

9 "Mathematical Theory of Elasticity," by I. S. Sokolnikoff, McGraw-Hill Book Company, Inc., New York, N. Y., first edition, 1946, p. 170.

10 "Some Questions Concerning the Theory of Bending of Thin Plates," by S. G. Lechnickii, Akademia Nauk SSSR, Prikladnaya Matematika i Mehanika, vol. 2, 1938, p. 181.

11 "Bending of a Thin Isotropic Plate Having an Aperture," by M. M. Friedman, Akademia Nauk SSSR, Prikladnaya Matematika i Mehanika, vol. 4, 1945, p. 334.

12 "Koncentraciya napryaženii okolo otverstii" ("Stress Concentration Near Holes"), by G. N. Savin, Moscow-Leningrad, USSR, first edition 1951, p. 348.

13 "Sur l'équation $\Delta\Delta u = 0$," by E. Goursat, Bulletin de la Societé Mathématique de France, vol. 26, 1898, p. 236.

14 "Theory of Plates and Shells," by S. Timoshenko, McGraw-Hill Book Company, Inc., New York, N. Y., first edition, 1940, p. 88.

15 "The Effect of Transverse-Shear Deformation on the Bending of Elastic Plates," by E. Reissner, JOURNAL OF APPLIED MECHANICS, Trans. ASME, vol. 67, 1945, p. A-69.

[9] See reference (12), p. 366.

[10] See, for instance, reference (14), p. 88.

Impulsive Response of Beams in the Elastic and Plastic Regions[1]

By W. T. THOMSON,[2] LOS ANGELES, CALIF.

The problem of the impulsive response of a beam in the elastic and plastic regions is discussed. The beam in the plastic region is simulated by yield hinges where the moment reaches a constant yield value. Transition from the elastic to the plastic beam, including the satisfaction of the initial conditions imposed on the plastic beam, is accomplished automatically in terms of the normal mode solution of each. A practical computing scheme making use of the electronic analog computer is described. Some elastic-plastic solutions obtained by the computer are presented.

Nomenclature

The following nomenclature is used in the paper:

$y(x, t)$ = deflection at x at time t, in.
$p(x, t)$ = intensity of load at x at time t, lb per in.
$m = m_o m(x)$ = mass per unit length, lb sec^2 in.$^{-2}$
m_o = reference mass per unit length, lb sec^2 in.$^{-2}$
$m(x)$ = nondimensional mass distribution
E = Young's modulus, psi
I = moment of inertia of beam cross section, in.^{4}
$\phi_i(x)$ = normal mode deflections of original beam (nondimensional)
$\psi_i(x)$ = normal mode deflections of beam with moment hinge (nondimensional)
ω_i = natural frequencies of original beam, radian/sec (rps)
Ω_i = natural frequencies of hinged beam, radian/sec
l = length of beam
$\beta_i l$ = eigenvalue of normal mode equation (nondimensional)
$Y_i(t)$ = time-dependent coefficient of deflection expansion, in.
$P_i(t)$ = time-dependent coefficient of loading expansion, lb/in.
P_o = total load at $f(t) = 1.0$, (lb)
$p(x)$ = space distribution of loading (nondimensional)
$f(t)$ = time distribution of loading (nondimensional)
K_i = participation factor defined by Equation [12] (nondimensional)
$D_i(t)$ = dynamic load factor defined by Equation [14] (nondimensional)
$U'(x - a)$ = unit impulse function at $x = a$, (in.$^{-1}$)
M_o = moment, lb-in.
$\theta(x, t)$ = slope at x at time t (nondimensional)
t_1 = time at which moment reaches a yield limit
t_2 = time corresponding to maximum hinge rotation

Elastic-Plastic Response of a Beam

When a beam of any stiffness and mass distribution is excited by a force of arbitrary space and time distribution, its response in the elastic range can be expressed in terms of its normal modes of oscillation. The development of these equations for various types of loading are given in the Appendix.

When the beam is loaded beyond the elastic range the problem becomes too complex to solve without simplifying assumptions. A solution is possible, however, under the following assumptions:

1 The region of plastic behavior represents a small fraction of the beam span.

2 The plastic zone constitutes a yield hinge where the moment reaches a constant yield value.

3 The positions of the yield hinges remain unchanged.

4 The beam sections between yield hinges behave elastically and are excited by forces and moments developed at the hinge of the original beam.

Briefly, the problem in the elastic-plastic range can be described as follows: Letting $\phi_i(x)$ be the normal modes of the elastic beam with its original constraints, and $\psi_i(x)$ the normal modes of the plastic beam with the yield hinge or hinges, the equations in term of $\phi_i(x)$ apply until a yield hinge is formed at time t_1. After t_1, the response of the beam must be expressed in terms of $\psi_i(x)$ where the deflection and velocity of the original beam at t_1 now become the initial conditions for the plastic beam with the hinge. The moment at the hinge now remains constant while the beam continues to deflect. The equations in terms of $\psi_i(x)$ apply until the angle of discontinuity at the hinge reaches a maximum value, say at time t_2, after which the moment at the hinge returns elastically. The third phase subsequent to t_2 must now be expressed in terms of $\phi_i(x)$, the deflection and velocity of the plastic phase at t_2 becoming the initial conditions for the third phase. It is possible, however, for a second hinge to form before the angle of discontinuity at the first hinge reaches a maximum value, in which case the beam may become a linkage capable of sustaining load by axial tension.

The description just mentioned has been followed without modification by other investigators (1).[3] Generally, the mathematical difficulties encountered in transposing from one configuration $\phi_i(x)$ to another $\psi_i(x)$ with its necessary initial conditions are so great that only a few simple problems could be treated by such a scheme.

The procedure to be described here follows the sequence of behavior described previously without the difficulties of transposing from one beam configuration to another. The initial conditions at time t_1 are also satisfied automatically. The procedure is best illustrated by the following example.

---

[1] Research underlying this paper was conducted at the University of California at Los Angeles under Contract Noy 73231 with the U. S. Naval Civil Engineering Research and Evaluation Laboratory, Port Hueneme, Calif.

[2] Professor of Engineering, University of California, Los Angeles, Calif. Mem. ASME.

Presented at the West Coast Meeting of the Applied Mechanics Division, Berkeley, Calif., June 21–23, 1954 of The American Society of Mechanical Engineers.

Discussion of this paper should be addressed to the Secretary, ASME, 29 West 39th Street, New York, N. Y., and will be accepted until October 11, 1954, for publication at a later date. Discussion received after the closing date will be returned.

Note: Statements and opinions advanced in papers are to be understood as individual expressions of their authors and not those of the Society. Manuscript received by ASME Applied Mechanics Division, December 15, 1953. Paper No. 54—APM-5.

[3] Numbers in parentheses refer to the Bibliography at the end of the paper.

Clamped-Clamped Beam (Scheme 1)

Consider here a clamped-clamped uniform beam loaded by a concentrated force of arbitrary time variation $f(t)$ at the mid-span as shown in Fig. 1(a). For such a configuration, the dynamical moment at the clamped ends at the end of the elastic range is approximately 1.6 times that at the center, and hence the yield hinge will first form at the clamped ends, and then later at the mid-span.

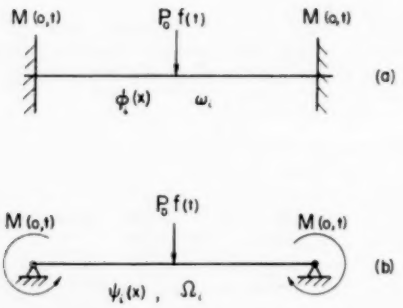

Fig. 1

Fig. 1(b) shows the hinged beam loaded by the same force at mid-span and also by the end moments $M(0, t)$ developed in the clamped beam. Thus the two configurations (a) and (b) should give identical results, the only difference being that in (b) the response is expressed in terms of $\psi_i(x)$ with natural frequencies Ω_i whereas in (a) the equations are expressed in terms of $\phi_i(x)$ and ω_i. In the last section of the Appendix it is shown that the two results are identical in that the quantities in terms of the natural frequencies Ω_i of the hinged beam cancel out leaving only quantities in terms of the natural frequencies ω_i of the clamped beam.

Having established the fact that (b) is identical to (a) even if the equations are generated in terms of $\psi_i(x)$ and Ω_i, it is a simple matter to go from the elastic into the plastic region by merely limiting the moment $M(0, t)$ at the yield value. It should be noted that the initial conditions are then automatically satisfied since configuration (b) applies to both the elastic and plastic regions.

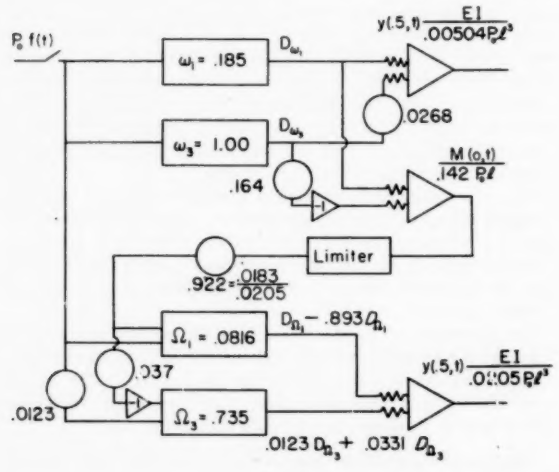

Fig. 2

Fig. 2 shows an analog-computer circuit to carry out the foregoing operation. As described in a previous paper (2), the computer generates the dynamical load factors $D_i(t)$ which can be summed with proper space coefficients to obtain deflection or moment at any point. The computer is then calibrated for a step-function input, after which the response for any time variation of input becomes known.

In Fig. 2 the first two symmetric modes of the clamped beam are summed to develop the deflection at the center and the moment at the clamped ends. If the configuration of Fig. 1(b) is used, the end moment is passed through a limiter and applied together with the central load to the modes of the hinged beam. With proper settings of the potentiometers, the output of the hinged modes can represent deflection at any point. It should be noted here that when the limiter is by-passed the two deflections, Fig. 1 (a and b), must be equal except for a constant multiplier. The effect of the limiter then is equivalent to applying a moment opposing part of the elastic moment.

Clamped-Clamped Beam (Scheme 2)

The computing scheme shown in Fig. 2 has certain practical disadvantages. As mentioned previously the terms in the dynamic load factor containing Ω_i must cancel in the elastic range, leaving only terms relating to the original clamped modes of frequency ω_i. In many cases the terms to be canceled are larger than the terms to be retained, thereby imposing a serious accuracy requirement on the computer (3).

To avoid this difficulty a second scheme of Figs. 3 and 4 is proposed. Fig. 3(a) is now equivalent to the superposition of Fig. 3 (b and c) where the constant yield moment is obtained by the difference between the elastic moment M_e and the plastic moment M_p. The beam (c) has zero deflection up to time t_1 after which the deflection in the plastic region is given by the sum of (b) and (c). This procedure then requires no cancellation of modes and hence avoids the difficulty mentioned previously.

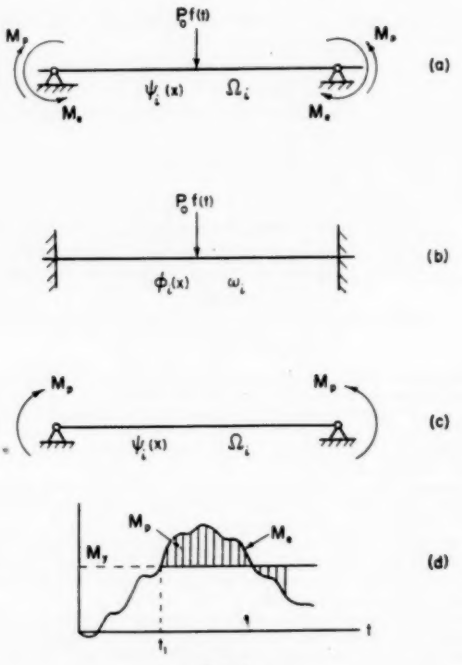

Fig. 3

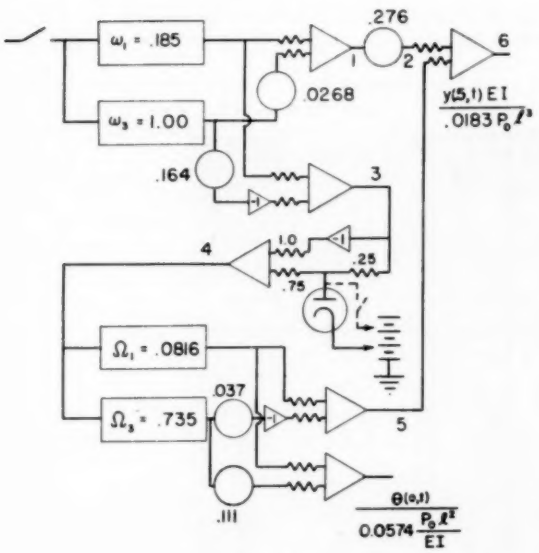

FIG. 4

rence of the maximum hinge angle or the formation of a second hinge at mid-span. Equations pertinent to the circuit of Fig. 4 are given in the Appendix.

The motion of the beam subsequent to time t_2 needs consideration only if a second hinge does not form. In this case the beam ends must be suddenly clamped at time t_2 as shown in Fig. 5 and the subsequent motion must be elastic with initial displacement and velocity imposed by the previous configuration of Fig. 3 at time t_2. The maximum hinge angle θ_{max} now remains fixed while the deflection and hinge moment decrease elastically until a yield moment in the opposite sense is reached.

A computer to accomplish the latter phase of transition from the plastic to the elastic motion entails some difficulties which are undergoing study at present. One possible approach is to assume the velocity of the pinned-pinned beam at time t_2 to be zero everywhere instead of only at the hinge. This is equivalent to ignoring the velocities of the higher modes of the pinned beam. With this assumption the computer generating M_p and the deflection of the pinned beam can be placed on "hold," in which case the subsequent displacement and hinge moment becomes the superposition of Fig. 3(*b*) and the frozen configuration of Fig. 5 including M_p.

Computer Solutions. The machine solutions presented here were obtained by the second scheme shown in Fig. 4 and apply to the clamped beam with the central load. In Figs. 6 and 7 the

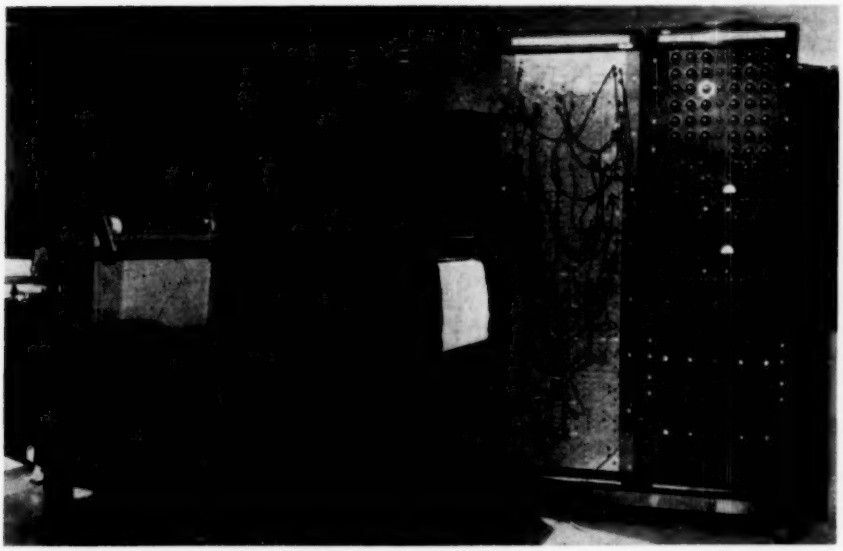

FIG. 4(*a*) VIEW OF COMPUTER

The computer for the second scheme of Fig. 3 is shown in Fig. 4. A photograph of the computer is shown in Fig. 4(*a*). Referring to the equations in the Appendix, the upper banks of the computer generate the elastic deflection at the center, and the elastic moment at the ends, of a fixed-ended beam. The elastic moment is passed through a limiter, the difference between the limited and the unlimited moment being applied to the ends of the pinned-pinned beam for which the dynamic load factor is generated by the lower banks of the computer. The upper and lower banks are then summed with proper multiplying factor to give the entire response through the elastic and into the plastic region. The results are then valid up to time t_2 corresponding to the occur-

FIG. 5

time variation $f(t)$ is a step function. The top curves in Fig. 6 represent the moment M_p applied to the hinges at the end. It should be noted that with no limiting this moment is zero. Fig. 7 shows the results for the same loading; however, the angle $\theta(0, t)$ at the ends is now shown by the top curves instead of M_p.

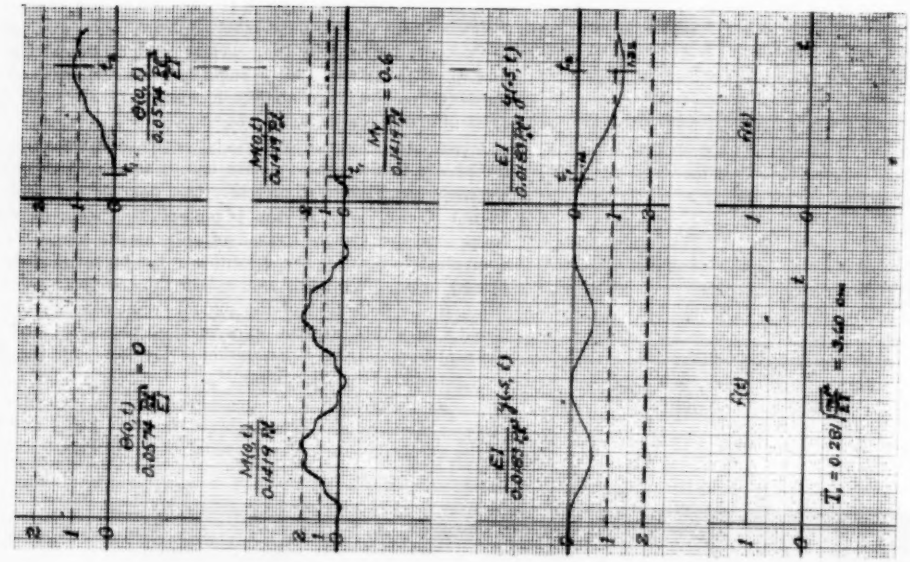

Fig. 7

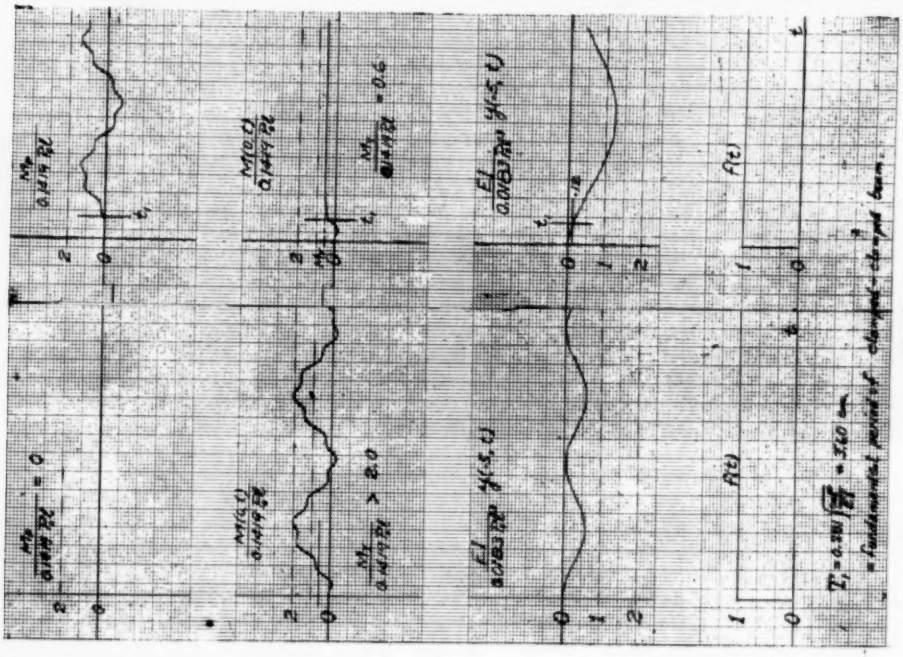

Fig. 6

Figs. 8 and 9 show solutions for larger and smaller yield moments with both the step and an arbitrary time variation of the load.

The solutions presented assume that the subsequent hinge at mid-span does not form and hence is applicable to time t_2.

The machine solutions presented are in nondimensional form and hence are applicable to any beam with the same load and boundary conditions. To illustrate its numerical evaluation, consider a steel beam 1 in. × 1 in. × 20 in. for which $EI/l^3 = 312$. Using 35,000 psi for the elastic limit, a yield moment of 8750 in-lb can be assumed. Referring to the plastic solution in Fig. 7 and using the foregoing yield moment, we have

$$\frac{M_y}{0.1419\,P_o l} = \frac{8750}{0.1419 \times 20 \times P_o} = 0.6$$

$$P_o = 5140 \text{ lb}$$

Thus a load of 5140 lb will produce the response shown in Fig. 7.

The maximum elastic deflection at mid-span is found from the deflection curve at t_1 to be

$$\frac{312}{0.0183 \times 5140}\, y(0.5, t_1) = 0.14$$

$$y(0.5, t_1) = 0.0421 \text{ in.}$$

Similarly, the maximum deflection into the plastic region is

$$\frac{312}{0.0183 \times 5140}\, y(0.5, t_2) = 1.22$$

$$y(0.5, t_2) = 0.368 \text{ in.}$$

Thus a permanent set in deflection of 0.326 in. can be expected at the center, with a permanent set in the angle at the supports of $\theta(0, t_2) = 0.0567$.

Conclusions

An analog scheme has been developed for computing the deflection of beams in the elastic and plastic regions. The procedure outlined is applicable only to symmetric cases and requires modifications for unsymmetric loading, or where the positions of the yield hinges change with deflection. The accuracy obtainable with the analog computer depends to a great extent on the operator setting up the problem and to the number of modes included in the computation. A fair estimate on the equipment used is approximately 10 per cent.

BIBLIOGRAPHY

1 "Impulsive Motion of Elastic-Plastic Beams," by H. H. Bleich and M. G. Salvadori, Proceedings of the ASCE, vol. 79, September, 1953, p. 287.

2 "Analog Solution for Beams Excited by an Arbitrary Force,"

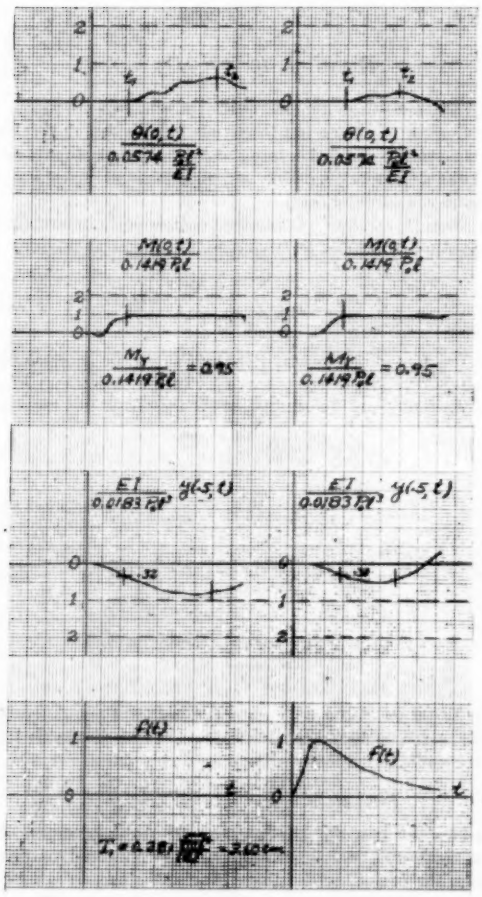

Fig. 8

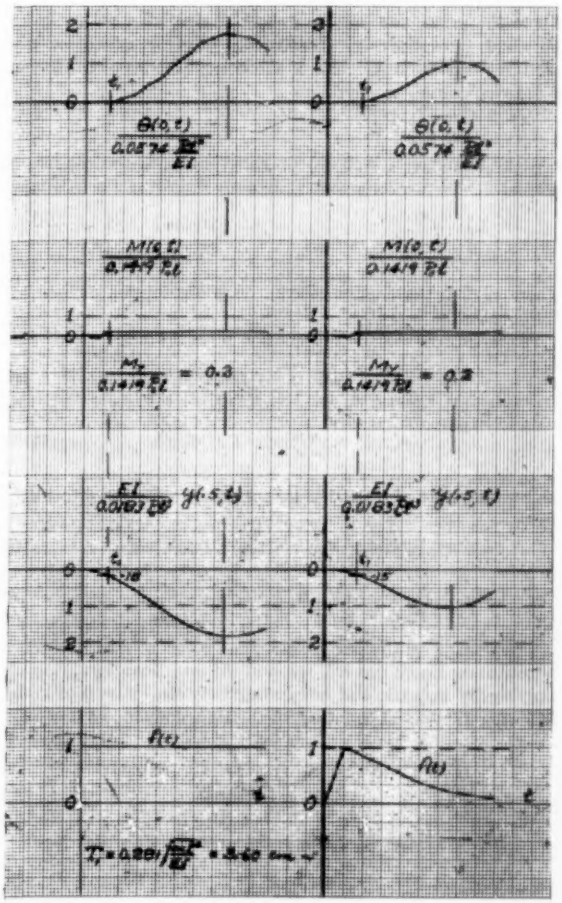

Fig. 9

by W. T. Thomson and T. A. Rogers, JOURNAL OF APPLIED MECHANICS, Trans. ASME, vol. 75, 1953, pp. 482–484.

3 "Dynamic Response of Beams in and Beyond the Elastic Range," by W. T. Thomson, J. M. English, and J. A. Cheney, University of California Engineering Report 53–19, August, 1953.

4 "Mechanical Vibrations," by W. T. Thomson, second edition, Prentice-Hall, Inc., New York, N. Y., 1953, p. 186.

5 "Tables of Characteristic Functions Representing Normal Modes of Vibration of a Beam," by D. Young and R. P. Felgar, Jr., University of Texas Publication No. 4413, July 1, 1949.

6 "Laplace Transformation" by W. T. Thomson, Prentice-Hall, Inc., New York, N. Y., 1950, pp. 25–27.

7 "Dynamic Load Characteristics in Plastic Bending of Beams," by P. S. Symonds, JOURNAL OF APPLIED MECHANICS, Trans. ASME, vol. 75, 1953, pp. 475–481.

8 "Large Plastic Deformations of Beams Under Transverse Impact," by E. H. Lee and P. S. Symonds, JOURNAL OF APPLIED MECHANICS, Trans. ASME, vol. 74, 1952, pp. 308–314.

9 "On the Development of Plastic Hinges in Rigid-Plastic Beams," by M. G. Salvadori and F. Di Maggio, Quarterly of Applied Mathematics, vol. XI, 1953, pp. 223–230.

Appendix

General Equations

When the effect of rotatory inertia and deflection due to shear are negligible the flexural motion of a beam of variable stiffness and mass distribution is governed by the differential equation

$$[EI\ y''(x,t)]'' + m\ \ddot{y}(x,t) = p(x,t) \quad [1]$$

where the prime and dot represent differentiation with respect to x and t, respectively. Equation [1] can be solved for any arbitrary excitation in terms of the normal modes of oscillation $\phi_i(x)$ which satisfy the equation

$$[EI\ \phi_i''(x)]'' - m\omega_i^2\ \phi_i(x) = 0 \quad [2]$$

and the boundary conditions of its space configuration. Such normal modes are orthogonal functions satisfying the relation

$$\frac{1}{l}\int_0^l m(x)\phi_i(x)\phi_j(x)\,dx = \begin{cases} 0 \text{ for } i \neq j \\ 1 \text{ for } i = j \end{cases} \quad [3]$$

where $m(x)$ is the nondimensional mass distribution defined by the equation $m = m_o\,m(x)$.

Expressing the solution of Equation [1] in the form

$$y(x,t) = \sum_i Y_i(t)\,\phi_i(x) \quad [4]$$

$$p(x,t) = \sum_i m(x)\,P_i(t)\phi_i(x) \quad [5]$$

and taking note of Equation [3] the time coefficients become

$$Y_i(t) = \frac{1}{l}\int_0^l m(x)y(x,t)\phi_i(x)\,dx \quad [6]$$

$$P_i(t) = \frac{1}{l}\int_0^l p(x,t)\phi_i(x,t)\,dx \quad [7]$$

Substituting Equations [2], [4], and [5] into Equation [1], multiplying by $\phi_i(x)dx$, and integrating between limits 0 to l, the following differential equation for the time domain is obtained

$$\ddot{Y}_i(t) + \omega_i^2 Y_i(t) = \frac{1}{m_o l}\int_0^l p(x,t)\phi_i(x)\,dx \quad [8]$$

We will assume here that the intensity of loading can be expressed by the following product

$$p(x,t) = \frac{P_o}{l}\,p(x)f(t) \quad [9]$$

where $p(x)$ and $f(t)$ are the nondimensional space and time distribution of the loading. P_o can then be defined as the total load at $f(t) = 1$, in which case we have the normalizing relationship

$$\frac{1}{l}\int_0^l p(x)\,dx = 1 \quad [10]$$

Equation [8] then reduces to

$$\ddot{Y}_i(t) + \omega_i^2 Y_i(t) = \left(\frac{P_o K_i}{m_o\omega_i^2 l}\right)\omega_i^2 f(t) \quad [11]$$

$$K_i = \frac{1}{l}\int_0^l p(x)\,\phi_i(x)\,dx \quad [12]$$

The quantity K_i determines the extent to which the various modes contribute to the motion of the beam and hence is appropriately called the participation factor.

The solution of Equation [11] is of the form

$$Y_i(t) = Y_i(0)\cos\omega_i t + \frac{1}{\omega_i}\dot{Y}_i(0)\sin\omega_i t + \left(\frac{P_o K_i}{m_o\omega_i^2 l}\right)\omega_i\int_0^t f(\xi)\sin\omega_i(t-\xi)\,d\xi \quad [13]$$

where $Y_i(0)$ and $\dot{Y}_i(0)$ are the ith mode components of the initial conditions which are taken to be zero when the beam is started from rest. The nondimensional quantity

$$D_i(t) = \omega_i\int_0^t f(\xi)\sin\omega_i(t-\xi)\,d\xi \quad [14]$$

is generally called the dynamic load factor for the ith mode, the significance of the name implying that if the static deflection of the beam is also expanded in terms of $\phi_i(x)$, a comparison between it and the dynamical equation will show that each term of the expansion will differ by $D_i(t)$.

Equation [4] can now be expressed conveniently in terms of the participation factor and the dynamic load factor as follows

$$y(x,t) = \frac{P_o}{m_o l}\sum_i \frac{K_i\phi_i(x)}{\omega_i^2}\,D_i(t) \quad [15]$$

For the nonuniform beam, $\phi_i(x)$ and ω_i can be determined by the tabular method of reference (4). In the case where EI and m are constant along the beam

$$\omega_i^2 = (\beta_i l)^4\,\frac{EI}{m_o l^4} \quad [16]$$

where $\beta_i l$ is the eigenvalue of the normal mode equation and depends only on the boundary conditions. For uniform beams $\phi_i(x)$, $\beta_i l$, and ω_i are tabulated by Young and Felgar (5). By substituting from Equation [16], Equation [15] for the uniform beam reduces to

$$y(x,t) = \frac{P_o l^3}{EI}\sum_i \frac{K_i\phi_i(x)}{(\beta_i l)^4}\,D_i(t) \quad [17]$$

where all terms within the summation sign are nondimensional. The slope, moment, and shear are obtained from Equation [15] or Equation [17] by successive differentiations.

Equations for Specified Loadings

Besides the case for the arbitrary space distribution, three special cases of load distribution are encountered frequently, namely, the uniformly distributed force, the concentrated force, and the concentrated moment. The load distribution affects only

the participation factor, the development of which is given for the foregoing cases as follows:

(*a*) Uniformly distributed force, $p(x) = 1$

$$K_i = \frac{1}{l}\int_0^l \phi_i(x)\,dx \quad \ldots\ldots [18]$$

(*b*) Concentrated force at $x = a$: The loading $p(x)$ corresponding to the concentrated force at $x = a$ can be represented by an impulse function (6) $lU'(x - a)$ as shown in Fig. 10.

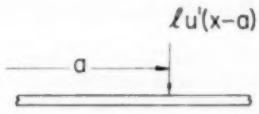

FIG. 10

The participation factor thus becomes

$$K_i = \frac{1}{l}\int_0^l lU'(x-a)\phi_i(x)\,dx = \phi_i(a) \quad \ldots\ldots [19]$$

The equation for the deflection for this case is

$$y(x, t) = \frac{P_o l^3}{EI}\sum_i \frac{\phi_i(a)\phi_i(x)}{(\beta_i l)^4} D_i(t) \quad \ldots\ldots\ldots [20]$$

(*c*) Concentrated moment $M_o f(t)$ at $x = a$: The loading $p(x)$ corresponding to the concentrated moment is the limiting case of two impulse functions shown in Fig. 11 as $c \to 0$. The participation factor then becomes

$$K_i = \lim_{c\to 0}\frac{1}{l}\int_0^l \frac{l^2}{c}\,[U'(x-a) - U'(x-a-c)]\phi_i(x)\,dx$$

$$= l\lim_{c\to 0}\left[\frac{\phi_i(a) - \phi_i(a+c)}{c}\right] = l\,\frac{d\phi_i(a)}{dx} = \beta_i l\,\phi_i'(a) \quad [21]$$

where

$$\beta_i\phi_i'(a) = \frac{d\phi_i(a)}{dx}$$

The deflection for this case becomes

$$y(x, t) = \frac{M_o l^2}{EI}\sum_i \frac{\phi_i'(a)\phi_i(x)}{(\beta_i l)^3} D_i(t) \quad \ldots\ldots [22]$$

Equations for Clamped-Beam Problem

For the beam of Fig. 3(*b*) the deflection at mid-span and the moment at the ends are obtainable from Equation [20] as follows

$$y(0.5, t) = \frac{P_o l^3}{EI}\sum_i \frac{\phi_i^2(0.5)}{(\beta_i l)^4} D_i(t)$$

$$= \frac{P_o l^3}{EI}\,0.0050388\,[D_1(t) + 0.02684\,D_3(t) + 0.004455\,D_5(t) + \ldots] \quad [23]$$

$$M(0, t) = P_o l\sum_i \frac{\phi_i(0.5)\phi_i''(0)}{(\beta_i l)^3} D_i(t)$$

$$= P_o l\,0.14197\,[D_1(t) - 0.16382\,D_3(t) + 0.06674\,D_5(t) + \ldots] \quad \ldots\ldots [24]$$

If $M(0, t)$ is applied to the ends of the hinged beam of Fig. 3(*c*), the deflection at its center can be determined from Equations [22] and [24] to be

$$y(0.5, t) = 2\,\frac{P_o l^3}{EI}\,0.14197\sum_i \frac{\psi_i'(0)\psi_i(0.5)}{(\beta_i l)^3}\mathfrak{D}_i(t)$$

$$= \frac{P_o l^3}{EI}\,0.018315\,[\mathfrak{D}_1(t) - 0.03704\,\mathfrak{D}_3(t) + 0.004115\,\mathfrak{D}_5(t) \ldots] \quad [25]$$

where the dynamic load factor $\mathfrak{D}_i(t)$ is the response due to

$$[D_1(t) - 0.16382\,D_3(t) + 0.06674\,D_5(t) - \ldots] \quad \ldots\ldots [26]$$

Adding the two deflections given by Equations [23] and [25] and factoring out a common term, the result is

$$\frac{EI}{0.018315\,P_o l^3}\,y(0.5, t) = [\mathfrak{D}_1(t) - 0.03704\,\mathfrak{D}_3(t) + 0.004115\,\mathfrak{D}_5(t) - \ldots] + 0.27512\,[D_1(t) + 0.02684\,D_3(t) + 0.004455\,D_5(t) + \ldots] \quad [27]$$

The slope at the hinge is obtained by differentiating Equation [25]

$$\theta(0, t) = \frac{2P_o l^2}{EI}\,0.14197\sum_i \frac{\psi_i'(0)\psi_i'(0)}{(\beta_i l)^2}\mathfrak{D}_i(t)$$

$$= 0.0574\,\frac{P_o l^2}{EI}\,[\mathfrak{D}_1(t) + 0.1111\,\mathfrak{D}_3(t) + \ldots] \quad \ldots\ldots [28]$$

Circuit diagram for the computation of Equations [27] and [28] is shown in Fig. 4.

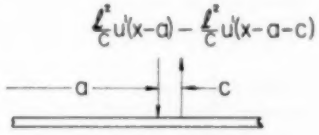

FIG. 11

Cancellation of Modes for Scheme 1

Assuming a step function for $f(t)$, the beam configurations shown in Fig. 1 (*a* and *b*) can be shown to be equivalent as follows:

The deflection at the mid-span of the simply supported beam due to a step-function load at center is

$$y(0.5, t) = \frac{P_o l^3}{EI}\,[0.020532\,D_1(t) + 0.00025348\,D_3(t) + 0.00003285 D_5(t) + \ldots] \quad [29]$$

Subtracting from Equation [29] the deflection due to the end moments $M(0, t)$ given by Equation [25], the equation to be evaluated is

$$y(0.5, t)\,\frac{EI}{P_o l^3} = 0.020532\,D_1(t) + 0.00025348\,D_3(t) + 0.00003285\,D_5(t) - 0.018315\,\mathfrak{D}_1(t) + 0.00067839\,\mathfrak{D}_3(t) - 0.000075366\,\mathfrak{D}_5(t) \quad [30]$$

where for the step-function load the dynamic load factors are

$$D_i(t) = (1 - \cos\omega_i t) \quad \ldots\ldots [31]$$

and

$$\mathfrak{D}_i(t) = \frac{1}{1 - \left(\frac{\Omega_i}{\omega_j}\right)^2}(1 - \cos \Omega_i t) + \frac{1}{1 - \left(\frac{\omega_j}{\Omega_i}\right)^2}(1 - \cos \omega_j t) \quad [32]$$

for each of the components $D_j(t)$ in Equation [26]. Thus with three modes there will be six terms for each of the $\mathfrak{D}_i(t)$. For the clamped and the hinged beams, the following numerical values are available (5):

i	ω	Ω
1	22.373	9.8696
3	120.903	88.827
5	298.556	246.741

With these numerical values, Equation [30] becomes

$$\begin{aligned} y(0.5, t)\frac{EI}{P_o l^3} &= 0.00507(1 - \cos \omega_1 t) + 0.000126(1 - \cos \omega_3 t) \\ &+ 0.0000078(1 - \cos \omega_5 t) - 0.000411(1 - \cos \Omega_1 t) \\ &- 0.000016(1 - \cos \Omega_3 t) - 0.000021(1 - \cos \Omega_5 t) \\ &\cong 0.00507[(1 - \cos \omega_1 t) + 0.0248(1 - \cos \omega_3 t)] \\ &- 0.000411(1 - \cos \Omega_1 t) \end{aligned}$$

This result indicates that with three modes it is approaching Equation [23] for the clamped-clamped beam. The terms containing $(1 - \cos \Omega_i t)$ will further diminish with the inclusion of higher modes.

Although a step function load was assumed for this proof, it can be shown that the same conclusion can be obtained for an arbitrary load variation.[4]

[4] Reference (3), p. 13.

Abstracts of Papers

Presented at the

Second U. S. National Congress of Applied Mechanics

Appearing below are authors' abstracts of all papers which have been accepted for publication in the Proceedings of the Second U. S. National Congress of Applied Mechanics. The papers were presented at the Congress, which was held at the University of Michigan, from June 14 to June 17, 1954. The Proceedings of the Congress, which will be published by The American Society of Mechanical Engineers, are to appear within the year following the Congress.

The abstracts given here are grouped according to subject matter and session schedule. In view of the current space limitations of the JOURNAL OF APPLIED MECHANICS, it has been necessary to omit at this place the titles of the authors as well as any references to sponsorship of the investigations concerned; complete information of this nature will be contained in the Proceedings. If necessary, authors may be reached through the Chairman of the Editorial Committee, Professor Paul M. Naghdi, University of Michigan, Ann Arbor, Michigan.

The Editorial Committee wishes to express its sincere appreciation to the staff of the JOURNAL OF APPLIED MECHANICS, in particular to the editor, Professor John M. Lessells, for their efforts in connection with the present publication of these abstracts.

Session 1: Limit Design; Plastic Failure

Large plastic deformations of beams under blast-type loading. P. S. Symonds, Brown University.

Plastic deformations of supported beams under dynamic loading are determined under the assumption of negligible elastic strains. Particularly simple solutions are in several cases obtained when the load-time curve is of a class defined in the paper which includes typical blast pressure curves and rectangular pulses as simple examples.

Combined concentrated and distributed load on ideally-plastic circular plates. D. C. Drucker, H. G. Hopkins, Brown University.

This paper has two main objectives. One is to extend the work on circular plates to the experimentally realizable cases of large or small overhang. The other is to demonstrate that answers may be obtained in a straightforward manner for any yield condition and almost any radially-symmetric loading. As an example, the Tresca yield criterion is assumed and the collapse condition is calculated for an overhanging circular plate subjected to both a central force and a uniformly distributed pressure within the support circle. Solutions for the simply supported and for the built-in plate appear as special cases.

The deflection of plates in the elastic-plastic range. R. M. Haythornthwaite, Brown University.

The deflections of plates with circular symmetry are computed for an elastic-plastic material that obeys the yield condition of Tresca and the associated flow rule. At any point on the plate the entire thickness is assumed to be either fully elastic or fully plastic. An annular plate simply supported at the outer radius and clamped to a centrally loaded rigid disk is analyzed in detail, the simply supported circular plate with a central concentrated load being included as a limiting case. The testing of a steel plate is described and the results obtained are compared with the theory.

An experiment on circular plates in the plastic range. R. M. Cooper, G. A. Shifrin, University of Michigan.

Nine simply supported mild-steel circular plates were loaded well into the plastic range under concentric, uniformly distributed load. Deflection, strain, and slope data were observed as functions of load. Comparison is made with the predicted limit loads of Hopkins and Prager.

The influence of shearing forces on the plastic bending of wide beams. E. T. Onat, R. T. Shield, Brown University.

The theory of the slip-line field in plane plastic flow is used to obtain critical combinations of bending moment and shearing force for a wide beam of rectangular cross section.

Session 2: Fluid Flow (Jets, Boundary Layer, Incompressible)

The stall performance of cascades. William G. Cornell, General Electric Company.

A theory is developed for the stalled performance of two-dimensional compressor and turbine cascades, yielding fluid deflection and total pressure loss. The cascade blades, idealized as infinitesimally thin flat plates, are assumed to separate at the leading edges. The flow in the jets between the separated regions is analyzed by free streamline theory. The jets are assumed to mix at constant momentum, yielding a uniform exit flow. Experimental data compare well with the theory for cascade solidities of order unity and greater. A simple approximate theory is developed, good for high solidity.

Laminar incompressible mixing of two-dimensional and axially symmetric jets. T. P. Torda, University of Illinois; W. J. Thompson, North American Aviation, Inc.; B. K. Genetti, General Electric Company.

The analysis of viscous, laminar, incompressible mixing of two-dimensional and axially symmetric jets is presented. In particular, the second region of mixing (downstream of the "potential core") of two-dimensional jets, and the third region of mixing (past the second in which the effect of the upstream boundary layers are dissipated) of axially symmetric jets are treated in detail.

Free jet boundary with consideration of initial boundary layer. A. J. Chapman, The Rice Institute; H. H. Korst, University of Illinois.

The equation of motion within the mixing region is simplified to the heat-conduction equation in an intrinsic system of co-ordinates where the solution has to satisfy the same initial and boundary conditions as in a reference system attached to the fictitious inviscid jet boundary. The momentum integral method is then applied to the velocity profiles thus obtained, leading to their localization in the reference system of co-ordinates. The turbulent problem requires the experimental determination of two empirical quantities. Numerical values for these quantities are presented for low-velocity air flow, with one apparently a constant, the other related to a boundary-layer-form parameter.

Axially symmetric diffusion in a radial-velocity field. B. A. Fleishman, Johns Hopkins University.

Soluble material, placed in a fluid with an axially symmetric radial velocity of magnitude $U(r) = a/r$, moves with the fluid and is also dispersed by molecular diffusion. Given an initial concentration distribution of solute, the concentration distribution at any subsequent time is sought. The basic equations, a diffusion-convection differential equation and an unusual type of boundary condition, are used to formulate initial-value problems for two domains, one infinite, the other bounded by a cylinder of radius R, for which formal general solutions are obtained. Several examples are worked out for specific initial data.

Pressure-probe response in fluctuating flow. R. E. Kronauer, H. P. Grant, Harvard University.

Theory predicts and experiment confirms that the equilibrium pressure recorded by conventional probes deviates considerably from the time average of the imposed fluctuation (by as much as 15 per cent of the fluctuation amplitude if the probe hole is short or the frequency low) when fluctuations are nonsymmetrical about the average. The analysis is for incompressible flow. Curves useful in predicting probe behavior are presented.

Session 3: Vibrations (Miscellaneous); Beams

A simple approximation for the fundamental frequencies of two-span and three-span continuous beams. A. S. Veletsos, N. M. Newmark, University of Illinois.

A rapid approximate method is presented for calculating the fundamental frequencies of flexural vibration of two-span beams and of particular arrangements of three-span beams which are continuous over nondeflecting supports and are elastically restrained against rotation at their end supports. The stiffnesses of the end restraints are assumed to be positive. The mass per unit of length and the flexural rigidity of the cross section of the beams may vary from one span to the next, but in any one span these quantities are considered constant. The application of the method is illustrated by two numerical examples.

Determination of the natural frequencies of continuous beams on flexible supports. A. S. Veletsos, N. M. Newmark, University of Illinois.

The purpose of this paper is to present a method for calculating the undamped natural frequencies of flexural vibration of continuous beams on flexible supports. The supports are represented by a set of mutually independent, linearly elastic, deflectional and rotational springs. The effects of concentrated masses, attached either directly to the beam or through a spring, are also considered.

Coupled bending torsion vibration of a trapezoidal box beam with warping restraint. Hsu Lo, R. J. H. Bollard, Purdue University.

An integrodifferential equation in terms of axial warping is established for the determination of the effect of secondary stresses on the fundamental frequency and mode of vibration of a cantilever box beam of trapezoidal cross section, having a concentrated mass at any station along its length. The equation is solved exactly as a characteristic value problem.

An experimental device for obtaining elastic rotational constraint on boundary of a plate. W. H. Hoppmann, II, Joshua Greenspon, Johns Hopkins University.

For use in various technological investigations requiring the flexural vibrations of plates, there is presented in this paper an experimental method for providing prescribed elastic rotational constraint on the boundary of a plate. In particular, it is shown how the conditions known as simple support or hinged edge can be obtained satisfactorily. To obtain the various edge conditions a 90 deg V-notch of given depth to plate thickness ratio is provided at the boundary of the plate leaving a narrow flat rim extending beyond. This rim is then mounted rigidly in a surrounding support.

The use of self-equilibrating functions in solution of beam problems. G. Horvay, J. S. Born, General Electric Company.

A method is presented for the analysis of deep beams. It involves the use of approximate stress functions which satisfy all the boundary conditions of the problem.

Session 4: Nonlinear Vibrations

On the stability of a nonlinear nonautonomous system. R. M. Rosenberg, University of Toledo.

The stability of solutions of the equation $\ddot{x} + a^2x + f(t)\,x^3 = 0$ is investigated for several functions $f(t)$. This type of differential equation arises in the stability of rolling elastic missiles, and in dynamic systems where the forcing function is proportional to the square of the displacement. The cases investigated include those where $f(t)$ is monotone and (a) does not, or (b) does go to infinity with t, or (c) it is periodic with arbitrary period. In case

(a) the solutions are found to be stable; in case (b) they are not; and in case (c) the solutions are stable or not with those of a Mathieu equation.

Steady-state motion of one and two-degrees-of-freedom vibrating systems with a nonlinear restoring force. Patarasp Rustomji Sethna, Bendix Aviation Corporation.

In this paper are studied the steady-state motions of one and two-degrees-of-freedom vibrating systems with quadratic or cubic nonlinear restoring forces and under the influence of external sinusoidal excitations.

The first and second approximations are given for some one-degree-of-freedom undamped systems, and first approximations are given for the undamped and damped cases of a two-degrees-of-freedom system.

The adequacy of the methods employed is demonstrated by comparing the results obtained by them with those obtained from an Electronic Analog Computer.

On the stability of harmonic solutions of a modified form of Duffing's equation. Dana Young, P. N. Hess, Yale University.

Theoretical analyses of the stability of periodic solutions of Duffing's equation indicate certain unstable regions for which the practical significance has not been determined. This paper reports an investigation of the actual behavior in these theoretically unstable regions. The work was carried out on an analog computer using a modified form of the equation which has an exact harmonic solution. The results verify that the harmonic solutions became unstable in the predicted regions. In addition, it is found that certain unusual nonharmonic periodic solutions are stable in these regions.

The attenuation of damped free vibrations and the derivation of the damping law from recorded data. K. Klotter, Stanford University.

An approximate method, known in nonlinear mechanics as the "Kryloff-Bogoliuboff Method," allows describing in closed form the attenuation of free damped vibrations, for a large variety of damping laws, provided the damping forces are sufficiently weak. From the expressions for the attenuation it is possible to derive rules for finding the damping law from a set of observed data.

Subharmonic oscillations in nonlinear systems of two degrees of freedom. T. C. Huang, University of Illinois.

This paper deals with subharmonic oscillations in particular systems of two degrees of freedom with nonlinear restoring force. Qualitative results for subharmonics of order one third are developed for (1) subharmonic response with damping neglected, and (2) subharmonics with viscous damping. In the first case, frequency ranges at which subharmonics can exist are shown; while in the second case, it is verified that the coefficient of viscous damping should be small in order that subharmonic oscillations can occur. Fourier series has been chosen to treat the problem and the iteration method has been illustrated to calculate the coefficients of the series.

Session 5: Fluid Flow (Potential, Wave Phenomena)

Two-dimensional potential flow in a gravitational field with a known free stream. Kin N. Tong, Syracuse University.

This paper contains a method of analytic continuation which can be used to determine the flow in the neighborhood of a known free streamline whose shape can be described by a real analytic function $y = f(x)$.

On surface waves generated by traveling disturbances with circular symmetry. R. C. F. Bartels, University of Michigan; A. C. Downing, Jr., Oak Ridge National Laboratory.

Kelvin's ship wave problem for the surface waves produced by a distribution of pressure moving with constant velocity on the surface of a body of water with infinite depth is formulated in terms of a singular integrodifferential equation. The expression for the predominant part of the surface wave produced behind the moving source of disturbance is obtained from the solution of this equation with the aid of the Abelian theorems for the complex inversion integral in the theory of Laplace transforms. The special case of a moving pressure point is given careful treatment.

Flow through a cascade in flapping oscillation. Chieh-Chien Chang, Wen-Hua Chu, University of Maryland.

In a uniform flow a cascade of flat-plate airfoils is subject to small flapping oscillation and is treated analytically with conformal mapping technique. Normal force and moment are given essentially in closed forms. The interference effects among the cascade airfoils are so significant that the usual approximation with single-airfoil theory is questionable. Some examples are given to demonstrate this point. The wake interference is expressed in ratio of hypergeometrical functions involving parameters, such as reduced frequency and gap-chord ratio. As the gap goes to infinity, it reduces to Theodorsen's function as a special case.

Stability of parallel laminar flow with a free surface. Chia-Sun Yih, State University of Iowa.

The stability of parallel laminar flow with respect to wave formation at the free surface is investigated. Since the flow can be expected to become unstable at low Reynolds numbers, the well-known Sommerfeld-Orr equation is solved by a series expansion in ascending powers of the Reynolds number. For a specified slope of the primary flow, the relationship between the Reynolds number and the wave number for neutral stability can be obtained. Numerical calculations carried out for the case of vertical flow show that the flow becomes unstable at very low Reynolds numbers. The present work should contribute to the understanding of wave phenomena occurring in a flowing viscous liquid.

Ducts for accelerated flow. T. C. Lin, Brown University.

A method of design for two-dimensional contracting ducts for incompressible and inviscid flow has been developed which gives a rapid change of cross section with no pressure discontinuity or adverse pressure gradient. While giving essentially uniform flow

on both ends it yields ducts of smaller over-all length and shorter wall length than those given by existing methods for any contraction ratio. The design is based on a fan-shaped boundary chosen in the hodograph plane, for which the flow is found by conformal mapping. As examples of the method, the design of ducts of contraction ratios 3 and 10 is carried out.

Session 6: Shells

General instability of ring-reinforced cylindrical shells subject to hydrostatic pressure. W. A. Nash, David Taylor Model Basin.

An analytical solution is presented for the problem of the general instability failure of a geometrically perfect ring-stiffened cylindrical shell subject to external hydrostatic pressure. In this type of failure both the shell and the reinforcing rings collapse simultaneously into a number of lobes spaced uniformly around the circumference of the cylinder and extending between bulkheads closing the ends of the cylinder. This distance is a significant parameter in this problem. In this study a displacement configuration is introduced which implies clamped ends at the bulkheads.

Analysis of stresses in the conical elements of shell structures. C. E. Taylor, E. Wenk, Jr., David Taylor Model Basin.

The Love-Meissner analysis for thin shells has previously been applied to cones of uniform wall thickness, and solutions for the stress resultants were given in terms of Kelvin's functions. Since tabulation of these functions for large arguments is not practical, considerable computation was still required. In the present paper the authors define special functions which eliminate the necessity of evaluating Kelvin's functions and which may be used with simple algebraic and trigonometric functions to compute the boundary forces and displacements for cones for various loading conditions. These special functions also make clear the magnitude of errors which result from Geckeler's and other approximate solutions.

Sound radiation from an elastic cylindrical shell submerged in an infinite medium. H. H. Bleich, Columbia University.

Based on results from a previous publication, the paper determines the sound field due to a periodic force acting on an infinitely long elastic shell which is submerged in an acoustic medium. The radiation is expressed by a Fourier integral which can be evaluated simply for points at large distances.

To obtain realistic results for the radiation at resonant frequencies structural damping is introduced in the analysis in an approximate manner.

While the theory assumes an unstiffened steel shell it is approximately applicable to ring-stiffened shells. Numerical results are given for a ring-stiffened steel shell in water.

The response of a cylindrical shell to a transverse shock wave. Melvin L. Baron, Columbia University.

The elastic response of a cylindrical shell to a transverse shock wave in an acoustic medium is obtained by an expansion of the response into normal modes of oscillation of the structure, including both inextensional and extensional effects in all modes. The axis of the shell is parallel to the wave front.

An approximate mathematical solution is obtained for the response of the shell. This is compared with the results obtained from a previously published theory by R. D. Mindlin and H. H. Bleich, which neglects extensional effects in all but the dilatational mode, $n = 0$.

On the in-vacuo vibrations of simply supported, ring-stiffened cylindrical shells. Gerard D. Galletly, David Taylor Model Basin.

An analytical solution is presented for the problem of determining the in-vacuo frequencies of vibration of a simply supported thin cylindrical shell, which is reinforced by equally spaced, equal-strength circular ring stiffeners. The displacement configuration assumed permits inter-ring deformation of the shell. Numerical calculations were made for a cylindrical shell with various sizes of stiffening rings and curves were plotted which show the effect of the rings upon the frequency of vibration. The numerical values obtained were also compared with those calculated by approximate methods and were found to agree within ± 10 per cent.

Session 7: Elasticity

The solution of a class of mixed-mixed boundary-value problems in plane elasticity. A. Cemal Eringen, Purdue University.

With the use of some linear operators, a class of mixed-type plane problems of elasticity for an orthotropic rectangular region is solved. The boundary conditions consist of specifying normal and tangential components of displacement vector at two parallel boundaries and normal stress and tangential displacement components at two other boundaries as arbitrary functions of the tangential co-ordinates. Thus the solution is a functional of eight arbitrary boundary functions which may be chosen to suit the particular purpose.

On the singularity at a concentrated load applied to a curved surface. E. Sternberg, R. A. Eubanks, Illinois Institute of Technology.

This paper deals with the singularity at the point of application of a concentrated load acting perpendicular to a curved boundary of an elastic body. In a neighborhood of the point of application, the boundary is assumed to be representable by a sufficiently smooth arbitrary surface of revolution, the axis of which coincides with the load axis. In the event the surface is locally analytic, it is shown that the singularity is identical with that appropriate to a concentrated load applied normal to a plane boundary if and only if the curvature of the meridian of the surface vanishes at the load point. The required modified singularity for the case of nonvanishing curvature is determined in a closed form to the extent where the residual surface tractions are finite and continuous.

Generalization of the theory of elasticity to porous bodies. Arthur Lubinski, Stanolind Oil and Gas Company.

Elasticity problems of porous bodies may be solved without knowledge of pore shape, by using the four following constants: two elastic constants of the porous matter; one elastic bulk constant of the interpore material; and porosity. The method uses

a special stress-strain relationship and makes allowance for body forces due to flow through the medium and for permeable and impermeable boundaries. The method is equivalent to superimposing a hydrostatic stress; a stress similar to thermal stress; and a stress resulting from subjecting the body, assumed nonporous, to pressure. Stresses in long cylinders subjected to radial flow are investigated.

Session 8: Transonic Flow

On the flow over a wedge in the upper transonic region. Hideo Yoshihara, Wright Air Development Center, USAF.

The flow over a wedge is computed using the transonic small perturbation method for that portion of the upper transonic region in which the bow shock is attached. The drag and the lift curve slope at zero angle of attack are calculated. The results indicate that a maximum in the lift curve slope occurs at the detachment Mach number.

A transonic approximation. J. B. Diaz, G. S. S. Ludford, University of Maryland.

This approximation is based on obtaining that pressure-density relation which best fits that of a polytropic gas near the sonic point, whilst retaining the analytical simplicity of the Tricomi gas. Third-order contact can be obtained at the sonic point, and there still remains a parameter, which can be chosen in two ways so as to give good supersonic agreement. These two choices give practically identical results. For this approximation the general solution of the partial differential equation for the stream-function is expressible in terms of Bessel functions, as also are the product solutions.

New applications of Tricomi solutions to transonic flow. P. Germain, Brown University.

New applications of an approximate method for subsonic and transonic flow of a compressible fluid are given. In this approximation the stream function of any flow can be expressed in terms of a solution of the Tricomi equation. After a brief statement of the basic ideas of this method, simple applications are made to problems involving jets or wedges. This method is applicable for finite as well as for infinitesimal perturbations of the basic flow. In this latter case the results agree with the classical transonic similarity laws.

Session 9: Numerical and Experimental Methods

Graphical field-plotting methods in mechanics. H. Poritsky, R. P. Jerrard, General Electric Company.

The use of graphical field-plotting methods in applied mechanics is reviewed and extended. Examples are given in torsion, ideal fluid flow, beam bending, viscous flow, and two-dimensional stress problems. While the main emphasis is on the solution of the Laplace and Poisson equations in two dimensions, it is shown how graphical methods may be applied in cases with axial symmetry, and to considerably more complicated differential equations. These include torsion of an axially symmetric shaft whose radius varies with axial distance and certain compressible-flow problems.

A grid method to determine strains in rubber-like materials. A. J. Durelli, R. L. Lake, S. Okubo, Armour Research Foundation.

This paper deals with a development of the old idea of determining strains by drawing or scratching lines. True stresses, natural strains, and Poisson's ratio as function of strain can be deduced in a direct manner. The grids used are made of rubber-latex threads (0.008 in. in diameter), they are stretched and then cemented to the specimen by means of latex emulsion. The record of strain is taken photographically. The slight errors introduced by changes in optical magnification are studied in the appendix. An example of application to one of the Thiokol products is given.

A study of photoplasticity: the photoelastic effect in the region of large deformation in polyethylene. B. Fried, N. H. Shoup, State College of Washington.

The photoelastic effect in polyethylene is found to vary linearly with principal strain difference well beyond the range of stress-strain linearity for this material. The nondimensional stress-strain curve for polyethylene over the range of strain rates here employed is found to be similar to that of 3-S aluminum. Results of a photoplastic study of the shear-strain distribution in a polyethylene model are compared with those measured directly on a 3-S aluminum prototype strained beyond its elastic limit.

Session 10: General Lecture

Shear flow turbulence. Howard W. Emmons, Harvard University.

The development of ideas of turbulent flows is briefly presented. The eddy viscosity and mixing-length assumptions are traced and the statistical theory of turbulence which replaces them for isotropic turbulence is considered. Against this background, the use of the turbulent-energy equation in a new approximate method of approach is discussed. The degree of agreement between the turbulent-energy approach and experimental data, behind grids, in turbulent wakes, in a free jet, in a channel, and in a boundary layer are noted. It is shown that the appropriate scale of turbulence is rather simply related to the size of the flow system so that rough predictions are possible in new cases where no experimental work is available to guide the analysis. It is finally pointed out that for further improvement of understanding and prediction of turbulent flows, it is necessary to introduce, at least in an approximate way, an equation for the transfer of turbulent energy between the various possible eddy sizes, thus permitting a more logical prediction of the appropriate turbulence scale.

Session 11: Plasticity

Plastic flow in deeply notched bars with sharp internal angles. A. J. Wang, E. H. Lee, Brown University.

We consider the plastic flow in deeply notched bars with cylindrical notches pulled in plane strain. The notch surfaces consist of planes joined by circular fillets. By letting the radii of these approach zero, we obtain limiting solutions for sharp corners. These are compared with previous solutions for a V-notch and a rectangular notch, which are not limiting solutions in this sense. The differences are due to different assumptions about points forming the notch surfaces. This question is discussed in detail.

Analysis of chip formation in the turning operation. Bernard W. Shaffer, New York University.

Continuous chips may be formed, during machining, by a simple shearing process between the uncut material and newly formed chip. It was shown that for the turning operation this shearing action takes place along a circular shear line. Equations were derived which describe the radius and the position of the shear line relative to the cutting tool.

Equations were also derived which express the machining force and the chip-thickness ratio in terms of the rake angle of the tool, coefficient of friction, the appropriate yield stress of the work, and the radius of the workpiece.

On obtaining plane strain or plane-stress conditions in plasticity. D. C. Drucker, Brown University.

Symmetrically notched sheets and perforated sheets in tension provide basic examples of the required conditions for achieving plane stress and plane strain in elasticity and in perfect plasticity. The significant parameter in elasticity is the ratio of sheet thickness to radius of the discontinuity in the region of greatest stress concentration. The radius is of no importance for perfectly plastic material of unlimited ductility. It is replaced by a material dimension such as the distance between notches. Enormously thicker sheets will often be required in the plastic range, for what is customarily termed plane strain, than are needed in the elastic.

Session 12: Turbulence: Supersonic Flow

Some remarks on von Kármán's equation of isotropic turbulence. L. Persen, Brown University.

It is shown in this paper that introducing a slightly generalized form of the similarity law originally suggested by von Kármán makes it possible to deduce expressions for the rate of decay, the correlation functions, and the spectral functions, which have all the main features which one expects them to have from information gained by experiments, and which are not affected by the objections to such an approach made by G. I. Taylor, *Journal of Aeronautical Sciences* (1938). However, the triple-correlation function is proportional to r and not to r^3 for small r, thus indicating that the range of validity of the proposed approach is rather restricted.

On turbulence in rarefied gases. M. Z. V. Krzywoblocki, University of Illinois.

Grad's representation of equations of motion, continuity, and energy is used to describe turbulent vector field of a flow in the realm of rarefied gases. The method of space Fourier spectrum is applied to show that the field variables (velocity, density, pressure, and temperature fields) separate into a few distinct groups: one corresponding to eddy turbulence, the other associated with fluctuating acoustical waves, etc. From that standpoint the result is analogous to that one obtained by previous authors using simplified Navier-Stokes equations. Derivation of equations of motion for spectral tensors closes the paper.

Two-dimensional supersonic shear flow around a corner. Shih I. Pai, University of Maryland.

An approximate solution for two-dimensional supersonic rotational flow of a perfect gas in the neighborhood of a corner around which the flow expands is given.

The solution is applied to two cases: (1) A parallel shear flow passes over a wall with an edge; and (2) a parallel shear flow discharges into a medium of constant but lower pressure.

Session 13: Viscoelastic Problems

On mixed boundary-value problems of linear viscoelastic solids. Harold G. Lorsch, The City College of New York; Alfred M. Freudenthal, Columbia University.

While the elastic-viscoelastic analogy solves first and second boundary-value problems for viscoelastic solids, it is shown that mixed boundary-value problems require an additional stress-strain state. Equations for these additional stresses and strains are given for Maxwell and Kelvin solids subject to time-independent boundary forces under plane strain. The method is extended to time-dependent boundary forces; a moving line load on a semi-infinite Maxwell solid in plane stress and plane strain. Strain recovery and volume stress relaxation are demonstrated for the case of plane strain.

On the attenuation of a sinusoidal pulse in a cylindrical specimen held between elastic bars. R. A. Eubanks, Illinois Institute of Technology; D. Muster, General Electric Company; E. Volterra, Rensselaer Polytechnic Institute.

The attenuation of a sinusodial pulse as it moves along a cylindrical specimen held between the plane ends of two cylindrical steel bars is analyzed. The following stress-strain relationships for the material are considered: (*a*) Elastic (Hookean model); (*b*) Elastoviscous (Voigt model); (*c*) Hereditary (Boltzmann model). In an appendix of the paper the problem is solved under the approximate assumption that the stress is uniformly distributed along the entire length of the specimen.

Thermal stresses in thick-walled cylinders exhibiting temperature-dependent viscoelastic properties of the Kelvin type. Harry H. Hilton, University of Illinois.

A solution is presented for the thermal stresses and strains in a thick-walled circular cylinder under the influence of a steady-state radial temperature. The stress-strain relationship used is that of a Kelvin viscoelastic body with temperature-dependent material properties. The solution is in a closed form and holds for any arbitrary temperature distribution. A numerical example is computed, which shows that the elastic solution and temperature-independent Kelvin body solution are extremely conservative.

Session 14: General Lecture

Discontinuous fields of plastic stress and flow. William Prager, Brown University.

The role of discontinuous stress and velocity fields in the theory of perfectly plastic solids is illustrated by examples that are representative of a wide range of applications. It is shown that the discontinuous fields discussed in the literature fall into two classes. The fields of the first class satisfy all equations of the

theory of perfectly plastic solids and would actually occur in such solids. The fields of the second class, however, violate some of the fundamental equations; they cannot occur in perfectly plastic solids but may furnish a mathematically simple, approximate description of actual stress and velocity fields in such solids. The importance of discontinuous fields for the practical solution of problems in two and three dimensions is discussed.

Session 15: Shells; Plates

Effects of large deflections and imperfections on the elastic buckling of cylinders under torsion and axial compression. Tsu-Tao Loo, Rensselaer Polytechnic Institute.

A large-deflection theory for thin circular cylinders in torsion is presented, which reveals most of the characteristics observed experimentally. The powerful effect of the large-deflection terms on post buckling resistance is shown. A new formula is proposed for initial defects in actual specimens, the considered cause for scattered and low buckling strengths. This formula is applicable to both torsion and axial compression. From this, new theories having identical assumptions are developed. The results are in fair agreement with experiment. They are also shown to be in good agreement, when modified, with previous small and large-deflection theories.

Deformation of elastic ellipsoidal shells of revolution. P. M. Naghdi, C. Nevin De Silva, University of Michigan.

Deformation of thin elastic ellipsoidal shells of revolution of uniform thickness under axisymmetric loading are considered in detail. By means of a more recent method of asymptotic integration due to Langer, a solution is obtained which is valid at the apex of the shell and involves Kelvin functions. This solution reduces in the limit to the known theory of shallow spherical shells. Specifically, the stress distribution is obtained for ellipsoidal shells under both distributed and edge loadings.

Symmetrical bending of circular sandwich plates. Melvin Zaid, Bulova Research and Development Laboratories.

General solutions are obtained for a circular sandwich plate under arbitrary symmetrical loading and boundary conditions. Bending of the face layers is considered in a manner similar to that by N. J. Hoff for rectangular plates. The case of a simply supported plate is examined in detail. For a constant-pressure load, this solution is compared to E. Reissner's work in which the face layers are considered as membranes. For most practical cases the bending factor is negligible. Where this is not true, the results of this paper should be used.

Session 16: Fluid Flow (Miscellaneous)

The growth of an axisymmetric turbulent boundary layer in an adverse pressure gradient. Earl M. Uram, Pennsylvania State University.

Axisymmetric boundary-layer growth in an adverse pressure gradient was studied using a conical diffuser. Static pressure distributions and detailed velocity profiles were measured for thick and thin inlet boundary layers. Pressure-gradient effects on the velocity profiles and the difference between two and three-dimensionally defined boundary-layer parameters are shown quite clearly. The wall shear-stress coefficients computed from the Ludwieg-Tillmann and Law of the Wall formulas are compared. The data was applied to the recent semiempirical analyses of Maskell, Rubert and Persh, and Ross for calculating turbulent boundary layers to investigate their validity or extensibility to axisymmetric flows.

Some experimental results on wing-body interference at supersonic speeds. H. E. Bailey, University of Michigan; R. E. Phinney, Johns Hopkins University.

Some of the experimental results obtained on a wing-body configuration which was tested in the University of Michigan Supersonic Wind Tunnel are presented. These results, which are in the form of static pressures measured on the body in the presence of the wing, are compared with the linearized theory in an attempt to evaluate some of the effects of viscosity on wing-body interference. The china-clay-film technique has been used to visualize the flow in the boundary layer on the body in the vicinity of the wing-body juncture.

In addition, the effect on the pressures measured on the body of a gap between the wing and the body is investigated.

Oscillatory motion of a spheroid. V. G. Szebehely, David Taylor Model Basin, U. S. Navy, University of Maryland, George Washington University.

The effect of frequency, amplitude of oscillation, speed of advance, and presence of a free surface on the virtual mass, on the damping coefficient, and on the hydrodynamic moment of a prolate spheroid are discussed. The body performs free oscillations in the horizontal plane around its shorter axis and moves with a uniform forward velocity in its plane of oscillation in the direction defined by the mean position of its longitudinal axis. The amplitude and the dimensionless frequency are not "small" permitting the study of unsteady and nonlinear effects.

Session 17: Fatigue; Creep; Friction

Combined bending and torsion fatigue tests of 25S-T aluminum alloy. W. N. Findley, W. I. Mitchell, D. E. Martin, University of Illinois.

Fatigue data for 25S-T aluminum alloy are presented for completely reversed cycles of bending, torsion, and three different combinations thereof.

The *S-N* diagrams of these data are presented in terms of the alternating principal shear stress τ_1 and shown to be expressible by the power relation $\tau_1 = BN^{\alpha}$.

The merits of six theories of failure, relative to their agreement with these test data, are discussed. Further consideration was given to the physical significance of several of these theories, and to the possible effect of anisotropy on the *fatigue behavior* under combined stress.

Prediction of creep under fluctuating stress and damping from creep under constant stress. G. F. Weissmann, Bell Telephone Research Laboratories; Yoh-Han Pae, E. I. du Pont de Nemours and Company, Inc.; Joseph Marin, Pennsylvania State University.

The first part of this paper presents a theory for predicting creep strains under dynamic fluctuating stresses from an assumed static creep strain-stress-time relation. A comparison of the theoretical dynamic creep strain values with preliminary experimental results on plastics shows good agreement between the theoretical and test results.

A second part of this investigation presents a theory for predicting internal damping of materials under dynamic stress based upon short-time static tension creep data. For the material considered the theoretical internal-damping value agrees well with the actual damping constants obtained by tests.

The friction of boundary-lubricated surfaces. Ernest Rabinowicz, Massachusetts Institute of Technology.

In this paper are discussed several different methods, based on friction and metal-transfer measurements, of determining the relative importance, during the sliding of lubricated surfaces, of the shearing of the lubricant layer and of the penetration of the lubricant with the formation of welded junctions. An extension of these methods suggests that the total friction force is the linear sum of the two separate components due to the lubricant layer and the metal junctions. In consequence, fresh light is thrown on the stick-slip phenomenon and its prevention by the use of good boundary lubricants.

Session 18: General Lecture

Mechanics of granular media. R. D. Mindlin, Columbia University.

Some recent work, on the mathematical theory of the deformation and vibration of materials composed of elastic grains, has been aimed at taking into account tangential forces between grains. Sufficient progress has been made in the development of the theory to enable several interesting predictions, based on it, to be tested experimentally. The theory and the experiments are described in this lecture.

Session 19: Plasticity (Stress-Strain Relations)

A proposed theory of plasticity based on slips. T. H. Lin, University of Detroit.

This paper shows a method for calculating the incremental stress-strain relations in the plastic range, under varying ratios of principal stresses, from uniaxial tests. Metals of face-centered cubic crystals like aluminum and its alloys are studied. The deformation of each crystal is taken to be the same as that of the aggregate. The principle of minimum virtual work is applied to determine the five operative slip systems for incremental strain. This method has been applied to find the plastic axial and torsional strains of thin-walled cylinders first compressed beyond elastic limit and then twisted. The present method gives good agreement with experimental results obtained at NACA.

Plastic stress-strain relations based on linear loading functions. J. L. Saunders, Jr., Brown University.

The stress-strain relations of incremental theories of plasticity have recently been generalized by Koiter, who introduced the use of any number of loading functions instead of only one. The present paper is concerned with incremental theory based on any number of linear loading functions. In this case the resulting plastic strain increments are integrable in a restricted sense and the stress-strain relations can be given in a form partially resembling deformation theories. The slip theory of Batdorf and Budiansky falls within the class of theories which are discussed in this paper.

Inelastic behavior under combined tension and torsion. Morris Feigen, Hughes Aircraft Company, Inc.

Tests conducted on thin-walled aluminum tubes under combined tension-torsion show test results which fall between the predictions of the flow theory and deformation theory. A specimen which is tensile-stressed into the plastic range will exhibit little or no plastic shearing strain under an applied torsion stress. With the torsion stress applied and held constant, however, plastic shearing strain will occur when the axial stress or axial strain is increased. If the torsion stress is removed after plastic shearing action has occurred and the axial strain is increased, the specimen will exhibit a plastic untwisting.

Session 20: Beam Vibrations; Traveling Waves in Bars

Vibrations of rotating beams of constant section. W. E. Boyce, Carnegie Institute of Technology; R. C. Di Prima, Massachusetts Institute of Technology; G. H. Handelman, Carnegie Institute of Technology.

Methods are discussed for determining approximate frequencies of a beam rotating at constant angular velocity about an axis at one end and vibrating transversely to the plane of rotation. Various boundary conditions at the restrained end are considered. The associated minimum principles and natural boundary conditions are developed. The Southwell principle yielding a lower bound on the first frequency is a well-known consequence. It is also shown that these principles can be made to yield lower bounds for all frequencies. A simple trial function yields close bounds on the first two frequencies.

Timoshenko's shear coefficient for flexural vibrations of beams. R. D. Mindlin, H. Deresiewicz, Columbia University.

It is pointed out that Timoshenko's shear coefficient, in his equations of flexural vibrations of beams, depends on both the shape of the cross section and the mode of motion. It is shown how the latter may be taken into account by matching solutions, of Timoshenko's equations and the three-dimensional equations, for simple thickness-shear motions of infinite beams of various cross-sectional shapes.

Traveling compressional waves in an elastic rod according to the more exact one-dimensional theory. Julius Miklowitz, U. S. Naval Ordnance Test Station.

The traveling-wave character of the Mindlin-Herrmann one-dimensional theory of compressional waves is established. A solution in accord with this theory is derived for the problem of a semi-infinite rod with an end excitation of a step-axial stress. A related finite rod traveling-wave solution is also derived. The velocity associated with the leading wave front in these solutions gives support for this theory as a physical model.

Session 21: Buckling of Bars

Buckling of columns with equal and unequal end eccentricities and equal and unequal rotational end restraints. P. P. Bijlaard, Cornell University.

A general analytical method is given for calculating the buckling stress of eccentrically loaded columns with any combination of end eccentricities and end restraints. In the general case the deflections will gradually increase with increasing load until, due to plastic action, a maximum is reached, which is the eccentric buckling load. However, for columns with equal end restraints and equal and opposite end eccentricities a bifurcation point is reached, at which the column buckles in a superimposed symmetrical mode.

A method for estimating allowable load capacities of columns subject to creep. R. L. Carlson, A. D. Schwope, Battelle Memorial Institute.

A method for estimating allowable load capacities of columns subject to creep is presented. The method utilizes approximate stress distributions derived from iso-stress-strain curves to determine column loads which are shown to be conservative for the time for which a determination is made.

An application of the method is made to test data on a stabilized 24S-T4 aluminum for two test temperatures. A comparison of the calculated load capacities with experimental load capacities indicates that the method satisfactorily estimates the decrease in column load capacity with increasing time.

Prediction of very short time creep buckling from very short time tensile-creep properties. Henry W. Baer, Hughes Aircraft Company, Inc.

Very short time tensile-creep data are used to predict local creep buckling of thin-walled cylinder shells. Strain-time behavior is described empirically by the formula $\epsilon = A + Bt + C(1 - e^{-\alpha t})$, A, B, C, and α being functions of stress and temperatures. From these relations isochronous stress-strain curves are constructed, yielding time-dependent tangent moduli, which are used in the applicable crippling formula to give time-dependent crippling stresses as functions of temperature. The criterion is shown to hold for QQ-M-44 magnesium alloy in both annealed and work-hardened conditions.

Session 22: General Lecture

Nonlinear vibrations of system with several degrees of freedom. J. J. Stoker, New York University.

In nonlinear systems with several degrees of freedom there exist, in general, no methods for determining the solutions explicitly, except purely numerical methods which then of course require that the parameters of the system be given numerical values. However, if the nonlinearities are small in some appropriate sense, the perturbation method of Poincare is available, particularly for the discussion of periodic motions. A description of this method for both regular and degenerate cases is given, together with a fairly typical example. If the motions to be treated are not periodic, considerable difficulties may arise; in particular, the famous "difficulty of small divisors" can occur. In systems with several degrees of freedom, this difficulty seems quite likely to arise in many cases of interest from the physical point of view. Attempts have been made to treat nonlinear continuous systems, which means systems with infinitely many degrees of freedom; in such cases the difficulty with small divisors may occur even in dealing with a purely periodic motion. The stability of periodic motions of nonlinear systems with several degrees of freedom, if treated by using the small oscillation criterion for stability, leads to systems of Hill's equations; a brief discussion concerning a few problems involving such systems will be given.

Session 23: Elasticity

Thermal stresses in rectangular strips. G. Horvay, General Electric Company.

Stresses and deformations ensuing from application of a step-function temperature distribution to a rectangular strip are calculated by precise biharmonic eigenfunction expansions, by Fourier integrals, and by self-equilibrating function expansions. Superiority of the latter method, because of its great speed and yet adequate reliability, is clearly established. It is also shown that, contrary to expectation (whereby $^1/_2 E \alpha T = \sigma_d$), the temperature step T is related to the design stress σ_d by $E \alpha T = \frac{5}{6} \sigma_d$.

Stresses in a centrally heated disk. Henry Parkus, Michigan State College.

Temperature and stress distribution in an infinite, thin disk heated by a temporary heat source which acts from $t = 0$ to $t = \theta$ are investigated. Dynamical effects are considered and residual stresses due to partly plastic flow in the disk are calculated.

An Airy integral analysis of beam-columns with distributed axial loading that deflects with the column. C. M. Tyler, Jr., W. T. Rouleau, Carnegie Institute of Technology.

An analytical method for determining the deflection, bending moment, and stability of beam-columns having partially uniformly distributed axial loads which deflect with the member (their direction of action remaining fixed) is developed in terms of Airy Integral Functions. A table of the required integrals of the Airy Integral Functions needed for numerical computations is included.

Stresses in a plate containing a ring of circular holes and a central circular hole. Peter P. Radkowski, Watertown Arsenal.

This paper gives the stress distribution that occurs in a plate perforated by a ring of uniformly distributed holes and a central hole. The plate is in a state of generalized plane stress and subjected to constant radial tension at infinity. The stress function is determined by constructing and then combining two series of periodic biharmonic functions. The first series relates to the infinite plate containing one circular hole; the second series relates to the ring of holes.

A method for determining the stress distribution in a plate due to a uniform pressure applied over the boundary of a square hole. Cliff Smith Barton, Rensselaer Polytechnic Institute.

This paper provides an analytical method whereby the stress distribution in a plate may be determined by superposition when

the boundary of a square hole in the plate is loaded with a uniform pressure. Experimental results are obtained utilizing an interesting application of the principle of superposition. Experimental results are used in the development of and for comparison with the analytical solution. Solutions for stresses normal to two radial lines are developed, one line at 90 deg and the other line at 45 deg to the flat of the hole. Graphs demonstrate the application of superposition and present the stress distributions.

Session 24: Fluid Flow (Boundary Layer, Heat Transfer)

Theoretical velocity and temperature profiles for the laminar boundary layer of the flow of a compressible fluid in the entrance region of a tube. Tau-Yi Toong, Joseph Kaye, Massachusetts Institute of Technology.

The boundary-layer equations of momentum, continuity, and energy for flow of a compressible fluid in the entrance region of a tube have been solved for the special case of constant values of fluid viscosity and thermal conductivity. These equations were transformed into a set of ordinary differential equations, suitable for integration by means of the M.I.T. Differential Analyzer.

The solutions presented here consist essentially of the velocity and temperature profiles in the laminar boundary layer. These profiles are compared with those for the laminar boundary layer of a compressible fluid flowing over a flat plate.

Experimental velocity profiles for supersonic flow of air in a tube with and without heat transfer. Joseph Kaye, Geo. A. Brown, Massachusetts Institute of Technology; John J. Dieckmann, United States Air Force; Edw. A. Sziklas, United Aircraft Corp.

Measurements of velocity profiles for supersonic flow of air in a round tube have demonstrated that a laminar boundary layer can be maintained for a relatively long length of supersonic flow in a tube. The measured velocity profiles of a laminar boundary layer for tube flow agree well with those measured and predicted for a laminar boundary layer on a flat plate with supersonic free-stream velocities. Velocity profiles for transitional and turbulent boundary layers for tube flow are also presented and compared with similar data for plate flow.

Heat transfer in crossflow. John L. Mason, AiResearch Manufacturing Company.

The crossflow heat-transfer equation is solved by use of the Laplace transform. The solution is in the form of an infinite series which converges more rapidly than previous solutions of the same problem, which were obtained by nonoperational methods. Engineering applications are cited.

Hydraulic analogy applied to crossflow heat exchangers. S. I. Juhasz, Midwest Research Institute; P. C. Hooper, University of Toronto.

The hydraulic analogy for steady-state parallel-flow heat exchangers is reviewed and its extension to the more complex problems of crossflow is presented.

Basically, the solution is made by subdividing the crossflow heat exchanger into several finite rectangular heat exchangers and solving each part in turn as a parallel-flow problem. A novel hydraulic-analogy arrangement, which permits this, is described.

The analog permits direct solution of crossflow problems involving complicated geometries and physical complications such as variable specific heat and heat leakage to surroundings. Slight modification of the analog allows the treatment of mixing in one fluid.

A new examination of the concepts of adiabatic wall temperature and heat-transfer coefficient. Tau-Yi Toong, Massachusetts Institute of Technology.

The laminar flow of an incompressible fluid over a flat plate with zero pressure gradient is studied in terms of the concept of the growth of an "incremental" boundary layer, when the thermal condition at the plate wall is subjected to an arbitrary change.

Two cases are illustrated. First, the distribution of adiabatic wall temperature is obtained for a flat plate, which is insulated downstream of an arbitrary length of constant temperature from the leading edge. Second, the variation of heat-transfer coefficient is obtained when the wall temperature is given a step change from the adiabatic value.

Session 25: Dynamics

Effects of mass distribution on critical speeds. C. A. Schulte, Ford Motor Company; R. A. Riester, Carrier Corporation.

This paper gives the results of an investigation of the critical speeds of overhung rotors excited by rotational unbalance. Rotors of approximately identical weights, but different mass distributions, were used to determine both analytically and experimentally the influence of the gyroscopic moment on critical speeds. No effort was made to provide external stimulus at frequencies other than the running speed

Nine different shaft and rotor combinations were investigated. In each case, actual tests revealed a resonance condition corresponding to the critical speed of forward precession. In six of the nine cases, the critical speed of backward precession was observed.

Application of dynamic vibration absorber to vehicles. James C. Settles, The Buckeye Steel Castings Company.

This paper deals with the use of dynamic vibration absorbers for simultaneous control of forced linear and rotational motions of vehicles or similar systems.

The equations for the motions of the main mass, the absorber masses, and the relative motion between the main and absorber masses are presented. The equation for the phase angle between the separately forced motions is also presented and the effects of variations in speed and load are discussed.

Examples are given of the application of the equations to systems in which (1) the absorber mass remains constant, and (2) the mass ratio remains constant.

Semigraphical method for plotting vibration response curves. Robert Plunkett, General Electric Company.

A semigraphical method is described for constructing the vibration-response curve, as a function of frequency, for a continuous system. It will be as accurate as the values of the natural frequencies and the integrated values of the kinetic-energy terms associated with the various modes. It is illustrated by applica-

tion to the construction of the vibration response (mobility) curve of the center of a free-free beam. This curve is compared with experimentally determined values.

An antiresonant damper for dancing cables. Joseph F. Shea, University of Michigan.

This paper analyzes a simple antiresonant damper for dancing aerial cables. The cable is treated as a string subjected to negative damping, the damper as a mass, spring, and dashpot at an arbitrary point in the span. The relationships among the damper parameters which render the system stable are derived. The results indicate that dampers weighing five pounds or less should prove satisfactory for most cables which dance, provided that the spring and viscous elements are properly chosen. The calculations are carried out for some typical cases.

The derivation of a new kinetic-energy formula from the energy aspect of matter. Jakob Mandelker, Georgia Institute of Technology.

It will be shown in this paper that the motion of a body, *whose mass increases with the velocity, is equivalent to motion with resistance*, of the character of a continuous inelastic impact. In this case, however, kinetic energy *cannot* become equal to the work performed but must remain smaller.

After introducing here the energy concept of matter mc^2 we obtain—strictly within the precincts of classical mechanics—the *identical* expressions for the mass, momentum, and work as in relativity mechanics, however a *different*, new kinetic energy formula. Only the latter conforms fully with relativistic kinematics and with the required relativistic Lagrangian.

Session 26: Plates

A theory for thick plates. L. H. Donnell, Illinois Institute of Technology.

A theory suitable for thick elastic plates is developed by starting with expressions suggested by classical thin-plate theory for the stresses as functions of the loading, and calculating additional terms so as to satisfy more and more exactly the theory of elasticity. Expressions are thus obtained for stresses and displacements in the form of infinite series involving higher and higher derivatives of the loading. Of especial interest is the information given regarding the most important errors in the classical theory.

Bending of a rectangular plate on an elastic foundation with two adjacent edges fixed and the others free. Gordon C. K. Yeh, Reed Research, Inc.

Ritz's energy method is used to obtain an approximate solution for the bending of a thin rectangular plate fixed at two adjacent edges and free at the other two edges which is supported by an elastic foundation. The solution applies to general distributions of lateral loads and foundation stiffnesses. It also includes the solution for a plate without foundation as a limiting case. Tables of coefficients necessary in setting up the simultaneous equations are given. Two numerical examples for square plates are presented and, in one case, the result checks with that obtained by another method.

The influence of a small hole or rigid inclusion on the transverse flexure of thin plates. Yi-Yuan Yu, Washington University.

In the present paper the influence of a small hole and that of a small rigid inclusion on the transverse flexure of thin plates are studied by means of the complex variable method. The hole or core is of the shape of an ovaloid, of which the circle, the ellipse, and the square with rounded corners are special cases. The plate is very large in size compared with the hole or core, and constant bending moments, twisting moments, or shearing forces are transmitted through the plate in an arbitrary direction. Results are compared with those obtained by previous authors.

Bending of thin rectangular plates. H. J. Fletcher, Brigham Young University; C. J. Thorne, University of Utah.

A Fourier series solution is obtained for the deflection of a thin rectangular plate subject to a transverse load and any of the standard boundary conditions. An infinite set of equations with an infinite number of unknowns must be solved to obtain a solution. A discussion of convergence is included.

Stress singularities in angular corners of plates having linear flexural rigidities for various boundary conditions. M. L. Williams, R. H. Owens, California Institute of Technology.

Eigensolutions of the small-deflection variable-thickness plate equation for various combinations of homogeneous boundary conditions extend earlier results, with particular emphasis in this paper on thickness distributions obeying any arbitrary power law in the radial direction. It is tentatively proposed that, in general, the linear-thickness variation separates cases for which singular eigenstresses may or may not exist. If $D \sim t^3 \sim r^{m/3}$ cusplike variations, $m > 3$, yield vanishing stresses as the origin is approached for all included angles, while for $m < 3$ (approaching the uniform thickness case as $m \to 0$) singular stresses may occur, depending upon the angle.

Session 27: Fluid Flow (Laminar, Drag, Hydrofoils)

Friction factor in the laminar entry region of a smooth tube. Ascher H. Shapiro, Robert Siegel, Massachusetts Institute of Technology; Stephen J. Kline, Stanford University.

Three theoretical methods of computation of the apparent friction factor for steady, incompressible flow in the laminar entry region of a smooth tube are presented.

The results are found to agree well with experimental data.

A critical comparison is made between the methods presented here and those of other investigators.

In the range where $\mathrm{Re}_x/\mathrm{Re}_D^2 < 10^{-3}$, the theory gives $4f_{APP}\mathrm{Re}_D = 6.88\left(\mathrm{Re}_D/\sqrt{\mathrm{Re}_x} - 5.76 + 333\sqrt{\mathrm{Re}_x/\mathrm{Re}_D}\right)$ where f_{APP} is the local *apparent* shear stress coefficient (based on pressure gradient), and Re_D and Re_x are, respectively, the diameter and length Reynolds numbers.

Form drag of composite surfaces. Hunter Rouse, Tien-To Siao, State University of Iowa.

Following a free-streamline analysis of two-dimensional flow past multiple plates, experimental data are presented for the drag

coefficient of axially symmetric and three-dimensional arrangements of sharp-edged disks, rings, and plates as a function of the number, form, and spacing of the elements. It is shown that the form drag of a composite surface of given solid area can be varied over nearly a twofold range by proper disposition of its parts.

On the flow and temperature fields in forced flow against a rotating disk. Arthur N. Tifford, Sheng To Chu, Ohio State University.

A single-parameter, exact analysis of the flow field associated with a rotating disk in forced flow is presented. Plots of the velocity components for ten different ratios of disk-rotating speed to forced-flow speed are given.

An exact solution, except for viscous heating effects, for the temperature field associated with a rotating disk in forced flow is obtained.

When the Prandtl number is one and the radial surface-temperature distribution is parabolic, an analogy exists between the frictional torque and the rate of heat transfer.

Limiting velocity by momentum relations for hydrofoils near the surface and airfoils in near-sonic flow. E. V. Laitone, University of California.

It is shown that the surface velocity over the upper surface of a two-dimensional hydrofoil has a definite limiting magnitude as the hydrofoil approaches the free water surface. This limiting condition is governed by the maximum depth available from the hydraulic jump relations.

Then it is shown that an analogous limiting surface velocity exists on a two-dimensional airfoil at high subsonic speeds. This limit in the magnitude of the surface velocity occurs in the local supersonic flow region and is similarly governed by the shock-wave relations.

A study of gust entry of sweptback wings. Theodore H. H. Pian, Holt Ashley, Massachusetts Institute of Technology.

The lift and moment growth on a swept wing upon entering a sharp-edged gust are determined by strip theory and by a "semi-three-dimensional" theory. The latter is based on the calculation of lift distribution of an infinite swept wing penetrating a gust front. This unsteady-flow problem is shown to be equivalent to a steady-flow problem involving an infinite swept wing with an angle-of-attack discontinuity at a spanwise station. Results indicate that, according to the improved theory, the airloads build up faster than what is shown by strip theory.

Session 28: Structures

A matric method of structural analysis. P. H. Denke, Douglas Aircraft Company, Inc.

Matric formulations of the equilibrium equations, the Maxwell-Mohr equations of continuity, the λ-equation of free vibration, and certain "linking equations," are derived for statically determinate and indeterminate structures. The matric Maxwell-Mohr equations account for the effects of thermal stress, creep, initial distortion, residual distortion, and settlement of the supports. The combined equations provide a complete matric formulation which greatly facilitates preparing and coding data for the automatic digital computer.

A large deflection theory of redundant structures. E. F. Masur, Illinois Institute of Technology.

The classical theory of structures is extended to include the nonlinear effect of the bar deflections on the condition of compatible axial deformations. The resultant theory is thus a counterpart of the von Kármán theory of plates subjected to large deflections.

Basic theorems (uniqueness, minimum energy, etc.) are derived. It is shown that the inclusion of the additional terms generally corresponds to a strengthening of the structure. A numerical example is presented to illustrate the theory.

Energy theory of buckling of circular elastic rings and arches. H. L. Langhaar, A. P. Boresi, University of Illinois; D. R. Carver, Kansas State College.

The hoop strain at any point in a circular ring or curved beam that is deformed in its plane is expressed in terms of the displacement vector of the centroidal axis. The most important quadratic terms in the displacement components are retained. The hoop-strain formula leads to a strain-energy expression that includes the most important cubic terms in the displacement components. As an illustrative application, this formula is applied to the problem of buckling of a semicircular arch loaded by a concentrated force at its center. Some related experimental data are presented.

Effective stiffness of a plate subjected to a local edge moment. I. A. Mohammed, E. P. Popov, University of California.

This paper deals with the analysis of a simply supported rectangular elastic plate subjected to an applied moment uniformly distributed over a finite distance. A general equation for the deflection of the loaded portion of a plate is derived. Then for the special case of an infinitely long plate with a moment applied at the middle of one of the long edges, rotation of the plate at the applied moment is formulated. Adopting this rotation as a measure of the plate's stiffness to an applied moment, the width of an equivalent simply supported beam is established.

PREPUBLICATION ORDER FORM

For Proceedings of the Second U. S. Congress of Applied Mechanics

Order Dept.
Amer. Soc. of Mech. Engrs. Date———
29 West 39 Street
New York 18, N. Y.

Please enter my order for ——— copies of the Proceedings of the Second U. S. National Congress of Applied Mechanics. Price: $10.00. (No discount allowed.) Available early in 1955. Bill and Proceedings should be sent to me at the following address:

Name———

Address———

City———Zone———State———

Design Data and Methods

It is important that the data contained in technical papers be made readily available to designing engineers. In order to satisfy these needs of industry, this section of the Journal includes a concise presentation of data and information drawn chiefly from papers previously published by the Applied Mechanics Division of The American Society of Mechanical Engineers.

A Simple Nomogram for the Ratios of Octahedral to Maximum Shearing Stresses and Its Physical Interpretation

By G. A. ZIZICAS,[1] LOS ANGELES, CALIF.

A nomogram constructed exclusively by means of straight lines is presented, giving the ratio of the octahedral to the maximum shearing stresses for all possible stress distributions in terms of the nondimensional ratios of the two principal stresses to the one of maximum absolute value. The physical interpretation of the nomogram is discussed. It is shown that states of stress with constant ratio of octahedral to maximum shearing stress are represented by straight lines. To such lines are found to correspond fixed values of the deviatoric parameter

$$\mu = \frac{2S_2 - S_1 - S_3}{S_1 - S_3}$$

in agreement with a recent observation by Novozhilov. The values of μ are given directly by the nomogram.

Nomenclature

The following nomenclature is used in the paper:

S_1 = principal stress of maximum absolute value, lb in.$^{-2}$
S_2, S_3 = two principal stresses of absolute value less or equal than absolute value of S_1, lb in.$^{-2}$
$\alpha = \frac{S_2}{S_1}$ = nondimensional parameter
α_{-1} = value of α for $\beta = -1$
$\beta = \frac{S_3}{S_1}$ = nondimensional parameter
γ = function of α and β defined by Equation [8]
γ_{min} = analytical minimum of admissible values of γ
γ_{max} = upper bound of admissible values of γ
ϵ = per cent difference between a value of ρ and its optimum value ρ_o
ϵ_{max} = maximum value of ϵ
$\mu = \frac{2S_2 - S_1 - S_3}{S_1 - S_3}$ = nondimensional deviatoric parameter of theory of plasticity
$\tau_{max} = \frac{S_1 - S_3}{2}$ = maximum shearing stress, lb in.$^{-2}$
τ_{oct} = octahedral shearing stress, lb in.$^{-2}$
$\rho = \frac{\tau_{oct}}{\tau_{max}}$ = nondimensional ratio of octahedral to maximum shearing stress
ρ_{max} = upper bound of admissible values of ρ
ρ_{min} = analytical minimum of admissible values of ρ
ρ_o = optimum value of ρ defined by Equation [19]

Introduction

Specific values of the octahedral shearing stress and the maximum shearing stress are often used as criteria of yielding for plastic materials. It is therefore of some practical importance to have a means of quick appraisal of their relative values. Such information, for instance, is the basis for an estimate of the differences in design that may result from the use of the one or the other criterion. In the following a simple nomogram is presented which in addition to satisfying this specific need gives an over-all conception of the interrelation between these two theories for all possible stress distributions.

Fundamental Relations

Let $$S_1, S_2 = \alpha S_1, S_3 = \beta S_1 \quad [1]$$

be the principal stresses in the neighborhood of a generic point of a deformable body, where S_1 is the principal stress with the largest absolute value. It is assumed, without loss of generality, that

$$1 \geqslant \alpha \geqslant \beta \geqslant -1 \quad [2]$$

Then the maximum shearing stress is

$$\tau_{max} = \frac{1 - \beta}{2} S_1 \quad [3]$$

and the octahedral shearing stress becomes

$$\tau_{oct} = \frac{S_1}{3}\sqrt{(1-\alpha)^2 + (1-\beta)^2 + (\alpha-\beta)^2} \quad [4]$$

---

[1] Assistant Professor of Engineering, University of California.

Presented at the West Coast Conference of the Applied Mechanics Division, Berkeley, Calif., June 21–23, 1954, of The American Society of Mechanical Engineers.

Discussion of this paper should be addressed to the Secretary, ASME, 29 West 39th Street, New York, N. Y., and will be accepted until October 11, 1954, for publication at a later date. Discussion received after the closing date will be returned.

Note: Statements and opinions advanced in papers are to be understood as individual expressions of their authors and not those of the Society. Manuscript received by ASME Applied Mechanics Division, March 10, 1954. Paper No. 54—APM-9.

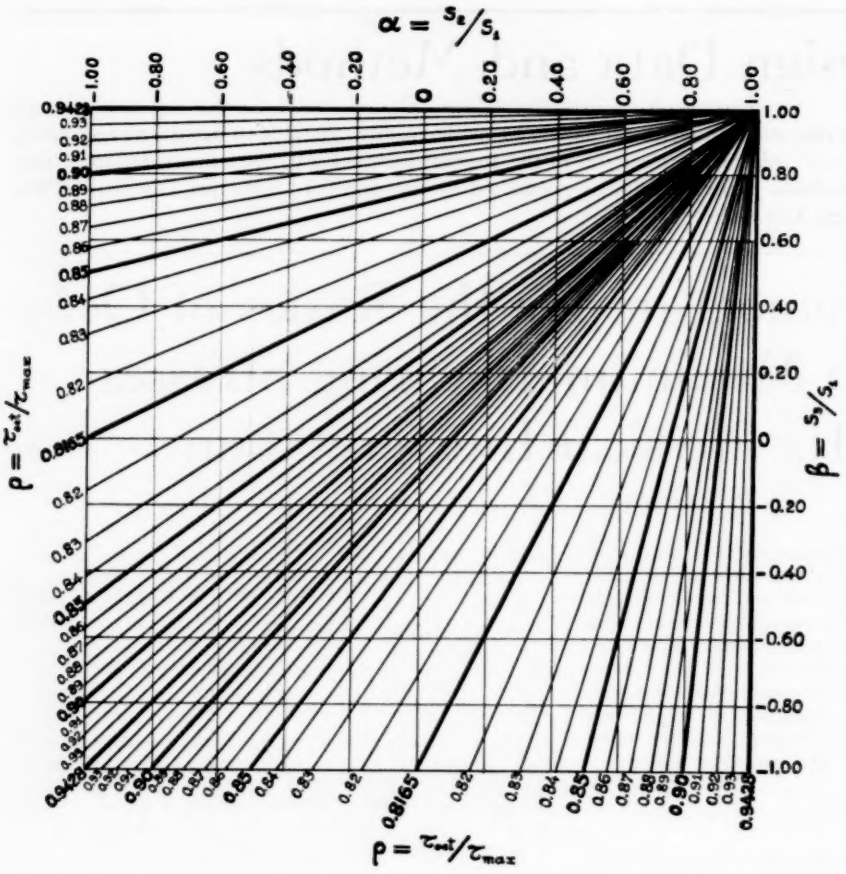

FIG. 1 NOMOGRAM FOR RATIOS ρ OF THE OCTAHEDRAL TO THE MAXIMUM SHEARING STRESS IN TERMS OF THE RATIOS $\alpha = S_2/S_1$ AND $\beta = S_3/S_1$ OF THE PRINCIPAL STRESSES TO THE STRESS S_1 OF THE MAXIMUM ABSOLUTE VALUE

so that the ratio ρ of τ_{oct} to τ_{max} is expressed by

$$\rho = \frac{\tau_{oct}}{\tau_{max}} = \frac{2\sqrt{(1-\alpha)^2 + (1-\beta)^2 + (\alpha-\beta)^2}}{3(1-\beta)} \quad \ldots [5]$$

If $\beta = 1$, Equation [2] implies $\alpha = 1$ and for

$$\alpha = \beta = 1, \quad \tau_{oct} = \tau_{max} = 0 \quad \ldots [6]$$

The value of the ratio ρ in this case is of little physical significance since Equations [6] answer completely the problem. Its mathematical value is undetermined and can be evaluated only by a limiting process, provided the path of α and β in approaching the value 1 (say, in an α, β-co-ordinate plane) is known. Such an analysis, however, depends on values $\beta \neq 1$ which are considered in the following:

When $\beta \neq 1$, Equation [5] can be written

$$\rho = \frac{2}{3}\sqrt{1+\gamma} \quad \ldots [7]$$

where

$$\gamma = \frac{(1-\alpha)^2 + (\alpha-\beta)^2}{(1-\beta)^2} \quad \ldots [8]$$

from which follows

$$2\alpha^2 - 2(1+\beta)\alpha - \gamma(1-\beta)^2 + 1 + \beta^2 = 0 \quad \ldots [9]$$

This equation solved for α gives

$$\alpha = \frac{1}{2}\left[(1+\beta) \pm (1-\beta)\sqrt{2\gamma - 1}\right] \quad \ldots [10]$$

or, in terms of the ratio ρ related to γ by Equation [7]

$$\alpha = \frac{1}{2}\left[(1+\beta) \pm (1-\beta)\sqrt{\frac{3}{2}(3\rho^2 - 2)}\right] \quad \ldots [11]$$

The last two equations show that for a fixed value of γ or ρ the corresponding values of α and β represent, in a Cartesian system of co-ordinates α, β, straight lines which all pass through the point $\alpha = \beta = 1$.

The range of admissible values of γ, hence also of ρ, is well known.[3] It will be specified here by determining its extremals when considered as a function of α and β which have values absolutely smaller than unity according to Equation [2]. Either one of the two necessary conditions $\partial\gamma/\partial\alpha = 0$ and $\partial\gamma/\partial\beta = 0$ applied on Equation [8] gives, when $\beta \neq 1$

$$2\alpha - \beta = 1 \quad \ldots [12]$$

and results in the following values of γ and ρ

$$\gamma_{min} = \frac{1}{2}, \quad \rho_{min} = \sqrt{\frac{2}{3}} = 0.8165 \quad \ldots [13]$$

which are readily checked to be minima. There are no analytical maxima, but γ and ρ have each an upper bound along the

[3] See, for instance, "Theory of Perfectly Plastic Solids," by W. Prager and P. G. Hodge, Jr., John Wiley and Sons, Inc., New York, N. Y., 1950, p. 24, or "Weight-Strength Analysis of Aircraft Structures," by F. R. Shanley, McGraw-Hill Book Company, Inc., New York, N. Y., 1952, pp. 300–303.

boundaries $\alpha = \beta$ and $\alpha = 1$ of the triangular domain defined by Equations [2]. These bounding values are

$$\gamma_{max} = 1, \quad \rho_{max} = \frac{2\sqrt{2}}{3} = 0.9428 \ldots\ldots\ldots [14]$$

The Nomogram and Its Physical Interpretation

In a Cartesian system with co-ordinates α and β, Fig. 1, the straight lines associated with constant values of γ or ρ in Equations [10] and [11] are readily drawn if, in addition to the common point $\alpha = \beta = 1$, their intersection with the line $\beta = -1$ is specified by the corresponding abscissa α_{-1}. According to Equations [10] and [11]

$$\alpha_{-1} = \pm\sqrt{2\gamma - 1} = \pm\sqrt{\frac{3}{2}(3\rho^2 - 2)} \ldots\ldots [15]$$

Its numerical values are given in Table 1 for values of ρ in steps equal to 0.01

TABLE 1 NUMERICAL VALUES OF γ AND $\alpha_{-1} = \pm\sqrt{2\gamma - 1}$

1	2	3	1	2	3
ρ	γ	$\pm\sqrt{2\gamma - 1}$	ρ	γ	$\pm\sqrt{2\gamma - 1}$
0.8165	0.5000	0	0.88	0.7424	±0.696
0.82	0.5129	±0.161	0.89	0.7822	±0.751
0.83	0.5500	±0.317	0.90	0.8225	±0.803
0.84	0.5876	±0.419	0.91	0.8632	±0.852
0.85	0.6256	±0.501	0.92	0.9044	±0.899
0.86	0.6641	±0.573	0.93	0.9460	±0.944
0.87	0.7030	±0.637	0.9428	1.0000	±1.000

On the basis of these data the simple nomogram of Fig. 1 has been constructed. It readily gives the value of $\rho = \tau_{oct}/\tau_{max}$ for any stress distribution for which the principal stresses are known. By including the symmetric of the nomogram with respect to the first diagonal $\alpha = \beta$ the restriction $\alpha \geqslant \beta$ has been removed. The only important assumption is that S_1 is the principal stress of maximum absolute value.

It is interesting to examine the physical meaning of the various elements of the nomogram. It is noted that each straight line emanating from the point $(+1, +1)$ corresponds to states of stresses with a fixed ratio of the octahedral to the maximum shearing stress. Moreover, the deviatoric parameter μ of plasticity[3]

$$\mu = \frac{2S_2 - S_1 - S_3}{S_1 - S_3} \ldots\ldots\ldots\ldots [16]$$

where $S_1 \geqslant S_2 \geqslant S_3$ are the three principal stresses, can be written in terms of α and β with minus sign in front of μ when $S_1 < 0$

$$\pm\mu = \frac{2\alpha - 1 - \beta}{1 - \beta} \ldots\ldots\ldots\ldots [17]$$

If Equations [10], [11], and [15] are taken into consideration the foregoing expression gives

$$\pm\mu = \pm\sqrt{2\gamma - 1} = \pm\sqrt{\frac{3}{2}(3\rho^2 - 2)} = \alpha_{-1} \ldots [18]$$

These relations establish in a different way the recent observation by V. V. Novozhilov to the effect that fixing the value of the parameter μ is equivalent to assuming a constant value of the ratio of the octahedral to the maximum shearing stress.[4] In terms of the nomogram of the present paper they show that the abscissas of the intercepts of lines of constant ratio ρ with the line $\beta = -1$ give the value of μ if $S_1 > 0$, or $-\mu$ if $S_1 < 0$, associated with this value of ρ. The value of ρ for all the possible states of stress having a given value of parameter μ is also given by the nomogram.

[3] See, for instance, "Theory of Flow and Fracture of Solids," by A. Nadai, McGraw-Hill Book Company, Inc., New York, N. Y., vol. 1, second edition, 1950, p. 106.

[4] "The Physical Meaning of the Stress Invariants of the Theory of Plasticity," by V. V. Novozhilov (in Russian), *Applied Mathematics and Mechanics*, Academy of Sciences of USSR Publication, vol. 16, 1952, pp. 617–619.

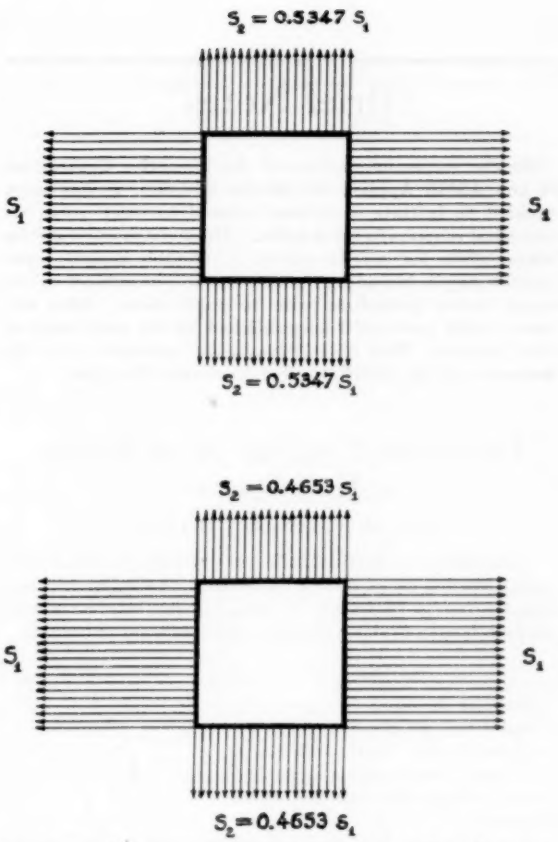

Fig. 2 Two-Dimensional Stress Distributions With Optimum Ratio of the Octahedral to the Maximum Shearing Stress

The difference between the octahedral shearing-stress and maximum shearing-stress criteria may be narrowed if in view of the small range of values of their ratio ρ this ratio is fixed at an optimum. Then the physical value of either τ_{max} or τ_{oct} may be chosen for each material so as best to fit experimental data for the occurrence of yielding under all possible stress distributions, or all stress distributions appearing in the problem under consideration. If the optimum value ρ_o of ρ is chosen so as to make the maximum difference between the values of any ρ and ρ_o, a minimum, then clearly

$$\rho_o = \frac{1}{2}(0.8165 + 0.9428) = 0.87965 \ldots\ldots [19]$$

leading to the maximum per cent difference

$$\epsilon_{max} = \frac{0.9428 - 0.87965}{0.87965} \times 100 = \frac{0.87965 - 0.8165}{0.87965} \times 100$$
$$= 7.18 \text{ per cent} \ldots\ldots [20]$$

The value $\rho_o = 0.87965$ given by Equation [19] corresponds, for instance, to the two-dimensional stress-distributions

$$S_1, S_2 = 0.5347S_1, \quad S_3 = 0 \ldots\ldots [21]$$

or

$$S_1, S_2 = 0.4653S_1, \quad S_3 = 0 \ldots\ldots [22]$$

which can be read off directly from the nomogram and are shown in the sketches of Fig. 2.

Brief Notes*

On the recommendations of the Executive Committee of the ASME Applied Mechanics Division, it has been decided to initiate a section devoted to brief notes on technical matters in mechanics. These notes must not be longer than 750 words (about 2½ double-spaced typewritten pages, including figures) and will be subject to the usual review procedure prior to publication. After approval such notes will be published in the next issue of the Journal. The notes should be submitted to the Secretary of the ASME Applied Mechanics Division.

Impulsive Loading on an Elastic Half-Space

By J. H. HUTH[1] and J. D. COLE[2]

This brief note considers the wave system resulting from a step loading on an elastic half-space. A similar problem was treated by H. Lamb[3] in 1904, but his interest was in surface tremors rather than the stresses treated herein.

Analysis

Consider the elastic half-space $z \geq 0$ and introduce the cylindrical coordinates r and z. At the time $t = 0$, let a unit normal loading be applied on the surface within a circular region of radius r_0.

It is well known that the displacement vector can be expressed as $\vec{u} = \text{grad } \phi + \text{curl } \vec{\psi}$. For cylindrical symmetry $\vec{\psi}$ has only one component, and we have

$$\left.\begin{aligned} \frac{\partial^2\phi}{\partial r^2} + \frac{1}{r}\frac{\partial\phi}{\partial r} + \frac{\partial^2\phi}{\partial z^2} &= \frac{1}{C_L^2}\frac{\partial^2\phi}{\partial t^2} \\ \frac{\partial^2\psi}{\partial z^2} + \frac{\partial}{\partial r}\left(\frac{1}{r}\frac{\partial(r\psi)}{\partial r}\right) &= \frac{1}{C_T^2}\frac{\partial^2\psi}{\partial t^2} \end{aligned}\right\} \quad \ldots\ldots [1]$$

The axial and shear-stress components are then

$$\left.\begin{aligned} \sigma_z &= 2\mu\left(\frac{1}{r}\frac{\partial^2(r\psi)}{\partial r\,\partial z} + \frac{\partial^2\phi}{\partial z^2}\right) + \lambda\left(\frac{\partial^2\phi}{\partial r^2} + \frac{1}{r}\frac{\partial\phi}{\partial r} + \frac{\partial^2\phi}{\partial z^2}\right) \\ \tau_{rz} &= \mu\left[2\frac{\partial^2\phi}{\partial r\,\partial z} - \frac{\partial^2\psi}{\partial z^2} - \frac{\partial}{\partial r}\left(\frac{1}{r}\frac{\partial(r\psi)}{\partial r}\right)\right] \end{aligned}\right\} \quad \ldots [2]$$

Here C_L and C_T are the longitudinal and transverse wave speeds, respectively, and λ and μ are Lamé's constants.

The boundary conditions are

$$\left.\begin{aligned} &\frac{\partial^2(r\psi)}{\partial r^2} - \frac{1}{r}\frac{\partial(r\psi)}{\partial r} - \frac{\partial^2(r\psi)}{\partial z^2} + 2r\frac{\partial^2\phi}{\partial r\,\partial z} = 0, \quad z = 0 \\ &\lambda\left[\frac{\partial}{\partial r}\left(r\frac{\partial\phi}{\partial r}\right)\right] + (\lambda + 2\mu)\,r\frac{\partial^2\phi}{\partial z^2} + 2\mu\frac{\partial^2(r\psi)}{\partial r\,\partial z} = \begin{cases} r & r \leq r_0 \\ 0 & r \geq r_0 \end{cases} z = 0 \end{aligned}\right\} \quad \ldots [3]$$

Laplace transforms of the solutions of Equations [1] appear as

$$\left.\begin{aligned} \bar{\phi} &= \int_0^\infty f(\beta)e^{-\sqrt{\beta^2 + s^2/C_L^2}\,z}\,J_0(\beta r)d\beta \\ \bar{\psi} &= \int_0^\infty g(\alpha)e^{-\sqrt{\alpha^2 + s^2/C_T^2}\,z}\,J_1(\alpha r)d\alpha \end{aligned}\right\} \quad \ldots\ldots [4]$$

Substitution of Equations [4] into the Laplace transform of Equations [3] leads to a pair of simultaneous integral equations for f and g. These may be solved with the aid of the inversion formula for the Hankel transform.

The resulting expression for the normal stress becomes

$$\sigma_z = \frac{r_0}{2\pi i}\int_{-i\infty}^{i\infty}\frac{e^{st}ds}{s}\left[\int_0^\infty \frac{J_0(r\beta)J_1(r_0\beta)(2\beta^2 + s^2/C_T^2)^2\,e^{-\sqrt{\beta^2 + s^2/C_L^2}\,z}\,d\beta}{\left[(2\beta^2 + s^2/C_T^2)^2 - 4\beta^2\sqrt{(\beta^2 + s^2/C_L^2)(\beta^2 + s^2/C_T^2)}\right]}\right.$$
$$\left. - \int_0^\infty \frac{J_0(r\beta)J_1(r_0\beta)(4\beta^2)\sqrt{(\beta^2 + s^2/C_L^2)(\beta^2 + s^2/C_T^2)}\,e^{-\sqrt{\beta^2 + s^2/C_T^2}\,z}\,d\beta}{\left[(2\beta^2 + s^2/C_T^2)^2 - 4\beta^2\sqrt{(\beta^2 + s^2/C_L^2)(\beta^2 + s^2/C_T^2)}\right]}\right] \quad \ldots [5]$$

The first double integral describes the longitudinal waves, the second describes the shear waves. Similar integrals exist for τ_{rz}.

These integrals contain the information shown in Fig. 1. At any instant the half space has four main regions:[4] Region I—unstressed; II—uniform stress; III—purely longitudinal stress field; IV—combined longitudinal and transverse fields.

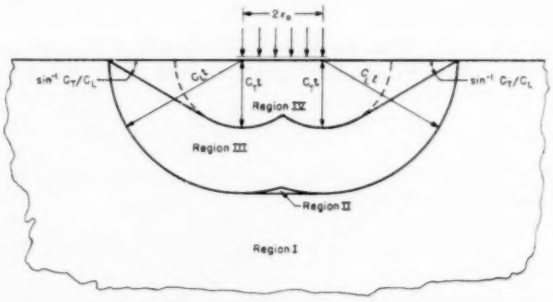

Fig. 1 Stress Field

Various approximations to Equation [5] can be studied. A starting point is the acoustic approximation (μ and $C_T \to 0$) for longitudinal waves which is exactly valid in region II, and shows both

[1] Missiles Division, Rand Corporation, Santa Monica, Calif.

[2] Consultant to the Rand Corporation and Assistant Professor, California Institute of Technology, Pasadena, Calif.

[3] "On the Propagation of Tremors Over the Surface of an Elastic Solid," by H. Lamb, Philosophical Transactions of the Royal Society of London, England, series A, vol. 203, 1904.

[4] For the two-dimensional concentrated load see "Der elastische Halbraum bei einer mechanischen Beeinflussing seiner Oberflanche," by F. Sauter, *Zeitschrift für Angewandte Mathematik und Mechanik*, vol. 30, July, 1950, pp. 203–215.

* Discussion of papers in Brief Notes should be addressed to the Secretary, ASME, 29 West 39th Street, New York, N. Y., and will be accepted until October 11, 1954, for publication at a later date. Discussion received after the closing date will be returned.

Note: Statements and opinions advanced in papers are to be understood as individual expressions of their authors and not those of the Society. Manuscript received by ASME Applied Mechanics Division, January 20, 1954.

regions II and III. Along the axis ($r = 0$) the acoustic stresses are:[5]

$$\left.\begin{array}{lll} z > C_L t & \sigma_z = 0 & \text{Region I} \\ \sqrt{C_L^2 t^2 - r_0^2} < z < C_L t & \sigma_z = 1, (\tau_{rz} = 0) & \text{Region II} \\ 0 \leq z < \sqrt{C_L^2 t^2 - r_0^2} & \sigma_z = 1 - \dfrac{z}{\sqrt{z^2 + r_0^2}} & \text{Region III} \end{array}\right\} \ldots [6]$$

Corrections can be studied with the aid of Equation [5].

Conclusions

The stresses in the one-dimensional "head" (Region III) are given exactly. The maximum width of this "head" is $2r_0$, and its depth along the axis falls off like $1/z^2$ for large z. However, the magnitude of the stresses within the "head" remain constant. This and the abrupt drop behind indicate the one-dimensional head could be of considerable importance in spalling problems, but it appears to have been overlooked by investigators in this field.[6] Integrals representing reflected waves can be obtained and treated by the same method.

Influence of Primary Creep on Column Buckling

By F. K. G. Odqvist,[1] Stockholm, Sweden

In his Wilbur Wright Memorial Lecture read before the Royal Aeronautical Society[2] in 1953, N. J. Hoff discussed the problem of the creep buckling of a hinged-hinged column with an idealized I-section consisting of two flanges each of a cross sectional area $A/2$. The material was assumed to follow Norton's power law for secondary creep rate.

In this note Hoff's formula will be generalized so as to include the effect of primary creep which was treated by the author in recent papers.[3,4] Thus the total creep rate at variable uniaxial stress σ may be put

$$(d\epsilon/dt) = k_0\sigma^{n_0-1}(d\sigma/dt) + k\sigma^n \ldots\ldots\ldots [1]$$

where k_0, n_0, k, and n are constants depending on temperature only. The case $k_0 = 0$ corresponds to Hoff's assumption. Values of the constants may be obtained from the author's previous paper,[4] but it should be remembered that n_0 and n of the present note correspond to $n_0 - 1$ and $n - 1$ of that reference.[4] The rule $n_0 < n$ holds for all cases investigated. In particular, $n_0 = 2$, $n = 3$ are sufficiently accurate choices for aluminum alloys at 200 C. Equation [1] is assumed to hold true for total strains ϵ of the order

$$10^{-3} < \epsilon < 10^{-2}$$

The first term in the right-hand member of Equation [1] corresponds to slip deformation within the grains and second term to viscous creep. This calls for a restriction as to the validity of Equation [1]. It can hold only if $d\epsilon/dt$ has the same sign throughout the process studied. If $d\epsilon/dt$ changes sign, the first term in the right-hand member of Equation [1], the "slip term," must be omitted because slip deformations are not recoverable. Similarly for three-dimensional cases, the plastic work, that is, the scalar product of the stress deviation tensor and the creep-rate tensor, has to be positive in order that the term corresponding to primary creep shall be retained.

In the buckling problem under consideration σ and ϵ are taken positive when they refer to compression. If the column is loaded at time $t = 0$ with a constant load P causing a bending moment M and a deflection y one has

$$P = (\sigma_c + \sigma_t)(A/2), \quad M = Py = (\sigma_c - \sigma_t)(Ah/4) \ldots [2]$$

where h is the distance between the flanges, and the subscripts c and t refer to the flanges on the concave and the convex sides, respectively, of the column. In consequence of the statements made earlier, the creep rate $d\epsilon_c/dt$ includes the slip term of Equation [1] while the creep rate $d\epsilon_t/dt$ does not. Bernoulli's assumption gives

$$(d\epsilon_t/dt) - (d\epsilon_c/dt) = h(\partial^2 y/\partial t\,\partial x^2)$$

Introduction of the dimensionless variables

$$w = 2y/h, \quad \pi x/L = \xi \ldots\ldots\ldots\ldots\ldots [4]$$

where L is the length of the column, and of the dimensionless constants Π, Λ

$$\Pi = 2k(L/\pi h)^2(P/A)^n, \quad \Lambda = 2k_0(L/\pi h)^2(P/A)^{n_0} \ldots [5]$$

result, after eliminations, in a single equation for the deflection of the column

$$\frac{\partial^2 w}{\partial t\,\partial \xi^2} = -\Lambda(1+w)^{n_0-1}\frac{\partial w}{\partial t} + \Pi\left[(1-w)^n - (1+w)^n\right] \ldots [6]$$

When $\Lambda = 0$, this equation reduces to the one derived by Hoff. As the case $n_0 = 2$, $n = 3$ is particularly simple and still of interest, e.g., for aluminum alloys, one may use Hoff's method of solution. Put $w = a(t)\sin\xi$ and retain only the first term of a Fourier series in ξ which satisfies the boundary conditions. The resulting ordinary differential equation for $a(t)$ can be integrated in closed form with the initial condition $t = 0$, $a = a_0$, where a_0 is the initial maximum deflection of the column. One obtains

$$\frac{3\Pi}{2}t = \frac{1-\Lambda}{8}\log\frac{a^2}{a_0^2}\cdot\frac{4+a_0^2}{4+a^2} - \frac{4\Lambda}{3\pi}\tan^{-1}\frac{2(a-a_0)}{4+aa_0} \ldots [7]$$

which is the proposed generalization of Hoff's results. It shows a more rapid growth of a with time when the initial deflections are equal.

It is obvious that the foregoing theory can hold only for such moderately slender columns for which the bending strains predominate over the uniformly distributed normal compressive strains. This excludes the possibility of passing to the limit $a_0 = 0$ and/or $\Pi = 0$ in Equation [6]. Moreover, Equation [7] should be used only as long as w does not exceed unity.

---

[5] For example, the exponential in the acoustic approximation can be related to a Bessel function of half-order. Then see "Theory of Bessel Functions," by G. N. Watson, twenty-fourth edition, Cambridge, 1948, p. 416, Equation (2) for evaluation of the Bessel function integral.

[6] "Some Quantitative Data Bearing on the Scabbing of Metals Under Explosive Attack," by J. Rinehart, *Journal of Applied Physics*, vol. 22, 1951, pp. 555–560.

[1] Professor of Applied Mechanics, Royal Institute of Technology.

[2] "Buckling and Stability," by N. J. Hoff, *Journal of the Royal Aeronautical Society*, January, 1954, p. 3.

[3] "Influence of Primary Creep on Stresses in Structural Parts," by F. K. G. Odqvist, Eighth International Congress of Applied Mechanics, 1952, Proceedings, Istanbul, Turkey, 1953, p. 99.

[4] "Influence of Primary Creep on Stresses in Structural Parts," (complete publication), by F. K. G. Odqvist, Transactions of the Royal Institute of Technology, Stockholm, Sweden, Nr 66, 1953, p. 17.

Manuscript received by ASME Applied Mechanics Division, April 9, 1954.

Bending of Plates Bounded by Conics and Clamped

By S. WOINOWSKY KRIEGER,[1] QUEBEC CITY, CANADA

A simple solution for a uniformly loaded wedge plate recently given by H. Reismann[2] suggests a just as simple generalization. Consider a thin plate clamped along the conic section

$$L \equiv ax^2 + 2hxy + by^2 + 2gx + 2fy + c = 0 \quad [1]$$

and subjected to a load of the intensity

$$p \equiv q + sx + ty \quad [2]$$

in which q, s, and t are constants.

Let

$$w = (\alpha + \beta x + \gamma y)L^2 \quad [3]$$

be the expression for the deflection of the plate, the required boundary conditions being then satisfied by any constant values of α, β, γ. Substituting this tentative solution into the differential equation

$$D\Delta\Delta w = p \quad [4]$$

in which D denotes the flexural rigidity of the plate one arrives at the result

$$\left.\begin{aligned} \alpha &= \frac{q - 32(3ag + 2fh + bg)\beta D - 32(3bf + 2gh + af)\gamma D}{8(3a^2 + 2ab + 3b^2 + 4h^2)D} \\ \beta &= \frac{1}{24ND}\,[(a^2 + 2ab + 5b^2 + 4h^2)s - 4(a + b)ht] \\ \gamma &= \frac{1}{24ND}\,[(b^2 + 2ab + 5a^2 + 4h^2)t - 4(a + b)hs] \end{aligned}\right\} \quad [5]$$

with

$$N = 16a^2b^2 + (5a^2 + 2ab + 5b^2)(a + b)^2 + 8(a - b)^2h^2 + 16h^4 \quad [6]$$

and thus the solution is established.

Taking especially an elliptical boundary one obtains some well-known solutions due to G. H. Bryan.[3] For a wedge plate submitted to a uniform load one has

$$L = y^2 - x^2 \tan^2 \alpha, \quad p = q \quad [7]$$

and, furthermore, $s = t = 0$; the result

$$w = \frac{q(y^2 - x^2 \tan^2 \alpha)^2}{8(3 \tan^4 \alpha - 2 \tan^2 \alpha + 3)D} \quad [8]$$

then is equivalent to that of H. Reismann.

The practical value of the obtained solution [3], quite evident in the case of a closed boundary, becomes rather questionable for plates bounded by parabolas, hyperbolas, or two intersecting straight lines, for the deflections and stresses then increase infinitely with the increasing distance from the given open boundary. Consequently, every additional boundary, practically inevitably, will lead to a complete dislocation of stresses resulting from the basic solution.

The general Solution [3] still holds in the event of an orthotropic plate with a load distributed according to Equation [2]; merely the constants α, β, and γ then must be altered as they become dependent on three rigidities[4] instead of being dependent on a single one, D.

Lastly it should be noted that just as in the case of Bryan's solutions for the elliptical plate a possible mode of stress distribution throughout an appropriately bounded thick elastic plate can be obtained from the general solution [3].

[1] Professor of Structural Engineering, Laval University.

[2] "Bending of Clamped Wedge Plates," by Herbert Reismann, JOURNAL OF APPLIED MECHANICS, Trans. ASME, vol. 75, 1953, p. 141.

[3] "A Treatise on the Mathematical Theory of Elasticity," by A. C. H. Love, University Press, Cambridge, England, fourth edition, 1934, pp. 484, 486.

Manuscript received by ASME Applied Mechanics Division, December 21, 1953.

On the Rate of Growth of Fatigue Cracks

By F. A. McCLINTOCK[1] AND F. J. RYAN,[2] CAMBRIDGE, MASS.

A. K. HEAD'S theory for the rate of growth of fatigue cracks[3] is derived from the model shown in Fig. 1, consisting of rigid-plastic elements P, of length a_0 which yield at stress s_y and work harden linearly until fracture at strain e_f; elastic elements E, with modulus E; and shear elements S, with elastic shear modulus $E/2$. If L = crack length, s = applied stress, N = number of cycles, and N_∞ = number of cycles to failure, he found

$$L^{-1/2} = [s^2/(s_y - s)^2][N_\infty - N][1/(24\sqrt{2}\,Ee_fa_0^{1/2})]$$

Thus a plot of $L^{-1/2}$ versus N should give a curve whose slope is a function of the yield stress of the material and the current level of repeated stress, but independent of the past stress level. For tests at a constant level of repeated stress, Head did find a constant slope. This note reports tests on specimens subjected to varying levels of stress.

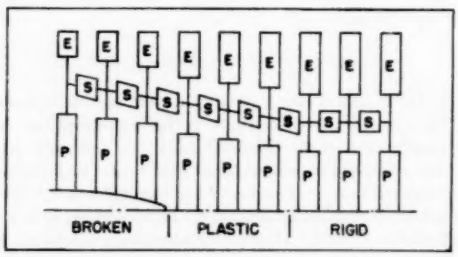

FIG. 1 MODEL SHOWING RATE OF GROWTH OF FATIGUE CRACKS

REPORT OF TESTS

The material was 1/8-in. cold-rolled B1112 steel with a proportional limit of 86,000 psi, a yield strength (0.2 per cent offset) of 107,000 psi, a tensile strength of 109,000 psi, and a 37 per cent reduction of area giving a logarithmic strain at fracture of 0.45. The specimens had a minimum diameter of 0.145 in. with a 1-in.

[4] "Theory of Plates and Shells," by S. Timoshenko, McGraw-Hill Book Company, New York, N. Y., first edition, 1940, p. 189.

[1] Assistant Professor of Mechanical Engineering, Massachusetts Institute of Technology. Assoc. Mem. ASME.

[2] Graduate Student, Massachusetts Institute of Technology.

[3] "The Growth of Fatigue Cracks," by A. K. Head, *Philosophical Magazine*, vol. 44, September, 1953, pp. 925–938.

Manuscript received by ASME Applied Mechanics Division, June 18, 1954.

TABLE 1 VALUES OF K

(*A*) Stress, Ksi	80	60	40	30	20	
(K, in.$^{5/2}$/lb)(—10^9)	1.8–2.3	1.8–2.8	1.3–1.7	2.0–3.5	4.2–8.4	
(*B*) Stress, Ksi	80	40	20	30	40	50
(K, in.$^{5/2}$/lb)(—10^9)	1.7–2.4	5.1–6.5	0	0.8–1.1	1.8–4.1	3.4–5.8
(*C*) Stress, Ksi	80	60	40	20	40	
(K, in.$^{5/2}$/lb)(—10^9)	3.4–4.5	1.3–1.9	1.0–1.7	3.8–9.3	1.2–2.6	

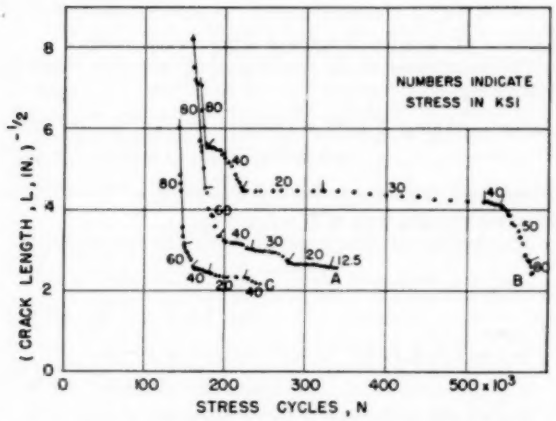

FIG. 2 RESULTS OF TESTS ON SPECIMENS SUBJECTED TO VARYING LEVELS OF STRESS

longitudinal radius of curvature. Final polishing was done with 4/0 emery in a diagonal direction. Rotary bending tests were run at 6000 rpm and an initial stress of 80,000 psi. The tests were stopped frequently for microscopic examination at 30X. Subsequent stress levels were lower to minimize work hardening of the specimen as a whole during crack growth.

Fig. 2 shows the results. Except for a brief "incubation period" after changes in stress, the slopes are fairly constant for any stress level and independent of past history. Twenty-to-one uncertainty intervals for the slopes were "guesstimated" from the original large-scale plots after the incubation periods. The theory predicts that the quantity $(dL^{-1/2}/dN)(s_y - s)^2/s^3$, defined as K, should be a constant. This constant is presented in Table 1, based on $s_y = 150{,}000$ psi. (Values of 120,000 to 190,000 psi would not affect the results seriously.) Constraint at the root of the crack may be the reason that the best fit is found with s_y higher than the tensile yield stress. While the slopes vary by a factor of as much as 100, in almost all cases the uncertainty interval for K extends to within a factor of 1.5 of -2.5×10^{-9} in.$^{5/2}$/lb, and variations from this value are not systematic. Thus Head's theory seems to explain most of the effect of stress level on the rate of crack growth. But while K seems constant, its magnitude is not satisfactory, for with $e_f = 0.45$, $E = 30 \times 10^6$ psi, and $a_0 = 10^{-4}$ to 10^{-2} in., the theory predicts -0.22×10^{-7} to -2.2×10^{-7} in.$^{5/2}$/lb.

CONCLUSION

Perhaps some of the assumptions of the theory should be reexamined. The width of the plastic region may not be constant as the crack proceeds. Perhaps the shear elements should have plastic, as well as elastic, properties. Provision should be made for carrying a compression load across the crack. Furthermore, the theory predicts that under static loading of a work-hardening material, a crack will propagate to failure when the mean stress reaches the yield point, which is not observed in notched tensile tests.

In conclusion, the authors feel that the foregoing results, while based on rather meager data, indicate both enough agreement and enough discrepancy between Head's theory and experimental data to make the theory of practical interest and at the same time to warrant further study.

Rounded Corner of a 90-Deg Elbow—Two-Dimensional Potential Flow

BY ROBERT LOWY[1]

THE two-dimensional irrotational flow of a frictionless incompressible fluid around sharp corners shows two extreme possibilities, either infinite velocity or separation. Solutions of avoiding the infinite velocity and the separation can be brought about by rounding-off or by rounding-out of the inner corner.

Problems of this nature are treated in the form of term papers by graduate students in Advanced Fluid Mechanics at the University of Pennsylvania and are published in condensed form by the author in bulletins of the Civil Engineering Department.

The simplest method of rounding-off can be obtained by assuming a constant velocity and constant pressure along the rounding-off (an example for a 90-deg elbow is shown in Bulletin No. 3, Problem No. 9) and is represented in the following expression

$$v_x + iv_y = (v_x^2 + v_y^2)\left(\sqrt{\tanh(\varphi + i\psi) + k} + \sqrt{\tanh(\varphi + i\psi) - k}\right)$$

where x, y are the co-ordinates; v_x, v_y are the velocity components; φ, ψ are the potential and stream-function of the flow system; and k is a constant.

The disadvantage of such a rounding-off is present in the fact that the pressure gradient is infinite at either end of the rounding-off curve, without pressure discontinuity. At the leaving end, with a sudden pressure increase, a separation almost certainly will occur in practice.

To avoid the possibility of a separation we must abandon the assumption of a constant velocity along the rounding-off curve and utilize a more general solution for such a 90-deg elbow as may be expressed in the relation

$$v_x + iv_y = (v_x^2 + v_y^2) \Sigma\, C_i\, [\tanh(\varphi + i\psi) + k_i]^{n + 1/2}$$

where C_i, k_i are constants with $+1 > k_i > -1$; n is a positive integer. The rounding-off curve on the inner wall, $\psi = 0$ starts and ends at the extreme values of k_i. The outer wall $\psi = \pi/2$, has the stagnation point in the corner at $\varphi = 0$.

We presume as an example, Fig. 1, of a 90-deg elbow having equal shank widths (B), with the average velocity v_0 therein. Furthermore, the flow should proceed in the direction from $x = +\infty$ to $y = -\infty$ with a short acceleration before the rounding-off and a small deceleration at the start of the rounding. Similar conditions exist in a venturi tube. The velocity gradient at the

---

[1] Special Lecturer in Civil Engineering, The Towne Scientific School, University of Pennsylvania, Philadelphia, Pa.; Associate Professor, Pennsylvania Military College, Chester, Pa. Mem. ASME.

Manuscript received by ASME Applied Mechanics Division, July 13, 1953.

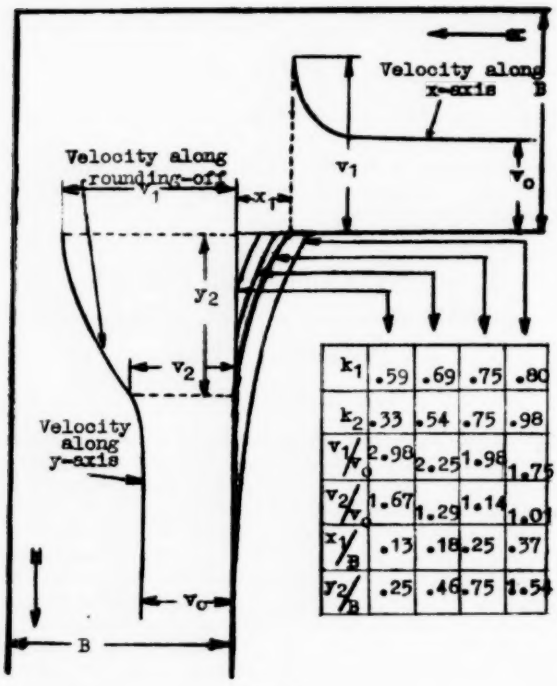

k_1	.59	.69	.75	.80
k_2	.33	.54	.75	.98
v_1/v_0	2.98	2.25	1.98	1.75
v_2/v_0	1.67	1.29	1.14	1.01
x_1/B	.13	.18	.25	.37
y_2/B	.25	.46	.75	1.54

FIG. 1

beginning of the rounding-off should be along the straight wall, $dv/dx = \infty$, and along the curve $dv/ds = 0$.

The particular solution for this case is expressed by

$$v_x + iv_y = (v_x^2 + v_y^2)\,[(\tanh(\varphi + i\psi) + k_2)^{3/2} + C(\tanh(\varphi + i\psi) - k_1)^{1/2}]$$

The foregoing conditions yield the relations between k_1, k_2, and C

$$1/v_0 = (1 + k_2)^{3/2} + C(1 - k_1)^{1/2} = (1 - k_2)^{3/2} + C(1 + k_1)^{1/2} = 2B/\pi$$

and $C = (k_1 + k_2)\sqrt{3}$ where B is the channel width.

The co-ordinates of the rounding-off curve can be found by integrating

$$dx/d\varphi = (\tanh\varphi + k_2)^{3/2} = t^{3/2}$$

$$\text{and } dy/d\varphi = C(k_1 - \tanh\varphi)^{1/2} = Cu^{1/2}$$

where t and u are new variables (functions of φ) which change along the rounding from $\sqrt{k_1 + k_2}$ to zero.

The co-ordinates of the rounding can then be computed from

$$x = (1 + k_2)^{3/2}\tanh^{-1}\sqrt{t/(1 + k_2)} + (1 - k_2)^{3/2}\tan^{-1}\sqrt{t\,(1 - k_2)} - 2\sqrt{t}$$

$$y = \left[\sqrt{1 + k_1}\tanh^{-1}\sqrt{u/(1 + k_1)} - \sqrt{1 - k_1}\tan^{-1}\sqrt{u/(1 - k_1)}\right](k_1 + k_2)\sqrt{3}$$

The velocity at the start of the rounding is $v_1 = 1/(k_1 + k_2)^{3/2}$ and at the end of the rounding-off curve is $v_2 = v_1/\sqrt{3}$.

Typical examples of such roundings are presented in Fig. 1. The velocity and pressure conditions along such a curved border wall and on the subsequent straight wall are far better than for a rounding with constant velocity.

If we had more knowledge concerning the boundary layer and the permissible velocity gradient without producing separation in diffusors we could obtain an even better 90-deg two-dimensional elbow by making use of the foregoing general equation by using more terms with various exponents of n.

Discussion

Analysis of a Nonlinear Dynamic Vibration Absorber[1]

KARL KLOTTER.[2] The author's conclusion reads: "The effect of the nonlinearity of the spring of the dynamic absorber is to prevent the existence of sharp resonant peaks and to introduce odd harmonic components of relatively small amplitudes in the motion of the two masses."

This statement contains two essential points; i.e. (1) nonexistence of sharp resonant peaks, (2) introduction of higher harmonics. On both of these points and two minor additional ones I wish to comment.

1 If the first part of the statement is to mean that there cannot exist any unlimited values for the amplitudes of the displacements of the two masses in the absence of damping (or equivalently, no high values of the amplitudes for small damping), I am sorry that I have to disagree with the author.

The author's statement in essence is based on the discussion of his Equation [35], called the "Amplitude Equation." The discussion, as given, does not reveal any unbounded values; in particular, at the crucial frequency ω_0 the author finds (see his Equation [38]) a single and finite value for the amplitude A of the relative displacement

$$A \equiv B/a = \frac{P_0}{k}\frac{m_1 + m_2}{m_2} \quad \ldots\ldots\ldots\ldots [1]$$

It is the author's discussion of his Amplitude Equation [35] for this particular frequency $\omega = \omega_0$, however, which I consider incomplete. It appears that the author has overlooked the possibility of the quantity $B \equiv A/a$ tending toward infinity whilst the factor $(\omega_0^{-2} - \omega^{-2})$ goes toward zero. A limiting process reveals two possibilities:

(*a*) The author's result, as listed here in Equation [1],

(*b*) $B \to \ln \dfrac{\omega_0^2}{\omega_0^2 - \omega^2}$, if $\omega \to \omega_0$ from below.

In order to demonstrate these results, we start from the author's Equation [35], which may be written as

$$-\left(\frac{\omega^2}{\omega_1^2} - 1\right) B + \frac{2k_0}{k}\omega_2^2\left[\frac{1}{\omega_0^2} - \frac{1}{\omega^2}\right] I_1(B) = \frac{aP_0}{k} \quad [2]$$

and we propose to find the values of B as ω^2 tends toward ω_0^2. For this purpose we denote $\omega^2 = \omega_0^2(1 + \epsilon)$ or conversely $\epsilon = (\omega^2 - \omega_0^2)/\omega_0^2$. The bracket in Equation [2] then becomes $[\omega_0^{-2} - \omega^{-2}] = \epsilon/\omega_0^2$. Introducing, furthermore, the frequency ratios ω_0^2/ω_1^2 and ω_2^2/ω_0^2 according to their definitions, we obtain from Equation [2]

$$B\frac{m_2}{m_1 + m_2} + 2\frac{k_0}{k}\frac{m_1 + m_2}{m_1}\epsilon I_1(B) = \frac{aP_0}{k} \quad \ldots\ldots [3]$$

and we wish to learn what values B may assume as ϵ tends toward zero. Obviously, two possibilities are to be considered:

(*a*) B stays finite as $\epsilon \to 0$.

In this case the term containing ϵ vanishes, and we find from Equation [3] the author's result, as denoted here in Equation [1].

(*b*) B goes toward infinity in such a way as to cause the product $\epsilon I_1(B)$ to stay finite.

In this case, Equation [3] of this discussion, after being divided through by B, simplifies to

$$\frac{(-\epsilon)I_1(B)}{B} \simeq \frac{1}{2}\frac{k}{k_0}\frac{m_2^2}{(m_1 + m_2)^2} \quad \ldots\ldots\ldots\ldots [4]$$

From this form we conclude first that ϵ is to be a negative (or $-\epsilon$ a positive) quantity, meaning that ω^2 is to approach the value ω_0^2 from below. Using the asymptotic expression for the modified Bessel functions

$$I_n(x) \simeq \frac{e^x}{\sqrt{2\pi x}}$$

and taking logarithms, we find

$$\ln(-\epsilon) + B - \frac{3}{2}\ln B - \ln 2\pi \simeq \ln\frac{1}{2}\frac{k}{k_0}\frac{m_2^2}{(m_1 + m_2)^2} \quad [5]$$

In this equation all terms but the first two are irrelevant as $(-\epsilon)$ tends toward zero and B toward infinity, and we are left with

$$\ln(-\epsilon) + B \simeq 0$$

or, equivalently

$$A \equiv B/a \simeq \frac{1}{a}\ln\frac{\omega_0^2}{\omega_0^2 - \omega^2}$$

as stated in the foregoing.

Thus infinite values for the amplitude A of the relative displacement $(x_1 - x_2)$ are possible and with them infinite values for the amplitudes of the displacements x_1 and x_2 themselves. ω_0 is a "resonant frequency" indeed, and the response curves do exhibit sharp resonant peaks.

The author has indicated a graphical procedure for solving the Amplitude Equation, but no response curves (amplitudes versus frequency) are given. At Stanford University we have investigated nonlinear systems of two degrees of freedom for quite some time. From our results, I wish to show the response curves for a system equivalent to the one treated by the author. The method used differs somewhat from the author's but this fact is immaterial in this connection. The system is built exactly like the one treated by the author with the sole exception that the restoring force-displacement relationship contains a linear and a cubic term only, whereas the author uses a transcendental relationship expressed by a hyperbolic sine function. This detail, however, does not influence the results appreciably. Fig. 1, herewith, shows the response curves for a system having the equations of motion

$$\left.\begin{aligned} m_1\ddot{x}_1 + c_1x_1 + c_2(x_1 - x_2)[1 + \mu_2^2(x_1 - x_2)^2] &= P\cos\Omega t \\ m_2\ddot{x}_2 + c_2(x_2 - x_1)[1 + \mu_2^2(x_2 - x_1)^2] &= 0 \end{aligned}\right\} \quad [6]$$

and one will recognize clearly that, in spite of the nonlinearity in the second spring, there is a definite frequency, designated by η_∞, and corresponding to the frequency ω_0 in the paper, for which the amplitudes of both masses, represented by the quantities

[1] By L. A. Pipes, published in the December, 1953, issue of the JOURNAL OF APPLIED MECHANICS, Trans. ASME, vol. 75, pp. 515–518.

[2] Professor of Engineering Mechanics, Stanford University, Stanford, Calif.

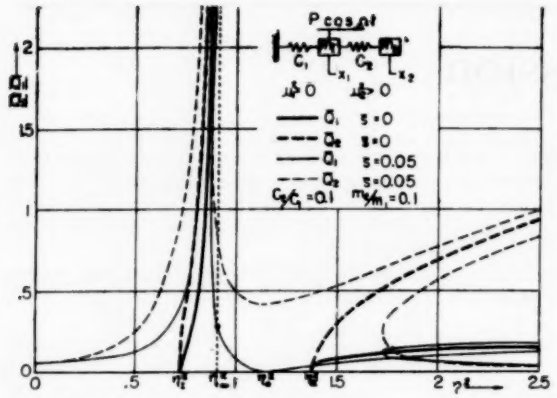

Parameters: $x_i = Q_i \cos \Omega t$, $\bar{Q}_i = \sqrt{3/4}\,\mu_2 Q_i$,

$s = \sqrt{3/4}\,\mu_2 \dfrac{m_2}{m_1} P/c_2$, $\eta^2 = m_2\Omega^2/c_2$

FIG. 1 RESPONSE CURVES

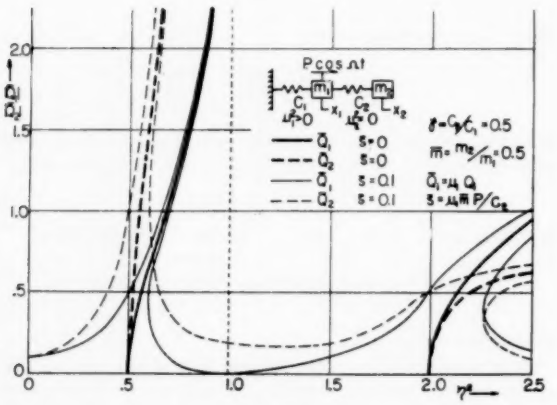

Parameter: $\eta^2 = m_2\Omega^2/c_2$

FIG. 2 RESPONSE CURVES

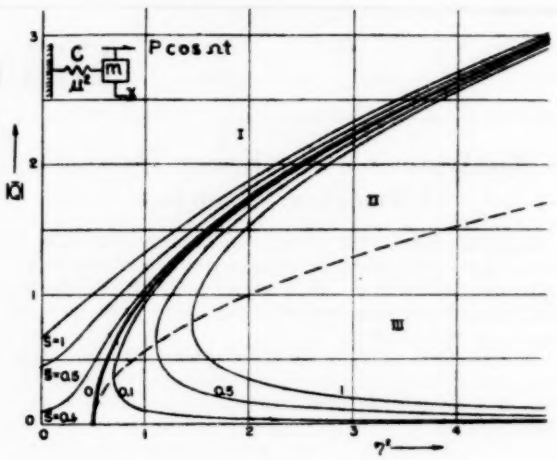

Parameters: $x = Q \cos \Omega t$, $\eta^2 = m\Omega^2/c$, $\bar{Q} = \sqrt{3/4}\,\mu Q$,

$\bar{s} = \sqrt{3/4}\,\mu P/c$

FIG. 3 RESPONSE CURVES OF SYSTEM HAVING EQUATION OF MOTION, $m\ddot{x} + cx(1 + \mu^2 x^2) = P \cos \Omega t$

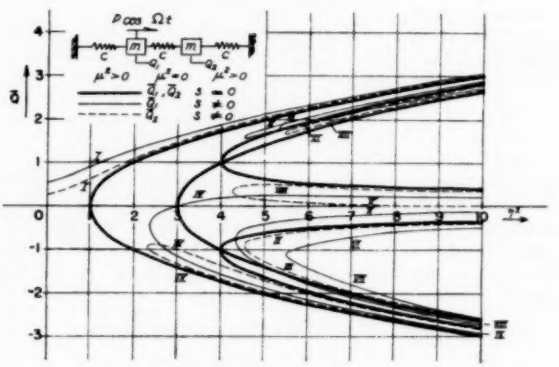

FIG. 4 RESPONSE CURVES

$\bar{Q}_1$ and $\bar{Q}_2$, become unbounded. The finite values for $\bar{Q}_1$ and $\bar{Q}_2$ at ω_0, corresponding to the value A of Equation [1] of this discussion, may be recognized as well (designated by o). If in the system, having two springs, not the second but the first spring is nonlinear, there exists also a resonant frequency; as is shown in Fig. 2 of this discussion.

The resonant frequency ω_0 has the value $\omega_0^2 = c_1/(m_1 + m_2)$ for the system having the nonlinearity in the second spring, whereas it has the value $\omega_0^2 = c_2/m_2$ if the nonlinearity is present in the first spring. In the first case the resonant frequency ω_0 coincides with the natural frequency of a single-degree-of-freedom system consisting of the first (linear) spring and the two masses combined, in the second case the resonant frequency coincides with the natural frequency of a system consisting of the second (linear) spring and the second mass alone. These results may be interpreted readily: Because the nonlinear springs are becoming increasingly stiffer as the displacements grow they finally turn into practically rigid connections. And the resonant frequencies are the natural frequencies of those linear systems in which the nonlinear springs have been replaced by rigid connections. One realizes immediately the importance of one spring being linear for the occurrence of the resonance phenomenon.

Let us contrast these systems with two others: The system of one degree of freedom has a response diagram as shown in Fig. 3, of this discussion. A system of two degrees of freedom having three springs, the outer two of which are nonlinear, possesses a response diagram as shown in Fig. 4. In either of *these* two cases there exists *no* finite frequency for which the amplitudes of the displacements would become unbounded; i.e., *no* resonant frequency. This result in turn agrees with the explanation given previously: There is no possibility of free vibrations if the nonlinear springs are replaced by rigid connections.

2 Turning now to the second part of the author's conclusion, I concur with his statement that higher-order terms are introduced into the solution. However, I wish to point out that these terms may have amplitudes which differ considerably from the ones given in the paper. The treatment of the higher-order terms in the paper appears to be inconsistent. Having neglected higher-order terms in his Assumption [27] the author should not carry such terms later. I would recommend omitting higher-order terms altogether from the formulas. The alternative, carrying all, or even some, of these terms in a consistent manner, would render the calculations quite a bit more involved.

3 The third point I would like to make has been touched upon already. I fail to see the significance and the advantage of the author's choice of a transcendental function for the force-displacement relationship in the absorber spring. A cubic term besides the linear one would suffice for the purpose and would render the picture, including the formulas, somewhat simpler.

4 Finally, I wish to repeat my suggestion, which I have offered already a number of times, to abolish the usage (introduced in 1938 by Mr. M. Rauscher, I suppose) of calling a nonlinear spring "hard" or "soft," if the slope of the force-displacement curve is increasing or decreasing. Instead, I wish to plead for the terms "hardening" or "softening," because the terms hard and soft are already customarily used in referring to the relative magnitude of the linear parts.

H. Norman Abramson.[3] Professor Pipes has presented a very illuminating analysis of a nonlinear vibration absorber. His approach to a seemingly very difficult fourth-order nonlinear differential equation is a striking example of the use of Duffing's method, and variations of it, in problems of this type.

The writer would like to add only a few comments concerning the possibility of jump phenomena and the interpretation of the author's Fig. 3 which provides the amplitude of relative motion. This writer does not agree that resonance phenomena will not be exhibited (a complete and detailed analysis of this very important question is given by Dr. K. Klotter in a separate discussion of the subject paper). The author is correct, however, in stating that jump phenomena may occur, as is easily seen from Fig. 3, when the solution yields three roots. A remark concerning stability of motion will be given in a later paragraph.

The analysis shows clearly how one may determine the relative amplitude, and then the motions of the individual masses, when all of the constants are given. The author mentions that for large values of the exciting frequency the amplitude of relative motion will be small. However, although it may be desirable to maintain a low relative amplitude, the essential point is that the amplitude of the main mass remain small. Since, by Equation [50], the amplitude of the main mass depends on the amplitude of relative motion in large measure, this is a valuable criterion.

Close examination of Fig. 3 of the paper shows that one may obtain any one of three different types of results, depending on the value of the exciting frequency. These are: (*a*) one root, corresponding to a motion in-phase with the exciting force; (*b*) two roots, one in-phase and one out-of-phase; (*c*) three roots, one in-phase and two out-of-phase. This strongly suggests an analogy with the usual response diagram for an undamped single-degree-of-freedom nonlinear system with hardening spring. In this case, the out-of-phase motion having the larger amplitude is unstable. For proper "tuning" then, one should use values of the absorber constants which will insure that the motion always remains on the lower branch. In terms of Fig. 3 of the paper, one must choose the constants so that $Y_2(B)$ intersects $Y_1(B)$ in at least two points on the lower portion, for all values of the exciting frequency within the spectrum for which the absorber is to be tuned. Thus a second criterion is provided which will aid in choosing the constants.

The tangency condition between $Y_2(B)$ and the lower portion of $Y_1(B)$ is the point at which a jump could occur (but only if the exciting frequency were being reduced). In practice, some damping will always exist. It would seem that the effect of a small amount of damping would be to make the amplitude of the upper branch of the response curve finite, and thus provide a second value of exciting frequency at which a jump would occur. Because of the presence of jump phenomena, one must be extremely cognizant of the range of exciting frequencies which will be encountered in the particular application.

[3] Associate Professor of Aeronautical Engineering, Agricultural and Mechanical College of Texas, College Station, Texas. Assoc. Mem. ASME.

Author's Closure

The author wishes to thank Professor Klotter and Professor Abramson for their interesting and valuable discussion of his paper. In his discussion Professor Klotter presents a rather lengthy analysis involving a limiting process and concludes that there is a sharp resonant peak in the relative amplitude A of the two masses of the system when the driving force has the angular frequency

$$w = w_0 = [k/(m_1 + m_2)]^{1/2} \quad [7]$$

Because of the importance of this point, it is well to analyze this question more fully by the extended Duffing's method used in the paper. The analysis of the performance of the vibration absorber is based on Equation [19] of the paper. This equation may be written in the following form

$$(m_1m_2D^2 + km_2D^2)x + [(m_1 + m_2)D^2 + k]F(x) = -m_2w^2P_0 \sin(wt) \quad [8]$$

where D is the time-derivative operator, x the relative displacement of the masses, and the function $F(x)$ expresses the characteristics of the nonlinear spring. In the paper $F(x)$ is taken to be the hyperbolic function $(k_0/a)\sinh(ax)$, but as is pointed out by Professor Klotter, the salient features of the analysis are preserved by taking a simple polynomial expression of the form

$$F(x) = k_0x \pm bx^3 \quad [9]$$

If the positive sign is taken in this expression, the function represents the characteristics of a "hardening" spring while if the negative sign is taken, Equation [9] represents the characteristics of a "softening" spring to use the descriptive terminology suggested by Professor Klotter.

The extended Duffing method of analysis consists of assuming an approximation for the solution of Equation [8] of the following form

$$x_0 = A \sin(wt) \quad [10]$$

If this approximate solution is substituted into Equation [8] and the coefficients of $\sin(wt)$ of both members of the resulting equation are equated, the following relation is obtained

$$(km_2w^2 - m_1m_2w^4)A + [(m_1 + m_2)w^2 - k](k_0A \pm 3/4bA^3) = m_1w^2P_0 \quad [11]$$

If b is zero, the absorber spring reduces to a linear one and Equation [11] reduces to the following linear equation in A

$$(km_2w^2 - m_1m_2w^4)A + [(m_1 + m_2)w^2 - k]k_0A = m_2w^2P_0 \quad [12]$$

An examination of this equation reveals the fact that if the angular frequency of the driving force has the value $w = w_0$ as given by Equation [7], the second term of Equation [12] vanishes and the relative amplitude of the masses is given by the well-known result

$$A = \frac{P_0}{km_2}(m_1 + m_2) \quad [13]$$

This is the relative amplitude of a linear absorber when the frequency of the driving force is w_0. Now, if a small amount of

nonlinearity is introduced into the system by giving the parameter b a small value, it should not be expected that A suddenly will assume an infinite value, from physical considerations, since this would mean shifting the resonant peak from $w = (k/m_1)^{1/2}$ to w_0 by the addition of an infinitesimal nonlinearity. That A remains finite in the nonlinear case may be seen by placing $w = w_0$ in Equation [11]. For this value of w the second term of the equation vanishes and the equation is again reduced to a linear equation in A whose solution is given by Equation [13] regardless of the type of nonlinearity assumed. Since Equation [11] reduces to a linear equation in A it possesses only one solution and this is given by Equation [13].

A convenient form of Equation [11] may be obtained by introducing the following notation

$$\theta_1(w) = [(m_1 + m_2)w^2 - k] \quad [14]$$

and

$$\theta_2(w) = (km_2w^2 - m_1m_2w^4) \quad [15]$$

With this notation, Equation [11] may be written in the following form

$$\left[\left(\pm 3b\,\frac{A^2}{4} + k_0\right)\theta_1 + \theta_2\right] = m_2w^2\,\frac{P_0}{A} = y(A) \quad [16]$$

This equation may be used as a basis for the graphical determination of the amplitude A. If the left member of Equation [16] is plotted against A, the resulting curve is a parabola. The plot of the right member is a hyperbola. The possible values of A are those for which the two curves intersect. If $w = w_0$, $\theta_1 = 0$ and the parabola degenerates into a straight line parallel to the A-axis. The values of A obtained from the graphical construction must be interpreted in the light that when $w = w_0$, the original Equation [11] reduces to a linear equation in A and has only the one solution, Equation [13]. If this fact is not clearly kept in mind, there is a possibility that extraneous roots might be introduced by allowing w to approach w_0 by a limiting process. An analogous situation would arise if one attempted to solve the following linear equation

$$bx + c = 0 \quad [17]$$

by first solving the quadratic equation

$$ax^2 + (bx + c) = 0 \quad [18]$$

whose roots are

$$x = -\frac{b}{2a} \pm \frac{(b^2 - 4ac)^{1/2}}{2a} \quad [19]$$

by allowing a to approach zero. If one did not use considerable care, one might conclude that Equation [17] has two infinite roots.

The author agrees with Professor Klotter's point regarding harmonic terms. The amplitudes of these terms should be calculated directly from Equation [19] of the paper and not as has been done in the paper. The choice of the hyperbolic form for the spring characteristic $F(x)$ is irrelevant and, as Professor Klotter points out, the form [9] is considerably simpler and preserves all the salient features of the analysis. Professor Klotter's choice of the terminology hardening and softening is very descriptive and will no doubt come into common usage to describe spring characteristics.

Professor Abramson's remarks concerning jump phenomena and his comments on criteria for tuning the absorber add much to the analysis.

In addition to the phenomena considered in the paper and in the discussion, it would seem that an analysis of the possible subharmonic oscillations of the system should be undertaken for completeness. The author has investigated subharmonics of order one third by searching for a solution of the form

$$x = B \sin(wt/3) \quad [20]$$

of Equation [8] with $F(x)$ given by Equation [9]. The results indicate that for certain values of the parameters of the system, Equation [20] is an exact solution. The analysis of the stability of the solution is a difficult one because of the high order of the resulting variational equation and the number of parameters involved, and conclusive results have not yet been reached.

Stress Concentration Due to Elliptical Holes in Orthotropic Plates[1]

E. P. Popov.[2] This paper discusses two interesting problems of stress concentration for an elliptical hole in an orthotropic plate. The behavior of anisotropic materials is beginning to receive ever-increasing attention. In prestressed reinforced-concrete design, the different amount of prestressing in two directions makes the slab orthotropic. In the design of some steel bridges in Germany spectacular economy was achieved by designing the steel bridge decks as orthotropic plates. From the information reaching us in this country it appears that this field of research has been highly developed in the USSR, and it seems significant to call attention to their work. This subject is treated in several Russian books. Two of them were written by S. G. Lekhnitskii.[3] Some 56 references to research literature are given in the first book; 80 papers are listed in the second.

Professor Timoshenko in his book[4] in a section on two-dimensional problems in elasticity states, "S. Lechnitski obtained solutions of this equation (differential equation for orthotropic plates) for rectangular beams, circular rings, and circular and elliptic holes, similar to those previously mentioned for isotropic plates."

In Chapter 5 of Lekhnitskii's book on "Anisotropic Plates" the problem of stress concentration around elliptical and circular holes is discussed. Functions of a complex variable are used to set up a general problem for an elliptical hole with an arbitrary edge loading. Then several special cases are considered for an infinitely large plate. For an elliptical hole, these are as follows:

1 Equal pressure acting normal to the contour of the ellipse.

2 Shearing stress of equal intensity acting tangentially to the contour of the ellipse.

3 Tension acting at an arbitrary angle with the major axis of the ellipse. (A special case of this problem corresponding to case b of the author's paper is also discussed.)

4 Pure shear.

5 Pure bending. The special case of an ellipse whose major axis is parallel to the edge of the plate also is treated.

The same cases are discussed for stresses in an orthotropic plate with a circular hole, and in addition the following:

---

[1] By H. D. Conway, published in the March, 1954, issue of the Journal of Applied Mechanics, Trans. ASME, vol. 76, pp. 42–44.

[2] Professor of Civil Engineering, University of California, Berkeley, Calif.

[3] The first of these books, "Anisotropic Plates" ("Anisotropnie plastinki"), was published in 1947; the second, "Theory of Elasticity of an Anisotropic Body" ("Teoriya uprugosti anisotropnogo tela"), in 1950; reviews of the books were published in *Applied Mechanics Reviews*, vol. 5, 1952, Rev. 1014.

[4] "History of Strength of Materials," by S. P. Timoshenko, McGraw-Hill Book Company, Inc., New York, N. Y., 1953, p. 408.

1 Equal tensions in two mutually perpendicular directions.

2 Compression of a plate whose transverse deformation is prevented.

3 Stresses caused by equal radial displacements at the boundary.

4 Stresses caused by prescribed angular rotation of the whole boundary in the plane of the plate.

5 Stresses in a plate with a rigid circular core.

A book by G. N. Savin[5] published in 1951 touches on the same subject. Chapter 3 of this book is devoted to stress concentrations in an orthotropic plate near elliptic and circular openings. Again, the general problem using the method of a complex variable is discussed, and the results of investigations for several special cases are given. A number of these treat other problems than those given in Lekhnitskii's book. Among these, the stresses caused by concentrated equal and opposite forces applied along the axis of the ellipse are given.

Author's Closure

The author is indebted to Professor Popov for calling attention to the work of Lekhnitskii and Savin in the USSR. The subject of orthotropic plates has also received considerable attention in Japan.[6]

It is perhaps relevant to mention that the two problems treated by the author were chosen without any great significance, the main aim of the paper being to show that the stresses around elliptical holes can be obtained very simply from those around corresponding circular ones, the general solution for the circular hole being already well established.

On Application of a Quasi-Static Variational Principle to a System With Damping[1]

J. P. Russell[2] This paper is another example of the author's ability to extract from the mathematical and physical aspects of a particular problem workable results that can be analyzed and used by the engineer. The author considers the problem of the transverse vibrations of a beam under a damping force proportional, at each point of the beam, to the velocity and, by eliminating the time variable, develops a stationary condition for the formulated nonconservative variational problem. It is in the extension of variational methods to this type of eigenvalue problem and the approximate formulas so developed that this paper makes its important contribution.

In assuming that an exponential time function will reduce Equation [1] to an ordinary differential equation of type [3] in the paper, it is well to note that the mathematical conditions must insure that the original partial differential equation be linear, homogeneous, with coefficients functions only of x. If these necessary restrictions are met, then the method employed is applicable.

The reduced ordinary differential equation, with its boundary conditions, is then transformed in standard manner into its corresponding variational form, and by apparently reasonable physical considerations, the author is led to assume that the deflection shape in any principal mode will be affected negligibly by the damping term. The formulas are developed in a convenient, useful, and familiar form; however, their accuracy depends, of course, on the foregoing assumption. It seems reasonable, however, that the error in the frequencies computed from Equations [6a] and [6b] will be less than the error introduced by assuming the shapes the same for the damped and undamped cases. Moreover, let us consider the differential equation for damped and undamped cases, viz.

$$[EIy_0'']'' + m(x)p_0^2y_0 = 0 \quad \ldots\ldots\ldots\ldots [10]$$

for the undamped case and

$$[EIy'']'' + m(x)p\left[\frac{f(x)}{m(x)} + p\right]y = 0 \quad \ldots\ldots [11]$$

for the damped case.

Comparing Equations [10] and [11], we see that if the coefficients of y_0 and y are the same in the two equations, then similar boundary conditions and the uniqueness property of the solution lead us to conclude that the solutions of the two equations must be the same, and the deflection shapes are unaffected by the damping term as long as

$$p_0^2 = p\left[\frac{f(x)}{m(x)} + p\right]$$

or

$$\frac{p_0^2 - p^2}{p} = \frac{f(x)}{m(x)} \; (= k) \quad \ldots\ldots\ldots\ldots [12]$$

Since the left-hand side of Equation [12] is constant, the right-hand side also must be constant, say, k. Furthermore, if the right-hand side is constant, and similar boundary conditions prevail, then if the p's are computed using Equation [12], with p_0 and k known, then the solution for this physically possible [$f(x) = km(x)$] damped situation is exactly the same as for the undamped case. The author shows this in the Appendix in a slightly different manner, and it is clearly one of the grounds which supports the assumption that the shapes for the damped and undamped cases will be similar for arbitrary $f(x)$. If $f(x)$ is small, then it may be expected that the damping will have a negligible effect on the mode shapes regardless of the function [$f(x)/m(x)$].

The question of developing a quantitative measure of the error involved by introducing this assumption is fraught with difficulties. However, an investigation may be attempted by considering special cases of $f(x)$ and $m(x)$ which give rise to known functions as solutions of the fourth-order linear Equation [10] of this discussion. Comparing these with the results obtained using the formulas derived in the paper for the eigenvalues, Equations [6a] and [6b], we will have some measure of the error.

---

[5] "Stress Concentrations Near Openings," (Koncentracia naprajeni okolo otversti), a book by G. N. Savin, published in 1951; a review of this book was published in *Applied Mechanics Reviews*, vol. 5, 1952, Rev. 1318.

[6] See, for example: "Calculation of the Stresses of the Orthotropic Strip With a Hole," by M. Higuchi, Reports of Research Institute for Applied Mechanics, vol. 1, no. 1, January, 1952.

"The Stresses in the Orthotropic Semi-infinite Plate Due to a Rigid Bolt Compressed Against Its Edge," by M. Higuchi, Reports of Research Institute for Applied Mechanics, vol. 2, no. 6, June, 1953.

"On the Stresses Due to Pressure on the Periphery of the Hole in an Orthotropic Plate," by M. Higuchi, Reports of Research Institute for Applied Mechanics, vol. 2, no. 6, June, 1953.

"Orthotropic Semi-infinite Plate With a Hole," by M. Higuchi, Report of Research Institute for Applied Mechanics, vol. 2, no. 7, September, 1953.

"A Note on the Two-Dimensional Stresses of Orthogonally Aelotropic Plates," by K. Washizu, Trans., Japan Society of Mechanical Engineers, vol. 18, no. 68, 1952.

"On the Bending of Orthogonally Aelotropic Plates," by K. Washizu, Proceedings of First Japan National Congress for Applied Mechanics, 1951.

[1] By Morris Morduchow, published in the March, 1954, issue of the Journal of Applied Mechanics, Trans. ASME, vol. 76, pp. 8–10.

[2] Polytechnic Institute of Brooklyn, Brooklyn, N. Y.

This procedure probably would contain mathematical difficulties not unlike the original problem itself.

D. E. WHITFORD.[3] For the particular system considered, the success of the method used depends upon the elimination of the time. This is equivalent to the usual process of separating the variables, except that in this case a single ordinary differential equation results. If $f(x)/m(x) \neq$ const, then it would be found that the variables cannot readily be separated by this usual procedure; but the immediate use of the factor e^{pt} accomplishes this quite easily.

The variational procedure leads directly to Equation [4] of the paper, which exists under the general boundary conditions stated. The principle of virtual work was applied to obtain the left-hand member of Equation [4] which represents the first variation. Since this variation vanishes, by Equation [4], the integral must be stationary.

By using the Relation [5], the work integral becomes a function of the single variable a_n, and the method of Rayleigh then gives the eigenvalues for p corresponding to the nth mode of deflection shape $y_n(x)$. Owing to the fact that Equation [5] contains only the one parameter a_n, the solutions are only approximate.

The method used by the author is elegant, in that the results are obtained in a straightforward manner, and are expressed by formulas that are easy to work with in practice, and have a simple physical interpretation. These Formulas [6*a*] and [6*b*] also possess the added virtue of showing the analogy between the approximate solution for small damping effect and that for constant damping. So far as the literature shows, the variational method has not been expounded previously for the quasi-static case.

AUTHOR'S CLOSURE

The author would like to thank Professor Russell and Professor Whitford for their interesting comments.

It may be worth while, from a practical as well as logical standpoint, to note again that the *only* approximating assumption made in the analysis is that the damping negligibly affects the mode shapes. No assumption, for example, that the damping has a negligible effect on the natural frequencies has been, or need be, made. In this connection it may be observed, as has Professor Russell, that the error made in the natural frequency obtained by Rayleigh's method is usually less than that made in the assumed deflected shape, and that this is one of the important advantages of Rayleigh's method here. [For the case of undamped vibrations of a beam, for example, it can be readily seen that if a first-order-small error is made in the assumed deflected shape, then the error in the natural frequency obtained by Rayleigh's method will tend to be second-order-small. This follows essentially from the fact that, as described in, e.g., Reference (7) of the original paper, the natural frequency must have a stationary value with respect to variations in the deflected shape.] As indicated in the original paper, the fact that the mode shapes will be exactly unaffected by the damping when $f(x)/m(x) =$ constant shows, among other things, that the results obtained here can be approximately valid, under certain conditions, even when the damping is large.

It is, finally, of mathematical interest to add that in the analysis presented in the original paper, it is not necessary and would actually be disadvantageous to first eliminate the $\dot{Y}$ (damping) term from the partial differential Equation [1]. Indeed, the standard type of substitution for this purpose would in this case be

$$Y(x, t) = v(x, t) \exp.\{[f(x)/2m(x)]t\}$$

Such a substitution, however, despite the elimination of a first-time-derivative term, would result in this case in a much more complicated partial differential equation for $v(x, t)$ when $f(x)$ is not exactly proportional to $m(x)$.

[3] Associate Professor of Mathematics, Polytechnic Institute of Brooklyn, Brooklyn, N. Y.

Note on Thermal Stresses[1]

YI-YUAN YU.[2] The utility of the complex variable method in solving two-dimensional thermal-stress problems had been well established by previous authors. Although the presentation is different, the content of the note may be seen to have been covered in a paper by H. Poritsky[3] on steady-state thermal stresses; the example given in the note is the same as one of the three cases solved in the latter paper. These cases are well known to be the only ones which give rise to nonvanishing thermal stresses in the plane of the cross section of hollow circular cylinders.

The author's statement, "The derivation . . . can be modified also to yield analog equations when $\nabla^2 T \neq 0$" is also misleading. The application of the complex variable method to unsteady-state thermal-stress problems had been discussed by N. Lebedew[4] and B. E. Gatewood.[5] These authors as well as N. I. Muschelisvili[6] also considered the steady-state problem of the hollow circular cylinder.

The writer also would like to take the liberty to report that a research project has been proposed in which the problem of thermal stresses in an eccentric hollow circular cylinder will be solved by the complex variable method. This problem does not seem to have been solved before, although the case of a composite body with the cross section as two eccentric circles and subjected to constant temperature has been discussed by Gatewood.[5]

AUTHOR'S CLOSURE

The author wishes to thank Professor Yi-Yuan-Yu for his comments.

With regard to the utility of complex potentials in the solution of two-dimensional thermal-stress problems, the author is in agreement with Professor Yu. However, the stated purpose of the Note (See paragraph 1, sentence 1) was simply to *emphasize* the utility of the method. (See, for example, pp. 427–433 of the first reference).

The simple forms of Equations [4*c*] and [4*d*] are of some interest as they reveal the analogy between thermal loading and dislocations of the type described by Mann,[7] and Bogdanoff.[8] It was not claimed in the Note, however, that either the presentation or the problem solved was original.

Due to a misprint, the word "analog" appeared in place of *analogous*.

[1] By J. L. Bogdanoff, published in the March, 1954, issue of the JOURNAL OF APPLIED MECHANICS, Trans. ASME, vol. 76, p. 88.

[2] Assistant Professor, Department of Mechanical Engineering, Syracuse University, Syracuse, N. Y. Assoc. Mem. ASME.

[3] "Thermal Stresses in Cylindrical Pipes," by H. Poritsky, *Philosophical Magazine*, vol. 24, 1937, pp. 209–223.

[4] "Über die Warmespannungen in Elastizitätstheorie," by N. Lebedew, *Journal of Applied Mathematics and Mechanics*, vol. 2, 1934, pp. 52–60 (in Russian with German summary).
"Thermal Stresses in Circular Ring," by N. Lebedew, ibid., vol. 3, 1936, pp. 76–84 (in Russian).

[5] "Thermal Stresses in Long Cylindrical Bodies," by B. E. Gatewood, *Philosophical Magazine*, vol. 32, 1941, pp. 282–301.

[6] "Some Basic Problems of the Mathematical Theory of Elasticity," by N. I. Muschelisvili, translated by J. R. M. Radok, P. Noordhoff Ltd., Groningen, Holland, 1953, pp. 233–236.

[7] "An Elastic Theory of Dislocations," by E. Mann, Proceedings of the Royal Society of London, England, series A, vol. 199, no. 1058, 1949, p. 376.

[8] "On the Theory of Dislocations," by J. L. Bogdanoff, *Journal of Applied Physics*, vol. 21, no. 12, 1950, p. 1258.

Book Reviews

Fluid Dynamics

MODERN DEVELOPMENTS IN FLUID DYNAMICS—HIGH SPEED FLOW. Composed under the aegis of the Fluid Motion Subcommittee of the Aeronautical Research Council and edited by L. Howarth with the assistance of H. B. Squire and the late C. N. H. Lock. Oxford Engineering Science Series, Oxford University Press, New York, N. Y. 1953. Cloth, 6 × 9 in. Vol. 1, xvi and 475 pp.; Vol. 2, viii and pp. 477 to 875, illus.; 2 volumes, $17.

REVIEWED BY ASCHER H. SHAPIRO[1]

ALTHOUGH its title and sponsorship are similar, the present two-volume work covers subject matter completely different from that in the 1938 two-volume work on "Modern Developments in Fluid Dynamics," edited by S. Goldstein. The Goldstein volumes gave an extended account of theory and experiment relating to boundary layers, turbulent motion, and wakes, which topics by the late 1930's had acquired some maturity. Since 1938 the great new developments have been in the realm of compressible fluid motions. The Howarth volumes are intended to give a comprehensive account of the present status of high-speed flows at a time when this subject has also acquired some maturity. In several respects the Goldstein and Howarth works are alike: The same guiding spirits lay behind their designs, they are much alike in style, and the newer volumes seem also destined to become a classic reference source.

In all, 15 authors contributed to the two volumes. The first volume is given almost exclusively to the mathematical theory of compressible flows. The second is devoted mainly to experimental methods and results, except for the final section on heat transfer. One of the unfortunate consequences of assigning individual chapters to different authors is that there is little coherence between the theoretical treatments in the first volume and the experimental presentations in the second, a consequence which causes both the theoretical and experimental accounts to suffer.

The range of subject matter is indicated by the following chapter outlines. After the chapter title is indicated the author of the chapter and, in parentheses, the number of pages.

VOLUME 1

1. Introduction, by L. Howarth (33). An outline of fundamental notions in compressible flow, and a preview of the various phenomena treated in detail in the remainder of the work.

2. The Equations of Flow in Gases, by L. Howarth (37). A searching formulation of the governing equations of compressible, viscous flows.

3. The Method of Characteristics, by R. E. Meyer (36). General presentation of the theory of characteristic curves with two independent variables, and application to plane steady flows, axisymmetric steady flows, and unsteady flows.

4. Section 1. Shock Waves, by C. R. Illingsworth (42). Relations for oblique and normal shock waves and their interactions.

4. Section 2. Blast Waves, by G. J. Kynch (21). Analysis of spherically-spreading wave systems.

5. Some Exact Solutions of the Equations of Steady Homentropic Flow of an Inviscid Gas, by W. G. Bickley (33). Miscellaneous collection of exact solutions, mostly supersonic: vortex; source flow; spiral flow; Prandtl-Meyer flow; supersonic nozzle design; supersonic flow past wedge, past flat-plate airfoil, and past double-wedge airfoil; supersonic flow past cone.

6. One-Dimensional Flow, by O. A. Saunders (37). Theory of one-dimensional steady flow, showing effects of area change, friction, and heat transfer.

7. The Hodograph Transformation, by M. J. Lighthill (56). Determination of physical flows from mathematical solutions in hodograph co-ordinates.

8. Approximate Methods, by G. N. Ward (59). Miscellaneous collection of approximate methods: linear and second-order theories of subsonic and supersonic flows; electrical analogy; conical flows; transonic similarity law.

9. Unsteady Motion, by G. Temple (53). Unsteady flow past wings and bodies of revolution at subsonic and supersonic speeds.

10. Boundary Layers, by A. D. Young (105). Theory of compressible boundary layers in laminar and turbulent flow.

VOLUME 2

11. Experimental Methods, by D. W. Holder, D. C. McPhail, and J. S. Thompson (135). Wind-tunnel design and operation; uncertainties and corrections in wind-tunnel tests; measurements; visualization of fluid motion.

12. Flow Past Aerofoils and Cylinders, by W. A. Mair and J. A. Beavan (80). Extensive collection of experimental results.

13. Flow Past Bodies of Revolution, by W. F. Cope (69). Extensive collection of experimental results.

14. Heat Transfer, by H. B. Squire (127). A revision of the two chapters on heat transfer originally appearing in the Goldstein work, with additional application to high-speed flows.

The index, which is of great importance for a book like this, is of generous size and has numerous cross references.

A tremendous amount of subject matter is encompassed in volume one, necessarily in condensed style. The treatment is highly mathematical, so much so as to restrict considerably the usage of the volume. Indeed, the reviewer feels that an overattentiveness to mathematical questions and generality of treatment has tended to obscurity and to a camouflage of the really significant methods and results. The subject matter of vol. 1 would have been enlivened, and that of vol. 2 been given greater significance, it is believed, had they been more thoroughly mixed.

Notwithstanding these comments, the reviewer believes this work to be a landmark and unhesitatingly recommends it to all who have passed the neophyte stage in gas dynamics.

Aeronautical Dynamics

INTRODUCTION TO AERONAUTICAL DYNAMICS. By Manfred Rauscher. John Wiley & Sons, Inc., New York, N. Y., 1953. Cloth, 6½ × 9½ in., xv and 644 pp., 479 figs., $12.

REVIEWED BY MARTIN BLOOM[2]

THIS work is an excellent contribution to the literature available to those concerned with teaching or learning the fundamentals of solid and fluid dynamics on the upper-undergraduate or even the lower-graduate levels. Distinctive for its clarity and unique point of view, it is a product of the author's more than 20 years of careful preparatory writing and of teaching these subjects according to the plan utilized at the Massachusetts Institute of Technology. Covering the difficult plane that lies just above the barely elementary (beginning at the Junior year), the book seeks to prepare students for subsequent detailed studies of the dynamic stability of aircraft. This accounts for the co-presentation of solid and fluid dynamics. Although the subject matter is so organized that these topics can readily be separated for use in

[1] Professor of Mechanical Engineering, Massachusetts Institute of Technology, Cambridge, Mass. Mem. ASME.

[2] Assistant Professor of Aeronautical Engineering, Polytechnic Institute of Brooklyn, Brooklyn, N. Y.

separate courses in either solid dynamics or fluid dynamics, the interrelation of the topics is stressed in a useful and interesting fashion. Many illustrative examples and chapter-concluding problems emphasize practical aeronautical applications; and quite a number of the explanations and applications are unique and will not be found readily elsewhere. Typical of these is the discussion of a spinning cylinder in a viscous fluid. However, according to the author, the present volume is meant to be supplemented particularly by other literature and courses in applied aerodynamics.

While the basic treatment of the various topics is mainly in a classical vein, the methods of formal vector analysis are purposely avoided. Moreover, the use of concrete, practical tie-up discussions is always emphasized for purposes of information and motivation. For example, in the chapter entitled "Dynamics of a Particle," sections are included on the following topics: Soaring in wind with a vertical velocity gradient, rocket propulsion, air-fed rockets, and rocket flight to great altitudes.

The chapter headings are given as follows: Preliminary—Newton's law and the conservation of matter; 1 kinematics of a point; 2 dynamics of a particle; 3 dynamics of groups of particles; 4 fundamental equations of fluid motion; 5 stream function and velocity potential; 6 fluid motion about simple bodies; 7 transformations; 8 airfoils; 9 airfoils in three dimensions; 10 viscosity; 11 kinematics of rigid bodies; 12 dynamics of rigid bodies; 13 oscillations of systems with one degree of freedom; 14 oscillations of systems with more than one degree of freedom.

The clarity and excellence of the figures warrant special mention.

Some of the topics not discussed are pointed out in Professor Rauscher's own words ". . .I am aware that in some respects the book is not as complete as it might be. Particularly noticeable is the absence of discussions of compressible flows in more than one dimension, of thin airfoils as surfaces of discontinuity, under unsteady as well as under steady conditions, of three-dimensional flow problems, and of servomechanisms. My failure to include these topics is due to lack of time so far to write them up." The reason for these omissions really serves to point up the careful thought with which the large amount of material covered in the book has been presented.

Instruments Engineering

INSTRUMENT ENGINEERING. Vol. 2. Methods for Associating Mathematical Solutions With Common Forms. By C. S. Draper, W. McKay, and S. Lees. McGraw-Hill Publications in Aeronautical Science, McGraw-Hill Book Company, Inc., New York, N. Y., 1953. Cloth, 8½ × 11 in., xxviii and 827 pp., illus., $15.

REVIEWED BY ENRICO VOLTERRA[3]

A FEW months ago, in a review of the first volume of *Instrument Engineering* for the JOURNAL OF APPLIED MECHANICS, the chief features and objectives of this work were described.[4] It is with great pleasure that one now sees published the second volume of this excellent work which will be useful to anyone interested in the field of measurement and control in instrument engineering. Whereas the first volume dealt with the description of physical devices and variations in physical quantities by graphical and analytical methods, the second volume gives the theoretical background for associating solutions with these forms.

This second volume consists of fourteen chapters. The first chapter of the second volume (which is the fourteenth chapter of the total group of three volumes) deals with nondimensionalization of linear integrodifferential equations, the second with the classical method of solving linear integrodifferential equations, the third with operational methods of solving linear integrodifferential equations with constant coefficients. The successive chapters discuss solutions of first and second-order differential equations, transient stability of mathematical solutions, and methods of solving third and fourth-order characteristic equations. Graphical methods of determining transient stability are given. The last two chapters deal with representation of solutions for differential equations with nonlinear terms of the rate-determined step type, and numerical analysis by the number-series transformation method.

The third volume is to consist of examples in which the theory and techniques, described in the first two volumes, are applied to typical cases.

There is no doubt that for many years to come this work, which presents in an orderly and clear way materials which until now have been scattered through the literature, will constitute the chief reference in the field of instrument engineering. The authors, all three authorities in the field, should be congratulated on their achievement.

[3] Professor of Mechanics, Rensselaer Polytechnic Institute, Troy, New York. Mem. ASME.

[4] JOURNAL OF APPLIED MECHANICS, Trans. ASME, vol. 76, 1953, p. 155.

Complex Variable and Transform Calculus

COMPLEX VARIABLE THEORY AND TRANSFORM CALCULUS WITH TECHNICAL APPLICATIONS. By N. M. McLachlan. Second edition. Cambridge University Press, New York, N. Y., 1953. Cloth, 5½ × 8½ in., xi and 388 pp., illus., $10.

REVIEWED BY A. ALI KHEIRALLA[5]

THE book is divided into four parts of which the last is simply a set of appendixes. The first section constitutes an engineering introduction to those portions of the theory of functions of a complex variable which are most commonly applied to the operational solution of differential equations. Although the later applications of this part of the text are almost exclusively limited to contour integration, various other topics of general background value are discussed. Analytic functions and their singularities are presented. The theorems of Cauchy, Taylor, Laurent, and Morera are considered and the Gamma, error, and Bessel functions introduced. A considerable proportion of the first section is devoted to the evaluation of contour integrals by means of the theorem of residues. This is, of course, directed toward establishing a facility in the inversion of the Laplace transform, the application of which is the main objective of the succeeding parts two and three. Special attention is given to a discussion of branch points and their influence on choice of contour is illustrated by numerous examples.

Part two presents the Laplace integral, formal solution of ordinary differential equations by transform technique, and frequency spectra associated with impulses. The various formal properties (translation, differentiation, integration) of the transformation as well as the inversion formula are exhibited. The Laplace transform of periodic functions is introduced. A short section on ordinary differential equations (with constant coefficients) follows. The last section of part two is a concise exposition of the intuitive connection between impulses and their frequency spectra. Avoiding the mathematical delicacies of Fourier analysis, the author presents simply and forcefully the fundamental formal technique. No attempt is made to state or prove theorems in full generality. This is, however, strictly consistent with the author's purpose to equip the reader with

[5] Lessells and Associates, Inc., Boston, Mass.

formal problem-solving methods and refer him to more extensive mathematical treatises for refinements, exceptions, and a rigorous development.

Part three consists of five chapters of which the first handles simple electric circuits, torsional oscillations, gun recoil effect on aeroplane, beam deflection, and coupled systems. The next chapter treats applications to radio and television-receiver circuits. In chapter 13 the topics are partial differential equations, electrical transmission lines, and electrical wave filters. Submarine cables and high and low-pass filters are covered. The next chapter treats the metal core solenoid, the condenser microphone, and the loudspeaker horn. The final chapter discusses the solution of the diffusion equation. Heating of automobile brakes, a refrigerator problem, annealing of a steel rod, and absorption of moisture by a slab are presented.

A collection of 102 problems follows chapter 15. The appendixes contain selected lemmas, theorems, and applications. Included are a couple of examples of Watson's theorem on the asymptotic expansion of Laplace transforms, a more extended discussion of the inversion formula and the convolution theorem on products of transforms.

The text is profusely illustrated with graphical representations of functions and contours. Although the author has elected to use "p—multiplied" Laplace transform in conformity with the operational notation of Heaviside, this introduces at most a minor inconvenience.

In general, the book should help to fill the gap between the more rigorous treatises of Doetsch and Widder and the handbook-type compilations of formal rules of operational calculus. Especially worthy of note is the fact that the complex variable material, so essential to an understanding of the Laplace transform theory, is used as an introduction to the subject and not relegated to the status of a neglected side issue as is so often the case in books on manipulative technique.

Elasticity

APPLIED ELASTICITY. By Chi-Teh Wang. McGraw-Hill Book Company, Inc., New York, N. Y., 1953. Cloth, 6 × 9 in., ix and 355 pp., illus., $8.

REVIEWED BY P. S. SYMONDS[6]

THIS book provides an introduction to the theory of elasticity and to the approximation techniques and numerical methods which are often required to obtain useful results for engineering purposes. A book having this size and level can take up only the fundamentals of a restricted list of topics, but the book under review supplies references to many of the important sources in the recent literature. This reviewer feels that the well-balanced choice of topics and the accurate and lucid exposition make this book a distinctive contribution.

The first three chapters deal with the fundamentals of stress and strain and the general equations of elasticity, the next two chapters taking up problems of plane stress and strain and of torsion, respectively. This leads naturally to the presentation in chapter six of a concise but readable introduction to numerical analysis by finite-difference approximations and by relaxation techniques, both exemplified by treating the problem of torsion of a square bar.

Chapter seven contains an authoritative and clear introduction to the variational principles of complementary energy and potential energy, basing the development on the principle of virtual work. Illustrations are given of the use of the Rayleigh-Ritz method with both variational principles, and the author also briefly outlines Galerkin's method and that of Biezeno and Koch. Chapter eight provides an introduction to complex variable methods for treating problems of torsion and plane strain.

Chapter nine discusses the stability of beams under axial thrust while the following chapter takes up numerical techniques for handling buckling problems: finite difference and relaxation schemes of computation and the use of Rayleigh's principle, with a brief treatment of devices for finding lower bounds. Bending and buckling of thin plates are discussed in chapter eleven, while the closing chapter twelve introduces the theory of thin shells, starting with vector geometry of surfaces and ending with the classical theory of buckling of a circular cylindrical shell under uniform axial compression (the author points out the deficiencies of this treatment and gives references to recent improvements).

The book has some defects inevitable in a new book; for example, Fig. 11.4 is so crowded as to be hardly intelligible. Some omissions seem unfortunate, such as the absence of reference to the upper and lower-bound theorems due to Prager and Synge, and the lack of mention of nonuniform torsion or of torsional buckling. The addition of further references, with brief annotation, would make an already excellent book still more valuable.

[6] Professor of Engineering, Brown University, Providence, R. I. Mem. ASME.

Stress and Strain

FORMULAS FOR STRESS AND STRAIN. By Raymond J. Roark. McGraw-Hill Book Company, Inc., New York, N. Y., third edition, 1954. Cloth, 6 × 9 in., xiii and 381 pp., 45 figs., 19 tables, $7.50.

REVIEWED BY JOSEPH MARIN[7]

THE publication of a third edition of this book indicates that it has been used by many engineers. This is no doubt because many useful results in stress analysis have been summarized in a compact and useful form readily usable by the design engineer.

In this new edition the author has brought the contents up to date in several ways. Throughout the book additional references have been added so that the reader can become acquainted with the most recent developments in each particular subject. Test data and empirical formulas reported in the second edition have been revised so that they are in keeping with the latest available information. New material has been added throughout this third edition which includes recent information on shear lag, stress and deflection of circular arches, flat plates with large deflection, pressure vessels and shells, and stress concentration. Material has also been added to various tables for flat plates, used to determine stress, deflection, and edge-slope in plates. This book should continue to be a valuable addition to the machine and structural designer's library.

Discontinuous Automatic Control

DISCONTINUOUS AUTOMATIC CONTROL. By Irmgard Flügge-Lotz. Princeton University Press, Princeton, N. J., 1953. Cloth, 6 × 9¼ in., viii and 168 pp., 102 figs., tables, appendixes, index, $5.

REVIEWED BY JOHN A. HRONES[8]

THE book deals with the control of systems describable with a second-order linear differential equation

$$a^*\ddot{\phi} + 2b^*\dot{\phi} + c^*\phi = M^* \quad \ldots\ldots\ldots\ldots [1]$$

ϕ is the difference between the actual value and the desired value

[7] Head, Department of Engineering Mechanics, The Pennsylvania State University, State College, Pa. Mem. ASME.

[8] Professor of Mechanical Engineering, Massachusetts Institute of Technology, Cambridge, Mass. Mem. ASME.

of the quantity to be controlled and M^* is the manipulated quantity. (See Fig. 1.)

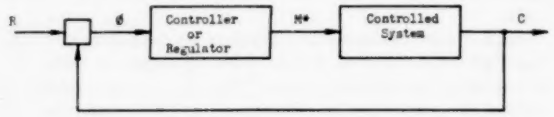

FIG. 1

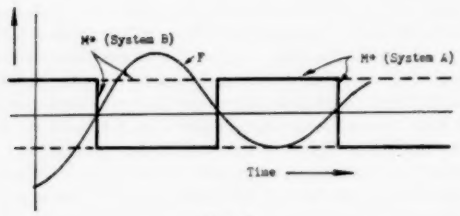

FIG. 2

$$\phi = C - R \quad \text{.....[2]}$$

The controllers considered are discontinuous in operation. One class of such controllers referred to as "position controllers" is defined by the following relationships

$$M^* = N^*\beta \quad \text{.....[3]}$$

$$\beta = \pm\beta_0 \operatorname{sgn} \rho_1(\phi + \rho\dot{\phi}) \quad \text{.....[4]}$$

$$\operatorname{sgn} x = \frac{x}{|x|} = +1 \quad \text{when } x > 0$$

(1)

$$\operatorname{sgn} x = -1 \qquad \text{when } x < 0$$

Two general systems of control are discussed. In system A the negative sign of Equation [4] is used. In system B the positive sign of Equation [4] is used. If the function $(\phi + \rho\dot{\phi}) = F$ is as shown in Fig. 2, the manipulated quantity M^* will be as indicated for systems A and B.

A second category of regulation discussed as "velocity control" has regulator transfer characteristics as defined below

$$M^* = N^*\beta \quad \text{.....[5]}$$

where

$$\dot{\beta} = \pm\gamma \operatorname{sgn} (\rho_1\phi + \rho_2\dot{\phi}) \quad \text{.....[6]}$$

Again, two cases are discussed, one case involving the negative sign of Equation [6] and the other employing the positive sign of Equation [6], see Fig. 3.

In addition, control functions of the following form are also discussed. Such a function is obtained by feedback around the controller. (See Fig. 4.)

$$F = \rho_1\phi + \rho_2\dot{\phi} + \rho_3\beta \quad \text{.....[7]}$$

Certain imperfections of control elements are discussed. They include the existence of a dead zone and the existence of a constant time delay.

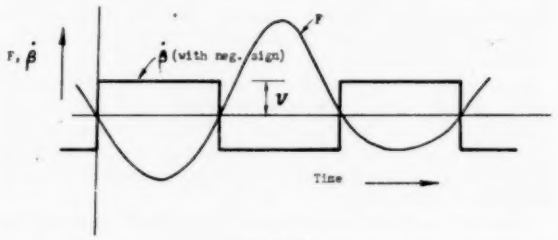

FIG. 3

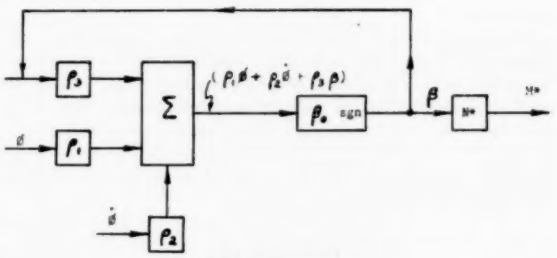

FIG. 4 CONTROLLER

Phase plane representation (ϕ plotted against $\dot{\phi}$) is used throughout in the analysis. Simple approximate construction methods are presented. A number of cases are discussed, all briefly. The final chapter is devoted to a consideration of the control of the longitudinal motion of a missile.

The book has only 159 pages and the reader has the distinct impression that the author has not exploited the material as fully as desirable. It is a welcome addition to the limited literature covering systems controlled by discontinuous-type regulations.

AN ASME PAPER

Its Preparation, Submission and Publication, and Presentation

To a large degree the papers prepared and presented under the ASME sponsorship are evidence by which its professional standing and leadership are judged. It follows, therefore, that to qualify for ASME sponsorship, a paper must not only present suitable subject matter, but it must be well written and conform to recognized standards of good English and literary style.

The pamphlet on "AN ASME PAPER" is designed to aid authors in meeting these requirements and to acquaint them with rules of the Society relating to the preparation and submission of manuscripts and accompanying illustrations. It also includes suggestions for the presentation of papers before Society meetings.

CONTENTS

PREPARATION OF A PAPER—

General Information—Style, Preferred Spelling, Length Limitation, Approvals and Clearances.

Contents of the Paper—Title, Author's Name, Abstract, Body of Paper, Appendixes, Acknowledgments, Bibliographies, Tables, Captions, Photographs, Other Illustrations.

Writing the Paper—Outline Tabulations, Tables, Graphs, Charts for Computation, Drawings, Mathematics, Accuracy, Headings and Numbering, Lantern Slides, Motion Pictures, Typing, Number of Copies.

SUBMISSION AND PUBLICATION OF A PAPER—

Intention to Submit Paper Required in Advance, Meeting Dates, Due Dates for Manuscript, Discussers, Review and Acceptance, Proofs, Advance Copies and Reprints, Discussion and Closure, Publication by Others.

PRESENTATION OF A PAPER—

Time Limit, Addressing Your Audience, Public Address Systems, Use of Slides.

REFERENCES—

References on Writing and Speaking, Engineering Standards.

Price 20¢. 20% Discount to ASME Members

THE AMERICAN SOCIETY OF MECHANICAL ENGINEERS

29 West 39th Street, New York 18, N. Y.

GENERAL DISCUSSION ON HEAT TRANSFER

This is the complete record of the 1951 Conference sponsored by the ME-ASME, the purpose of which was to review a decade's development in heat transfer and in the design of apparatus relating thereto. In ninety-three papers, this reference provides first-hand accounts of experimental and analytical investigations, descriptions of various methods and apparatus used, information on actual performance of fundamental data, essential conclusions from researches, technical and laboratory data needed for more accurate control of design, a considerable amount of bibliographical material, and a complete record of the discussion.

The contents is grouped under five sections: heat transfer with change of state; heat transfer between fluids and surfaces; conduction in solids and fluids; convection, radiation, instrumentation and measurement techniques; and special problems with the entire subject covered in a way that will enable one to accurately appraise fundamental discoveries of the field and to take advantage of new practical applications of known principles.

1951 $10.00

GLOSSARY OF TERMS IN NUCLEAR SCIENCE AND TECHNOLOGY

Now, under one cover, precise definitions for about 2000 terms used in the fields of reactor theory, reactor engineering, chemistry, chemical engineering, biophysics and radiobiology, instrumentation, isotopes separation, metallurgy, and physics. The Glossary is divided into nine sections to enable the user to readily locate the terms peculiar to each of the afore-mentioned fields. An alphabetical arrangement of the terms has also been included to indicate the section or sections in which the definitions and the terms will be found.

Seventeen scientific and technical societies, ten governmental agencies, and four divisions of the National Research Council have co-operated in the preparation of this Glossary.

$7.50

DIGITAL AND ANALOG COMPUTERS AND COMPUTING METHODS

This book summarizes the present state of high speed computation in the field of applied mechanics. It discusses the use of analog computers and their application to aircraft design problems and to mechanical problems. It also shows how digital analog computers are being used to solve linear algebraic equations and to find eigenvalues and eigenvectors.

1958 $5.00

DESIGN DATA AND METHODS APPLIED MECHANICS

This collection of papers covers new design methods and procedures in the field of strength of materials, fluid mechanics, vibration and balancing, and lubrication. Each paper is an original and practical contribution to the field. The section on Strength of Materials contains stress and deflection methods applied to circular and rectangular plates, analysis of circular beams, hydrostatic loading problems, piping, stress concentrations, torsion, helical compression and tension springs, thermal stresses, stresses in pressure vessels, shrink-fitted assemblies, and thick-walled cylinders. The Fluid Mechanics section includes two-dimensional supersonic flow, gas-flow problems, and shock waves in water. Articles on lubrication discuss method of applying bearing theory to the analysis and design of journal bearings. In the Vibration and Balancing section, various types of vibration problems are dealt with, also balancing with rotating apparatus, torsional vibration modes of tapered bars, engine torque curves, and frequency vibration of rectangular plates.

1953 $4.00

ASME HANDBOOK

METALS ENGINEERING-DESIGN

Comprising 46 sections and written by 43 well-known authorities, it provides: Criteria for facing the over-all problems of selection of materials; facts on potential weaknesses of various metals and ways of making the metals strong; details of the specific problems of corrosion and the mechanical factors which influence corrosion; present knowledge of testing by nondestructive methods; special requirements of design and surface finish set up by mass production; modern basic information on the design theory, design practice, experimental design; and the special requirements of aluminum and magnesium. Here, too, are the equations for determining such factors as stress, creep, impact strength; the results of such methods as the use of residual stresses to improve fatigue resistance, and the use of flame hardening to increase resistance to fatigue failure; and the methods for making your structure or machine part stronger, such as shot peening, cold working, and case carburizing.

450 pages 880 Illustrations $10.00

METALS PROPERTIES

A practical accumulation of tabulated data on the properties of more than 500 metals in common industrial use—AISI steels, ASTM steels, cast copper alloys, aluminum alloys, tin, magnesium, etc. Specially prepared for design engineers, this book provides such information as chemical composition...industrial uses...density, electrical resistivity, volume conductivity, and other physical properties...draw temperatures, tensile strength, yield point, and other mechanical properties...treatment temperatures for forging, annealing, normalizing, and quenching...thermal conductivity...critical points...end-quench hardenability...Rockwell "C" core hardness...hot-working temperature...weldability...fatigue strength...coefficient of thermal expansion...brazing and soldering.

In brief, METALS PROPERTIES is the reference manual that will help you select the right metal for each part or product, see that it meets specifications, and make sure it will stand up under typical conditions.

448 pages $11.00

THE AMERICAN SOCIETY OF MECHANICAL ENGINEERS

29 W. 39th St., New York 18, N. Y.

25% DISCOUNT TO ASME MEMBERS